Flexural behaviour of RC beams strengthened with multi-layer steel reinforced grout (SRG) composites

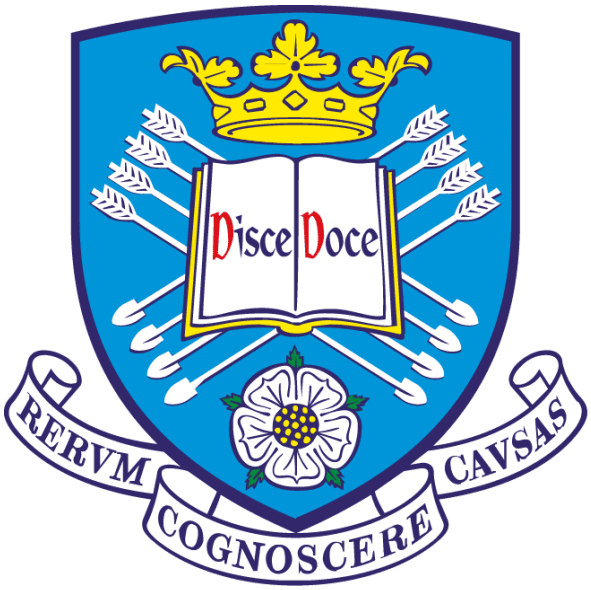

A thesis presented for the degree of

Doctor of Philosophy in Civil and Structural Engineering

at The University of Sheffield

By

Sultan Alotaibi

Sheffield

October 2021

To my brother Moqrin, joy died the day you died

To my son Moqrin, joy was reborn the day you were born

Abstract

Several events can cause damage to existing structures including natural and man-made disasters. Even if some structures are less vulnerable to such extreme events, damage can be still introduced by several other events including change of codes or use, increase of demands on structural performance, deterioration with age, deficient design or construction. Different systems have been used in the retrofit industry including section enlargement, steel plate bonding, welded steel meshes, external post-tensioning, and the use of composites including Fibre Reinforced Polymers (FRP), Steel Reinforced Polymers (SRP), Fabric reinforced cementitious matrices (FRCM), and Steel Reinforced Grout (SRG). This latter system received much attention recently as the use of the grout has addressed many drawbacks associated with the use of the epoxy matrix in FRP and SRP systems. Furthermore, the use of the steel textiles as an alternative to other synthetic textiles used in FRCM systems was advantageous from economic and design perspectives. SRG systems were investigated in several applications including flexural and shear strengthening, confinement of columns and joints, out-of-plane and in-plane strengthening of walls. However, the knowledge on the flexural behaviour of RC beams strengthened with SRG systems is very limited, especially the use of multiple layers of these systems which is often considered for strengthening large structural members.

The aim of this research was to investigate the flexural behaviour of RC beams strengthened with SRG composites comprising different number and densities of the steel textiles. However, the flexural behaviour is largely influenced by the tensile behaviour of the composite and the bond between the composite and the substrate. To achieve the aim of this work, three experimental programmes were conducted on a total of 200 specimens. The first programme was devoted to investigating the tensile behaviour of the SRG composites. Mechanical characterisation was conducted by performing a total of 104 direct tensile tests on bare single cords, bare textiles, and SRG coupons. The bond behaviour between the SRG composites and the concrete substrate was investigated in the second experimental programme. This was achieved by conducting a total of 90 direct shear bond tests on different SRG systems comprising multiple layers of steel textiles and different densities applied to concrete substrates with different compressive strengths. Finally, the last experimental programme was conducted on 6 full-scale RC beams strengthened with different SRG systems to study their flexural behaviour.

The results of the tensile tests showed that the SRG coupons comprising dense steel textiles exhibited a tensile stress-strain behaviour similar to that developed by those comprising low density textiles. Increasing

the number of layers resulted in an increase in the axial stress and the corresponding strain. This increase was sound for the transition from one to two layers. However, increasing the density of the textiles led to a decrease in the axial stress and the corresponding strain. All tested coupons developed a comparable crack pattern and eventually failed by textile rupture. However, the coupons strengthened with multiple layers of textiles (i.e., high reinforcement ratio) experienced a greater number of cracks at failure with relatively less crack width and spacing. Shear bond tests indicated that the effective bond length of the SRG system is insignificantly influenced by the reinforcement ratio (function in the density of textile and the number of layer). In general, the effective bond length for the SRG system was found to lie between 200 mm and 300 mm. The SRG systems comprising three layers of textiles always failed by debonding at the substrate interface, while those comprising dense steel structure in most cases experienced the failure at the textile interface. Increasing the density of the textiles and the number of layers was found to decrease the axial stress and the corresponding slip. The bending tests conducted on the RC beams showed that beams strengthened with low density textiles exhibited a less stiff behaviour in elastic and post-cracking stages. It was also found that increasing the density of the textiles insignificantly increased the load at yield and at the failure of the SRG system. All the beams strengthened with low-density textiles mobilised a full utilisation of the textiles as they eventually failed by rupture, while the beam strengthened with only one layer of the dense textiles failed by interlaminar shearing at textiles interface. The use of two layers of the dense textiles resulted in the debonding of the SRG system at the substrate interface. Analytical modelling was also carried out on some existing bond models originally proposed for the FRP systems to evaluate their adoptability for the SRG system. It was found that some of these models were accurate in estimating the debonding load for the SRG systems. However, they could not capture all the parameters of the experimental programme. A new model was suggested for shear bond tests based on the reinforcement ratio and the bond length of the SRG composite. The proposed model was able to capture the overall behaviour of the SRG system. The debonding load was predicted with a coefficient of variation of only 9%, while the accuracy of predicting the mode of failure was 97%. The proposed mode for the shear bond tests was then utilised to predict the failure load and mode in RC beams strengthened with SRG systems. A design recommendations and guidelines were given to help engineers when using SRG system in the strengthening industry.

Acknowledgements

I would like to thank my supervisors Dr Iman Hajirasoulih and Dr. Maurizio Guadagnini for their invaluable help and endless support throughout my PhD journey. Also, a very special gratitude goes to Dr. Georgia Thermou who helped in laying out the first brick in my PhD project when she visited the University of Sheffield in 2017 as a “Marie Curie” individual fellow. The collaboration with Dr. Georgia continued after she left the University of Sheffield to join the University of Nottingham as an assistant professor. This work would not have been accomplished without the help and coordination provided by Dr. Iman, Dr. Maurizio, and Dr. Georgia.

My parents and my siblings, I am really in shortage of words to express how I’m lucky to have you in my life. You were beside me in the difficult times, I pray to Allah that you stay with me in the good times for many years to come.

My sponsor Ministry of Education, Shaqra University, and Saudi Cultural Bureau (SACB), my PhD would not have been possible without you, thank you all.

Very special thanks to KeraKoll S.p.A for providing the steel textiles and the cement for the experimental programmes.

My wife, you have always been the remedy for the tough days in my life. It does not take more than a look at you to fix any crack in my soul. You are the strengthening system for my life that never debonded and will never do.

CEE Group

Prof. Kypros Pilakoutas
Dr Zuhal Ozdemir
Dr Shan-Shan Huang
Dr Giacomo Torelli
Dr Harris Angelakopoulos
Dr Panos Papastergiou
Dr Francesca Roscini
Mr Yifan Li
Mr Imad El Khouri
Mr Mohammad Nora
Mr Soheil Khoshkholghi
Mr Mohammad Moavi
Mr Seyed Mojtabaei
Mr Ioannis Papargyriou
Mr Ilya Sianko
Miss Niki Trochoutsou
Mr Talal Alshamri
Mrs Tracey McNeilly
Dr Abdulaziz Alsaif
Dr Zahran Al-Kamyani
Mr. Shaun Waters
Dr Matteo Di Benedetti
Dr Stefano De Santis
Dr Szymon Cholostiakow
Dr David Margarit
Dr Hamed Fergani
Dr Fabio Figueiredo
Dr Nelson Flores Medina
Dr Reyes Garcia
Dr Hang Hu
Dr Lampros Koutas
Mr Spyridon Maroudas
Dr Neda Nabid
Mr Spyros Polydoropoulos
Dr Samar Raffoul
Miss Francesca Rech
Dr Asif Hussain Shah
Mr Sándor Sólyom
Dr Zhao Wang
Ms Veronica Zoni

Technical staff

Dr Paul Bentley
Mr Paul Blackbourn
Mr Alex Cargill
Mr Andrew Fairburn
Mr Mark Foster
Mr. Robin Markwell
Mr Alan Grundy
Mr Don Jenkins
Mr Kieran Nash
Mr Martin Taylor
Mr Samuel Whitehouse
Mr. Bez khan

Unaizah group

Mr. Fawaz Awad
Mr. Marzouq Awaed
Dr. Ahmad Theeb
Mr. Obaid Motlaq
Mr. Ahmad Awad
Mr. Mohammad Awad
Mr. Ghazi Mohammad
Mr. Mohammad Naif
Mr. Safr Motlaq
Mr. Omar Qodaemes
Mr. Bandar Mohaemeed
Mr. Abdulmohie Bonider

Double-Digit Club

Dr!. Mansoor Alruqi
Mr. Seraj Alsofiani
Mr. Omar Almutairi
Mr. Mohannad alqulaity
Dr?. Khalid alsolius
Mr. Mohammed jeza
Mr. Moaud Alnaami
Mr. Adel Alhuthali
Mr. Jeza Darmooh
Mr. Bandr Aldubakhi
Mr. Dokhi Mohaemeed

Otaibis-in-Nottingham

Dr. Yasser Alotaibi
Dr. Turki A Alotaibi
Mr. Yasser M Alotaibi
Dr. Khalid Alotaibi
Mr. Abdulrahman Alotaibi
Mr. Khalid Alotaibi
Dr. Turki M Alotaibi
Dr. Abdulaziz Alotaibi
Mr. Mohammad Alotaibi
Mr. Ghazi Alotaibi
Dr. Rakan Alotaibi
Dr. Sultan Alotaibi
Mr. Khalf Alotaibi
Mr. Fahad Alotaibi
Mr. Naif Alotaibi
Dr. Adel Alotaibi
Dr. Yousef Alotaibi
Mr. Bandr Alotaibi

PeerPower Project

Mr. Yousef Almalky
Mr. Khalid Albalawi
Mr. Mohammad Alenzi
Mr. Ahmed Alamri
Mr. Abdulatif Alzahrani

Heaven's corridor

Dr. Hammad
Dr. Asif
Dr. Tawfiq
Dr. Mohammad Nora
Dr Abdulaziz Alsaif

Special Thanks To

Dr. Mohammad Qodaemes
Dr. Mohammad Alghasab
Mr. Abdullah Alalwi
Mr. Nasser Alenzi
Mr. Saud Alotaibi

Early 20s

Mr. Naif Alharbi
Mr. Motlaq almutairi
Mr. Abdulrazaq Alotaibi
Mr. Abdullah Alharbi
Mr. Mohammad alharbi

Royal Plaza

Mr. Thabet Alzahrani
Mr. Abdulmonaem
Mr. Mshari Alotaibi
Mr. Hani Alqahtani
Mr. Fawaz Almutari
Mr. Hazaa Alqorashi
Mr. Faisal Alqahtani
Mr. Omar Alshamri
Mr. Wael Alsaedi
Mr. Bader Alotaibi
Mr. Mohammad aljohani

THANK YOU ALL

List of Figures

List of Tables

List of Abbreviations

RC	Reinforced Concrete
EB	Externally Bonded strengthening system
EB	Externally Bonded strengthening systems
IRS	Inhibiting Repairing Strengthening systems
FRCM	Fibre Reinforced Cementitious Matrices
FRGM	Fibre Reinforced Geopolymer Matrices
TRM	Textile Reinforced Mortars
TRC	Textile Reinforced Concrete
C-FRCM	Carbon-Fibre Reinforced Cementitious Matrices
G-FRCM	Glass-Fibre Reinforced Cementitious Matrices
PBO-FRCM	Polyparaphenylene BenzobisOxazole -Fibre Reinforced Cementitious Matrices
B-FRCM	Basalt-Fibre Reinforced Cementitious Matrices
A-FRCM	Aramid-Fibre Reinforced Cementitious Matrices
S-FRCM	Steel-Fibre Reinforced Cementitious Matrices
SRG	Steel Reinforced Grout
PVA	Polyvinyl Alcohol
PP	PolyproPylene
PE	PolyEthylene
STZ	Stress Transfer Zone
HTSS	High Tensile Strength Steel
ULS	Ultimate Limit State
SLS	Serviceability Limit State
FRC	Fibre Reinforced Concrete
DIC	Digital Image Correlation measurement system
AOI	Areas Of Interest for the DIC system
S4	The steel textile that has a density of 4 cords/in
S8	The steel textile that has a density of 8 cords/in
LVDT	Linear Variable Differential Transducer

List of Symbols

n	the total number of cords in the dry steel textiles or the SRG composite.
n_{cords}	The number of the steel cords.
ρ_{tx}	The density of the textile defined as the number of cords per unit length.
ρ_{com}	The maximum load in the single-cord specimens.
$t_{tx,1}$	The equivalent thickness of one layer of the steel textile.
t_{tx}	The equivalent thickness of the steel textile (all layers).
t_{com}	The overall thickness of the SRG coupon.
$\mathrm{A_{cord}}$	The cross-sectional area of a typical steel cord.
A_{tx}	The area of the steel textile.
$\mathrm{A}_{tx,1}$	The area of the steel textile in a single layer.
A_{com}	The cross-sectional area of the SRG composite.
b_{com}	the width of the SRG composite.
b_{sb}	the width of the substrate or the beam.
L_{com}	the length of the SRG composite.
L_{eff}	The effective bond length of the SRG composite.
$d_{ext.}$	the reading of the extensometer mounted to the SRG coupon.
L	the gauge length in direct tensile tests.
P_u	The ultimate load acquired from the testing machine.
$P_{u,cord}$	The maximum load in the single-cord specimens.
$f_{u,cord}$	The maximum axial stress in the single-cord specimens.
ε_{cord}	The strain corresponding to the maximum load in the single-cord specimens.
$E_{cord,I}$	The modulus of elasticity of the single-cord specimens in the first zone on the stress-strain curve.
$E_{cord,II}$	The modulus of elasticity of the single-cord specimens in the second zone on the stress-strain curve.
$P_{u,tx}$	The maximum load in the dry-textile specimens.
$f_{u,tx}$	The maximum axial stress in dry-textile specimens.
$\varepsilon_{u,tx}$	The strain corresponding to the maximum load in dry-textile specimens.
$E_{tx,I}$	The modulus of elasticity of dry-textile specimens in the first zone on the stress-strain curve.
$E_{tx,II}$	The modulus of elasticity of dry-textile specimens in the second zone on the stress-strain curve.
$P_{u,com}$	The maximum load in the single-cord specimens.
$f_{u,com}$	The maximum axial stress in the single-cord specimens.
$\varepsilon_{com,ext.}$	the strain in the grout of the SRG composite coupons obtained from the extensometer.
$\varepsilon_{com,DIC}$	the strain in the grout of the SRG composite coupons obtained from the DIC system.
$E_{com,I}$	The modulus of elasticity of the single-cord specimens in the first zone on the stress-strain curve.
$E_{com,II}$	The modulus of elasticity of the single-cord specimens in the second zone on the stress-strain curve.
$E_{com,III}$	The modulus of elasticity of the single-cord specimens in the second zone on the stress-strain curve.
n_w	The strain corresponding to the maximum load in the single-cord specimens.
w_{av}	The maximum load in the dry-textile specimens.
S_{av}	The maximum axial stress in dry-textile specimens.

s	The slip of the composite.
$s_{com,LVDT}$	the slip of the SRG composite obtained from the LVDTs.
$s_{com,DIC}$	the slip of the SRG composite obtained from the DIC system.
$\tau\ (s)$	The analytical interfacial shear stress at the matrix-to-substrate interface.
A and B	Parameters for calibrating the shape of the curve and the peak value of the shear stress while.
$\tau_{u,an}$	The analytical ultimate shear bond stress.
$s_{u,an}$	The slip corresponding to the analytical ultimate shear bond stress.
$\tau_{u,exp}$	The experimental interfacial shear stress.
F_y	The yield load.
δ_y	The deflection at the mid-span of the beam corresponding to the yield load.
F_u	The ultimate load.
δ_u	The deflection at the mid-span of the beam corresponding to the ultimate load.
μ_δ	The displacement ductility index.
ε_{fd}	The design strain of the external reinforcement.
f_{sd}	The strength of the external reinforcement at debonding.
k_q	A coefficient to account for load distribution.
k_b	a geometrical corrective factor.
$k_{G\ ,2}$	A corrective factor calibrated against experimental results.
η_a	An environmental conversion factor.
γ_f	A partial safety factor for systems sensitive to debonding.
C_E	An environmental conversion factor.
$f_{c,sb}$	The compressive strength of the substrate (cubic strength at 28 days).
$f_{t,sb}$	The tensile strength of the substrate (cubic strength at 28 days).
$f_{c,mx}$	The compressive strength of the matrix (cubic strength at 28 days).
$f_{t,mx}$	The tensile strength of the matrix (cubic strength at 28 days).
$P_{deb,1}$	The debonding load at the matrix-to-substrate interface.
$P_{deb,2}$	The debonding load at the matrix-to-textile interface.
P_{rup}	The theoretical load that can cause a rupture to the external reinforcement.
α	A calibration factor for the debonding at the matrix-to-substrate interface.
β	A coefficient to account for the influence of the bond length.
ξ	A coefficient to account for the effect of the number of the steel textile layers.
φ	A calibration factor for the debonding at the matrix-to-textile interface.
ζ	A calibration factor for the tensile rupture.
F_s	The internal force in the tensile reinforcement.
F_s'	The internal force in the compression reinforcement.
F_c	The internal force in the concrete block.
F_f	The internal force acting upon the external reinforcement.
d	The effective length of the tensile reinforcement.
d'	The effective length of the compression reinforcement.
d_f	The effective length of the external reinforcement.
x	The depth of the neutral axis.
a	The shear span.
h	The height of the beam.
b	The width of the beam.
c	The concrete cover.
λ	A factor defining the effective height of the compression zone
η	A factor defining the effective strength of the concrete

A_s	The cross-sectional areas of the tensile reinforcement.
A_s'	The cross-sectional areas of the compression reinforcement.
f_y	The yield strength of the tensile rebars.
f_c	The cubic compressive strength of the concrete.

Table of contents

Chapter 1 Introduction

This chapter presents a brief background on the retrofit and repair industry in terms of why and when structures need to be strengthened and what are the strengthening systems used in that industry, in particular, the systems that utilise the use of composite materials. This chapter also highlights the significance and motivation to conduct this research and presents its aim and objectives. The scope, limitation, contribution, thesis layout, and publication outputs are also provided herein.

1.1Background

1.1.1 The need for retrofit and repair

Structures are prone to various extreme events that can cause either local or global damage including natural disasters (e.g., earthquakes and fire) and man-made disasters (e.g., explosions) (see Fig. 1.1). Even if some structures are less vulnerable to such extreme events, damage can be still introduced by several different ways including change of codes or use, increase of demands on structural performance, modifications of structural lay-out in existing structures, deterioration with age, deficient design or construction [1, 2].

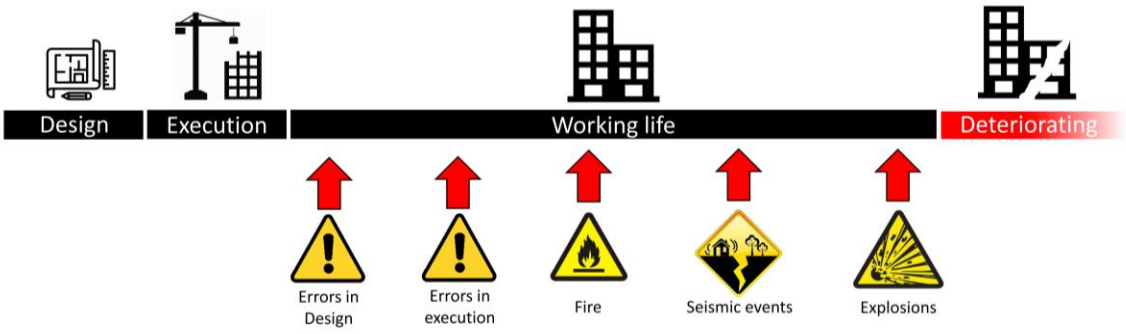

Figure 1.1 *Different events introducing local or global damage to structures.*

Structures that experienced, or are vulnerable to, damage arising from different events can be either demolished or repaired. Demolition, however, might be prohibited either to economic, religious, or historical considerations. The cost of retrofitting a mildly deteriorated building would be, in most cases, less than the cost of demolition and reconstruction. Also, structures of religious value (e.g., Kaaba in Mecca, Saudi Arabia) are sensitive to the idea of demolition and rebuilding. Structures that are considered part of the architectural heritage (e.g., Mada'in Salih, Taj Mahal, or Colosseum) hold the historical value within its old shape and materials and hence destroying these materials strips its very own value (see Fig. 1.2).

(a) **(b)** **(c)**

Figure 1.2 *(a) Mada'in Salih in Hegra, Saudi Arabia [courtesy: S. Six via Wikimedia Commons], (b) Taj Mahal in Agra, India [courtesy: G. Eichmann via Wikimedia Commons], and (c) Colosseum in Rome, Italy [courtesy: D. ILIFF via Wikimedia Commons.*

Retrofit is a preventive action to upgrade a structure to meet certain functions or requirements e.g., upgrading residential buildings to a commercial or industrial use, upgrading old buildings to conform to new or amended building codes, or upgrading vulnerable structures in seismic regions to account for expected future events. On the other hand, repair is a remedial action to restore the function of a partially damaged structure that might be caused by different events.

1.1.2 Composite-based strengthening systems

Different systems have been used in the retrofit industry including section enlargement, steel plate bonding, welded steel meshes, or external post-tensioning [3]. However, the use of composite-based strengthening systems received much of the research community attention due to the promising advantages associated with the use of these systems, noticeably the high strength-to-weight ratio and corrosion resistance. These composite-based systems can be broadly categorised into two main categories based on the nature of the matrix used to impregnate the reinforcement (see Fig. 1.3):

- Organic-based strengthening composites. In these systems, the textiles are impregnated in matrices of organic nature typically epoxy. Different acronyms are used to refer to these systems based on the type of the textiles utilised in the system including Fibre Reinforced Polymers (FRP) and Steel Reinforced Polymers (SRP).

- Inorganic-based strengthening composites which utilise matrices of inorganic nature typically mortar or grout. Several exchangeable terms are used to refer to these systems e.g., Fabric Reinforced Cementitious Matrices (FRCM), Textile Reinforced Mortar (TRM), Fabric Reinforced Composites (FRC), Mineral Based Composites (MBC), and Steel Reinforced Gout (SRG).

It is worth noting that theses system should not be confused with Textile Reinforced Concrete (TRC) which refers to new industrial products e.g., thin shells, cladding panels, and façade systems [3].

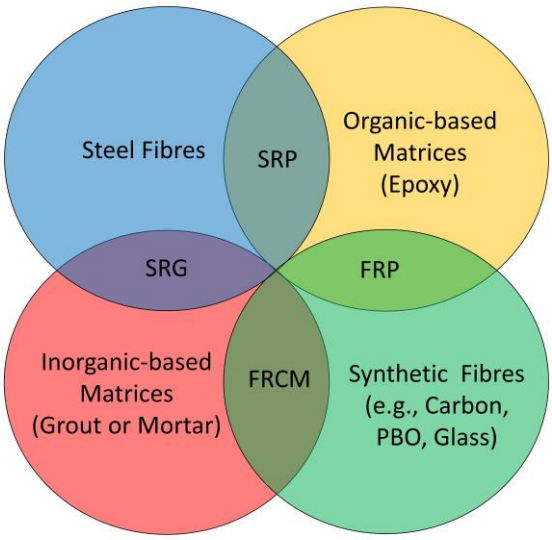

Figure 1.3 *Different composite-based strengthening composites.*

Although the so-called FRP system has shown many advantages in different strengthening applications, however this system has shown several drawbacks mainly associated with the use of the organic matrix including poor fire performance as epoxy degradation occurs at temperatures close to or above the matrix glass transition temperature [2, 4], poor compatibility with concrete and masonry substrates [5, 6], high labour and material cost, unfamiliarity with their mechanical behaviour [7], and potential hazards for the workers [8].

As many of these disadvantages were associated with the use of the organic-based matrix, the idea of replacing this matrix with an inorganic-based one (typically grout or mortar) was introduced in the scientific community. The use of grout or mortar in the FRCM systems was advantageous in terms of compatibility with the substrate, vapor permeability, improved fire performance, durability against detrimental agents, protecting the embedded textiles from UV ray exposure, ease of application on uneven surface, safety for the operators, low cost and less time of installation, and ability to dissipate energy through developing multi cracking patterns under cyclic loads [1, 5, 9- 11].

The use of steel fibres in the inorganic-based composites (i.e., SRG system) has drawn a special attention due to the advantages that steel fibres have shown compared to other synthetic fibres including excellent mechanical characteristics, relatively lower cost, and the familiarity with their mechanical behaviour.

1.1.3 Steel Reinforced Grout (SRG) composites

SRG composites are typically made by impregnating steel textiles in a grout matrix. The textiles are made of High Tensile Strength Steel (HTSS) micro strands which were initially developed to be used as internal reinforcement for tyres in the automotive industry [9]. The HTSS strands or filaments are combined in

several arrangements to form cords e.g., three straight strands and two twisted around (3X2) or twelve straight strands and one twisted around (12X). The resulted cords of a twisted shape provide a better impregnation with the matrix as all strands are in contact with the grout (see Fig. 1.4(a)). These cords are arranged parallel to each other to form a unidirectional textile. To control the spacing between the cords, a bidirectional glass fabric is used such that the cords are spaced and mounted to that glass fabric by means of strong adhesives. The number of cords per unit length (often inches) will determine the density of the textile e.g., 4 or 8 cords/in (see Fig. 1.4(b)). Steel textiles are produced in different densities ranging from 4 to 23 cords/in.

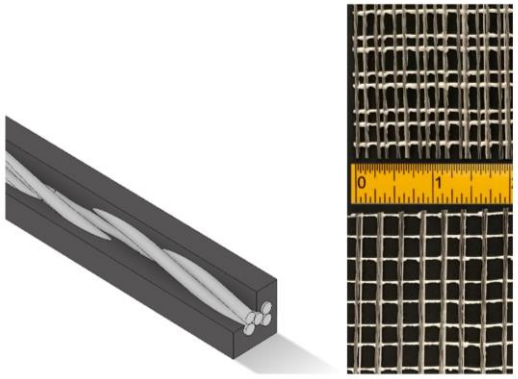

(a) ***(b)***

Figure 1.4 *Schematic of a 3X2 cord embedded in a grout matrix (a), steel fabrics of density 8 cord/in (b) and 4 cord/in (c).*

1.1.4 The flexural behaviour of RC beams strengthened with composites

The RC beams with external flexural strengthening systems have several interfaces that are prone to different modes of failure. Fig. 1.5 provides a schematic presentation of an RC beam strengthened with multi-layer strengthening system. Every direct contact between two different materials can be considered as a unique interface. The number of interfaces is a function in the number of the textile layers such that each textile layer will create two interfaces with the matrix in addition to the interface between the first layer of the matrix and the substrate. Almost all the interfaces in the RC beams strengthened with inorganic-based strengthening systems (e.g., FRCM or SRG) can be considered critical since they are prone to debonding or interlaminar shearing failures. On the contrary, FRP systems have only one critical interface i.e., the substrate-to-matrix interface. The failure at other interfaces (i.e., inside the composite) is prevented by the high shear strength of the organic matrix.

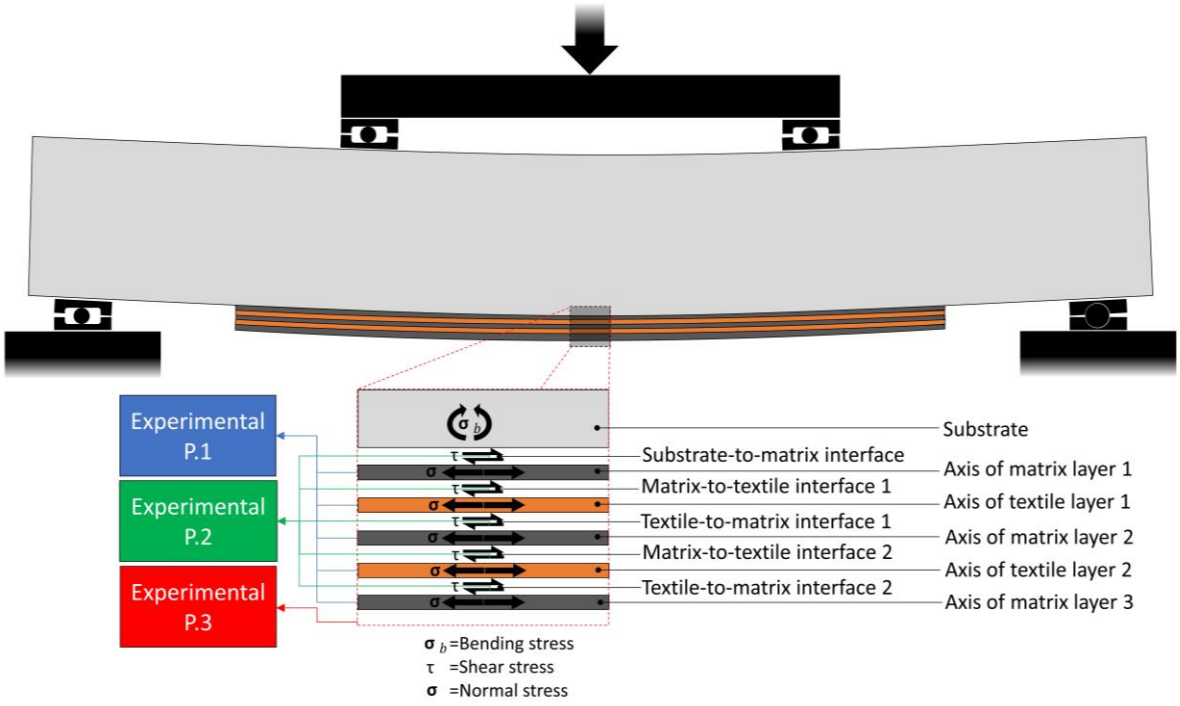

Figure 1.5 *Schematic presentation of the stress status at the midspan of an RC beam strengthened with a multilayer strengthening system.*

The bending stress in a strengthened RC beam will develop tensile stresses in the internal reinforcement (rebars), the substrate, the external reinforcement (textiles), and the matrix. All these materials are straining at different rates and hence this stain incompatibility will generate shear stresses at the interfaces between different materials (see Fig. 1.5). To comprehend the flexural behaviour of a strengthened RC beam, two topics must be understood first:

- The tensile behaviour of the composite and its constituent materials.
- the bond behaviour between the composite and the substrate.

The tensile behaviour of the strengthening composite largely affects the flexural response of the strengthened beam since the stresses in the composite is partly transferred as tensile stresses in the textile and the matrix as established earlier. The tensile behaviour of the inorganic-based composites can be investigated by conducting mechanical characterisation tests on the bare textiles and the coupons of the textiles impregnated in the matrix. These tensile tests provide a better understanding of the mechanical properties of the constituent materials including the ultimate tensile strength and strain of the textiles, the mode of failure, the crack patterns in the composite, and the tension stiffening effect of the grout. Several experiments were carried out to study the tensile behaviour of the FRCM [1-20] and SRG [4,6, 19, 21-27] composites.

The other crucial component to the flexural response of a strengthened beam is the shear bond behaviour. In fact, the first link in the stress transfer mechanism is the substrate-to-matrix interface where the stresses are transferred to the composite as interfacial shear stresses. Furthermore, stresses are dissipated within the composite by means of shear stresses between the textiles and the matrix. Shear bond tests are conducted to derive key information on the bond performance including the relative slip between the composite and the substrate, the stress-slip response, the strain at debonding, the mode of failure, and the crack patterns. The shear bond behaviour was investigated in several studies for FRCM [1, 9, 13, 28-38], SRG [26, 29, 30, 39-47], and FRP [48-52] systems.

Once a sufficient understanding of the tensile and the bond behaviour of the strengthening composite is established, the flexural behaviour of the RC beams strengthened with these composites can be then investigated. The flexural performance of strengthened RC beams can be explored by performing bending tests which provide important design parameters e.g., the stress in the external reinforcement at the debonding of the composite which is crucial in the design for the Ultimate Limit State (ULS). Also, they provide information on the influence of the external strengthening system on the crack width in the strengthened beam which is often a design parameter for the Serviceability Limit State (SLS). Different experimental investigations were conducted to study the flexural behaviour of RC beams strengthened with SRG [53-55, 64, 67-74], FRCM [56-60, 62, 63, 71], and FRP [54, 55, 61, 63-66, 70, 73, 74]. The technical details of the above-mentioned studies will be provided in the literature review in Chapter 2.

In the present work, the experimental campaign was divided into three main programmes. The first experimental programme aims at understanding the tensile behaviour of the SRG composites comprising single and multiple layers of the steel textiles. The shear bond behaviour between the SRG composites and the concrete substrates will be investigated in the second experimental programme. Finally, the results obtained from the previous experimental programmes will be utilised to conduct the last experimental programme to explore the flexural behaviour of the RC beams externally strengthened with the SRG composites. Further discussion on these experimental programmes will be provided in the relevant sections.

1.2 Research significance and motivation

The research on the tensile, bond, and flexural behaviour of the RC beams strengthened with SRG composites can be considered important by considering the following aspects:

- General consideration, as any strengthening system derives its importance from the importance of the structure to be strengthened. These strengthening systems are tools to preserve structures of religious, historic, economic, and social values. They can also be of paramount importance when

it comes to the safety of human lives e.g., strengthening vulnerable residential building in seismic regions.

- Safety and economic considerations: the use of the grout in the SRG systems is less hazardous and relatively cheaper than the epoxy used as a matrix in the organic-based systems. Also, the use of the steel textiles in the SRG systems is considerably cheaper than other synthetic textiles e.g., carbon.

There is, also, a lack of knowledge on the tensile and bond behaviour of the inorganic-based composites, especially for the SRG composites. In particular, the behaviour of the composites comprising multiple layers of the textiles which is often required when strengthening large structural member. Also, the flexural behaviour of the RC beams strengthened with multiple layers of the FRCM composites is very limited, not to mention the SRG systems. Furthermore, much of the scientific contribution on the bond behaviour of the SRG systems is devoted to the masonry substrates as masonry buildings constitute more than 70 % of the buildings worldwide since masonry is the world oldest construction system [20]. The introduction of the reinforced concrete (RC) system is relatively recent, compared to the masonry system. This makes the masonry structures seem of more historical value than the RC structures. However, the vast number of existing RC structures today not to mention the high construction rate in concrete industry will make addressing the structural needs of RC structures inevitable at some point in the near future. Furthermore, some of the present-day RC structures will be of a historical value to future generations. A solid knowledge on the behaviour of different strengthening SRG systems applied to these structures needs to be established today.

1.3 Research aim and objectives

The aim of the research is to investigate and understand the flexural behaviour of RC beams strengthened with the SRG composites. This understanding will help in suggesting models that can provide key design parameters. However, understanding the flexural behaviour of RC beams strengthened with any composite system is crucially dependent on two aspects including:

- The tensile behaviour of the textile, the matrix, and the composite of the two.
- The bond behaviour between the textiles and the matrix and between the composite and the substrate.

For the sake of simplification, these two aspects will be considered as sub aims to the main aim of this work, such that:

- Sub aim 1: Investigating the tensile behaviour of the SRG composites to understand the influence of applying multiple layers of the steel textiles on the performance of the composite including the mode of failure, the crack patterns, and the contribution of the grout to the overall composite behaviour (i.e., tension stiffening effect).
- Sub aim 2: Investigating the bond behaviour between the SRG composites and the concrete substrates to understand the stress transfer mechanism in these systems. This investigation will help, also, in understanding different modes of failure that might take place in these composites.

These aims will be achieved through a set of objectives that can be broadly categorised into theoretical and experimental parts. The theoretical part includes two objectives including the literature review and the analytical modelling. On the other hand, the experimental part is divided into three main experimental programmes. Experimental programme 1 addresses the tensile behaviour of the SRG composites, while the bond and flexural behaviours are addressed in the experimental programmes 2 and 3, respectively. Fig. 1.6 provides a flowchart that depicts the sequence of these objectives. The following bullet points provide a brief description on each objective:

Objective 1. Literature Review: aims at exploring the current state of knowledge on the inorganic-based composites including FRCM and SRG composites in terms of tensile, bond, and flexural behaviour. This objective will help in understanding the current state of knowledge of the topic under investigations. Furthermore, it will help in designing the experimental programmes in terms of experimental parameters, specimens geometry, strengthening layout, and test setup.

Objective 2. Experimental programme 1: aims at investigating the tensile behaviour of the SRG composites by conducting direct tensile test on the constituent materials of the SRG system including the dry single steel cords, the dry steel textiles, and the composite of the steel textiles and the grout. This programme will help to get a better understanding of different aspects of the tensile behaviour of the SRG composites especially those comprising multiple layers of the steel textiles in terms of stress-strain response, mechanical interlock, crack patterns, mode of failure, and tension stiffening effect of the matrix.

Objective 3. Experimental programme 2: to get an insight into the bond behaviour between the SRG composites and the concrete substrate. Direct shear bond tests will be conducted on different SRG composites comprising different number of layers and different bond lengths applied to concrete substrate that have different strengths. The purpose of the experimental programme

is to evaluate the influence of different parameters on the bond behaviour in terms of the stress-slip response and the mode of failure.

Objective 4. Experimental programme 3: the knowledge obtained on the tensile and bond behaviour in the previous experimental programmes will help in designing this programme which aims at investigating the flexural behaviour of RC beams strengthened with the SRG composites. Four-point bending tests will be conducted on full-scale beams strengthened with different SRG composites to evaluate the effectiveness of this systems in terms of the enhancement to the load-carrying capacity, the exploitation of the reinforcement in the SRG systems, and the stress and strain at the failure of the strengthening system.

Objective 5. Analytical modelling: reviews the existing bond models suggested for the FRP systems and evaluates its validity to the SRG system. The process of validation and verification will be carried out on the data obtained from the three experimental programmes. Modifications to the existing models will be made, if necessary, to capture the behaviour of the SRG composites comprising multiple layers of the steel textiles. Based on the outputs of this objective, a model will be suggested to allow the designers to estimate the debonding load for the SRG systems which is a key parameter for the design of the strengthening system.

1.4 Research scope and limitations

The scope of this work concerns the externally Bonded (EB) inorganic-based strengthening systems that are mainly reinforced with steel textiles i.e., SRG composites. Although, the FRCM composites (reinforced with other synthetic fibres) often exhibit a relatively similar behaviour to that of the SRG system, however they are not considered in the experimental campaign, not to mention the FRP systems.

Different systems, apart from EB, are not considered in this work including Fibre Reinforced Concrete (FRC) which refers to new RC elements reinforced with short steel fibres and Inhibiting Repairing Strengthening (IRS) system where new reinforcement, typically carbon or glass rebars, is inserted into groves in the concrete cover of an existing RC member for the purpose of strengthening.

In particular, this research addresses the flexural behaviour of the RC beams and the aspects that are necessary to understand that subject, namely the tensile behaviour of the SRG composite and the bond behaviour between the composite and the concrete substrate. Masonry substrates are not covered in the experimental part of this research since it was mainly designed to investigate the flexural behaviour of the RC beams. Apart from the flexural strengthening of beams, there are other structural members that might require strengthening including beams (for shear), confinement of columns and joints, out-of-plane and in-

plane strengthening of walls and strengthening of slabs. However, this work is only limited to the flexural strengthening of beams.

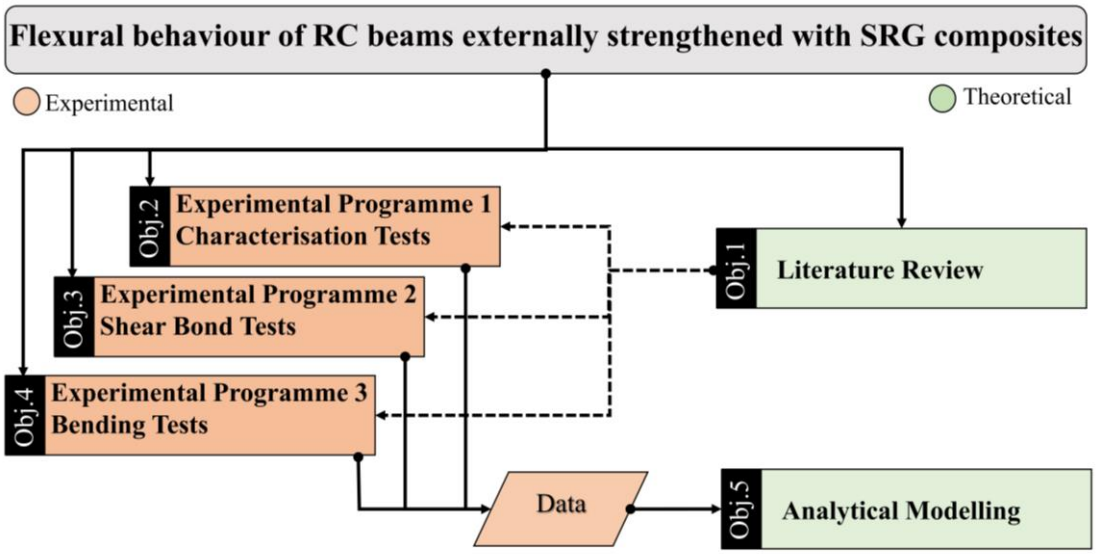

Figure 1.6 *Flowchart of the objectives of the research.*

In fact, addressing the behaviour of different strengthening systems for different structural members is far too difficult to be comprehend within a single work. Not to mention the limitations on the current work including the constraints on time, fund, and technical issues related to the use of the laboratories in terms of space and availability of technical support. Nonetheless, much effort has been made to conduct a solid and valid work that can meet the standards of the scientific community and the current constraints.

1.5 Research contribution

This work will fill the gap in the current literature and provide a better understanding of different aspects related to the use of the SRG system to strengthen RC beams including:

- The mechanical properties of the SRG composites, in particular, the behaviour of the multi-layers SRG composites which has not been investigated to date.
- The bond performance between the SRG composites and the concrete substrates in terms of stress-slip response and the mode of failure especially when using SRG systems comprising multiple layers of the steel textile. The data on these latter systems is very limited in the available literature.
- The flexural behaviour of full-scale RC beams externally strengthened with the SRG composites and how can different combinations of these composites comprising different

steel textiles and different number of layers affect the load carrying capacity and the mode of failure.

Owing to the lack of the bond models that can predict the bond behaviour and the debonding load in the RC beams strengthened with the SRG systems, this present work provides an evaluation of the current bond models suggested for the FRP systems and assess their accuracy in predicting the debonding load in the SRG systems. Furthermore, this current work suggests a model to predict the debonding load in the SRG systems comprising steel textiles having different densities and different number of layers. The output of research will help in laying the first building blocks for future contributions on the flexural behaviour of the RC beams strengthened with the SRG systems that can be then employed in design guidelines for these systems.

1.6 Thesis layout

This thesis consists of seven chapters and eight appendices. Beside the introduction and the conclusions, there are three chapters comprising the three experimental programmes followed by a chapter presenting the analytical modelling part. A brief description of the content of each chapter is provided in the following bullet points:

- Chapter 1: introduction to the thesis including a background to the topic under investigation, research significance and motivation, aim and objectives, scope and limitations, contribution, thesis layout, and publication outputs.
- Chapter 2: an up-to-date literature review on the mechanical characterisations and the tensile behaviour of the inorganic-based composites, the bond behaviour between these composites and different substrates, and finally the flexural behaviour of RC beams strengthened with these systems.
- Chapter 3: the experimental programme conducted on the materials of the SRG composites including dry single steel cords, dry steel textile, and SRG composite coupons to derive their mechanical properties and to gain a better undertraining of the tensile behaviour of the SRG composites.
- Chapter 4: the experimental programme comprising shear bond tests to investigate the bond behaviour between the SRG composites and the concrete substrate.
- Chapter 5: the experimental programme performed on the full-scale RC beams strengthened with multiple layers of the SRG composites to evaluate their flexural behaviour.

- Chapter 6: the analytical modelling consisting of the process of the validation and verification of the data obtained from the outputs of the experimental programmes.
- Chapter 7: conclusions made on the previous experimental programmes and design recommendations based on the analytical modelling.
- Appendix A: a joint conference paper with Roma Tre University. This paper was titled "Mechanical characterization of multi-ply steel reinforced grout composites for the strengthening of concrete structures" submitted to CICE conference held in Paris, France 2018.
- Appendix B: a conference paper titled "Tensile behaviour of multi-ply steel-reinforced grout (SRG) composites" submitted to COMPDYN conference held in Crete, Greece 2019.
- Appendix C: a conference paper titled "Bond behaviour of multi-layer steel reinforced grout (SRG) strengthening systems to concrete" submitted to ACIC conference held in Birmingham, UK 2019.
- Appendix D: a joint conference paper with Roma Tre University. This paper was titled "Shear bond behaviour of multi-ply steel reinforced grout composites for the strengthening of concrete structures" submitted to SECED conference held in London, UK 2019.
- Appendix E: an abstract and presentation titled "Flexural Strengthening of RC Beams with SRG" at 74th RILEM Annual Week & 40th Cement and Concrete Science Conference held in Sheffield, UK (online) 2020.
- Appendix F: a joint journal article with Roma Tre University. This article was titled "Bond Behaviour of Multi-Ply Steel Reinforced Grout Composites" published in Construction and building materials journal 2020.
- Appendix G: a database of existing bond models for FRP systems.
- Appendix H: manufacturers' datasheets for the materials used in the experimental programmes including the steel textiles and the cement.

1.7 Publication outputs

A total of nine publication outputs will be produced from this work including four journal articles and five conferences contributions. Three journal articles comprising the three experimental programmes are provided in chapters 1, 2, and 3. The fourth journal article, provided in the appendices, is an output of a collaboration with a research team from Roma Tre University, Italy. All the five conference contributions are provided in the appendices. The key information about these outputs is provided in Table 1.1.

Table 1.1.1 *Key information about the publication outputs*

Title	Authors	Journal/Conference	Status	Notes
Mechanical characterization of multi-ply steel reinforced grout composites for the strengthening of concrete structures	Georgia Thermou Gianmarco de Felice Stefano De Santis Sultan Alotaibi Francesca Roscini Iman Hajirasouliha Maurizio Guadagnini	9th International Conference on Fibre-Reinforced Polymer (FRP) Composites in Civil Engineering (CICE) July 17 - 19, 2018 Paris, France	Published	Appendix A
Tensile behaviour of multi-ply steel-reinforced grout (SRG) composites	Sultan Alotaibi Georgia Thermou Iman Hajirasouliha Maurizio Guadagnini	7th ECCOMAS Thematic Conference on Computational Methods in Structural Dynamics and Earthquake Engineering (COMPDYN) June 24 – 26, 2019 Crete, Greece	Published	Appendix B
Bond behaviour of multi-layer steel reinforced grout (SRG) strengthening systems to concrete	Sultan Alotaibi Georgia Thermou Iman Hajirasouliha Maurizio Guadagnini	9th Advanced Composites in Construction (ACIC) September 3 - 5, 2019 Birmingham, UK	Published	Appendix C
Shear bond behaviour of multi-ply steel reinforced grout composites for the strengthening of concrete structures	Georgia Thermou Gianmarco de Felice Stefano De Santis Sultan Alotaibi Francesca Roscini Iman Hajirasouliha Maurizio Guadagnini	SECED Conference on Earthquake and Civil Engineering Dynamics September 9 - 10, 2019 London, UK	Published	Appendix D
Flexural Strengthening of RC Beams with SRG	Sultan Alotaibi Georgia Thermou Iman Hajirasouliha Maurizio Guadagnini	74th RILEM Annual Week & 40th Cement and Concrete Science Conference September 1 – 4, 2020 Sheffield, UK (online)	Abstract & presentation	Appendix E
Bond Behaviour of Multi-Ply Steel Reinforced Grout Composites	Georgia Thermou Gianmarco de Felice Stefano De Santis Sultan Alotaibi Francesca Roscini Iman Hajirasouliha Maurizio Guadagnini	Construction and building materials	Published	Appendix F
Mechanical characterisation of multi-layers SRG composites	Sultan Alotaibi Georgia Thermou Maurizio Guadagnini Iman Hajirasouliha	Construction and building materials	Draft is ready	Chapter 3
Bond behaviour of RC substrates strengthened with multi-layers SRG systems	Sultan Alotaibi Georgia Thermou Maurizio Guadagnini Iman Hajirasouliha	Construction and building materials	Draft is ready	Chapter 4
Flexural behaviour of RC beams strengthened with SRG system	Sultan Alotaibi Georgia Thermou Maurizio Guadagnini Iman Hajirasouliha	Construction and building materials	Draft is ready	Chapter 5

References

[1] A. Bilotta, F. Ceroni, E. Nigro and M. Pecce, "Experimental tests on FRCM strengthening systems for tuff masonry elements", *Construction and Building Materials*, vol. 138, pp. 114-133, 2017.

[2] T. D'Antino and C. Papanicolaou, "Comparison between different tensile test set-ups for the mechanical characterization of inorganic-matrix composites", *Construction and Building Materials*, vol. 171, pp. 140-151, 2018.

[3] J. Donnini, V. Corinaldesi and A. Nanni, "Mechanical properties of FRCM using carbon fabrics with different coating treatments", *Composites Part B: Engineering*, vol. 88, pp. 220-228, 2016.

[4] C. Pellegrino and T. D'Antino, "Experimental behaviour of existing precast prestressed reinforced concrete elements strengthened with cementitious composites", *Composites Part B: Engineering*, vol. 55, pp. 31-40, 2013.

[5] T. D'Antino, A. Calabrese and C. Poggi, "Experimental procedures for the mechanical characterization of composite reinforced mortar (CRM) systems for retrofitting of masonry structures", *Materials and Structures*, vol. 53, no. 4, 2020.

[6] R. Contamine, A. Si Larbi and P. Hamelin, "Contribution to direct tensile testing of textile reinforced concrete (TRC) composites", Materials Science and Engineering: A, vol. 528, no. 29-30, pp. 8589-8598, 2011.

[7] M. Leone et al., "Glass fabric reinforced cementitious matrix: Tensile properties and bond performance on masonry substrate", *Composites Part B: Engineering*, vol. 127, pp. 196-214, 2017.

[8] U. Ebead, K. Shrestha, M. Afzal, A. El Refai and A. Nanni, "Effectiveness of Fabric-Reinforced Cementitious Matrix in Strengthening Reinforced Concrete Beams", Journal of Composites for Construction, vol. 21, no. 2, p. 04016084, 2017.

[9] J. Donnini and V. Corinaldesi, "Mechanical characterization of different FRCM systems for structural reinforcement", *Construction and Building Materials*, vol. 145, pp. 565-575, 2017.

[10] L. Mercedes, L. Gil and E. Bernat-Maso, "Mechanical performance of vegetal fabric reinforced cementitious matrix (FRCM) composites", *Construction and Building Materials*, vol. 175, pp. 161-173, 2018.

[11] F. Carozzi et al., "Experimental investigation of tensile and bond properties of Carbon-FRCM composites for strengthening masonry elements", Composites Part B: Engineering, vol. 128, pp. 100-119, 2017.

[12] A. Younis, U. Ebead and K. Shrestha, "Tensile characterization of multi-ply fabric-reinforced cementitious matrix strengthening systems", *Structural Concrete*, vol. 21, no. 2, pp. 713-723, 2019.

[13] S. De Santis, F. Carozzi, G. de Felice and C. Poggi, "Test methods for Textile Reinforced Mortar systems", *Composites Part B: Engineering*, vol. 127, pp. 121-132, 2017.

[14] D. Arboleda, F. Carozzi, A. Nanni and C. Poggi, "Testing Procedures for the Uniaxial Tensile Characterization of Fabric-Reinforced Cementitious Matrix Composites", *Journal of Composites for Construction*, vol. 20, no. 3, p. 04015063, 2016. Available: 10.1061/(asce)cc.1943-5614.0000626.

[15] I. Colombo, A. Magri, G. Zani, M. Colombo and M. di Prisco, "Textile Reinforced Concrete: experimental investigation on design parameters", *Materials and Structures*, vol. 46, no. 11, pp. 1933-1951, 2013.

[16] A. Bilotta, F. Ceroni, G. Lignola and A. Prota, "Use of DIC technique for investigating the behaviour of FRCM materials for strengthening masonry elements", *Composites Part B: Engineering*, vol. 129, pp. 251-270, 2017.

[17] F. Roscini, S. De Santis and G. de Felice, "Experimental investigation on the mechanical behaviour of mortar-based strengthening systems", in *SAHC'16 - 10th International Conference on Structural Analysis of Historic Constructions*, Leuven, Belgium, 2016.

[18] C. Caggegi et al., "Experimental analysis on tensile and bond properties of PBO and aramid fabric reinforced cementitious matrix for strengthening masonry structures", Composites Part B: Engineering, vol. 127, pp. 175-195, 2017

[19] T. D'Antino and C. Papanicolaou, "Mechanical characterization of textile reinforced inorganic-matrix composites", *Composites Part B: Engineering*, vol. 127, pp. 78-91, 2017.

[20] S. De Santis and G. de Felice, "Tensile behaviour of mortar-based composites for externally bonded reinforcement systems", *Composites Part B: Engineering*, vol. 68, pp. 401-413, 2015.

[21] T. D'Antino and C. Papanicolaou, "Comparison between different tensile test set-ups for the mechanical characterization of inorganic-matrix composites", *Construction and Building Materials*, vol. 171, pp. 140-151, 2018.

[22] A. Bilotta, F. Ceroni, E. Nigro and M. Pecce, "Experimental tests on FRCM strengthening systems for tuff masonry elements", *Construction and Building Materials*, vol. 138, pp. 114-133, 2017.

[23] G. Thermou et al., "Mechanical characterization of multi-ply steel reinforced grout composites for the strengthening of concrete structures", in *CICE 2018. 9th International Conference on Fibre-Reinforced Polymer (FRP) Composites in Civil Engineering*, Paris, France, 2021.

[24] S. Mazzuca, H. Hadad, L. Ombres and A. Nanni, "Mechanical Characterization of Steel-Reinforced Grout for Strengthening of Existing Masonry and Concrete Structures", *Journal of Materials in Civil Engineering*, vol. 31, no. 5, p. 04019037, 2019.

[25] B. Ghiassi, D. Oliveira, V. Marques, E. Soares and H. Maljaee, "Multi-level characterization of steel reinforced mortars for strengthening of masonry structures", *Materials & Design*, vol. 110, pp. 903-913, 2016.

[26] S. De Santis et al., "Round Robin Test on tensile and bond behaviour of Steel Reinforced Grout systems", *Composites Part B: Engineering*, vol. 127, pp. 100-120, 2017.

[27] S. De Santis and G. de Felice, "Steel reinforced grout systems for the strengthening of masonry structures", *Composite Structures*, vol. 134, pp. 533-548, 2015.

[28] V. Alecci, M. De Stefano, R. Luciano, L. Rovero and G. Stipo, "Experimental Investigation on Bond Behavior of Cement-Matrix–Based Composites for Strengthening of Masonry Structures", *Journal of Composites for Construction*, vol. 20, no. 1, p. 04015041, 2016.

[29] G. de Felice et al., "Mortar-based systems for externally bonded strengthening of masonry", *Materials and Structures*, vol. 47, no. 12, pp. 2021-2037, 2014.

[30] L. Ascione, G. de Felice and S. De Santis, "A qualification method for externally bonded Fibre Reinforced Cementitious Matrix (FRCM) strengthening systems", *Composites Part B: Engineering*, vol. 78, pp. 497-506, 2015.

[31] F. Carozzi, G. Milani and C. Poggi, "Mechanical properties and numerical modeling of Fabric Reinforced Cementitious Matrix (FRCM) systems for strengthening of masonry structures", *Composite Structures*, vol. 107, pp. 711-725, 2014.

[32] S. Sueki, C. Soranakom, B. Mobasher and A. Peled, "Pullout-Slip Response of Fabrics Embedded in a Cement Paste Matrix", *Journal of Materials in Civil Engineering*, vol. 19, no. 9, pp. 718-727, 2007.

[33] L. Sneed, T. D'Antino, C. Carloni and C. Pellegrino, "A comparison of the bond behavior of PBO-FRCM composites determined by double-lap and single-lap shear tests", *Cement and Concrete Composites*, vol. 64, pp. 37-48, 2015.

[34] O. Awani, A. Refai and T. El-Maaddawy, "Bond characteristics of carbon fabric-reinforced cementitious matrix in double shear tests", *Construction and Building Materials*, vol. 101, pp. 39-49, 2015.

[35] T. D'Antino, L. Sneed, C. Carloni and C. Pellegrino, "Influence of the substrate characteristics on the bond behavior of PBO FRCM-concrete joints", *Construction and Building Materials*, vol. 101, pp. 838-850, 2015.

[36] C. Caggegi, D. Sciuto and M. Cuomo, "Experimental study on effective bond length of basalt textile reinforced mortar strengthening system: Contributions of digital image correlation", *Measurement*, vol. 129, pp. 119-127, 2018.

[37] F. Carozzi and C. Poggi, "Mechanical properties and debonding strength of Fabric Reinforced Cementitious Matrix (FRCM) systems for masonry strengthening", *Composites Part B: Engineering*, vol. 70, pp. 215-230, 2015.

[38] A. Younis and U. Ebead, "Bond characteristics of different FRCM systems", *Construction and Building Materials*, vol. 175, pp. 610-620, 2018.

[39] M. Matana, A. Nanni, L. Dharani, P. Silva and G. Tunis, "BOND PERFORMANCE OF STEEL REINFORCED POLYMER AND STEEL REINFORCED GROUT", in *Proceedings of International Symposium on Bond Behaviour of FRP in Structures (BBFS 2005)*, Hong Kong, China, 2005.

[40] M. Santandrea, F. Focacci, C. Mazzotti, F. Ubertini and C. Carloni, "Determination of the interfacial cohesive material law for SRG composites bonded to a masonry substrate", *Engineering Failure Analysis*, vol. 111, p. 104322, 2020.

[41] F. Bencardino, A. Condello and A. Ashour, "Single-lap shear bond tests on Steel Reinforced Geopolymeric Matrix-concrete joints", *Composites Part B: Engineering*, vol. 110, pp. 62-71, 2017.

[42] F. Ascione, M. Lamberti, A. Napoli and R. Realfonzo, "Experimental bond behavior of Steel Reinforced Grout systems for strengthening concrete elements", *Construction and Building Materials*, vol. 232, p. 117105, 2020.

[43] A. Razavizadeh, B. Ghiassi and D. Oliveira, "Bond behavior of SRG-strengthened masonry units: Testing and numerical modeling", *Construction and Building Materials*, vol. 64, pp. 387-397, 2014.

[44] S. De Santis, "Bond behaviour of Steel Reinforced Grout for the extrados strengthening of masonry vaults", *Construction and Building Materials*, vol. 150, pp. 367-382, 2017.

[45] L. Carabba, M. Santandrea, C. Carloni, S. Manzi and M. Bignozzi, "Steel fiber reinforced geopolymer matrix (S-FRGM) composites applied to reinforced concrete structures for strengthening applications: A preliminary study", *Composites Part B: Engineering*, vol. 128, pp. 83-90, 2017.

[46] F. Ascione, M. Lamberti, A. Napoli, G. Razaqpur and R. Realfonzo, "An experimental investigation on the bond behavior of steel reinforced polymers on concrete substrate", *Composite Structures*, vol. 181, pp. 58-72, 2017.

[47] F. Bencardino, M. Nisticò and S. Verre, "Experimental Investigation and Numerical Analysis of Bond Behavior in SRG-Strengthened Masonry Prisms Using UHTSS and Stainless-Steel Fibers", *Fibers*, vol. 8, no. 2, p. 8, 2020.

[48] R. Perera, A. Recuero, A. Diego and C. López, "Adherence analysis of fiber-reinforced polymer strengthened RC beams", *Computers & Structures*, vol. 82, no. 23-26, pp. 1865-1873, 2004.

[49] M. Valluzzi et al., "Round Robin Test for composite-to-brick shear bond characterization", *Materials and Structures*, vol. 45, no. 12, pp. 1761-1791, 2012.

[50] A. Serbescu, M. Guadagnini and K. Pilakoutas, "Standardised double-shear test for determining bond of FRP to concrete and corresponding model development", *Composites Part B: Engineering*, vol. 55, pp. 277-297, 2013.

[51] J. Chen, Z. Yang and G. Holt, "FRP or steel plate-to-concrete bonded joints: Effect of test methods on experimental bond strength", *Steel and Composite Structures*, vol. 1, no. 2, pp. 231-244, 2001.

[52] X. Zou and L. Sneed, "Bond Behavior Between Steel Fiber Reinforced Polymer (SRP) and Concrete", *International Journal of Concrete Structures and Materials*, vol. 14, no. 1, 2020.

[53] L. Sneed, S. Verre, C. Carloni and L. Ombres, "Flexural behavior of RC beams strengthened with steel-FRCM composite", *Engineering Structures*, vol. 127, pp. 686-699, 2016.

[54] A. Napoli and R. Realfonzo, "Reinforced concrete beams strengthened with SRP/SRG systems: Experimental investigation", *Construction and Building Materials*, vol. 93, pp. 654-677, 2015.

[55] X. Huang, V. Birman, A. Nanni and G. Tunis, "Properties and potential for application of steel reinforced polymer and steel reinforced grout composites", *Composites Part B: Engineering*, vol. 36, no. 1, pp. 73-82, 2005.

[56] S. Babaeidarabad, G. Loreto and A. Nanni, "Flexural Strengthening of RC Beams with an Externally Bonded Fabric-Reinforced Cementitious Matrix", *Journal of Composites for Construction*, vol. 18, no. 5, p. 04014009, 2014.

[57] A. Jabr, A. El-Ragaby and F. Ghrib, "Effect of the Fiber Type and Axial Stiffness of FRCM on the Flexural Strengthening of RC Beams", *Fibers*, vol. 5, no. 1, p. 2, 2017.

[58] L. Ombres, "Flexural analysis of reinforced concrete beams strengthened with a cement based high strength composite material", *Composite Structures*, vol. 94, no. 1, pp. 143-155, 2011.

[59] A. D'Ambrisi and F. Focacci, "Flexural Strengthening of RC Beams with Cement-Based Composites", *Journal of Composites for Construction*, vol. 15, no. 5, pp. 707-720, 2011.

[60] H. Elsanadedy, T. Almusallam, S. Alsayed and Y. Al-Salloum, "Flexural strengthening of RC beams using textile reinforced mortar – Experimental and numerical study", *Composite Structures*, vol. 97, pp. 40-55, 2013.

[61] A. Lopez, N. Galati, T. Alkhrdaji and A. Nanni, "Strengthening of a reinforced concrete bridge with externally bonded steel reinforced polymer (SRP)", *Composites Part B: Engineering*, vol. 38, no. 4, pp. 429-436, 2007.

[62] L. Ombres, "Debonding analysis of reinforced concrete beams strengthened with fibre reinforced cementitious mortar", *Engineering Fracture Mechanics*, vol. 81, pp. 94-109, 2012.

[63] S. Raoof, L. Koutas and D. Bournas, "Textile-reinforced mortar (TRM) versus fibre-reinforced polymers (FRP) in flexural strengthening of RC beams", *Construction and Building Materials*, vol. 151, pp. 279-291, 2017.

[64] F. Bencardino and A. Condello, "Structural behaviour of RC beams externally strengthened in flexure with SRG and SRP systems", *International Journal of Structural Engineering*, vol. 5, no. 4, p. 346, 2014.

[65] G. Mitolidis, T. Salonikios and A. Kappos, "Tests on RC Beams Strengthened at the Span with Externally Bonded Polymers Reinforced with Carbon or Steel Fibers", *Journal of Composites for Construction*, vol. 16, no. 5, pp. 551-562, 2012.

[66] A. Prota, K. Tan, A. Nanni, M. Pecce and G. Manfredi, "Performance of shallow reinforced concrete beams with externally bonded steel-reinforced polymer", *CI Structural Journal*, vol. 103, pp. 163-170, 2006.

[67] F. Bencardino and A. Condello, "Eco-friendly external strengthening system for existing reinforced concrete beams", *Composites Part B: Engineering*, vol. 93, pp. 163-173, 2016.

[68] L. Ombres and S. Verre, "Flexural Strengthening of RC Beams with Steel-Reinforced Grout: Experimental and Numerical Investigation", *Journal of Composites for Construction*, vol. 23, no. 5, p. 04019035, 2019.

[69] C. Papakonstantinou and K. Katakalos, "Flexural behavior of reinforced concrete beams strengthened with a hybrid inorganic matrix - steel fiber retrofit system", *Structural Engineering and Mechanics*, vol. 31, no. 5, pp. 567-585, 2009.

[70] A. Balsamo, F. Nardone, I. Iovinella, F. Ceroni and M. Pecce, "Flexural strengthening of concrete beams with EB-FRP, SRP and SRCM: Experimental investigation", *Composites Part B: Engineering*, vol. 46, pp. 91-101, 2013.

[71] C. Menna et al., "Use of geopolymers for composite external reinforcement of RC members", *Composites Part B: Engineering*, vol. 45, no. 1, pp. 1667-1676, 2013.

[72] P. Larrinaga, L. Garmendia, I. Piñero and J. San-José, "Flexural strengthening of low-grade reinforced concrete beams with compatible composite material: Steel Reinforced Grout (SRG)", *Construction and Building Materials*, vol. 235, p. 117790, 2020.

[73] E. Wobbe et al., "Flexural capacity of RC beams externally bonded with SRP and SRG", in *International SAMPE Technical Conference*, Long Beach, USA, 2004, pp. 3009-3016.

[74] A. Prota, G. Manfredi, A. Nanni, E. Cosenza and M. Pecce, "Flexural strengthening of RC beams using emerging materials: Ultimate behavior", in *Proceedings of 2nd International Conference on FRP Composites in Civil Engineering (CICE 2004)*, Adelaide, Australia, 2004, pp. 163–170.

Chapter 2 Literature Review

This chapter provides a technical literature review on different aspects of the flexural behaviour of the inorganic-based strengthening composites i.e., FRCM and SRG systems. It is divided into five sections such that the first section reviews the tensile behaviour of these composites, while the bond behaviour is presented in the second section. The third section reviews the available studies on the flexural behaviour of the strengthened RC beams. Finally, the bond models that were suggested to predict key design parameters for these systems are presented in the last section. Owing to the similarities between organic-based and inorganic-based systems, the FRP system might be referred to in this chapter mainly for comparison purposes.

2.1 Tensile behaviour of inorganic-based systems

2.1.1 The materials

Tensile tests were conducted on coupons comprising different materials including carbon [1-6], glass [1, 6-10], E glass [11], Alkali-Resistant (AR) glass [5, 9, 11, 12], basalt [1, 4, 10, 11], steel [1, 8, 10, 13-17], aramid [11, 18], Polyparaphenylene benzobisoxazole (PBO) [2, 4, 6, 18], vegetal fibres [19]. The coupons strengthened with PBO FRCM were reported to develop an axial stiffness half of that reported for carbon for the same amount of reinforcement [2]. Furthermore, the use of carbon-FRCM enabled the composite to carry higher tensile loads and hence the composite developed denser crack pattern compared to glass-FRCM [5]. The use of steel textiles developed a better stress transfer within the matrix evident by the widespread crack pattern along the length of the coupon [8]. Polymer coating of the textile was investigated in several studies on carbon [4, 24, 25], basalt [4, 25], glass [25], and vegetal fibres [19] textiles. It was reported to improve the adhesion between the textile and the matrix and prevent slippage [4, 19]. The ability of polymer coating to prevent the telescopic failure of yarns (i.e., relative slippage between the core and sleeve filaments) is solely dependent on the ability of polymers to penetrate to the core filaments and that depends on viscosity of the polymers [19]. Furthermore, zinc coating was reported to improve the durability of the steel cords as it preventing corrosion resulting when subjected to salt attack [16].

Different matrices were investigated including cement-based mortar [e.g., 1, 4, 7], lime-based mortar [e.g., 14-17, 20], and mineral-based mortar [14, 17]. The lime-based mortar is generally of low strength and high vapor permeability which makes it ideal for the purpose of strengthening old masonry structures requiring less load upgrade and high vapor permeability as the moisture trapped within the substrate might cause damage to the masonry structure. On the other hand, the cement-based matrices are usually used the RC elements requiring high load upgrade and improved bond performance [4, 14, 15]. Cement-based matrices, compared to lime-based, were reported to provide an improved mechanical performance of the composite in terms of increasing the ultimate strength and altering the failure mode from the slippage of textile within the matrix to the rupture of the textile i.e.,

full exploitation of the textile [4]. Also, the high stiffness of the cement-based matrices will generally develop a larger carack saturation spacing and a higher stiffness of the composite in the first phases of the stress-strain response [17].

2.1.2 The geometry of the coupons

The shape of the tested coupons was also investigated in several studies. Two parameters play a significant role in determining the shape of the coupon including the ease of manufacturing and the sensitivity of ends to the gripping mechanism [11]. By examining the literature, coupons for the direct tensile tests were manufactured in four shapes including rectangular coupons [1, 4-18, 20], dumbbell coupons [1, 11], Bone-shape coupons [21], and V-notched coupons [22]. Rectangular and dumbbell coupons were reported to produce different tensile results due to the sensitivity of the clamping method [1].

Also, the geometry of the coupons was investigated by testing different lengths, widths, and thicknesses of the coupons. The investigated lengths found in the literature include 260 mm [3], 400 mm [3, 12, 18, 19], 410 mm [5, 6], 500 mm [3, 16, 18, 20], 510 mm [14, 18], 545 mm [3], 590 mm [18], 595 mm [3], 600 mm [3, 10, 13, 18], 650 mm [3]. Different widths were also examined including 40 mm [3], 45 mm [18], 50 mm [3, 5, 6, 13, 14, 16, 18, 19, 20], 54 mm [3], 70 mm [12], 75 mm [18], 90 mm [3], 96 mm [3], 100 mm [10, 18], 108 mm [3], 115 mm [3, 18]. Finally, the thickness of the coupon was investigated in few studies including 5 mm [5, 11], 6 mm [3,9,12], 9 mm [3, 9], 10 mm [2, 3, 6, 8-11, 16, 18, 19, 20], 12 mm [3, 9, 13], 14 mm [3, 9], 30 mm [9].

2.1.3 The number of layers

The tensile behaviour of coupons made of multiple layers of the FRCM systems was investigated for two [4-6, 11, 12] three [4, 5, 11], and four [5] layers of reinforcement. The tensile behaviour of coupons comprising overlap splice was also investigated [6, 12, 13]. The use of multiple layers was found to increase the ultimate tensile load and decrease the efficiency of the system [4]. However, this increase was found to be insignificant in [5] for two systems including carbon-FRCM and glass-FRCM. The alteration of failure mode was, also, observed when using multiple layers. Delamination was reported for FRCM comprising two and three layers of the textiles [4].

2.1.4 The test setup

The test setup largely influences the results of the direct tensile tests. Different aspects of the testing configuration were investigated including the gripping mechanism, the loading rate, and the instrumentation. Two gripping mechanisms were mainly utilised to grip the ends of the coupon in the testing machine including clevis articulation (AC 434[22]) [4-7,12-14, 17, 18] and clamping grips (hydraulics [18] or mechanical [6-8, 13, 15, 17, 18, 20]). The gripping system must serve two functions (1) preventing the relative slippage between the matrix and the gripping plates and that between the matrix and the embedded textiles and (2) preventing the crushing of the matrix in the gripping area [23]. The use of the clevis gripping mechanism is recommended for the strengthening applications

and on-site acceptance tests where the load-bearing capacity is to be investigated, while the clamping grip mechanism is preferred for the mechanical characterisation since it provides the right boundary conditions to study the trilinear stress-strain response [6]. For this latter mechanism, the jaws of the testing machine must provide a sufficient lateral force to prevent any slippage that might take place at the gripping area. To avoid crushing of the matrix that might arise from introducing excessive lateral pressure at the gripping area, different solutions were proposed including strengthening both ends of the coupon with FRP system [6, 10, 12, 13, 16, 17] or using sandwiching the ends of the coupon between two aluminium plates by means of strong adhesives [5, 15, 17, 20]. Strengthening the ends of the coupon with FRP system did not always prevent the formation of cracks near the gripping area, however this slightly affect the tensile behaviour [15]. Also, applying the gripping force to the dry textile extending from the composite at both ends was investigated [17]. In the clevis setup, the load is transferred to the coupon through shear stresses between the gripping tabs and the matrix and hence the contact length between the tabs and the coupon plays a significant role [4]. Different contact lengths were investigated in several studies including 50 mm [4], 55 mm [12], 60 mm [6], 90 mm [15, 17], 100 mm [4], 120 mm [13], 150 mm [4,5]. The optimal contact length between the tabs and the coupon in the clevis setup would depend on the tested FRCM system [4]. An optimal length of 150 mm was suggested in [4] for FRCM system comprising carbon and basalt textiles embedded in lime-based matrices.

In most cases, the tensile tests were performed in displacement-controlled rate. Different rates (mm/min) were examined including 0.10 [18], 0.25 [5, 6, 14, 18], 0.30 [6, 18, 20], 0.60 [13, 16, 17, 18], 1.00 [8, 10, 18], 1.20 [12, 15]. Reduction in strength and ductility was observed for low displacement rates since the behaviour of cement-based composites is dependent on the strain rate. Reducing the displacement rate was also found to influence the crack pattern (coarser pattern) and the stiffness of the composite [12]. Different instrumentations were utilised to obtain different properties including the strain of the textiles or the matrix and the crack pattern. Extensometers are generally used to obtain the strain of the composite. Extensometers with different gauge lengths were investigated including 50 mm [15], 100 mm [6, 14], 200 mm [15,18], 225 mm [18], 250 mm [16, 17, 18], 340 mm [18], 430 mm [18], 460 mm [11]. Digital Image Correlation (DIC) system was utilised in different studies to drive the stain in the textiles and the stain map of the composite [8, 10]. A large scatter in the tensile test results was observed with short gauge lengths [8]. Large gauge lengths will allow a sufficient number of cracks to be included in the measurement range and hence reducing the effect of crack distribution which is of a variable nature [23]. In general, there is a high variability in the tensile test results, and this can be attributed to geometrical imperfections in the matrix, misalignment of the textiles, and the location of the first crack with respect to the extensometer [14, 19]. Also, the In-plane and out-of-plane rotations can significantly affect the tensile behaviour of the coupons. This effect can be quantified by using two independent instrumentation systems at the back and the front of the tested coupon [1].

2.1.5 The stress-strain response

Direct tensile tests generally developed a trilinear stress-strain response characterising three distinct phases (see Fig. 2.1) including (1) uncracked section phase of high stiffness as both the matrix and the textile are resisting the applied load, and once the tensile strength of the matrix is reached, the first cracks form leading to (2) the second phase characterising a drop in the stiffness and the process of cracks formation and propagation. Finally (3) cracked section phase is introduced once cracks saturation is reached where the textile is almost the only component resisting the applied load and the stiffness of the composite in this stage is very similar to that developed by the bare textile [3, 8, 15, 16, 18, 20]. In the last stage, however, tension stiffening effect of the matrix will provide an enhancement to the textile as the chunks of the grout in the cracked section confining the cords/yarns will influence their behaviour in terms of axial stress and strain at failure. Tension stiffening effect largely depends on the matrix properties, the bond at the textile-to-matrix interface, and the layout of the textile [8, 20].

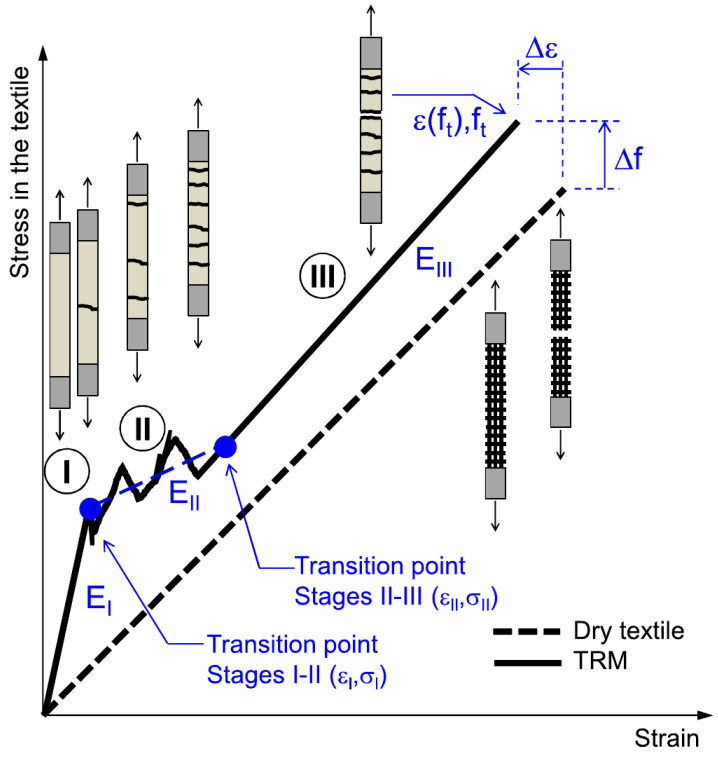

Figure 2.1 *The typical tensile response of FRCM composites (Adopted from [23]).*

It is worth to mention that some composite coupons developed a bilinear stress-strain curves such that the first phase (i.e., uncracked section) was not clearly recognised [7, 14] or the last phase (i.e., fully cracked section) could not be clearly identifiable [2, 8, 9, 18]. The absence of the first phase in some studies

was attributed to the relatively low stiffness matrix used to impregnate the relatively stiff textiles [7, 14], while the absence of the last stage in other studies was due to the slippage of the textiles [3] or the contemporaneously rupture

of the cords [8]. The use of clevis gripping system was reported to produce a bilinear stress-strain response as it was less effective in preventing the relative slippage at the grips [6].

The inorganic composites generally exhibit a slight reduction in the stiffness, the ultimate stress, and the peak strain due to the tension stiffening effect and stress concentrations in the cracked sections [17].

The contribution of the matrix is dominant in the uncracked and cracks development phases. However, this was only observed for composites comprising textiles of low stiffness. When the stiffness of the textiles is much higher than that of the matrix, the contribution of the latter becomes almost negligible [17].

2.1.6 The mode of failure

The coupons made of inorganic-based composites can fail in five scenarios including tensile rupture of the textiles at (a) either ends or (b) middle, (c) slippage of the textiles at the grips, (d) separation of the matrix, or (e) telescopic slippage of the core filaments (see Fig. 2.2). Premature rupture of the textile near the grips (Mode A) was reported in [5, 9]. It was attributed to the high localised stresses at the clamping areas arising from the simultaneous compression action coupled with the tensile load [9]. The tensile rupture of the textile at the middle of the coupon (Mode B) was the most common mode of failure observed for the inorganic-based coupons [3, 7]. Slippage of the textile at the clamping area (Mode C) was reported in [3] and was attributed to the efficiency of the clamping system. It is worth noting that this mode was also observed for lap-splice coupons between the overlapped textiles [13]. It was associated with the steel textiles of relatively high density.

Matrix separation or interlaminar failure (Mode D) was generally associated with the use of textiles that had a dense layout of cords or yarns as this hindered the penetration of the textile within the matrix and hence created weak interfaces that were prone to detachment at considerably lower stresses [7, 18]. This mode of failure was, also, reported for FRCM composites comprising multiple layers. However, it must be noted that some of the multilayer composites did not experience the interlaminar failure and they, instead, failed by premature rupture of the textiles [5]. This perhaps depends on the tensile properties of the textile and the stress concentrations in the gripping area. Finally, the telescopic failure (Mode E) was reported for some of the fibres or yarns that are made of straight filaments such that the matrix can only impregnate the sleeve filaments while the core filaments have, at best, a poor impregnation of the matrix [12].

2.2 Bond behaviour

The bond behaviour largely depends on several factors [15] including (1) the mechanical properties of the reinforcing textiles, the matrix, and the substrate, (2) the quality of shear transfer mechanism at the interfaces, (3) the manufacturing of the composite, preparation of the substrate, and the curing conditions, and (4) the experimental setup. The bond behaviour of the organic-based composites i.e., FRPs has been extensively investigated in the

research community (e.g., 26, 27, 28). The following sections provide detailed literature on the bond behaviour of the inorganic-based composites in terms of the textiles, the matrices, the number of layers, the test setup, and finally key findings related to the stress-slip response and the mode of failure.

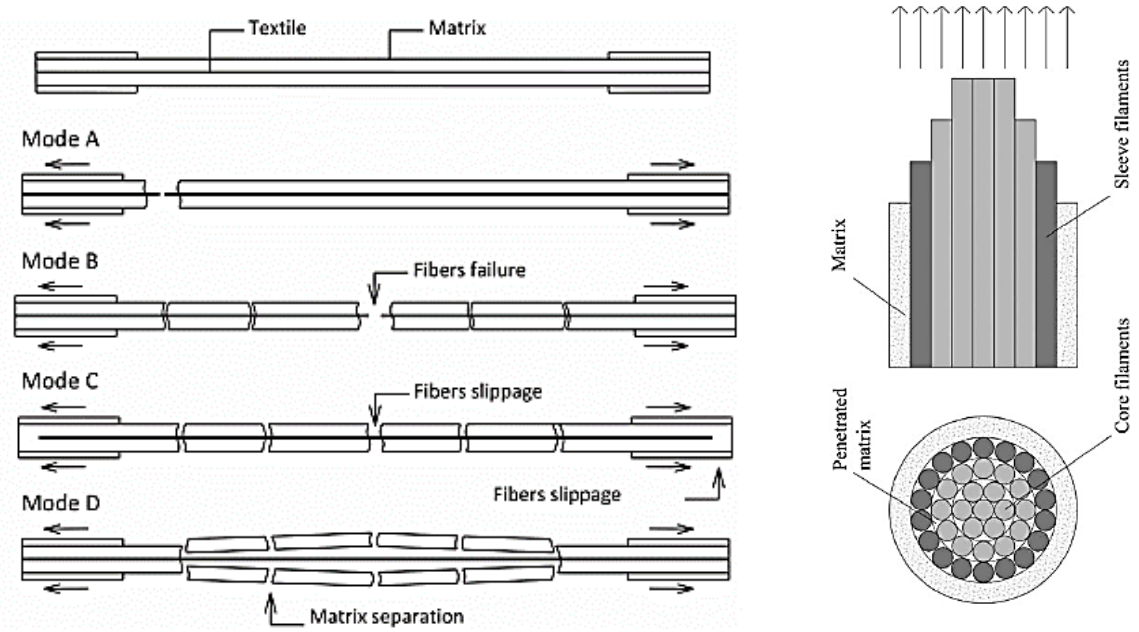

Figure 2.2 *Typical modes of failure for FRCM coupons; Modes A, B, C, D (left, adopted from [18]) and Mode E (right, adopted from [12]).*

2.2.1 The materials

The bond behaviour was investigated for inorganic-based composites comprising different reinforcing materials including steel [8, 15, 29-38], glass [8, 39-43], PBO [39, 42-45], carbon [30, 31, 39, 42, 43, 46], basalt [30, 31, 47], polyvinyl alcohol (PVA) [41], polypropylene (PP) [41], polyethylene (PE) [41]. The mechanical properties of the reinforcing textiles significantly influence the bond strength and the mode of failure [43]. Rigid and brittle behaviour was observed for composites comprising PBO reinforcement [39, 43].

Different matrices have been used to impregnate the textiles including lime-based [15, 30, 32, 36, 40], pozzolan-based [15], fibre-reinforced cement-based [15, 30, 31], polymer-modified cement-based [15, 30, 33, 40], mineral-based [31, 34] matrices. The mechanical properties of the matrix were found to largely influence the bond behaviour [40].

The bond behaviour between the inorganic-based composites and different substrates has been investigated. Masonry and stone substrates received the highest attention in the scientific community [8, 15, 23, 30, 32, 35, 36, 38, 40, 42, 48] since most of today's historical buildings are made of masonry. Only view studies investigated the bond behaviour on concrete substrates [33, 34, 44, 45]. Apart from masonry and concrete, different substrates were also investigated e.g., timber [49]. Concrete batches of low compressive strength were often used to simulate old

existing concrete buildings [33]. The mechanical characteristics of the substrate were reported to have a slight, or no, effect on the bond behaviour since the substrate is not typically involved in the failure mechanism for FRCM systems [33, 34, 36].

2.2.2 The geometry of the composites

The influence of the length and the width of the FRCM composite on the overall bond behaviour was investigated in several studies. The bond length is the length of direct contact between the composite and the substrate. Different bond lengths were investigated including 50 mm [39, 40], 75 mm [43, 46], 100 mm [34, 39, 40, 43, 44, 46,], 125 mm [43], 150 mm [34, 39, 40, 43, 46], 200 mm [34, 39, 43, 44], 250 mm [39, 44], 300 mm [34], 320 mm [36], 330 mm [44, 45], 350 mm [34], 450 mm [36, 45], 580 mm [36]. Also, different widths of the FRCM composites were considered including 34 mm [44], 50 mm [34], 60 mm [44, 45], 75 mm [46], 80 mm [44, 45], 100 mm [34, 46], 150 mm [46]. FRCM systems with a longer bond length will develop a higher friction resisting mechanism [36]. Bond strength was found to be increasing when the bond length was increased [36, 43, 46], however this increase was non-proportionally in some studies [34].

2.2.3 The number of layers

The use of a single layer of the strengthening system might not be always sufficient to meet the target upgrade (e.g., large structural members) and hence multiple layers of the composite might be considered. The use of FRCM systems comprising multiple layers of the textiles was investigated in [8, 30, 34, 43]. The debonding at the matrix-to-substrate interface involving a thin layer of the substrate was often observed for FRCM system of multiple layers [34]. However, debonding at the matrix-to-textile interface was also observed for FRCM systems comprising two layers of the textiles [43].

2.2.4 The test setup

Four experimental setups were used to carry out shear bond tests including single-lap [30-38, 45, 47], double-lap single-prism [30, 40, 42, 43], double-lap double-prism [29, 30, 36, 40, 46, 50], and beam-type [51] setups. They were classified by considering the number of the substrate prisms and the number of the laps (i.e., the surfaces of contact between the composite and the prism) except for the last setup which was classified according to the loading mechanism (see Fig. 2.3). The first three setups were designed to exert pure shear stresses, while the stresses developed in the beam-type setup are bending stresses (mixed normal and shear stresses). The fact that the shear bond behaviour is assumed to be studies in a pure shear mode makes the use of the beam-type setup less favourable as it does not exert pure shear stresses contrary to the rest of the setups. Although the beam-type setup has a better simulation of the stress conditions in the real-life application, however it is difficult to implement. The double-lap setups suffer from a set of drawbacks, notably the possible misalignments between different laps of the composite. This is even worse in the case of double-lap double-prism setup with two more laps introducing more misalignment possibilities. Furthermore, load eccentricity can be responsible for triggering unsymmetrical debonding and the

consequent load redistribution which in turn might have a high impact on the results of the bond tests [44]. On the other hand, single-lap setup is easy to implement and has much less misalignment issues compared to the double-lap setups.

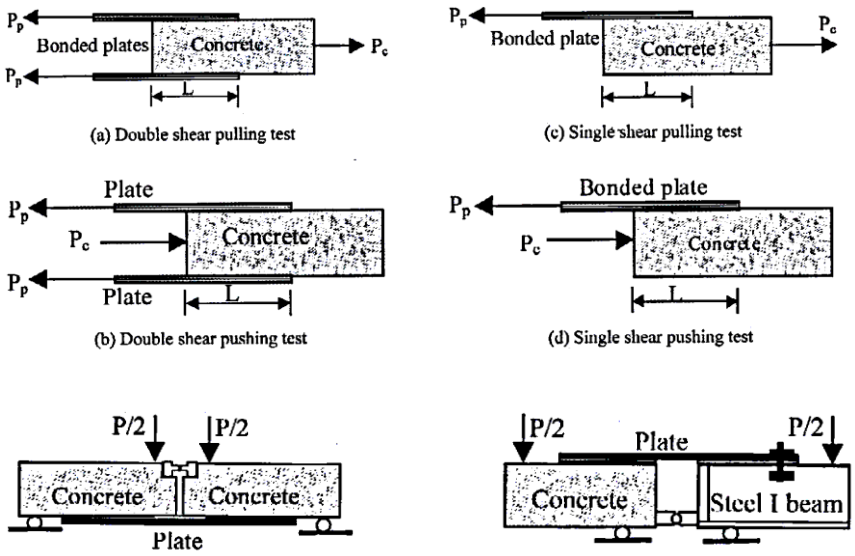

Figure 2.3 *Different setup for shear bond tests (adopted from [52]).*

Also, shear bond tests were also classified based on the boundary condition of the substrate (in addition to the number of laps between the substrate and the composite) into four categories [52] including single shear pulling (Single-Pull), single shear pushing (Single-Push), double shear pulling (Double-Pull), and double shear pushing (Double-push) test (see Fig. 2.4). Different stress states will develop in the substrate (near the composite) based on the setups utilised. The double-pull setup will generate compressive stresses in the substrate, while the double-push will develop tensile stresses. This latter setup is believed to have a good simulation of the stress state in beams strengthened in flexure [52]. High scatter in bond tests was reported [8, 15, 32] and attributed to several factors including the heterogeneity of mechanical properties of the substrate [8] or the matrix [32], the sensitivity of the shear transfer mechanism to the cracks [8], the possible misalignments during fabrication and testing [8, 15], and the differences in the test setup [15].

2.2.5 The stress-slip response

Stress-slip response can be obtained by plotting the stress against the relative slip between the composite and the substrate. FRCM systems was reported to exhibit a similar load-slip response to that of the FRP system [33]. Several studies reported a tri-linear load-slip response [36] including (1) un-cracked behaviour of the FRCM composite, (2) crack development in the composite, (3) debonding initiation (see Fig. 2.5). The first stage of the response characterising the elastic behaviour of the composite was mainly provided and governed by the contribution of the matrix. The initiation of the cracks in the matrix introduces the second stage of the nonlinear response with

significant drop in the stiffness and the load increases until the onset of the debonding mechanism. When the bond length of the composite is longer than the effective bond length, the shear stresses is only transferred through a certain zone of the interface called the stress transfer zone (STZ). Once the shear strength of the STZ is exceeded, debonding initiates at the loaded end and the STZ shifts away from the loaded end. This shifting mechanism continues until it reaches the free end of the composite where the remaining length is less than the effective bond length leading the complete detachment of the composite [44].

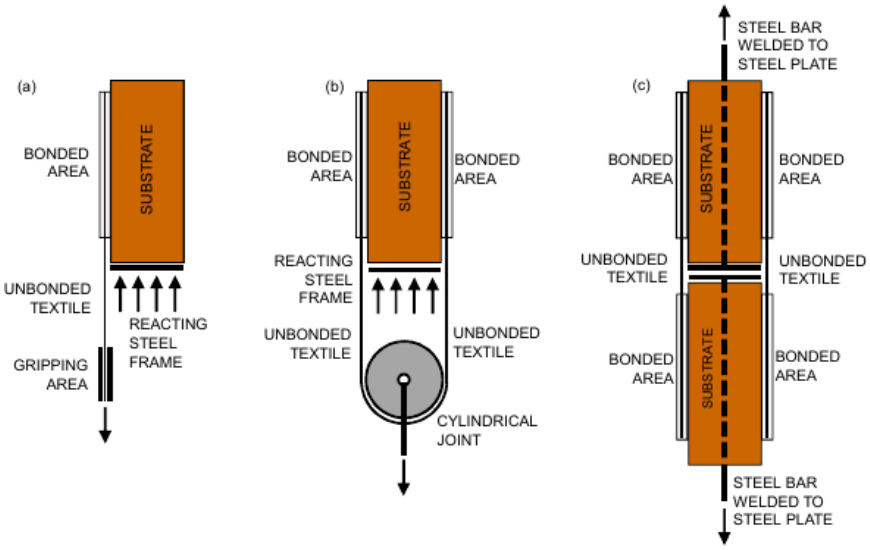

Figure 2.4 *Different setup for shear bond tests (adopted from [23]).*

Bi-linear stress-strain response was reported for some FRCM systems where only two stages were observed including the uncracked and the cracked stages [46]. The former was similar to that observed for trilinear response stress-slip response, while the latter characterised noticeable elongation in the reinforcement with explosive sounds indicating local debonding in the matrix and rupture of the textile.

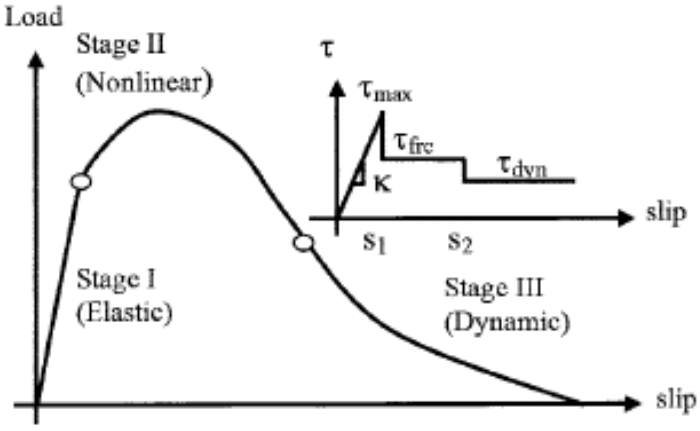

Figure 2.5 *The load-slip response curve of FRCM composites subjected to shear bond test (adopted from [41]).*

2.2.6 The mode of failure

Fig. 2.6 provide a schematic presentation of the possible modes of failure when conduction shear bond tests. The mode of failure in the inorganic-based composites generally occurs within the composite contrary to the FRP system where the cohesive failure inside the substrate (mode A) is typical. However, this latter mode was also observed for some of the FRCM systems comprising stiffer matrices [15] or subjected to normal stresses arising from misalignment during testing [30]. Furthermore, this mode of failure was also associated with the use of strengthening systems comprising short bond lengths [32, 43] or multiple layers of reinforcement [8, 43].

Debonding at the textile-to-matrix interface (mode B), also called interlaminar failure, was often reported for the FRCM systems [37, 38, 43, 46]. This mode of failure occurs usually starts as a micro-damage in the matrix near the loaded ended along the matrix-to-textile interface. This will appear as an interlaminar crack through the thickness of the composite initiating from the loaded ended. This crack will propagate towards the free end of the composite and will lead eventually to a full detachment of the textile and the upper layer of the matrix [38].

Slippage of the textiles within the matrix (mode D) was reported [44] for steel textiles comprising large number of cords per unit length (i.e., high density textiles). Composites comprising steel textiles of low cords density attained high loads sufficient to cause rupture (mode E1) to the textiles [8]. Furthermore, this mode of failure was also observed for Basalt-FRCM composites for bond length shorter than 125 mm [42, 47]. Rupture of the textiles can occur outside (mode E1) or inside the composite (mode E2). Mode E1 was often associated with systems comprising relatively low strength textiles [15, 42, 43] or with long bond lengths [47]. In the case of rupture of the textiles, progressive rupture (i.e., not simultaneous rupture) was often reported [42].

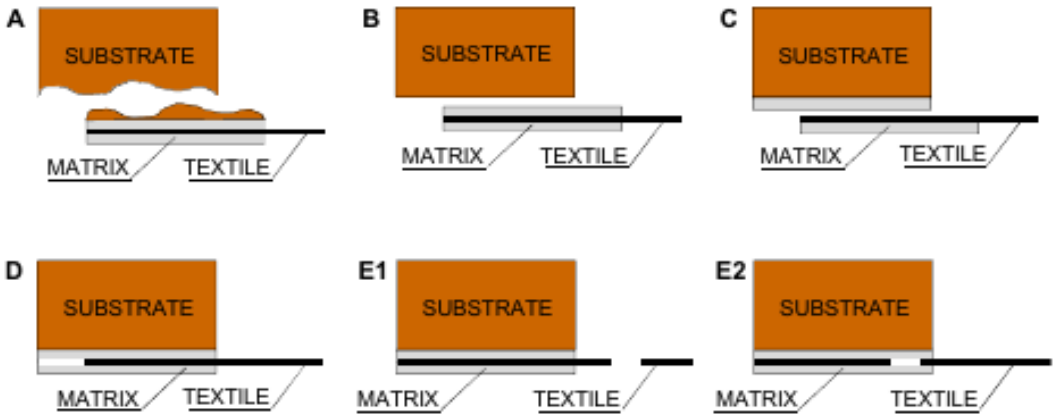

Figure 2.6 *The modes of failure for FRCM and SRG system in shear bond tests (adopted from [23]).*

2.2.7 The effective anchorage length

The effective anchorage length, also called the anchorage bond length, is defined as the maximum length beyond which there is no increase in the force transferred between composite and the substrate [39] or the minimum length needed to develop the load-carrying capacity of the interface [44].

Table 2.1.1 *The suggested effective anchorage length for different strengthening systems*

	Effective bond length (mm)				
System	100 ~ 150	150 ~ 200	200 ~ 250	250 ~ 300	> 300
Carbon-FRCM	[39]	[30]	--	--	--
Glass-FRCM	--	[39, 42]	--	--	--
PBO-FRCM	[39]	--	[30]	--	--
Steel-FRCM (SRG)	--	--	[32, 33, 34]	[34]	[29]
Basalt-FRCM	[47]	--	--	--	--

The formation of a plateau segment on the load-slip curve would suggest that the bond length of the tested specimen is more than the effective bond length. Similar load-slip curves were observed in [32]. Specimens that have a bond length more than the effective bond length will not always develop the sufficient load to cause rupture of the reinforcement. This is simply because the tensile stress required to cause rupture in the textiles can more than the shear stress of either interface (matrix-to-textile or matrix-to-substrate). In such cases, different failure mechanism will develop depending on the mechanical properties of the matrix, the textile, or the substrate. Also, the effective bond length largely depends on the shear transfer properties at the interface which is governed by the mechanical characteristics of the constituent materials. In fact, each strengthening system has its own effective bond length depending on the mechanical properties of the textiles and the matrix. Even for FRCM systems utilising the same reinforcement as the layout and the density of the textiles largely affect the failure mechanism. Table 2.1 provides some general suggestions for the effective bond length for different FRCM systems. As mentioned earlier, a single FRCM system (e.g., SRG) might have different effective bond lengths based on the constituent materials.

2.3 Flexural behaviour

The flexural behaviour of the RC beams strengthened with FRCM systems is governed by several parameters associated with each component of the whole system i.e., the beam and the strengthening composite. These parameters can be categorised into:

- Substrate-related parameters. This can include the geometry and detailing of the beam, the roughness of the substrate, the mechanical characteristics of the substate (e.g., the compressive or tensile strength of the concrete), or the curing conditions of the beam.

- Composite-related parameters. These parameters can be related to the matrix including the type of the grout (e.g., lime-based, or cement-based), or the compressive and tensile strength of the grout. Also, they involve the mechanical characteristics of the textiles (e.g., tensile strength, modulus of elasticity, and ultimate strain), the layout of the textiles (e.g., unidirectional, or bidirectional orientation), the microstructure of the fibres/cords (e.g., straight, or twisted filaments), the chemical modification of the fibres (e.g., zinc coating). Furthermore, there are several parameters related to the composite of the matrix and the textiles including the number of the textile layers, the geometry and layout of the composite, or the curing conditions.
- Setup-related parameters including the test setup configuration, the loading rate, or the anchorage system.

The following paragraphs review the different parameters that were considered to investigate their effect on the flexural behaviour of externally strengthened RC beams. they cover most of the available studies that mainly investigated the use of the FRCM and the SRG systems for strengthening RC beams. The flexural behaviour of RC beams externally strengthened with the FRP or the SRP systems can be found elsewhere [e.g., 53, 58].

2.3.1 Substrate-related parameters

Different geometries of the RC beams were considered including short [e.g., 54, 66, 74], long [e.g., 53, 66, 71], and shallow beams [e.g., 59, 73]. The spans were ranging from 1500 mm to 5000 mm, while the effective spans were in the range from 1350 mm to 4500 mm. Also, the depth of the tested beams varied from 140 mm to 400 mm with widths varying from 102 mm to 400 mm.

The substrate roughness plays a key role in the FRP systems since the typical mode of failure for these systems is the debonding at the matrix-to-substrate interface. However, this is not always the case for the FRCM systems the matrix-to-substrate interface is not always the weakest link in the system. Different surface preparation methods were used including surface grinding [56], sandblasting [66].

2.3.2 Composite-related parameters

Different inorganic-based strengthening systems were investigated which utilised several reinforcing materials including steel [53, 59, 70, 71, 73, 74], carbon [56, 66, 67, 73], basalt [56, 69], glass [56, 67], PBO [65-68, 70], Aramid [72]. Much higher enhancement in the load-carrying capacity was achieved by utilising the carbon in the FRCM system compared to the PBO reinforcement. However, the beams strengthened with PBO-FRCM systems exhibited more ductile behaviour compared to the beams strengthened with C-FRCM systems [2].

The influence of the use of multiple layers of the strengthening system has been investigated in several studies including one [65, 68], two [66-68], three [68], and four [65] layers of PBO, one [56], two [66, 67], three [56], and five [56] layers of carbon, four [67], and seven [56] layers of glass, and seven [56] and ten [69] layers of basalt.

The use of more than two layers of the C-FRCM system resulted in altering the mode of failure from the slippage of the textiles to the debonding at matrix-to-substrate interface [2]. Also, Increasing the number of the textile layers increased the yielding load and the load-carrying capacity [57, 61, 64]. This increase, however, was non-proportional due to the interruption of different modes of failure [64].

The mechanical properties of the matrix can significantly affect the flexural behaviour of the strengthened beams since the matrix is involved in different modes of failure that are reported for the beams strengthened with inorganic-based composites including the debonding at the matrix-to-textile interface and the relative slippage between the fibres/textiles and matrix. The flexural behaviour of beams strengthened FRCM systems was found to be largely affected by the type of the matrix used to impregnate the textiles. The matrix characterising higher compressive and tensile strength improved the bond between the textiles and the matrix which in turn improved the overall performance of the strengthening system [57].

2.3.3 Setup-related parameters

Most of the bending tests available in the literature were conducted in four-point bending configuration [e.g., 65] with different displacement-controlled rates including 0.18 mm/min [76], 0.87 mm/min [66], 1.00 mm/min [2 and 65], 1.20 mm/min [68], 1.50 mm/min [66], 2.00 mm/min [60 and 74], and 3.05 mm/min [73]. However, three-point bending test setup was also considered [e.g., 57]. The loading rate was reported to have an insignificant effect on the flexural behaviour [66]. Most of the available studies conducted bending tests on full scale beams of rectangular cross section. However, different sections were also considered including T-section [71] and double-T section [26].

The use of plain steel plates as an anchorage system was also considered [76]. The plates were mechanically fastened to the RC beams by means of bolts on the top of the composite and were providing lateral pressure to both ends of the composite. The use of the U-wrap anchorage system slightly improved the effectiveness of the strengthening, and it only prevented the composite from debonding. However, the relative slippage of the textile within the matrix was observed even with the presence of the U-wrap anchorage system [66, 64]. An improvement in the ductility was also observed for beams with U-wrap anchorage system [67]. The use of nail anchors did not improve the flexural performance of the SRG system [69]. This was attributed to the absence of the transverse cords in the unidirectional steel textile. Poor stress distribution and high local stress concentration at the anchors resulted in bearing failure in the matrix. Although the use of plain steel plates as an anchorage system was reported to prevent the complete debonding between the composite and the beam, however slippage of the fibres with the matrix was not prevented [76].

Different parameters were also investigated including the way the strengthening systems is applied such that the composite was applied to as-in-field beams as a counterpart to the beams strengthened in a laboratory condition

[68]. This parameter was considered to simulate the in-field operation of installing the strengthening system and to evaluate the impact of applying the system in the reverse direction.

Most of the available literature deal with Externally Bonded (EB) strengthening systems, however, Inhibiting Repairing Strengthening systems were also considered in few studies [e.g., 70]. This latter technique is often used to repairing RC structures with corroded reinforcement and deteriorated concrete cover.

2.3.4 The load-deflection response

The load-deflection response exhibited a tri-linear behaviour including (1) pre-cracking stage, (2) post-cracking stage, and (3) post-yielding stage [60, 61, 64, 73]. The first stage characterising a linear branch corresponds to the behaviour of the beam before the formation of the cracks in the concrete. Reduction in the stiffness characterises the second stage of the response as a result of cracks initiation and propagation. The third stage of a significantly reduced stiffness starts as soon as the tensile reinforcement yields and last by the failure in the strengthening system. After the failure of the strengthening system, the beam resembles the typical behaviour of an un-strengthened beam up until the crushing of concrete (see Fig. 2.7).

2.3.5 The mode of failure

The RC beams strengthened with EB composite system can fail by one of the following modes including (a) The tensile rupture of the external reinforcement, (b) crushing of concrete after the yielding of the tensile reinforcement, (c) shear failure, (d) cohesive failure within the substrate, (e) end debonding at the matrix-to-substrate interface, (f) flexural crack-induced debonding, and (g) shear crack-induced debonding (see Fig. 2.8). However, the FRCM systems is prone to additional modes of failure including the relative slippage between the textile and the matrix and the debonding at the matrix-to-textile interface or interlaminar shearing. these modes of failure are prevented in the FRP systems by the high bond strength between the textiles and the epoxy matrix.

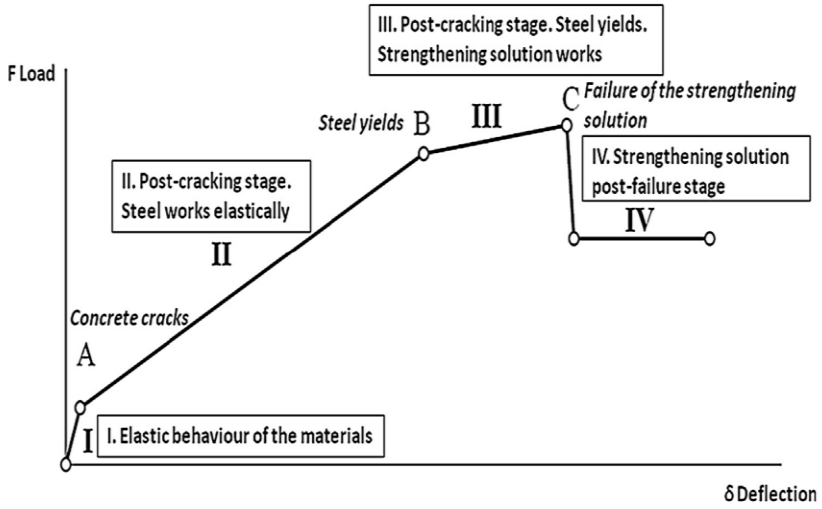

Figure 2.7 *The load-deflection curve of a typical RC strengthened beam (adopted from [76]).*

Rupture of the textiles was observed for beams strengthened with SRG systems comprising steel textiles of low-density cords layout [64, 68, 75]. The rupture of the textiles was generally reported in the constant-moment zone near the loading points [68] or at the midspan of the beam [68].

Concrete crushing after the yielding of the tensile reinforcement is typical for the RC beams designed to fail in flexure [2, 57, 61, 64, 65, 68, 73, 74]. Similar mode of failure was also reported for beams strengthened with only one layer of PBO-FRCM system [61].

Debonding at the matrix-to-substrate interface can be triggered in two different ways including end debonding generally observed for the FRCM systems without an anchorage system [67] and intermediate flexural/shear crack debonding (IC debonding). This mode was observed for beams strengthened with multiple layers of FRCM systems [2, 64, 77] and PBO-FRCM systems [61, 73] or those strengthened with FRCM systems comprising textiles of high-density cords/yarn layout [68]. This mode of failure was triggered by a longitudinal crack that initiated at the midspan of the beam and rapidly propagated towards either end of the composite to eventually cause the debonding at the matrix-to-substrate with [72, 77] or without involving the substrate [68, 73]. In [61], however, the propagation of the IC crack was described as "gradual" rather than sudden except for one beam where the sudden propagation of the IC crack was attributed to imperfections at the matrix-to-substrate interface during the application of the FRCM system. In fact, the speed of the debonding is governed by the bond length of the composite. The beams strengthened with FRCM systems with relatively long bond length could develop the "shifting" mechanism observed in bond shear tests for specimens comprising FRCM composites of bond length longer than the effective bond length [65]. Intermediate crack debonding is the governing mode of failure for the beams strengthened with FRCM systems without anchorage system [65, 67].

Debonding at the matrix-to-textile interface, also called interlaminar shearing, was reported. It was observed for beams strengthened with multiple layers of C-FRCM composites [2] and beams strengthened with SRG systems comprising steel textiles of high-density cords layout [26, 66]. Furthermore, this mode of failure was reported for beams strengthened with coated carbon fibres as coating prevented the relative slippage between the fibres and the matrix and forced the failure to occur at the matrix-to-textile interface [64]. Also, the use of Inhibiting Repairing Strengthening (IRS) strengthening technique caused the failure to occur at the matrix-to-textile interface (interlaminar shearing) as the composite was applied well inside the beam after removing the concrete cover. This enhanced the bond at the matrix-to-substrate interface and forced the failure to occur at the weakest link in the system i.e., the matrix-to-textile interface [70].

Slippage of the textile within the matrix was associated with beams strengthened with one and two layers of C-FRCM systems [2], one layer of PBO-FRCM systems [73]. Mixed mode of failure characterising slippage of the textile and debonding at the matrix-to-textile interface was observed for beams strengthened with PBO-FRCM

systems regardless of the number of the textile layers [2]. Also, slippage of the textile with the matrix with rupture of the fibres was reported for beams strengthened with C-FRCM systems [26]. Slippage of the textile and partial rupture of the yarns/cords was also reported. This mode of failure was observed for C-FRCM comprising dry carbon i.e., not coated [64]. This mode of failure can occur as a result of imperfections in the matrix during the installation of the system. Good mechanical interlock was developed for only some fibres which prevented slippage, and they eventually failed by tensile rupture.

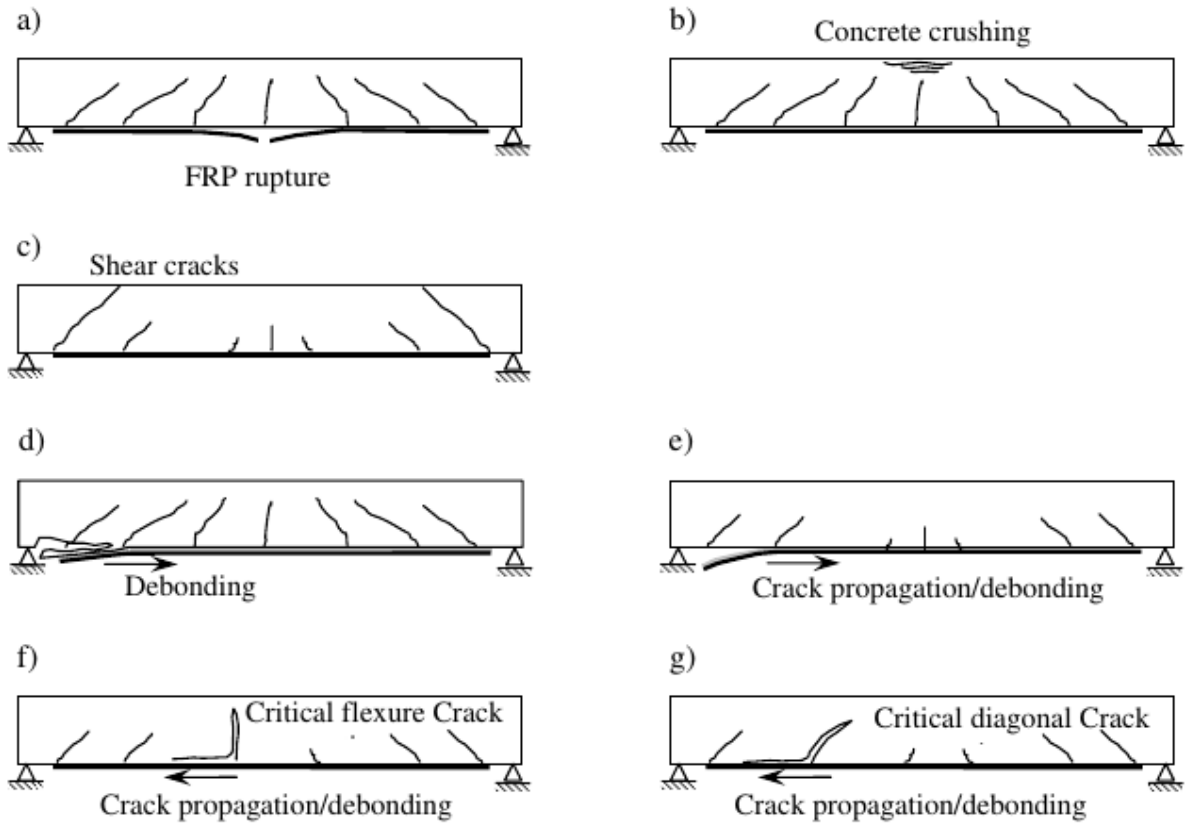

Figure 2.8 *Typical modes of failure for RC beams with EB strengthening systems (adopted from [75]).*

The relatively strong bond between the organic matrix and the embedded textiles in the FRP systems often derives the failure to occur within the concrete surface if the tensile strength of the textiles is not exceeded. However, the bond between the grout or mortar and the embedded textiles in the FRCM systems is not similar to that of the FRP system. This, in fact, introduces more modes of failure that can occur at different interfaces. Some of these modes is of a brittle nature e.g., full tensile rupture of the textiles or sudden end debonding at the matrix-to-substrate interface, although the brittleness of this latter is dependent on the bond length of the composite. On the other hand, the slippage of the textiles within the matrix is often gradual which makes the failure of a ductile nature. Also mixed modes of failure are reported including slippage of the textiles combined with either debonding at the matrix-to-

textile interface or partial rupture of fibres. Further discussion on these modes of failure will be provided in the following paragraphs.

2.3.6 The crack pattern and the strain distribution

In general, the typical crack pattern for beams tested in flexure is vertical cracks in the flexural span and inclined cracks in the shear span [67]. The strengthened beams exhibited a similar crack pattern to the un-strengthened control beams [68]. The cracks were spaced at a distance corresponding to the spacing of the shear reinforcement [68]. The beams strengthened with multiple number of FRCM layers developed higher strain hardening in post-yielding phase [2]. Furthermore, the strain distribution along the cross section of the beam was independent form the type and the amount of the external strengthening system [61].

2.4 Design theories and models

The ultimate load of RC beams strengthened with EB composite systems can be calculated through cross sectional analysis. ACI 318 and ACI 549 provide a detailed analysis to compute nominal flexural [65]. However, the stress and the strain at debonding of the strengthening system cannot be derived from such analysis. Different models were suggested in the research community to predict the strain of the external reinforcement at which the debonding might occur. These models can be classified according to their approach to (1) strength models, (2) fracture mechanics models, and (3) empirical or semi-empirical models [30]. Analytical [e.g., 75-98] and Numerical [e.g., 99-108] modelling was performed to predict different aspects of the bond behaviour including the shear stress, the debonding load and strain, and the effective length. A database of these suggested models is provided in Appendix G. A detailed discussion on this topic will be presented in Chapter 6.

2.5 Knowledge gap

While the research on the tensile and the bond behaviour of the FRP systems and their applications in the flexural strengthening of the RC beams is well established, the inorganic-based composite (FRCM and SRG) systems received less attention in the scientific community due to their relative novelty in the strengthening industry. In particular, the tensile and bond behaviour of the SRG systems is still in its infancy. The research on the tensile behaviour of the SRG composite system is very limited. Only a handful studies investigated the tensile behaviour of the SRG systems comprising a single layer of the steel textiles. The tensile behaviour of the multiple layers of this system is not investigated to date. Understanding this aspect is crucial to understand the bond and flexural behaviour of these composites when used as a flexural strengthening system for the RC beams. Most of the research on the bond behaviour of the SRG systems was focusing on masonry substrates. The bond behaviour between the SRG system and concrete substrates is very limited. Also, there was a very few studies devoted to investigating the flexural behaviour of the RC beams strengthened with the SRG composites. There is a need for a large experimental

campaign to address different aspects of the SRG system to bridge this gap. To this end, three experimental programmes will be conducted such that the first programme provides a mechanical characterising of the SRG system comprising two types of the steel textiles and different number of layers (Chapter 3). This will be achieved by conducting direct tensile tests on the SRG coupons to explore the effect of the textile density and the number of layers on the tensile behaviour. The bond behaviour of the SRG system will be investigated in Chapter 4 by performing direct bond shear tests on SRG systems comprising different bond lengths, number of layers, and textile densities. Finally, the flexural behaviour of full-scale RC beams strengthened with these systems will be investigated (Chapter 5) through bending tests on beams strengthened with different SRG composites.

References

[1] T. D'Antino and C. Papanicolaou, "Comparison between different tensile test set-ups for the mechanical characterization of inorganic-matrix composites", *Construction and Building Materials*, vol. 171, pp. 140-151, 2018.

[2] U. Ebead, K. Shrestha, M. Afzal, A. El Refai and A. Nanni, "Effectiveness of Fabric-Reinforced Cementitious Matrix in Strengthening Reinforced Concrete Beams", Journal of Composites for Construction, vol. 21, no. 2, p. 04016084, 2017.

[3] F. Carozzi et al., "Experimental investigation of tensile and bond properties of Carbon-FRCM composites for strengthening masonry elements", Composites Part B: Engineering, vol. 128, pp. 100-119, 2017.

[4] J. Donnini and V. Corinaldesi, "Mechanical characterization of different FRCM systems for structural reinforcement", *Construction and Building Materials*, vol. 145, pp. 565-575, 2017.

[5] A. Younis, U. Ebead and K. Shrestha, "Tensile characterization of multi-ply fabric-reinforced cementitious matrix strengthening systems", *Structural Concrete*, vol. 21, no. 2, pp. 713-723, 2019.

[6] D. Arboleda, F. Carozzi, A. Nanni and C. Poggi, "Testing Procedures for the Uniaxial Tensile Characterization of Fabric-Reinforced Cementitious Matrix Composites", *Journal of Composites for Construction*, vol. 20, no. 3, p. 04015063, 2016.

[7] T. D'Antino, A. Calabrese and C. Poggi, "Experimental procedures for the mechanical characterization of composite reinforced mortar (CRM) systems for retrofitting of masonry structures", *Materials and Structures*, vol. 53, no. 4, 2020.

[8] A. Bilotta, F. Ceroni, E. Nigro and M. Pecce, "Experimental tests on FRCM strengthening systems for tuff masonry elements", *Construction and Building Materials*, vol. 138, pp. 114-133, 2017.

[9] M. Leone et al., "Glass fabric reinforced cementitious matrix: Tensile properties and bond performance on masonry substrate", *Composites Part B: Engineering*, vol. 127, pp. 196-214, 2017.

[10] A. Bilotta, F. Ceroni, G. Lignola and A. Prota, "Use of DIC technique for investigating the behaviour of FRCM materials for strengthening masonry elements", *Composites Part B: Engineering*, vol. 129, pp. 251-270, 2017.

[11] R. Contamine, A. Si Larbi and P. Hamelin, "Contribution to direct tensile testing of textile reinforced concrete (TRC) composites", Materials Science and Engineering: A, vol. 528, no. 29-30, pp. 8589-8598, 2011.

[12] I. Colombo, A. Magri, G. Zani, M. Colombo and M. di Prisco, "Textile Reinforced Concrete: experimental investigation on design parameters", *Materials and Structures*, vol. 46, no. 11, pp. 1933-1951, 2013.

[13] G. Thermou et al., "Mechanical characterization of multi-ply steel reinforced grout composites for the strengthening of concrete structures", in *CICE 2018. 9th International Conference on Fibre-Reinforced Polymer (FRP) Composites in Civil Engineering*, Paris, France, 2021.

[14] S. Mazzuca, H. Hadad, L. Ombres and A. Nanni, "Mechanical Characterization of Steel-Reinforced Grout for Strengthening of Existing Masonry and Concrete Structures", *Journal of Materials in Civil Engineering*, vol. 31, no. 5, p. 04019037, 2019.

[15] S. De Santis et al., "Round Robin Test on tensile and bond behaviour of Steel Reinforced Grout systems", *Composites Part B: Engineering*, vol. 127, pp. 100-120, 2017.

[16] S. De Santis and G. de Felice, "Steel reinforced grout systems for the strengthening of masonry structures", *Composite Structures*, vol. 134, pp. 533-548, 2015.

[17] S. De Santis and G. de Felice, "Tensile behaviour of mortar-based composites for externally bonded reinforcement systems", *Composites Part B: Engineering*, vol. 68, pp. 401-413, 2015.

[18] C. Caggegi et al., "Experimental analysis on tensile and bond properties of PBO and aramid fabric reinforced cementitious matrix for strengthening masonry structures", Composites Part B: Engineering, vol. 127, pp. 175-195, 2017

[19] L. Mercedes, L. Gil and E. Bernat-Maso, "Mechanical performance of vegetal fabric reinforced cementitious matrix (FRCM) composites", *Construction and Building Materials*, vol. 175, pp. 161-173, 2018.

[20] B. Ghiassi, D. Oliveira, V. Marques, E. Soares and H. Maljaee, "Multi-level characterization of steel reinforced mortars for strengthening of masonry structures", *Materials & Design*, vol. 110, pp. 903-913, 2016.

[21] M. Raupach, J. Orlowsky, T. Büttner, U. Dilthey and M. Schleser, "Epoxy-impregnated Textiles in Concrete – Load Bearing Capacity and Durability", ICTRC, pp. 77–88, 2006.

[22] M.J. Roth, Ph.D Thesis, Mississippi State University, 2007.

[23] S. De Santis, F. Carozzi, G. de Felice and C. Poggi, "Test methods for Textile Reinforced Mortar systems", *Composites Part B: Engineering*, vol. 127, pp. 121-132, 2017.

[24] J. Donnini, V. Corinaldesi and A. Nanni, "Mechanical properties of FRCM using carbon fabrics with different coating treatments", *Composites Part B: Engineering*, vol. 88, pp. 220-228, 2016.

[25] T. D'Antino and C. Papanicolaou, "Mechanical characterization of textile reinforced inorganic-matrix composites", *Composites Part B: Engineering*, vol. 127, pp. 78-91, 2017.

[26] M. Valluzzi et al., "Round Robin Test for composite-to-brick shear bond characterization", *Materials and Structures*, vol. 45, no. 12, pp. 1761-1791, 2012.

[27] F. Ascione, M. Lamberti, A. Napoli, G. Razaqpur and R. Realfonzo, "An experimental investigation on the bond behavior of steel reinforced polymers on concrete substrate", *Composite Structures*, vol. 181, pp. 58-72, 2017.

[28] X. Zou and L. Sneed, "Bond Behavior Between Steel Fiber Reinforced Polymer (SRP) and Concrete", *International Journal of Concrete Structures and Materials*, vol. 14, no. 1, 2020.

[29] M. Matana, A. Nanni, L. Dharani, P. Silva and G. Tunis, "Bond performance of steel reinforced polymer and steel reinforced grout", in *Proceedings of International Symposium on Bond Behaviour of FRP in Structures (BBFS 2005)*, Hong Kong, China, 2005.

[30] G. de Felice et al., "Mortar-based systems for externally bonded strengthening of masonry", *Materials and Structures*, vol. 47, no. 12, pp. 2021-2037, 2014.

[31] L. Ascione, G. de Felice and S. De Santis, "A qualification method for externally bonded Fibre Reinforced Cementitious Matrix (FRCM) strengthening systems", *Composites Part B: Engineering*, vol. 78, pp. 497-506, 2015.

[32] M. Santandrea, F. Focacci, C. Mazzotti, F. Ubertini and C. Carloni, "Determination of the interfacial cohesive material law for SRG composites bonded to a masonry substrate", *Engineering Failure Analysis*, vol. 111, p. 104322, 2020.

[33] F. Bencardino, A. Condello and A. Ashour, "Single-lap shear bond tests on Steel Reinforced Geopolymeric Matrix-concrete joints", *Composites Part B: Engineering*, vol. 110, pp. 62-71, 2017.

[34] F. Ascione, M. Lamberti, A. Napoli and R. Realfonzo, "Experimental bond behavior of Steel Reinforced Grout systems for strengthening concrete elements", *Construction and Building Materials*, vol. 232, p. 117105, 2020.

[35] A. Razavizadeh, B. Ghiassi and D. Oliveira, "Bond behavior of SRG-strengthened masonry units: Testing and numerical modeling", Construction and Building Materials, vol. 64, pp. 387-397, 2014.

[36] S. De Santis, "Bond behaviour of Steel Reinforced Grout for the extrados strengthening of masonry vaults", *Construction and Building Materials*, vol. 150, pp. 367-382, 2017.

[37] L. Carabba, M. Santandrea, C. Carloni, S. Manzi and M. Bignozzi, "Steel fiber reinforced geopolymer matrix (S-FRGM) composites applied to reinforced concrete structures for strengthening applications: A preliminary study", *Composites Part B: Engineering*, vol. 128, pp. 83-90, 2017.

[38] F. Bencardino, M. Nisticò and S. Verre, "Experimental Investigation and Numerical Analysis of Bond Behavior in SRG-Strengthened Masonry Prisms Using UHTSS and Stainless-Steel Fibers", *Fibers*, vol. 8, no. 2, p. 8, 2020.

[39] V. Alecci, M. De Stefano, R. Luciano, L. Rovero and G. Stipo, "Experimental Investigation on Bond Behavior of Cement-Matrix–Based Composites for Strengthening of Masonry Structures", *Journal of Composites for Construction*, vol. 20, no. 1, p. 04015041, 2016.

[40] F. Carozzi, G. Milani and C. Poggi, "Mechanical properties and numerical modeling of Fabric Reinforced Cementitious Matrix (FRCM) systems for strengthening of masonry structures", *Composite Structures*, vol. 107, pp. 711-725, 2014.

[41] S. Sueki, C. Soranakom, B. Mobasher and A. Peled, "Pullout-Slip Response of Fabrics Embedded in a Cement Paste Matrix", *Journal of Materials in Civil Engineering*, vol. 19, no. 9, pp. 718-727, 2007.

[42] F. Carozzi and C. Poggi, "Mechanical properties and debonding strength of Fabric Reinforced Cementitious Matrix (FRCM) systems for masonry strengthening", *Composites Part B: Engineering*, vol. 70, pp. 215-230, 2015.

[43] A. Younis and U. Ebead, "Bond characteristics of different FRCM systems", *Construction and Building Materials*, vol. 175, pp. 610-620, 2018.

[44] L. Sneed, T. D'Antino, C. Carloni and C. Pellegrino, "A comparison of the bond behavior of PBO-FRCM composites determined by double-lap and single-lap shear tests", *Cement and Concrete Composites*, vol. 64, pp. 37-48, 2015.

[45] T. D'Antino, L. Sneed, C. Carloni and C. Pellegrino, "Influence of the substrate characteristics on the bond behavior of PBO FRCM-concrete joints", *Construction and Building Materials*, vol. 101, pp. 838-850, 2015.

[46] O. Awani, A. Refai and T. El-Maaddawy, "Bond characteristics of carbon fabric-reinforced cementitious matrix in double shear tests", *Construction and Building Materials*, vol. 101, pp. 39-49, 2015.

[47] C. Caggegi, D. Sciuto and M. Cuomo, "Experimental study on effective bond length of basalt textile reinforced mortar strengthening system: Contributions of digital image correlation", *Measurement*, vol. 129, pp. 119-127, 2018.

[48] F. Roscini, S. De Santis and G. de Felice, "Experimental investigation on the mechanical behaviour of mortar-based strengthening systems", in *SAHC'16 - 10th International Conference on Structural Analysis of Historic Constructions*, Leuven, Belgium, 2016.

[49] A. Borri and M. Corradi, "Strengthening of timber beams with high strength steel cords", Composites Part B: Engineering, vol. 42, no. 6, pp. 1480-1491, 2011.

[50] A. Serbescu, M. Guadagnini and K. Pilakoutas, "Standardised double-shear test for determining bond of FRP to concrete and corresponding model development", *Composites Part B: Engineering*, vol. 55, pp. 277-297, 2013.

[51] R. Perera, A. Recuero, A. Diego and C. López, "Adherence analysis of fiber-reinforced polymer strengthened RC beams", *Computers & Structures*, vol. 82, no. 23-26, pp. 1865-1873, 2004.

[52] J. Chen, Z. Yang and G. Holt, "FRP or steel plate-to-concrete bonded joints: Effect of test methods on experimental bond strength", *Steel and Composite Structures*, vol. 1, no. 2, pp. 231-244, 2001.

[53] A. Napoli and R. Realfonzo, "Reinforced concrete beams strengthened with SRP/SRG systems: Experimental investigation", Construction and Building Materials, vol. 93, pp. 654-677, 2015.

[54] X. Huang, V. Birman, A. Nanni and G. Tunis, "Properties and potential for application of steel reinforced polymer and steel reinforced grout composites", *Composites Part B: Engineering*, vol. 36, no. 1, pp. 73-82, 2005.

[55] A. Lopez, N. Galati, T. Alkhrdaji and A. Nanni, "Strengthening of a reinforced concrete bridge with externally bonded steel reinforced polymer (SRP)", *Composites Part B: Engineering*, vol. 38, no. 4, pp. 429-436, 2007.

[56] S. Raoof, L. Koutas and D. Bournas, "Textile-reinforced mortar (TRM) versus fibre-reinforced polymers (FRP) in flexural strengthening of RC beams", *Construction and Building Materials*, vol. 151, pp. 279-291, 2017.

[57] F. Bencardino and A. Condello, "Structural behaviour of RC beams externally strengthened in flexure with SRG and SRP systems", *International Journal of Structural Engineering*, vol. 5, no. 4, p. 346, 2014.

[58] G. Mitolidis, T. Salonikios and A. Kappos, "Tests on RC Beams Strengthened at the Span with Externally Bonded Polymers Reinforced with Carbon or Steel Fibers", *Journal of Composites for Construction*, vol. 16, no. 5, pp. 551-562, 2012.

[59] A. Prota, G. Manfredi, A. Nanni, E. Cosenza and M. Pecce, "Flexural strengthening of RC beams using emerging materials: Ultimate behavior", in *Proceedings of 2nd International Conference on FRP Composites in Civil Engineering (CICE 2004)*, Adelaide, Australia, 2004, pp. 163–170.

[60] A. Prota, K. Tan, A. Nanni, M. Pecce and G. Manfredi, "Performance of shallow reinforced concrete beams with externally bonded steel-reinforced polymer", *CI Structural Journal*, vol. 103, pp. 163-170, 2006.

[61] A. Balsamo, F. Nardone, I. Iovinella, F. Ceroni and M. Pecce, "Flexural strengthening of concrete beams with EB-FRP, SRP and SRCM: Experimental investigation", *Composites Part B: Engineering*, vol. 46, pp. 91-101, 2013.

[62] E. Wobbe et al., "Flexural capacity of RC beams externally bonded with SRP and SRG", in *International SAMPE Technical Conference*, Long Beach, USA, 2004, pp. 3009-3016.

[63] C. Pellegrino and T. D'Antino, "Experimental behaviour of existing precast prestressed reinforced concrete elements strengthened with cementitious composites", *Composites Part B: Engineering*, vol. 55, pp. 31-40, 2013.

[64] L. Sneed, S. Verre, C. Carloni and L. Ombres, "Flexural behavior of RC beams strengthened with steel-FRCM composite", *Engineering Structures*, vol. 127, pp. 686-699, 2016.

[65] S. Babaeidarabad, G. Loreto and A. Nanni, "Flexural Strengthening of RC Beams with an Externally Bonded Fabric-Reinforced Cementitious Matrix", *Journal of Composites for Construction*, vol. 18, no. 5, p. 04014009, 2014.

[66] A. D'Ambrisi and F. Focacci, "Flexural Strengthening of RC Beams with Cement-Based Composites", *Journal of Composites for Construction*, vol. 15, no. 5, pp. 707-720, 2011.

[67] A. Jabr, A. El-Ragaby and F. Ghrib, "Effect of the Fiber Type and Axial Stiffness of FRCM on the Flexural Strengthening of RC Beams", *Fibers*, vol. 5, no. 1, p. 2, 2017.

[68] L. Ombres, "Flexural analysis of reinforced concrete beams strengthened with a cement based high strength composite material", *Composite Structures*, vol. 94, no. 1, pp. 143-155, 2011.

[69] H. Elsanadedy, T. Almusallam, S. Alsayed and Y. Al-Salloum, "Flexural strengthening of RC beams using textile reinforced mortar – Experimental and numerical study", *Composite Structures*, vol. 97, pp. 40-55, 2013.

[70] F. Bencardino and A. Condello, "Eco-friendly external strengthening system for existing reinforced concrete beams", *Composites Part B: Engineering*, vol. 93, pp. 163-173, 2016.

[71] L. Ombres and S. Verre, "Flexural Strengthening of RC Beams with Steel-Reinforced Grout: Experimental and Numerical Investigation", *Journal of Composites for Construction*, vol. 23, no. 5, p. 04019035, 2019.

[72] C. Papakonstantinou and K. Katakalos, "Flexural behavior of reinforced concrete beams strengthened with a hybrid inorganic matrix - steel fiber retrofit system", *Structural Engineering and Mechanics*, vol. 31, no. 5, pp. 567-585, 2009.

[73] C. Menna et al., "Use of geopolymers for composite external reinforcement of RC members", *Composites Part B: Engineering*, vol. 45, no. 1, pp. 1667-1676, 2013.

[74] P. Larrinaga, L. Garmendia, I. Piñero and J. San-José, "Flexural strengthening of low-grade reinforced concrete beams with compatible composite material: Steel Reinforced Grout (SRG)", *Construction and Building Materials*, vol. 235, p. 117790, 2020.

[75] E. Sayed-Ahmed, R. Bakay and N. Shrive, "Bond strength of FRP laminates to concrete: State-of-the-art review", Electronic Journal of Structural Engineering, vol. 9, pp. 45-61, 2009.

[76] ACI 440.2R-08, "Guide for the Design and Construction of Externally Bonded FRP Systems for Strengthening Concrete Structures," American Concrete Institute, 2008.

[77] S. De Santis, G. de Felice, A. Napoli and R. Realfonzo, "Strengthening of structures with Steel Reinforced Polymers: A state-of-the-art review", Composites Part B: Engineering, vol. 104, pp. 87-110, 2016.

[78] F. Bencardino and A. Condello, "Reliability and adaptability of the analytical models proposed for the FRP systems to the Steel Reinforced Polymer and Steel Reinforced Grout strengthening systems", Composites Part B: Engineering, vol. 76, pp. 249-259, 2015.

[79] CNR-DT 200 R1/2013, "Guide for the Design and Construction of Externally Bonded FRP Systems for Strengthening Existing Structures", Consiglio Nazionale delle Ricerche, 2013.

[80] F. Bencardino and A. Condello, "SRG/SRP–concrete bond–slip laws for externally strengthened RC beams", Composite Structures, vol. 132, pp. 804-815, 2015.

[81] E. Grande, M. Imbimbo and E. Sacco, "Modeling and numerical analysis of the bond behavior of masonry elements strengthened with SRP/SRG", Composites Part B: Engineering, vol. 55, pp. 128-138, 2013.

[82] C. Mazzotti et al., "Design Procedures for the Use of Composites in Strengthening of Reinforced Concrete Structures: State-of-the-Art Report of the RILEM Technical Committee", Springer, 2016.

[83] L. Ombres, "Debonding analysis of reinforced concrete beams strengthened with fibre reinforced cementitious mortar", *Engineering Fracture Mechanics*, vol. 81, pp. 94-109, 2012.

[84] L. Bizindavyi and K. Neale, "Transfer Lengths and Bond Strengths for Composites Bonded to Concrete", Journal of Composites for Construction, vol. 3, no. 4, pp. 153-160, 1999.

[85] [15]C. Carloni, T. D'Antino, L. Sneed and C. Pellegrino, "Three-Dimensional Numerical Modeling of Single-Lap Direct Shear Tests of FRCM-Concrete Joints Using a Cohesive Damaged Contact Approach", Journal of Composites for Construction, vol. 22, no. 1, p. 04017048, 2018.

[86] F. Bencardino and A. Condello, "Experimental study and numerical investigation of behavior of RC beams strengthened with steel reinforced grout", Computers and Concrete, vol. 14, no. 6, pp. 711-725, 2014.

[87] J. Salsavilca, J. Yacila, N. Tarque and G. Camata, "Experimental and analytical bond behaviour of masonry strengthened with steel reinforced grout (SRG)", Construction and Building Materials, vol. 238, 2020.

[88] W. Figeys, L. Schueremans, K. Brosens and D. Van Gemert, "Strengthening of Concrete Structures using Steel Wire Reinforced Polymer", ACI Symposium Publication, vol. 230, 2005.

[89] F. Bencardino, C. Carloni, A. Condello, F. Focacci, A. Napoli and R. Realfonzo, "Flexural behaviour of RC members strengthened with FRCM: State-of-the-art and predictive formulas", Composites Part B: Engineering, vol. 148, pp. 132-148, 2018.

[90] F. Ceroni and P. Salzano, "Design provisions for FRCM systems bonded to concrete and masonry elements", Composites Part B: Engineering, vol. 143, pp. 230-242, 2018.

[91] T. D'Antino, F. Focacci, L. Sneed and C. Carloni, "Relationship between the effective strain of PBO FRCM-strengthened RC beams and the debonding strain of direct shear tests", Engineering Structures, vol. 216, p. 110631, 2020.

[92] G. Monti et al., "Design Procedures for the Use of Composites in Strengthening of Reinforced Concrete Structures: State-of-the-Art Report of the RILEM Technical Committee", Springer, 2016.

[93] A. Dalalbashi, B. Ghiassi and D. Oliveira, "Analytical Modeling of the Bond Behavior between Textile and Mortar Based on Pull-Out Tests", Key Engineering Materials, vol. 817, pp. 112-117, 2019.

[94] X. Zou and L. Sneed, "Bond Behavior Between Steel Fiber Reinforced Polymer (SRP) and Concrete", International Journal of Concrete Structures and Materials, vol. 14, no. 1, 2020.

[95] F. Ceroni and M. Pecce, "Cracking behaviour of RC beams externally strengthened with emerging materials", Construction and Building Materials, vol. 21, no. 4, pp. 736-745, 2007.

[96] J. Yao, J. Teng and J. Chen, "Experimental study on FRP-to-concrete bonded joints", Composites Part B: Engineering, vol. 36, no. 2, pp. 99-113, 2005.

[97] H. Yuan, J. Teng, R. Seracino, Z. Wu and J. Yao, "Full-range behavior of FRP-to-concrete bonded joints", Engineering Structures, vol. 26, no. 5, pp. 553-565, 2004.

[98] M. Pecce, F. Ceroni, A. Prota and G. Manfredi, "Response Prediction of RC Beams Externally Bonded with Steel-Reinforced Polymers", Journal of Composites for Construction, vol. 10, no. 3, pp. 195-203, 2006.

[99] F. Bencardino and A. Condello, "3D FE Analysis of RC Beams Externally Strengthened with SRG/SRP Systems", Fibers, vol. 4, no. 4, p. 19, 2016.

[100] A. Caggiano and E. Martinelli, "A unified formulation for simulating the bond behaviour of fibres in cementitious materials", Materials & Design, vol. 42, pp. 204-213, 2012.

[101] B. Barton et al., "Characterization of reinforced concrete beams strengthened by steel reinforced polymer and grout (SRP and SRG) composites", Materials Science and Engineering: A, vol. 412, no. 1-2, pp. 129-136, 2005.

[102] F. Bencardino and G. Spadea, "FE modeling of RC beams externally strengthened with innovative materials", Mechanics Research Communications, vol. 58, pp. 88-96, 2014.

[103] J. Hegger, "Load-bearing behaviour and simulation of textile reinforced concrete", Materials and Structures, pp. 0-0, 2005.

[104] E. Grande, M. Imbimbo and E. Sacco, "Numerical investigation on the bond behavior of FRCM strengthening systems", Composites Part B: Engineering, vol. 145, pp. 240-251, 2018.

[105] E. Bertolesi, F. Carozzi, G. Milani and C. Poggi, "Numerical modeling of Fabric Reinforce Cementitious Matrix composites (FRCM) in tension", Construction and Building Materials, vol. 70, pp. 531-548, 2014.

[106] J. Désir, M. Romdhane, F. Ulm and E. Fairbairn, "Steel–concrete interface: revisiting constitutive and numerical modeling", Computers & Structures, vol. 71, no. 5, pp. 489-503, 1999.

[107] J. Chen and W. Pan, "Three dimensional stress distribution in FRP-to-concrete bond test specimens", Construction and Building Materials, vol. 20, no. 1-2, pp. 46-58, 2006.

[108] V. Salomoni, G. Mazzucco, C. Pellegrino and C. Majorana, "Three-dimensional modelling of bond behaviour between concrete and FRP reinforcement", Engineering Computations, vol. 28, no. 1, pp. 5-29, 2011.

Chapter 3 Mechanical characterisation of single- and multi-ply Steel Reinforced Grout Composites

S. Alotaibi[1,2], G.E. Thermou[3], M. Guadanini[4], I. Hajirasouliha[4]

Abstract

This study investigates the tensile behaviour of single- and multi-ply Steel Reinforced Grout Composites. A total of 104 direct tensile tests were conducted on dry steel cords, textiles, and SRG coupons comprising one, two, and three layers of steel textiles that had density 4 and 8 cords/in. It was found that increasing the number of the steel textile layers was responsible for a reduction in the axial stress in the cords and the strain the grout. On the contrary, increasing the density of the steel textiles reduced the axial stress in the cords and the strain in the grout. Both steel textiles were found to develop a good composite action evident by the close and evenly distributed micro cracks. The average crack width and the crack spacing showed a decreasing trend when the reinforcement ratio was increased. The SRG coupons always failed by explosive rupture of the steel textile with a loud sound and a huge amount of dust and debris of grout expelled out of the coupons.

Keywords

Mechanical characterisation; steel reinforced grout (SRG); fabric reinforced cementitious matrix (FRCM); textile reinforced mortar (TRM); direct tensile test; composites; digital image correlation (DIC).

3.1 Introduction

Successful application of the Fabric Reinforced Cementitious Matrices (FRCM) and the Steel Reinforced Grout (SRG) composites have made them a promising candidate in the strengthening industry. These composites are made of different reinforcing materials (e.g., carbon, glass, or steel) embedded in inorganic matrices (typically grout or mortar). These inorganic systems have shown many advantages including compatibility with the substrate, ease of application, improved performance under elevated temperatures, and they are cost-efficient strengthening solutions [1-3]. These advantages enabled these systems to be a potential alternative to the Fibre Reinforced Polymer (FRP) system which suffered from a set of drawbacks mainly related to the use of the organic matrix used to impregnate the fibres in the FRP system including the relatively high cost, the poor fire performance, the lack of confidence in the long-term durability, and the poor compatibility with concrete and masonry substrates [4- 6].

The performance of the mortar-based composites in the real-life applications (e.g., confinement or flexural strengthening) is largely affected by the tensile behaviour of the reinforcing materials, the matrix, and the composite of both. This behaviour is further complicated when multiple layers of reinforcement are considered when strengthening large structural members requiring a high level of upgrade. Understanding the tensile behaviour of these composites is crucial to understand the bond and flexural behaviour. Mechanical characterisation tests are usually conducted to derive the tensile properties of these composites. Only few studies were conducted to investigate the tensile behaviour of the inorganic-based composites including FRCM and SRG systems. Direct tensile tests were caried out to evaluate the effect of different parameters including the type of the reinforcing material including carbon [5, 7-11], glass [8, 11-15], E glass [16], Alkali-Resistant (AR) glass [7, 15-17], basalt [11, 10, 13, 16], steel [1, 11-13, 18-21], aramid [16, 22], Polyparaphenylene benzobisoxazole (PBO) [8-10, 22], natural/vegetal fibres [23, 24], the type and the thickness of the matrix [5, 8, 10, 15, 16, 19], the type and the properties of the fibres [5, 8-10, 13, 16, 18, 19, 22, 23], the curing condition [15], the number of reinforcement layers [7, 8, 16], and the test setup [8, 10]. It was found that the ultimate behaviour of these composites is generally governed by the stiffer component (i.e., the embed reinforcement) whereas the contribution of the matrix is only dominant in the early stages of loading. However, the matrix was found to influence the tensile behaviour of the composite after cracking through the tension stiffening effect [1, 2, 13, 15]. Increasing the number of reinforcement layers was found to cause brittle mode of failure in FRCM composites comprising carbon, basalt, PBO, and glass textiles as it triggered delamination between the different layers of these textiles [7, 10].

Direct tensile tests generally develop a trilinear stress-strain response characterising three distinct phases including (1) uncracked section phase of high stiffness as both the matrix and the textile are resisting the applied load, and once the tensile strength of the matrix is reached, the first cracks form leading to (2) the second phase characterising a drop in the stiffness and the process of cracks formation and propagation. Finally (3) the cracked section phase is introduced once cracks saturation is reached where the textile is almost the only component resisting the applied

load and the stiffness of the composite in this stage is very similar to that developed by the bare textile [5, 12, 20-22, 25]. In the last stage, however, tension stiffening effect of the matrix will provide an enhancement to the textile as the chunks of the grout in the cracked section confining the cords/yarns will influence their behaviour in terms of axial stress and strain at failure. Tension stiffening effect largely depends on the matrix properties, the bond at the textile-to-matrix interface, and the layout of the textile [12, 25].

It is worth to mention that some composite coupons developed a bilinear stress-strain curves such that the first phase (i.e., uncracked section) was not clearly recognised [14, 19] or the last phase (i.e., fully cracked section) could not be clearly identifiable [9, 12, 15, 22]. The absence of the first phase in some studies was attributed to the relatively low stiffness matrix used to impregnate the relatively stiff textiles [14, 19], while the absence of the last stage in other studies was due to the slippage of the textiles [5] or the contemporaneously rupture of the cords [12]. The use of clevis gripping system was reported to produce a bilinear stress-strain response as it was less effective in preventing the relative slippage at the grips [8].

The inorganic composites generally exhibit a slight reduction in the stiffness, the ultimate stress, and the peak strain due to the tension stiffening effect and stress concentrations in the cracked sections [1]. The contribution of the matrix is dominant in the uncracked and cracks development phases. However, this was only observed for composites comprising textiles of low stiffness. When the stiffness of the textiles is much higher than that of the matrix, the contribution of the latter becomes almost negligible [1].

Different failure modes were reported including cracking of the matrix followed by the rupture of the reinforcement [5, 12, 15, 26], slippage of the reinforcement [5, 12, 13, 15, 26], and premature localised failure near the grip [15]. There are two different setups to perform the direct tensile tests on the coupons including the clamping grip recommended by RILEM TC 232 [27] and the clevis-grip recommended by the U.S. acceptance criteria AC434.13 [28]. Both setups are reported to produce results considerably different [14]. Furthermore, the tensile behaviour and the mode of failure of the mortar-based composites were reported to be very sensitive to the clamping method and the test setup [5, 10, 15, 26].

Among all the studies mentioned earlier, only few has considered investigating the tensile behaviour of the single-layer SRG system, not to mention the multiple layers of the same system. This study was conducted to gain a better understanding on the tensile behaviour of the SRG systems of single and multiple layers.

3.2 Experimental programme

This study investigates the mechanical behaviour of the SRG systems comprised of single and multiple layers of the steel textiles. The parameters of this study include (1) the density of the steel textiles (4 and 8 cords/in) and (2)

the number of the steel textiles layers (1, 2, and 3 layers). Direct tensile tests were carried out on a total of 104 specimens including 8 single-cord specimens, 48 dry steel textiles, and 48 SRG composite coupons.

All specimens had a total length of 600 mm. The number of the steel cords in the dry steel textile specimens was 7 or 15 cords for the specimens made of S4 or S8 textiles, respectively. All the SRG composite coupons had a width of 50 mm, while the thickness was 6 mm, 9 mm, or 12 mm for 1, 2, or 3 layers of textiles, respectively. At both ends of each specimen, a length of 100 mm was gripped in the testing machine leaving a total unbonded length of 400 mm. Further details on the gripping systems are provided in the relevant section. Fig. 3.1 provides a schematic presentation of the geometry and grip details of the specimens. Dry steel textile specimens and SRG coupons were labelled according to the following notation DTX-Y-Z where DT denotes direct tensile tests, X denotes the type of the tested specimen (T for dry textiles and C for SRG composite coupons), Y denotes the density of the steel textile (4 and 8 for the textiles that have a density of 4 and 8 cords/in, respectively), and Z denotes the number of the textile layers (1, 2, or 3 layers).

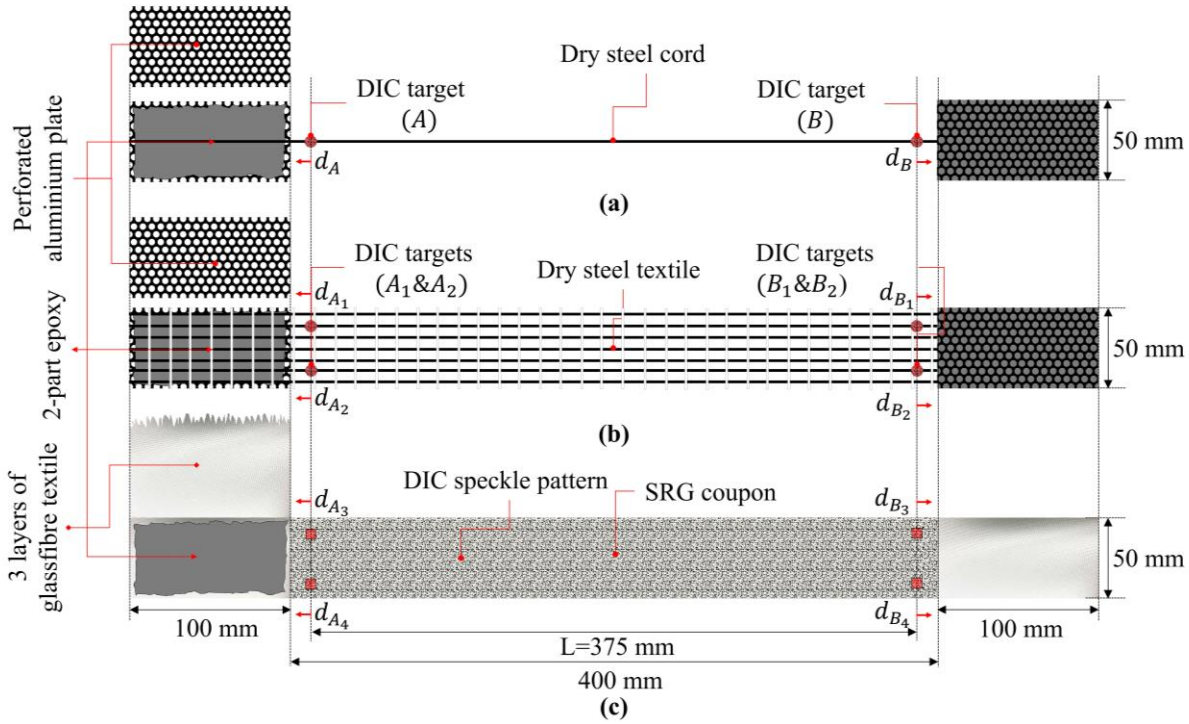

Figure 3.1 *The geometry, instrumentation, and grip details of (a) a typical single steel cord specimen, (b) a typical steel textile specimen, and (c) a typical SRG coupon.*

3.2.1 Materials

The steel textile is made of unidirectional ultra-high tensile strength steel (UHTSS) micro-cords, thermo-welded to a fibreglass micromesh. Each cord has a cross sectional area of 0.538 mm^2 and is obtained by joining 5 wires, 3 straight and 2 wrapped with a high torque angle to enhance the interlocking with the mortar. Wires have a cross

sectional area of 0.11 mm^2 and are galvanized (coated with zinc) to improve their durability. Two different textiles were used for the strengthening of the SRG coupons. These two textiles had the same mechanical properties but were different in terms of cords density namely 4 cords/in (corresponds to 1.57 cords/cm, labelled as S4) and 8 cords/in (3.15 cords/cm; S8). The steel cords in S4 textile are evenly arranged such that the clear spacing between two cords is 5.45 mm, whereas, in S8 textile, cords are paired such that the clear spacing between two pairs is 2.28 mm. The mechanical properties of the steel textiles found in the manufacturer's datasheet are provided in Table 3.1.

The matrix used to manufacture the SRG composite coupons was a pre-mixed geopolymer mortar with a crystalline reaction geo-binder base. It had average values of compressive and tensile strength of 60 N/mm^2 (CoV: 5 %) and 8 N/mm^2 (CoV: 7 %), respectively. These values were experimentally derived according to EN 1015-11 [29]. The modulus of elasticity under compression was equal to 25 kN/mm^2 according to the manufacturer's data sheet [32] The water-to-mortar powder mix ratio was 1:5 as recommended in the manufacturer's datasheet [32].

Table 3.1.1 *The mechanical properties of steel textiles according to the manufacturer's datasheet [30, 31]*

Property	S4	S8
	(N/mm^2)	(N/mm^2)
Number of cords, n	4	8
Textile density (cords/cm), ρ_{tx}	1.57	3.15
Surface mass density (g/m^2)	670	1300
Equivalent thickness of one layer (mm), $t_{tx,1}$	0.084	0.169
Average tensile strength (N/mm^2), $f_{u,tx}$	3200	
Ultimate strain (%), $\varepsilon_{u,tx}$	2.2	
Tensile modulus of elasticity (kN/mm^2), $E_{tx,II}$	186	

3.2.2 Manufacturing of the specimens

A specially designed mould made of acrylic was used to cast the SRG coupons. A typical SRG coupon was manufactured by applying a first layer of grout that had a thickness of 3 mm, then steel textile was placed on top and gently pressed by hand to ensure a good impregnation. Another layer of grout was then applied on top of the steel textile to form a sandwich with an overall thickness of 6 mm. This process was repeated for coupons with multiple layers of steel textiles. Care was taken to ensure alignment between the different layers of the steel textiles within a single coupon. This step is critical as any misalignment might introduce a nonuniform stress distribution between different layers of steel textiles. After manufacturing the SRG coupon, it was covered with a wet hessian to enhance the hydration process. Coupons were demoulded after at least three days and were then left in a place with controlled humidity (approximately 95 %) for at least 28 days.

To grip the specimens to the testing machine, two gripping systems were used. The first system was applied to the dry single cord and textile specimens. At both ends of each specimen, a total length of 100 mm was sandwiched between two perforated aluminium plates measuring 100 mm x 50 mm and impregnated in a two-part epoxy. For dry steel textile specimens with multiple layers, additional aluminium plates were added between steel textiles

inside the sandwich to keep the thickness similar to that of their SRG coupon counterparts. Similar to the SRG coupons, attention was paid to ensure the parallelism between different layers of the steel textiles in the specimen. Applying the grip directly to the cords would cause local stresses at the ends of the specimen that will trigger premature rupture. The holes in the aluminium plates will allow the epoxy to spread throughout the whole sandwich to prevent any interlaminar shear failure that might occur between different layers of the sandwich. On the other hand, the second gripping system was applied to the SRG coupons such that both ends of each coupon was strengthened with 3 layers of glass fibre textiles impregnated in a two-part epoxy adhesive (GFRP end strengthening). This step was made to prevent the brittle ends of the coupon from being crushed when gripped in the testing machine. The gripping systems and the manufacturing stages are provided in Figs. 3.2-3.3, respectively.

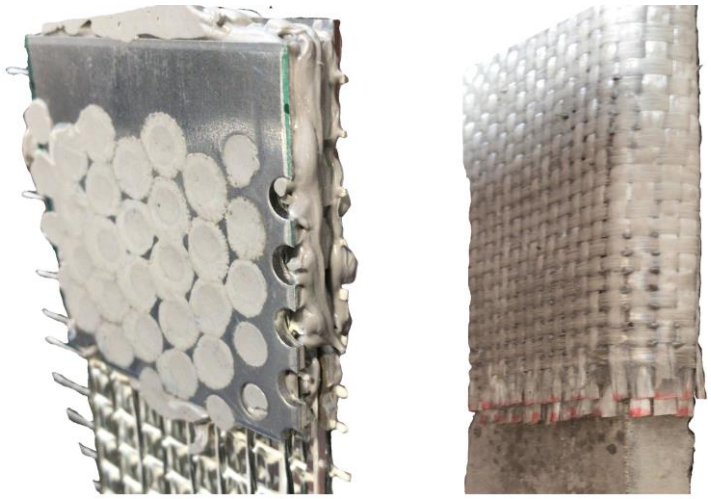

(a) **(b)**

Figure 3.2 *The grip system for (a) the dry single-cord and textiles specimens and (b) the SRG composite coupons*.

3.2.3 Test set-up and instrumentation

Direct tensile tests were carried out using a universal testing machine at a loading rate of 0.01 mm/s. Load was acquired directly from the integrated load cell in the testing machine. Strain was obtained by means of an extensometer and a Digital Image Correlation system (DIC). For the DIC system, still Images were captured at a frequency of 0.20 Hz with a digital camera of 20.2 effective megapixel resolution (canon EOS 70d). The camera was positioned at a distance of 750 mm from the tested specimen. The settings of the camera are presented in table 3.2. To enhance the contrast of the images, a LED light was pointed towards the tested specimen.

Table 3.2 *The settings of the camera for the DIC system.*

Model	Canon EOS 70D
F-stop	f/4.5
Exposure time	1/125 sec
ISO speed	ISO-160
Focal length	18 mm

Fig. 3.4 provides the general setup of the direct tensile tests. It was made sure that the sensor of the camera was parallel to the specimen to minimise any distortion. The images were processed in a digital image correlation (DIC) and evaluation software (GOM Correlate) with a facet size of 30 pixels and a point distance of 6 pixels. The extensometer was also used to obtain the strain of the grout in the SRG coupons. To attach the extensometer, two separate aluminium rods were attached to the back of the coupons by means of wooden bracket (375 mm apart) glued directly to the grout. Another two additional brackets were attached to the aluminium rods near the extensometer to keep the rods parallel to each other. These additional brackets were not glued to the coupon. Fig. 3.5 provides a schematic presentation of the extensometer setup for a typical SRG coupon.

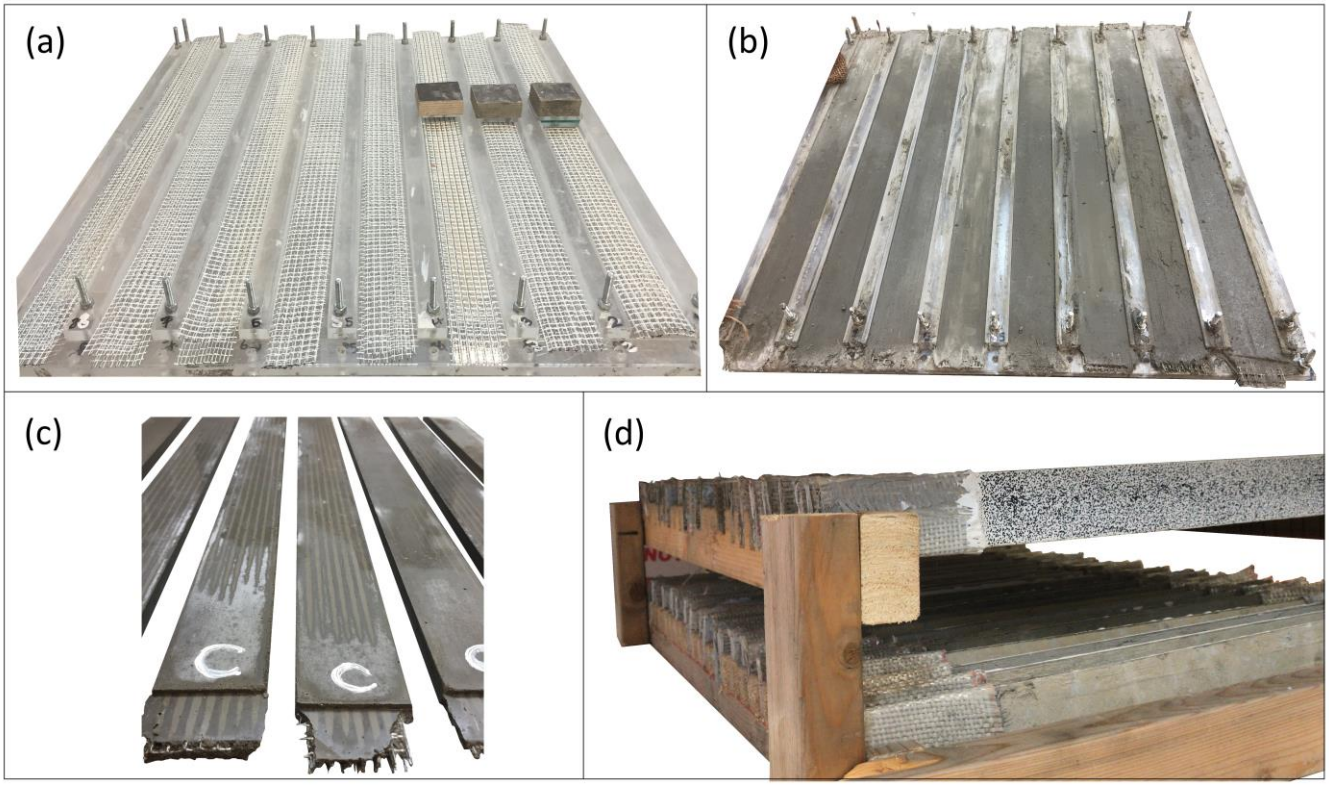

Figure 3.3 *The mould for casting the SRG coupons with the steel textiles cut to length (a), after casting (b), after demoulding (c), and the SRG coupons with GFRP end strengthening (d).*

The strain in the dry steel specimens could not be obtained by using the extensometer due to the complex geometry of the twisted steel cords and their relatively light weight. However, Digital Image Correlation (DIC) was used instead by attaching 4-mm diameter speckle targets to the cords by means of a strong adhesive. Two targets (A and B in Fig. 3.1) were attached to the dry single-cord specimens near the upper grip (A) and the lower grip (B) at a distance of 12.5 mm from the grips, whereas the dry steel textiles had four targets such that two were attached near the upper grip (Targets A_1 and A_2 in Fig. 3.1) while the other two were attached near the lower grip (Targets B_1 and B_2 in Fig. 3.1). All the targets were attached at a distance of 12.5 mm from the grips. On the other hand, both

extensometer and the DIC were used to obtain the strain of the SRG coupons. The DIC was also used to draw strain maps of the SRG coupons.

Figure 3.4 *The general setup for the direct tensile tests.*

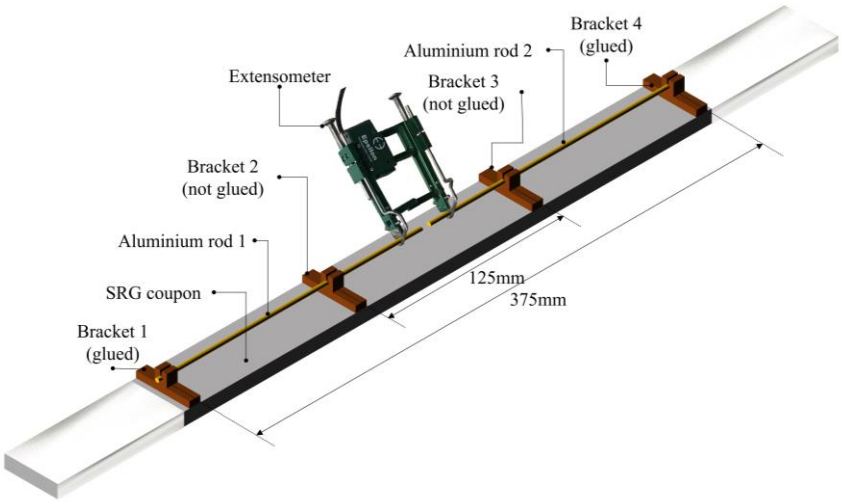

Figure 3.5 *Schematic presentation of the extensometer instrumentation setup for a typical SRG coupon.*

3.3 Test results and discussion

The main test results obtained from the direct tensile tests conducted on the single cords, the dry steel textiles, and the SRG composite coupons are presented in Tables 3.3-3.5 including the following:

- The ultimate load, P_u [kN], obtained directly from the load cell of the actuator.
- The ultimate axial stress, f_u [N/mm^2], obtained by dividing the maximum load, P_u, on the total area of the cords:

$$f_u = \frac{P_u}{n \times A_{cord}} \quad (1)$$

where n is the total number of cords in the dry steel textiles or the SRG composite and A_{cord} is the cross-sectional area of a typical steel cord, equal to 0.538 mm^2.

- The strain, in the dry single-cord specimens (ε_{cord}), the strain in the dry steel textiles (ε_{tx}), and the strain in the grout of the SRG composite coupons (ε_{com}). These strain values were calculated at the maximum load according to the following equations:

$$\varepsilon_{cord} = \frac{d_A + d_B}{L}, and\ \varepsilon_{tx} = \frac{(d_{A_1} + d_{A_2}) + (d_{B_1} + d_{B_2})}{2L} \quad (2)$$

where d_A, d_B, d_{A_1}, d_{A_2}, d_{B_1}, and d_{B_2} are defined in Fig. 3.1. L is the gauge length (375 mm).

The strain in the grout of the SRG composite (ε_{com}) was obtained from the extensometer ($\varepsilon_{com,ext.}$) and the DIC system ($\varepsilon_{com,DIC}$). They were calculated using the following equations:

$$\varepsilon_{com,ext.} = \frac{d_{ext.}}{L} \quad (3)$$

$$\varepsilon_{com,DIC} = \frac{(d_{A_3} + d_{A_4}) + (d_{B_3} + d_{B_4})}{2L} \quad (4)$$

where $\varepsilon_{grout,ext.}$ and $\varepsilon_{grout,DIC}$ are the strain of the grout obtained from the extensometer and the DIC system, respectively. $d_{ext.}$ is the reading of the extensometer, whereas d_{A_3}, d_{A_4}, d_{B_3}, and d_{B_4} are defined in Fig. 3.1.

- The moduli of elasticity of the dry steel textiles specimens and the SRG composite coupons. Fig. 3.6 provides a definition of these moduli for different zones on the stress-strain curve.

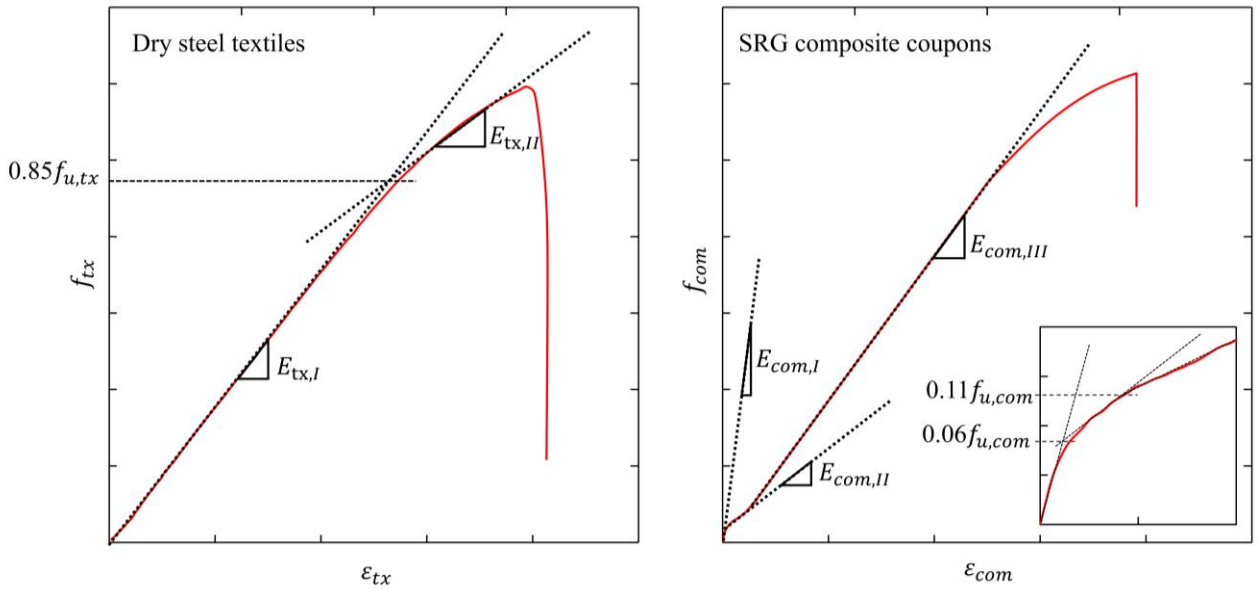

(a) **(b)**

Figure 3.6 *The definition of the modulus of elasticity for different zones on the stress-strain curve for (a) the dry steel textiles and (b) the SRG coupons.*

- The average crack width, w_{av}, the average saturation crack spacing, S_{av}, the number of cracks, n_w. For each crack, the width was measured along three longitudinal lines a, b, and c defined in Fig. 3.7. The average crack width was then calculated using the following expression:

$$w_{av} = \sum_{1}^{n=n_w} \frac{w_{av}^1 + w_{av}^2 + \cdots + w_{av}^n}{n_w} \tag{5}$$

where,

$$w_{av}^n = \frac{w_a^n + w_b^n + w_c^n}{3} \tag{6}$$

For each two consecutive cracks, the spacing was also measured along the three longitudinal lines mentioned earlier. Then, the average saturation crack spacing, S_{av}, was calculated as follows:

$$S_{av} = \frac{S_{av}^a + S_{av}^b + S_{av}^c}{3} \tag{7}$$

where,

$$S_{av}^a = \sum_{1}^{n=n_w-1} \frac{S_{1,2}^a + S_{2,3}^a + \cdots + S_{n,n_w}^a}{n_w - 1}, \tag{8}$$

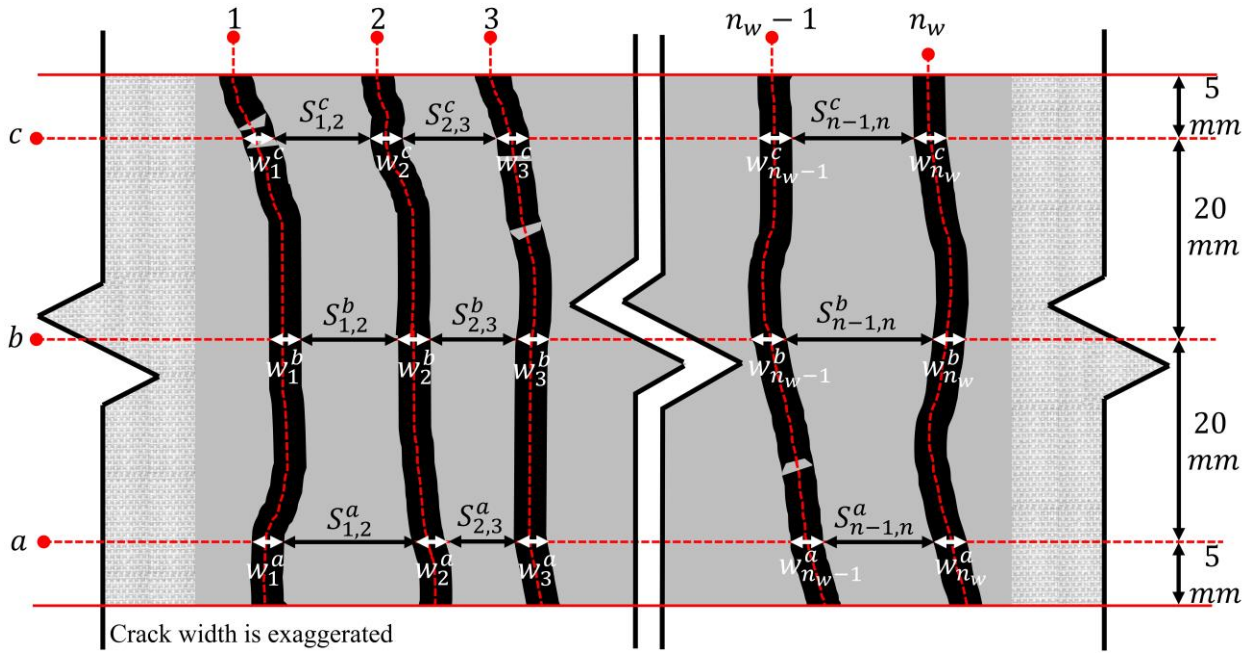

Figure 3.7 *The crack analysis for a typical SRG composite coupon.*

$$S^b_{av} = \sum_{1}^{n=n_w-1} \frac{S^b_{1,2} + S^b_{2,3} + \cdots + S^b_{n,n_w}}{n_w - 1}, and \tag{9}$$

$$S^c_{av} = \sum_{1}^{n=n_w-1} \frac{S^c_{1,2} + S^c_{2,3} + \cdots + S^c_{n,n_w}}{n_w - 1} \tag{10}$$

Table 3.3 *Results of direct tensile tests on the single steel cords.*

Specimen	$P_{u,cord}$ N	$f_{u,cord}$ N/mm^2	ε_{cord} με$\times 10^3$	$E_{cord,I}$ kN/mm^2	$E_{cord,II}$ kN/mm^2
DT-CORD-1	1633	3036	20.05	185	93
DT-CORD-2	1622	3016	18.56	193	97
DT-CORD-3	1640	3048	19.77	187	109
DT-CORD-4	1633	3035	20.86	181	96
DT-CORD-5	1635	3039	21.75	175	87
DT-CORD-6	1594	2963	19.11	183	98
DT-CORD-7	1608	2989	20.01	179	95
DT-CORD-8	1590	2955	18.21	188	102
Average	**1620**	**3011**	**19.79**	**184**	**98**
St. dev.	**20**	**37**	**1.17**	**6**	**7**
CV (%)	**2**	**2**	**6**	**4**	**7**

Table 3.4 *Results of direct tensile tests on the dry steel textile specimens.*

Specimen	$P_{u,tx}$ N	$f_{u,tx}$ N/mm^2	ε_{tx} με$\times 10^3$	$E_{tx,I}$ kN/mm^2	$E_{tx,II}$ kN/mm^2
DTT-4-1-1	11.15	2962	24.39	164	103
DTT-4-1-2	11.86	3148	21.05	175	88
DTT-4-1-3	11.51	3057	23.41	183	86
DTT-4-1-4	10.97	2914	17.13	206	125
DTT-4-1-5	11.72	3112	20.06	176	89
DTT-4-1-6	11.68	3100	20.48	182	97
DTT-4-1-7	10.82	2873	16.92	191	111
DTT-4-1-8	11.76	3123	18.22	188	92
Average	**11.43**	**3036**	**20.21**	**183**	**99**
St. dev.	**0.40**	**105**	**2.75**	**12**	**14**
CV (%)	**3.50**	**3.50**	**13.70**	**6.80**	**13.70**
DTT-4-2-1	22.46	2982	19.75	176	73
DTT-4-2-2	23.01	3055	22.2	171	87
DTT-4-2-3	23.41	3108	22.62	171	80
DTT-4-2-4	23.39	3106	19.18	179	91
DTT-4-2-5	22.87	3037	17.82	N/A	N/A
DTT-4-2-6	23.54	3125	20.6	174	79
DTT-4-2-7	23.38	3104	21.57	167	79
DTT-4-2-8	23.15	3074	18.95	181	90
Average	**23.15**	**3074**	**20.34**	**174**	**83**
St. dev.	**0.36**	**48**	**1.70**	**5**	**7**
CV (%)	**1.60**	**1.60**	**8.40**	**2.90**	**8.20**
DTT-4-3-1	32.05	2837	18.21	180	88
DTT-4-3-2	33.34	2951	19.55	180	83
DTT-4-3-3	33.42	2958	18.15	187	90
DTT-4-3-4	34.10	3018	18.52	203	101
DTT-4-3-5	34.52	3056	22.41	164	101
DTT-4-3-6	33.95	3005	20.43	182	97
DTT-4-3-7	33.55	2969	23.47	171	81
DTT-4-3-8	N/A	N/A	N/A	N/A	N/A
Average	**33.56**	**2971**	**20.11**	**181**	**91**
St. dev.	**0.79**	**70**	**2.12**	**12**	**8**
CV (%)	**2.40**	**2.40**	**10.60**	**6.90**	**9.00**
DTT-8-1-1	24.64	3054	21.81	169	85
DTT-8-1-2	24.65	3054	20.96	161	84
DTT-8-1-3	24.31	3012	20.56	178	90
DTT-8-1-4	24.29	3010	21.86	175	87
DTT-8-1-5	24.82	3076	19.54	190	83
DTT-8-1-6	24.62	3051	20.46	175	84
DTT-8-1-7	20.98	2600	18.07	172	N/A
DTT-8-1-8	23.36	2895	20.94	176	77
Average	**23.96**	**2969**	**20.53**	**174**	**84**
St. dev.	**1.29**	**159**	**1.24**	**8**	**4**
CV (%)	**5.40**	**5.40**	**6.10**	**4.80**	**5.00**
DTT-8-2-1	48.56	3009	22.62	172	97
DTT-8-2-2	49.85	3089	22.4	170	86
DTT-8-2-3	49.58	3072	20.96	176	77
DTT-8-2-4	49.52	3068	22.53	167	79
DTT-8-2-5	47.98	2973	21.22	165	61
DTT-8-2-6	49.25	3052	21.35	170	82
DTT-8-2-7	49.73	3081	20.13	185	90

DTT-8-2-8	49.17	3046	18.16	184	88
Average	**49.21**	**3049**	**21.17**	**174**	**82**
St. dev.	**0.64**	**39**	**1.50**	**7**	**11**
CV (%)	**1.40**	**1.30**	**7.10**	**4.30**	**13.40**
DTT-8-3-1	74.16	3063	22.85	156	78
DTT-8-3-2	72.30	2986	20.82	173	90
DTT-8-3-3	73.14	3021	20.19	173	85
DTT-8-3-4	73.56	3038	22.53	167	86
DTT-8-3-5	70.83	2926	18.26	186	96
DTT-8-3-6	73.32	3029	20.35	173	88
DTT-8-3-7	73.39	3032	20.22	178	N/A
DTT-8-3-8	73.05	3017	17.9	184	106
Average	**72.97**	**3014**	**20.39**	**174**	**90**
St. dev.	**1.01**	**42**	**1.76**	**10**	**9**
CV (%)	**1.40**	**1.40**	**8.70**	**5.60**	**9.80**

Table 3.5 *Results of direct tensile tests on the SRG composite coupons.*

Specimen	ρ_{com} %	$P_{u,com}$ N	$f_{u,com}$ N/mm^2	$\varepsilon_{com,ext.}$ με$\times 10^3$	$\varepsilon_{com,DIC}$ με$\times 10^3$	$E_{com,I}$ kN/mm^2	$E_{com,II}$ kN/mm^2	$E_{com,III}$ kN/mm^2	n_w	w_{av} mm	S_{av} mm
DTC-4-1-1	1.30	11.07	2940	16.25	16.42	330	120	160	53	0.35	6.64
DTC-4-1-2		11.10	2947	17.40	15.76	490	40	150	61	0.35	7.57
DTC-4-1-3		11.34	3011	16.12	17.30	780	80	170	57	0.37	7.12
DTC-4-1-4		11.40	3028	16.65	16.19	980	60	160	60	0.37	7.14
DTC-4-1-5		11.81	3135	N/A	16.85	N/A	N/A	N/A	55	0.33	6.78
DTC-4-1-6		11.73	3115	17.55	16.89	310	110	150	59	0.34	7.61
DTC-4-1-7		11.39	3025	16.84	17.66	420	90	150	56	0.36	8.08
DTC-4-1-8		11.93	3168	18.08	19.04	700	40	160	59	0.33	6.28
Average		**11.47**	**3046**	**16.98**	**17.01**	**573**	**77**	**157**	**58**	**0.35**	**7.15**
St. dev.		**0.32**	**85**	**0.72**	**1.02**	**253**	**32**	**8**	**3**	**0.02**	**0.59**
CV (%)		**2.80**	**2.80**	**4.30**	**6.00**	**44.20**	**41.50**	**4.90**	**4.70**	**4.05**	**8.23**
DTC-4-2-1	1.70	23.55	3127	16.78	19.11	890	83	172	55	0.34	7.14
DTC-4-2-2		22.65	3007	18.02	19.54	454	73	153	57	0.27	6.54
DTC-4-2-3		22.94	3045	17.96	17.87	745	107	166	60	0.27	6.49
DTC-4-2-4		23.71	3148	16.68	17.68	427	111	160	59	0.26	6.43
DTC-4-2-5		23.23	3084	16.67	17.52	558	116	161	63	0.29	5.84
DTC-4-2-6		22.56	2995	17.93	16.4	612	74	157	62	0.26	6.03
DTC-4-2-7		22.55	2994	16.94	15.51	472	110	164	61	0.36	6.78
DTC-4-2-8		23.53	3124	16.54	16.87	634	94	150	63	0.28	6.92
Average		**23.09**	**3066**	**17.19**	**17.56**	**599**	**96**	**160**	**60**	**0.29**	**6.52**
St. dev.		**0.48**	**64**	**0.66**	**1.33**	**158**	**17**	**7**	**3**	**0.04**	**0.43**
CV (%)		**2.08**	**2.09**	**3.90**	**7.60**	**26.50**	**18.20**	**4.50**	**4.80**	**12.89**	**6.65**
DTC-4-3-1	1.90	33.32	2949	16.85	18.82	475	84	154	58	0.25	6.19
DTC-4-3-2		35.35	3129	16.36	15.67	682	96	166	55	0.22	6.07
DTC-4-3-3		33.74	2986	17.18	15.77	480	94	158	61	0.31	4.96
DTC-4-3-4		35.09	3106	16.01	15.35	557	119	172	59	0.25	6.17
DTC-4-3-5		33.81	2993	17.09	19.7	524	99	148	62	0.31	5.51
DTC-4-3-6		35.73	3163	19.86	19.06	657	96	166	64	0.25	5.86
DTC-4-3-7		35.66	3156	N/A	18.23	N/A	N/A	N/A	65	0.32	6.51
DTC-4-3-8*		N/A	N/A	N/A	N/A	N/A	N/A	N/A	N/A	N/A	N/A
Average		**34.67**	**3069**	**17.23**	**17.51**	**563**	**98**	**161**	**61**	**0.27**	**5.90**
St. dev.		**1.01**	**90**	**1.37**	**1.85**	**89**	**12**	**9**	**4**	**0.04**	**0.52**
CV (%)		**2.92**	**2.94**	**8.00**	**10.60**	**15.80**	**11.80**	**5.60**	**5.75**	**13.77**	**8.76**
DTC-8-1-1	2.70	24.24	3003	18.93	19.42	678	103	154	56	0.32	6.79

DTC-8-1-2		23.79	2948	17.11	17.68	465	91	163	57	0.32	5.71
DTC-8-1-3*		N/A	N/A	N/A	N/A	N/A	N/A	N/A	N/A	N/A	N/A
DTC-8-1-4		24.67	3057	17.4	18.21	538	85	165	58	0.26	6.28
DTC-8-1-5		23.86	2957	16.29	N/A	341	97	189	61	0.32	5.54
DTC-8-1-6		24.36	3019	16.8	16.97	516	91	169	57	0.32	5.96
DTC-8-1-7		24.18	2996	18.31	17.76	301	117	171	59	0.30	6.31
DTC-8-1-8		23.52	2914	17.74	18.24	340	98	169	60	0.33	6.41
Average		**24.09**	**2985**	**17.51**	**18.05**	**454**	**97**	**169**	**59**	**0.31**	**6.14**
St. dev.		**0.39**	**48**	**0.90**	**0.82**	**136**	**10**	**11**	**2**	**0.02**	**0.43**
CV (%)		**1.62**	**1.61**	**5.20**	**4.60**	**29.90**	**10.70**	**6.40**	**3.05**	**7.33**	**7.04**
DTC-8-2-1	3.60	47.87	2966	18.81	19.36	302	109	158	61	0.21	5.45
DTC-8-2-2		49.84	3088	17.64	17.81	348	103	173	59	0.25	5.15
DTC-8-2-3		49.71	3080	18.89	19.89	577	118	170	62	0.30	5.26
DTC-8-2-4		48.23	2988	18.05	19.97	452	127	169	60	0.27	6.02
DTC-8-2-5		48.13	2982	N/A	18.97	N/A	N/A	N/A	64	0.22	4.92
DTC-8-2-6		47.88	2967	16.94	17.17	606	140	175	62	0.29	6.26
DTC-8-2-7*		N/A	N/A	N/A	N/A	N/A	N/A	N/A	N/A	N/A	N/A
DTC-8-2-8		47.13	2920	17.5	16.04	642	105	174	63	0.29	4.61
Average		**48.40**	**2999**	**17.97**	**18.46**	**488**	**117**	**170**	**62**	**0.26**	**5.38**
St. dev.		**1.00**	**62**	**0.77**	**1.49**	**142**	**14**	**6**	**2**	**0.04**	**0.59**
CV (%)		**2.07**	**2.07**	**4.30**	**8.10**	**29.20**	**12.30**	**3.70**	**2.78**	**13.77**	**10.91**
DTC-8-3-1	4.00	70.95	2931	19.41	17.8	318	119	150	65	0.25	5.61
DTC-8-3-2		74.27	3068	18.98	21.61	395	106	169	66	0.25	5.76
DTC-8-3-3		73.43	3033	17.77	17.5	358	150	166	60	0.26	4.71
DTC-8-3-4		71.28	2944	16.94	17.41	454	175	170	62	0.25	6.04
DTC-8-3-5		72.39	2990	17.15	18.58	638	122	169	58	0.24	3.94
DTC-8-3-6		73.09	3019	18.28	19.44	336	130	157	59	0.24	5.76
DTC-8-3-7		72.01	2974	17.5	16.83	463	145	167	64	0.23	4.41
DTC-8-3-8		74.76	3088	17.53	18.71	432	118	181	63	0.26	5.96
Average		**72.77**	**3006**	**17.95**	**18.49**	**424**	**133**	**166**	**63**	**0.25**	**5.28**
St. dev.		**1.36**	**56**	**0.88**	**1.52**	**102**	**22**	**9**	**3**	**0.01**	**0.80**
CV (%)		**1.87**	**1.87**	**5.00**	**8.30**	**24.00**	**16.80**	**5.60**	**4.61**	**4.45**	**15.16**

* Accidentally failed prior to loading

3.3.1 Stress-strain response

3.3.1.1 Tensile behaviour of steel cords and textiles

All the dry steel specimens including the single-cord specimens and the dry-textile specimens exhibited a stress-strain behaviour characterizing two distinct zones (Figs. 3.8-3.9). The first zone comprising a linear segment of the curve corresponding to the elastic behaviour of the cord that ended at approximately 85 % of the maximum axial stress of the cords (see Fig. 3.6). A considerable reduction in the stiffness characterised the second zone of the curve (Zone II) where the modulus of elasticity was reduced by approximately 47 % on average. The sing-cord specimens developed an average maximum load of 1.6 kN with a corresponding average axial stress of approximately 3000 N/mm^2. The corresponding strain at failure was in the range from 1.8 % to 2.2 %. The moduli of elasticity in the first and the second stages were 184 kN/mm^2 (CoV: 4 %) and 98 kN/mm^2 (CoV: 7 %), respectively.

On the other hand, the dry-textile specimens exhibited a similar behaviour to the single-cord specimens in terms of the strain at failure and the moduli of elasticity $E_{tx,I}$and $E_{tx,II}$. The maximum load resisted by the tested specimen

was proportional to the number of the steel cords. However, all the tested specimens developed a comparable average axial stress in the range from 2969 kN/mm^2 to 3074 kN/mm^2.

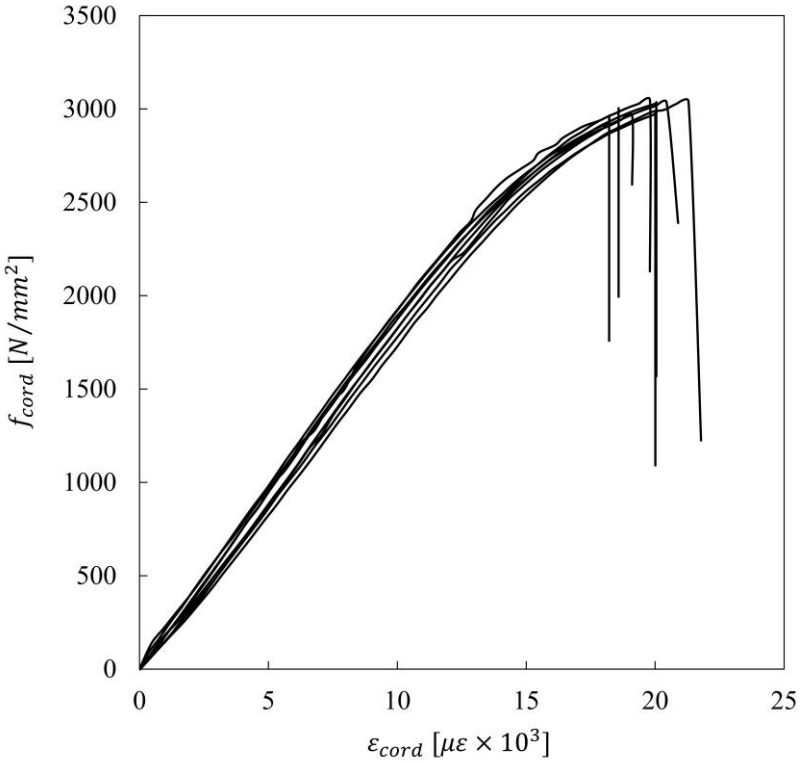

Figure 3.8 *The stress-strain curves for the direct tensile tests on dry single cords.*

3.3.1.2 Tensile behaviour of SRG coupons

The SRG composite specimens developed a three-zone stress-strain curves. The first zone was characterising a stiff behaviour due to the contribution of the grout to the system and lasted as soon as the first crack occurred in the coupons at a stress value of approximately 6 % of the maximum axial stress (see Fig. 3.6). In the second zone characterised a noticeable reduction in the stiffness with more new micro cracks were forming. This zone represents the transition phase where the stress transfer mechanism was gradually transferred from the cracking grout to the steel textile. This transition phase was completed when the grout was fully cracked, and this occurred at a stress level of approximately 11 % of the maximum attained stress (see Fig. 3.6). The third zone comprises coupons of cracked sections where the current cracks were widening. The last stage was governed by the behaviour of the textiles and the grout has no contribution except for tension stiffening effect which insignificantly enhanced the tensile behaviour of the cords as they failed at a slightly higher axial stress.

Figs. 3.9-3.11 provide a comparison between the stress-strain curves for the dry steel textiles and that of the SRG coupons. Each specimen of the dry steel textiles was plotted against that of the SRG coupons that had the same reinforcement (e.g., DTT-4-1 against DTC-4-1).

For the same steel textile reinforcement (in terms of the density and the number of layers), the SRG coupons exhibited a stiffer behaviour in the first stage compared to that of the dry textiles. This is mainly due to contribution of the grout confining each cord and hence limiting the strain in that cord. This principle holds true for the cracked sections where the chucks of the grout attached to the cords between cracks helped in reducing the strain in the cords at failure when compared to their dry textile counterparts.

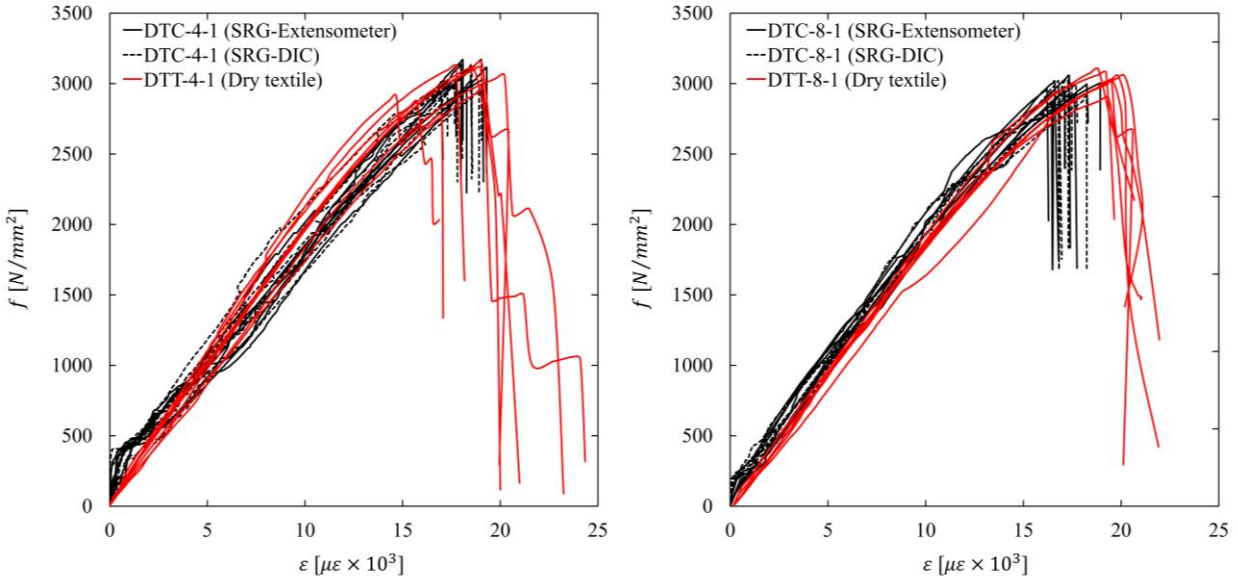

Figure 3.9 *The stress-strain curves for the direct tensile tests on the dry steel textiles and the SRG coupons for series 4-1 (left) and series 8-1 (right).*

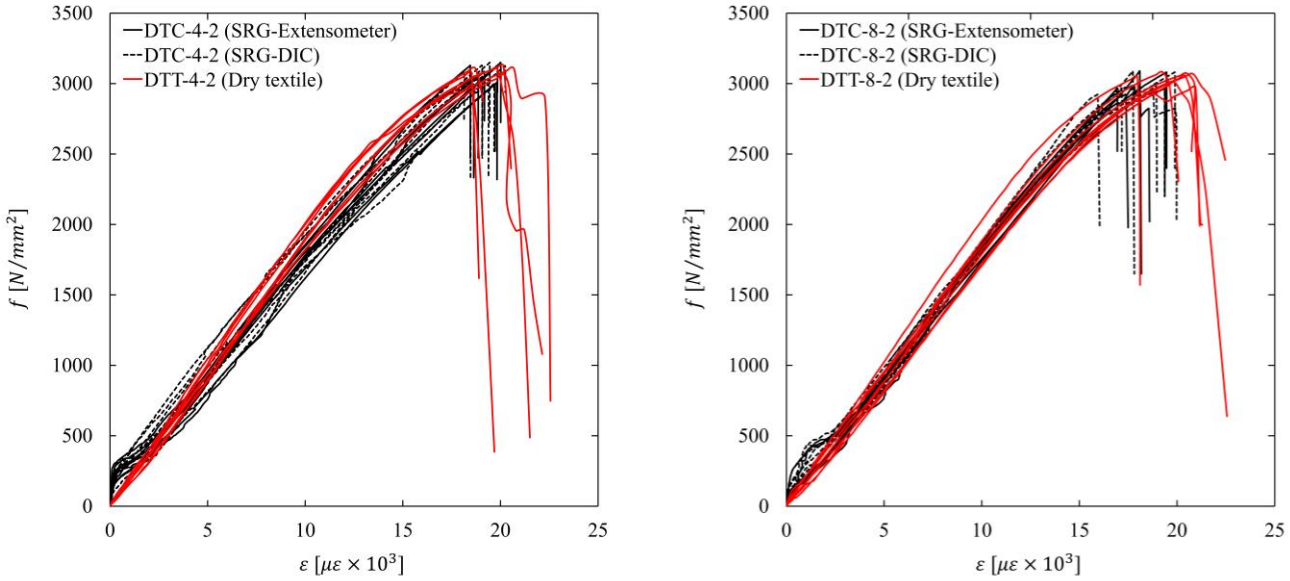

Figure 3.10 *The stress-strain curves for the direct tensile tests on the dry steel textiles and the SRG coupons for series 4-2 (left) and series 8-2 (right).*

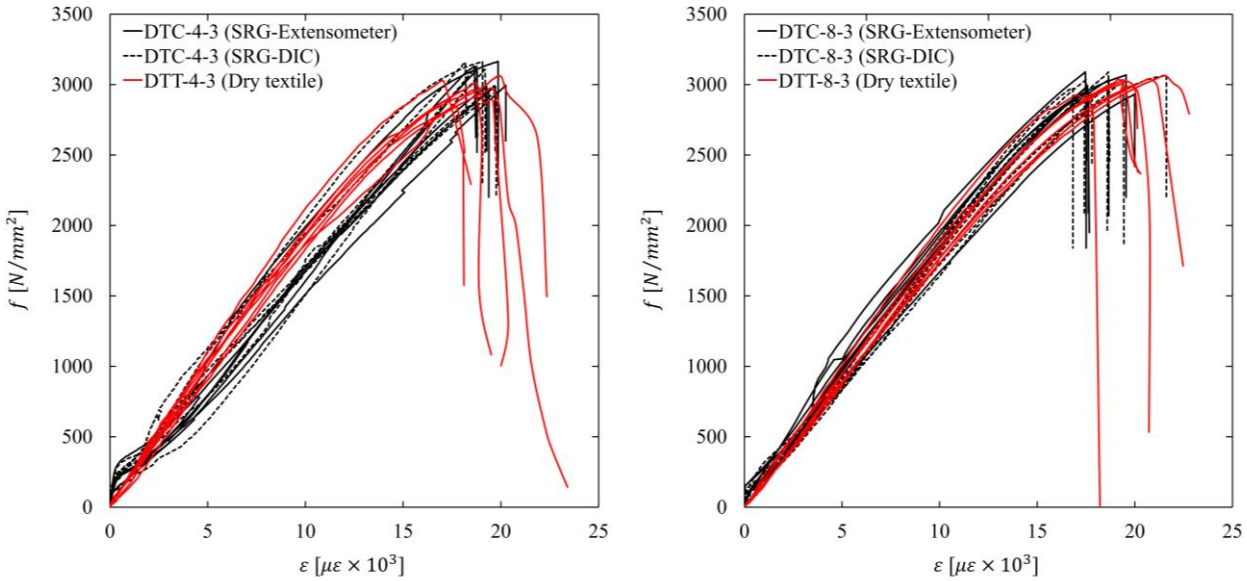

Figure 3.11 *The stress-strain curves for the direct tensile tests on the dry steel textiles and the SRG coupons for series 4-3 (left) and series 8-3 (right).*

3.3.2 Failure modes

3.3.2.1 Failure of the dry steel cords and textiles

All the dry single-cord specimens failed by tensile rupture at the middle of the cord (see Fig. 3.12) after the axial stress (approximately 3011 N/mm^2, on average) reached the ultimate tensile stress of the cord. The dry textile specimens failed in a fashion similar to that of the single cords at an axial stress of approximately 3018 N/mm^2 on average (see Fig. 3.13). The cords within a dry textile did not break simultaneously as they were not perfectly identical due to imperfections during manufacturing and testing, instead the break chain started with the rupture of a random cord immediately followed by progressive rupture of other cords and often ended by a simultaneous rupture of final bunch of cords with a loud rupture sound. It is worth noting that no signs of slippage at the grip area were observed during testing and this was confirmed by the visual inspection of the grip sandwich after each test.

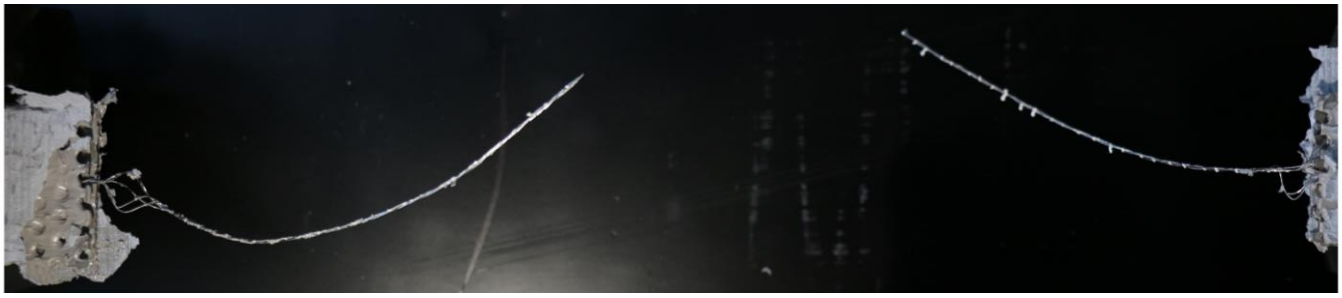

Figure 3.12 *Typical mode of failure for single steel cord specimens.*

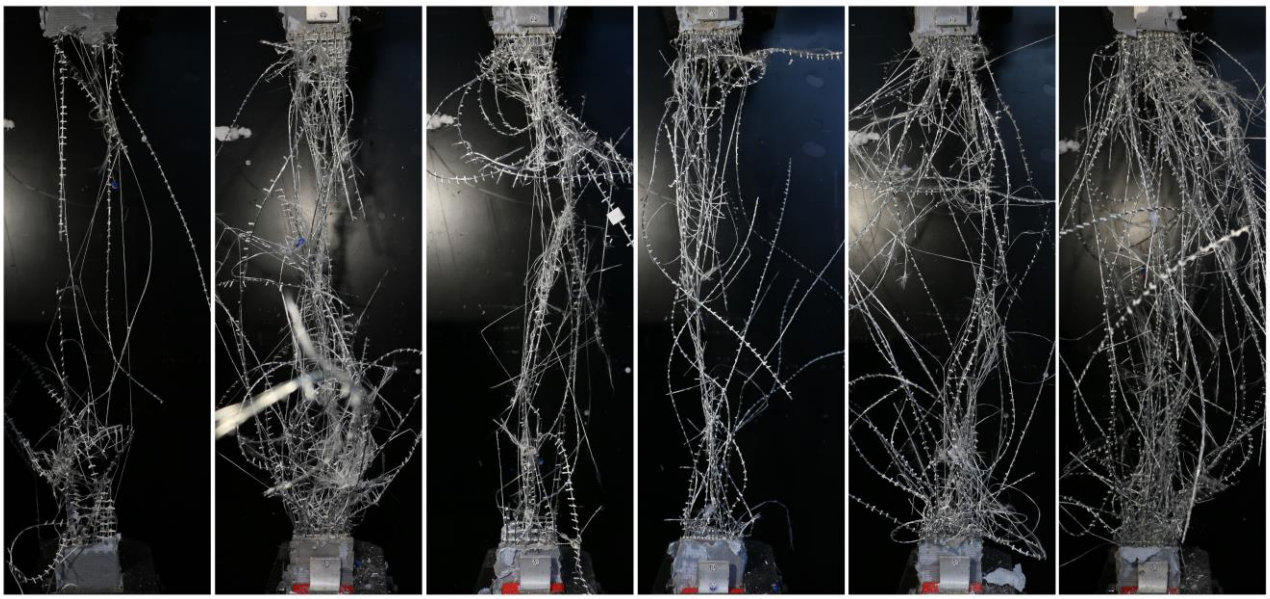

(a) **(b)** **(c)** **(d)** **(e)** **(f)**

Figure 3.13 *Typical mode of failure for dry steel textiles (a) series DTT-4-1, (b) series DTT-4-2, (c) series DTT-4-3, (d) series DTT-8-1, (e) series DTT-8-2, and (f) series DTT-8-3.*

3.3.2.2 Failure of the SRG coupons

The SRG composite coupon, on the other hand, exhibited hair cracks in the first zone and was confirmed by the DIC measurements (Fig. 3.14). These cracks firstly initiated at either ends of the coupon as a result of local stresses that was introduced by the clamping force. The cracks were, then, initiating along the full length of the coupon and were evenly distributed. This is an indication of the better bond between the steel textiles and the grout as the whole sections of the coupon were engaged in resisting the applied load (i.e., enhanced composite action). In most cases, the mode of failure observed for the SRG coupons was explosive with a loud sound and a huge amount of dust and debris of grout expelled out of the coupons. This energy release was more pronounced for the SRG coupons comprising multiple layers of S8 textiles as it resisted higher loads before failure and so the released energy was higher. Fig. 3.15 provides images after failure for representatives specimens from each tested series. All the tested SRG coupons develop comparable crack patterns (see Fig. 3.14).

In general, when the reinforcement ratio was increased, the average spacing between cracks and the average crack width were slightly decreased. For instant, series DTC-4-1 (one layer of textile; $\rho_{com} = 1.3$ %) developed 58 cracks on average spaced at 7.15 mm with an average crack width of 0.35 mm. When the reinforcement ratio was increased to 1.7 % in series DTC-4-2 (two layers), the number of cracks was 60 on average. However, the average crack spacing and the average crack width decreased by approximately 13 % and 17 %, respectively compared to series DTC-4-2. In series DTC-4-3 ($\rho_{com} = 1.9$ %), the decrease was 17 % and 23 %, respectively, compared to DTC-4-1. Similar trends were also observed in the SRG coupons strengthened with S8 textiles when the reinforcement ratio was increased.

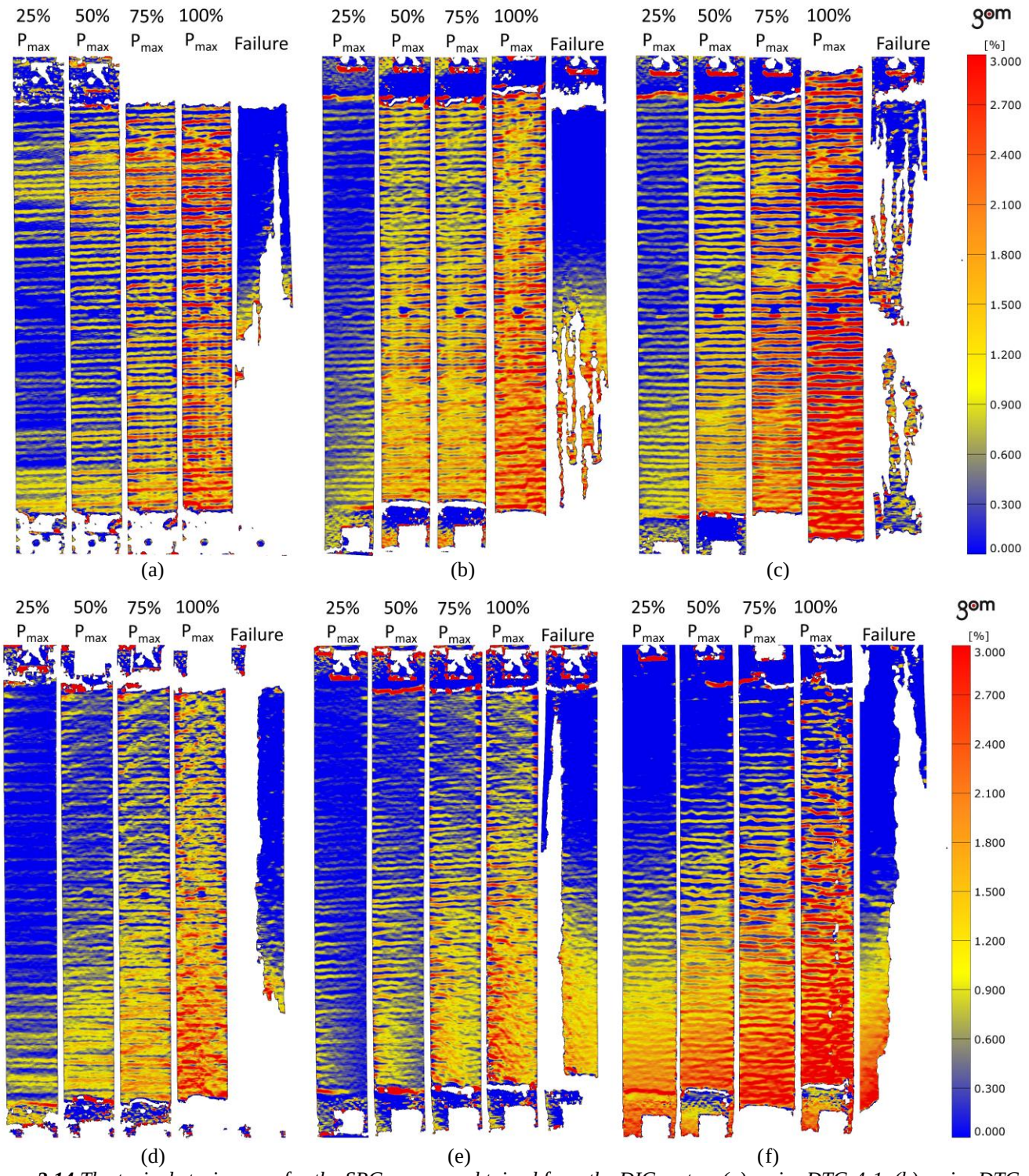

Figure 3.14 *The typical strain maps for the SRG coupons obtained from the DIC system (a) series DTC-4-1, (b) series DTC-4-2, (c) series DTC-4-3, (d) series DTC-8-1, (e) series DTC-8-2, and (f) series DTC-8-3.*

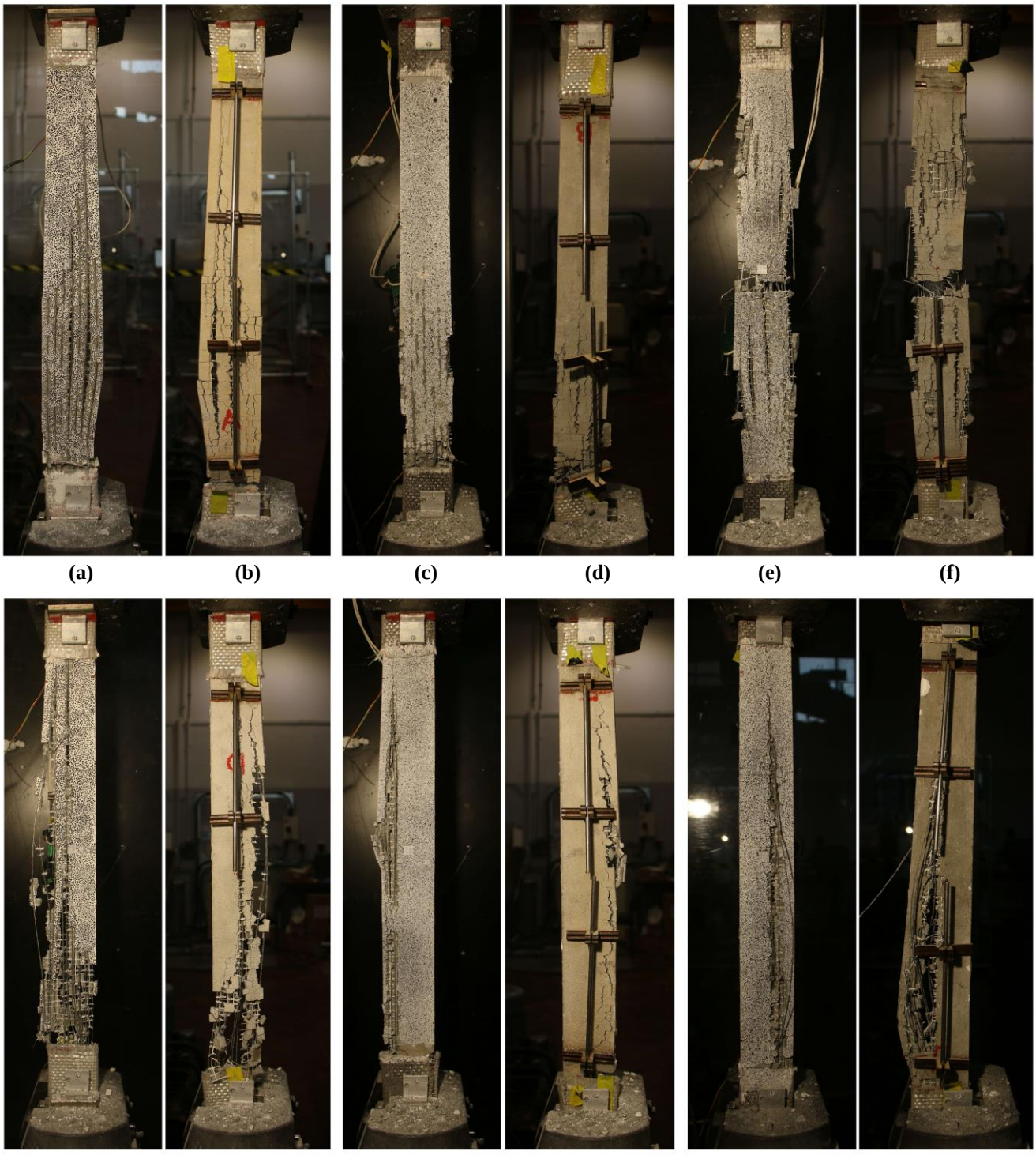

(a) **(b)** **(c)** **(d)** **(e)** **(f)**

(g) **(h)** **(i)** **(j)** **(k)** **(l)**

Figure 3.15 *Typical mode of failure for SRG coupons (a&b) series DTC-4-1, (c&d) series DTC-4-2, (e&f) series DTC-4-3, (g&h) series DTC-8-1, (i&j) series DTC-8-2, and (k&l) series DTC-8-3.*

3.3.3 Effect of the number of textile layers

Increasing the number of the steel textiles layers resulted in an insignificant increase in the axial stress in the cords for both steel textiles S4 and S8. The increasing trend can be observed in Fig. 3.16, as the axial stress was increased by adding a second layers of steel textiles. However, the increase in the axial stress associated with the use of three layers of the steel textile was considerably lower when compared to that observed for the transition from one to two layers of the steel textiles. As the number of the steel textiles layers was increased, the thickness of the SRG coupons was increased from 6 mm to either 9 mm or 12 mm for two and three layers, respectively. These new sections of larger areas required higher stresses to cause cracking in the grout and after these sections were fully cracked, the chunks of the grout between the cracks helped the cords to break at higher tensile stresses (i.e., tension stiffening effect) compared to one layer of the steel textiles. This also explains the similar trends that were observed for the strain of the grout. Similar to the effect on the axial stress, the increase in the strain of the composite in the transition from two to three layers was less pronounced. It is worth noting that this trend was observed for both instrumentation systems, the extensometer and the DIC system. The larger thickness of the SRG coupons comprising two and three layers of the steel textiles compared to that of one layer delayed the process of cracks propagation as they had to propagate through a larger surface area compared to the SRG coupons comprising only one layer of the steel textiles.

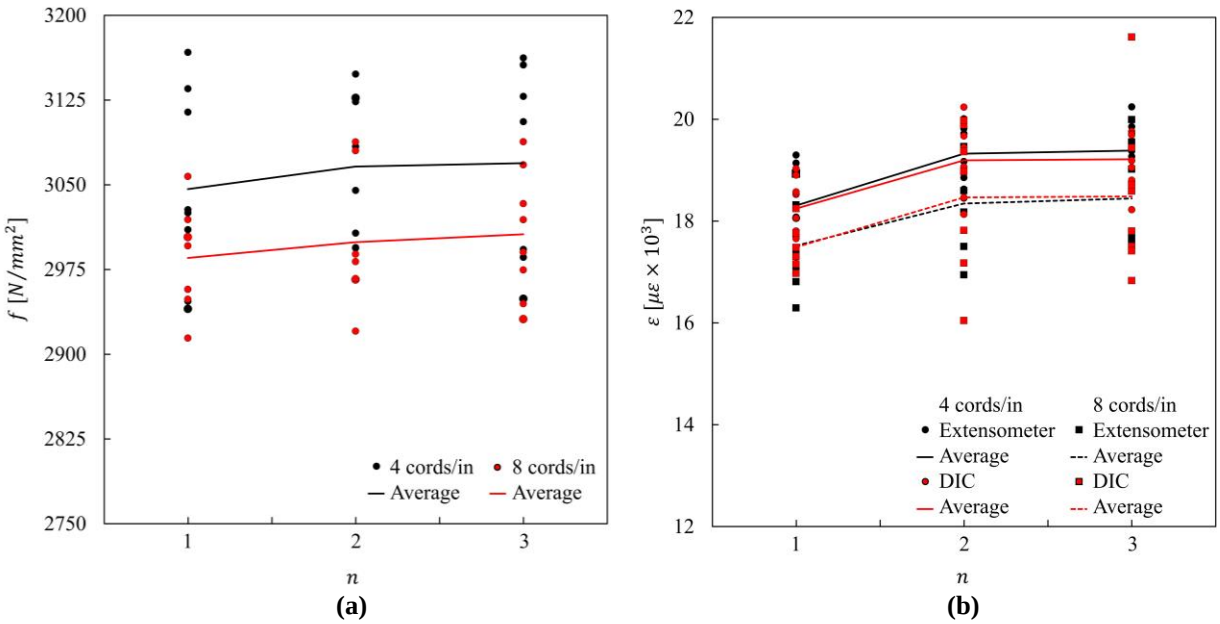

Figure 3.16 *The effect of the number of layers on (a) the axial stress in the dry textiles and (b) the strain of the SRG composites.*

3.3.4 Effect of the density of steel textile

Fig. 3.17 provides graphs to measure the effect of increasing the density of the steel textile on the tensile behaviour of the SRG composites in terms of the axial stress and the strain of the grout. There was a slight reduction in the axial stress in the cords as the density of the steel textile was doubled (4 to 8 cords/in). The reduction in the axial stress for the transition from one to two layers was more pronounced compared to that for the transition from two

to three layers of the steel textile. The denser structure of the S8 steel textiles hindered the process of full impregnation between the grout and the cords and created regions prone to cracking at lower stresses compared to that in the S4 steel textile. This caused the grout to crack at a lower axial stress and the chunks of the grout between the cracks that remined attached to the cords were lower in volume compared to that in the SRG coupons comprising S4 textiles. These chunks of grout that had a reduced volume insignificantly enhanced the tensile strength of the cords through tension stiffening effect. However, this enhancement was less than that provided by the bigger chunks of grout seen in the SRG coupons that had S4 textiles and this explains the reduction in the axial stress in the cords when the density of the steel textiles was increased from 4 to 8 cords/in. On the other hand, increasing the density of the steel textiles was of a contrary effect to that observed when increasing the number of the steel textile layers.

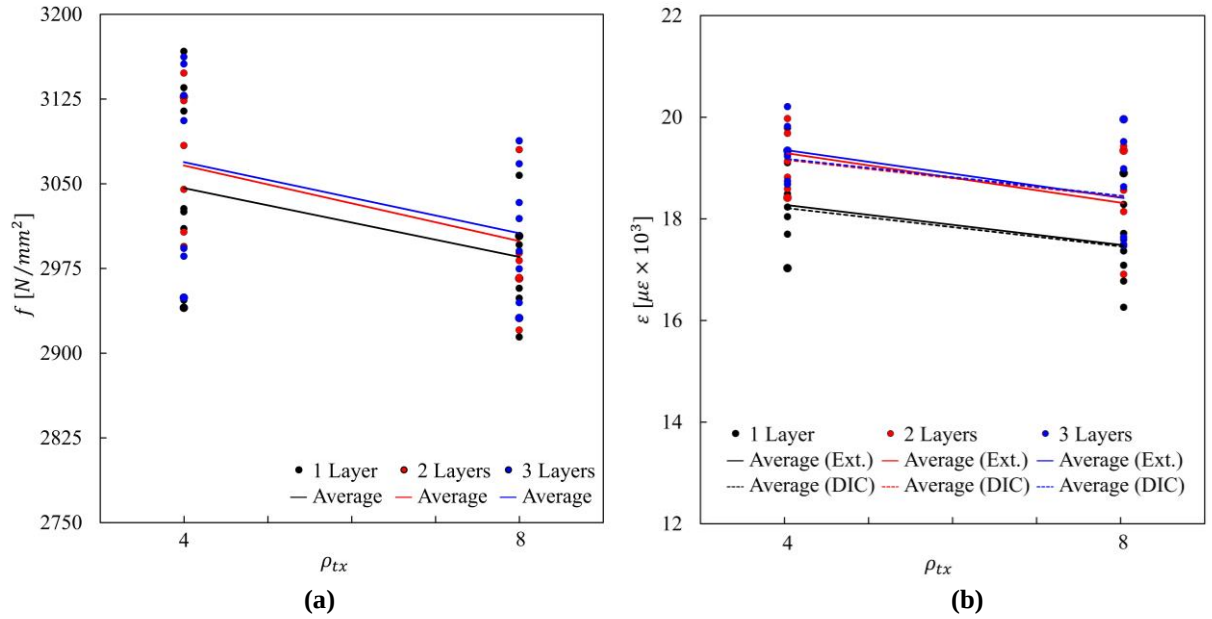

(a) **(b)**

Figure 3.17 *The effect of the density of textile on (a) the axial stress in the dry textiles and (b) the strain of the SRG composites.*

As explained earlier, the high density of the steel textile comprising 8 cords/in, relative to that of 4 cords/in, created weak surfaces between the cords and the grout that promoted cracks at earlier stages which ultimately caused the SRG coupons to strain at higher rates compared to that seen for the SRG coupons comprising S4 steel textiles. This also holds true for the SRG coupons comprising two and three layers of the steel textiles as there was a reduction in the strain of the grout when increasing the density of the steel textiles from 4 to 8 cords/in. This reduction was comparable to that observed for the SRG coupons that had one layer when increasing the density of the steel textiles.

3.3.5 Effect of the geometric reinforcement ratios

The geometric reinforcement ratio, ρ_{com}, is defined as the ratio of the cross-sectional area of the fibres, A_{tx}, to the cross-sectional area of the matrix, A_{com}. It can be calculated using the following expression

$$\rho_{com} = \frac{A_{tx}}{A_{com}} = \frac{n \cdot A_{cord}}{t_{com} \cdot b_{com}} \tag{11}$$

where t_{com} is the overall thickness of the SRG composite coupon (6 mm, 9 mm, and 12 mm for SRG coupons comprising one, two, and three layers, respectively) and b_{com} is the width of the SRG composite coupon (50 mm).

Fig. 3.18 provides graphs to explain the effect of increasing the geometric reinforcement ratio, ρ_{com}, on the axial tensile stress and the strain in the steel cords. The values of the moduli of elasticity for the SRG coupons in the three zones are expressed as a function in the geometric reinforcement ratio in Fig. 3.19.

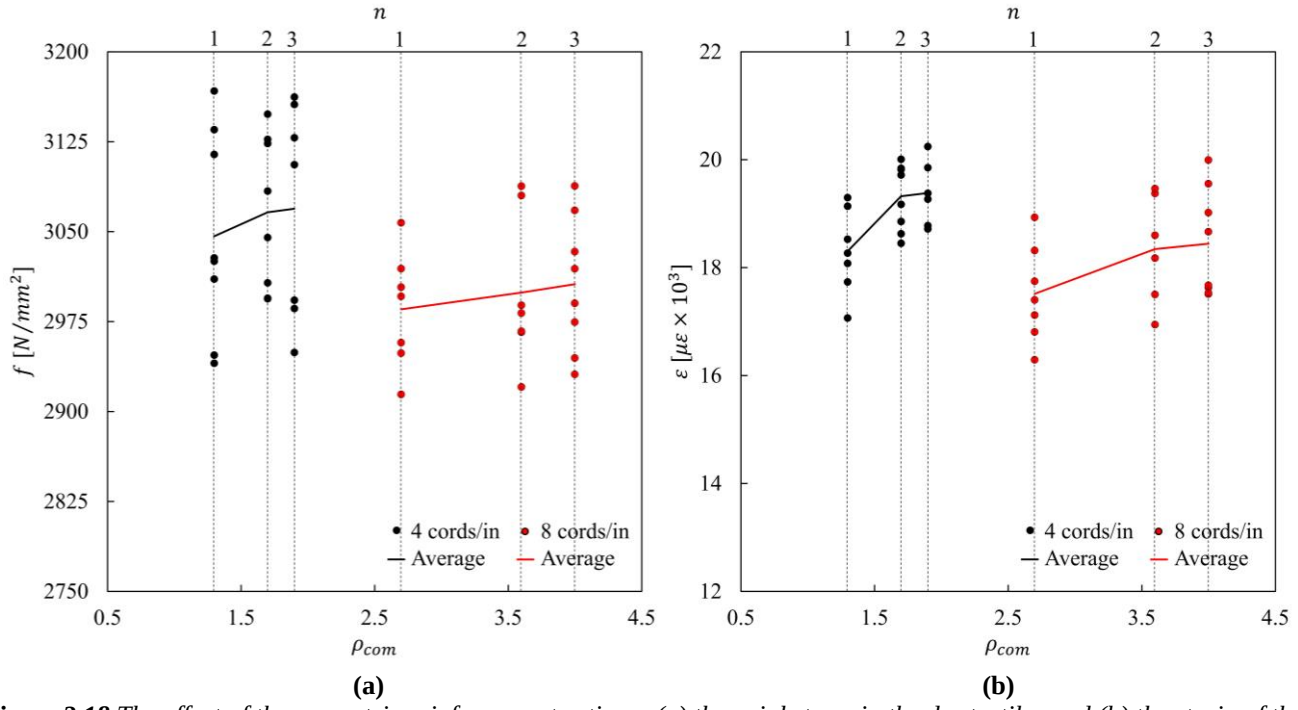

Figure 3.18 *The effect of the geometric reinforcement ratio on (a) the axial stress in the dry textiles and (b) the strain of the grout.*

It was observed that increasing the geometric reinforcement ratio was always associated with an increase in the maximum axial stress and the corresponding strain for both steel textiles S4 and S8. This increase was sound for the transition from one to two layers of both steel textiles. However, this increase was insignificant for reinforcement ratios greater than 1.7 for S4 textiles and 3.6 for S8 textiles (see Fig. 3.19). The modules of elasticity in the first zone, $E_{com,I}$, was in the range from 560 N/mm^2 to 600 N/mm^2 and from 420 N/mm^2 to 490 N/mm^2 for S4 and S8 steel textiles. There was an insignificant increasing trend in $E_{com,I}$ when the geometric reinforcement ratio was increased to approximately 30 % (i.e., increasing the number of layers from one to two for both steel textiles). This increase in $E_{com,I}$ was approximately 4 % and 7 % for S4 and S8 textiles, respectively. However, when ρ_{com} was further increased by approximately 11 % (from 2 to 3 layers), there was a slight decreasing trend in the values of the modulus of the elasticity $E_{com,I}$ for both steel textiles. The SRG coupons strengthened with the S4 textiles

exhibited a decrease in $E_{com,I}$ of approximately 7 %, while the percentage of decrease in their S8 textiles counterparts was 13 %.

When the cracking phase starts in the SRG coupon (represented by $E_{com,II}$ on the stress-strain curve) grout contribution to the stress transfer mechanism is still predominant and this evident by the increasing trend in the values of $E_{com,II}$. The increase in this latter was approximately 25 % and 21 % when ρ_{com} was increased by approximately 30 % for S4 and S8 textiles, respectively. However, when the ρ_{com} was increased by approximately 47 % (i.e., increasing the number of textile layers from 2 to 3) the SRG coupons strengthened with S4 textiles only exhibited a slight increase of only 2 % compared to the reinforcement ratio associated with only one layer. While their S8 textile counterparts developed an increase in $E_{com,II}$ of approximately 17 % with respect to the reinforcement ratio associated with one layer of the same textile. No significant changes were observed in the modules of elasticity in the third zone $E_{com,III}$ when the geometric reinforcement ratio was increased. All the tested specimens developed comparable values of $E_{III,SRG}$ ranging from 77 kN/mm^2 to 133 kN/mm^2.

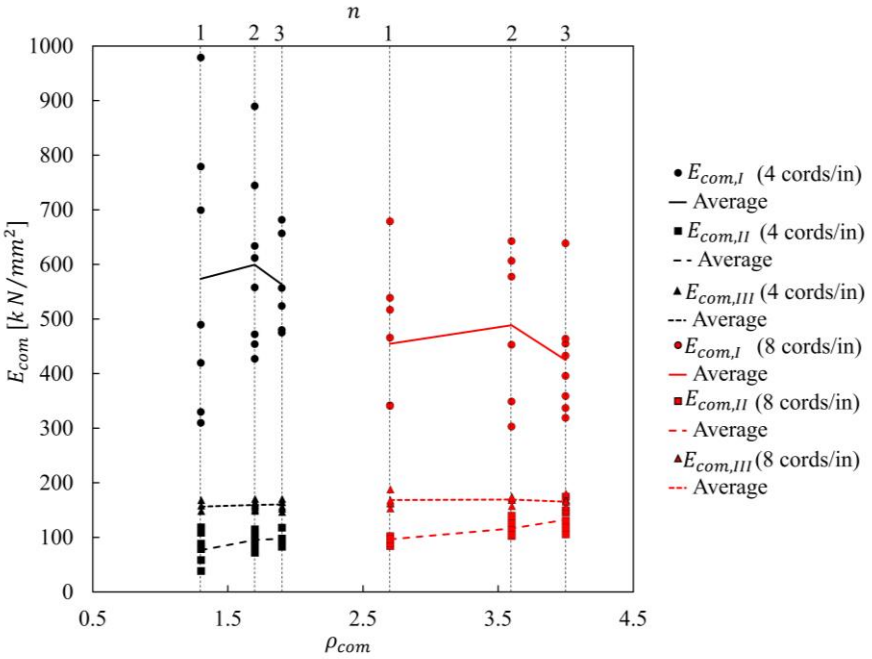

Figure 3.19 *The moduli of elasticity of the SRG composite coupons for different geometric reinforcement ratios and different number of layers.*

3.4 Conclusions

The aim of the study was to investigate the tensile behaviour of the SRG composites. Two parameters were investigated including the number and the density of steel textile layers. SRG coupons of one, two, and three layers were manufactured using steel textiles with two different densities (4 and 8 cords/in). Direct tensile tests were

conducted on a total of 104 specimens including single dry cords, dry textiles, and SRG coupons. The following conclusions are drawn:

1. The SRG coupons exhibited a three-zone stress-strain behaviour. The first zone had a stiff behaviour characterising the contribution of the grout, while the second zone described the process of cracks initiation and propagation. The end of this latter process led to the last stage where the applied load was mainly resisted by the steel textile only with a slight contribution of the grout (tension stiffening). The SRG coupons, compared to the dry textiles, developed a stiffer initial behaviour due to the contribution of the grout. Also, they developed a slightly higher axial stress due to the tension stiffening effect of the grout. It was found that increasing the number of the steel textile layers enhanced to axial stress in the cords and the strain of the grout. However, this enhancement was sound for the transition from one to two layers of the steel textiles.

2. The increased thickness of the SRG coupons comprising more layers helped the cords to attain higher axial loads as the chunks of grout providing tension stiffening were larger in volume compared to that for the SRG coupons comprising only one layer of the steel textiles. Also, the increased cross sections in the SRG coupons of multiple layers required higher energy to propagate cracks throughout the section and hence resulted in increasing the strain of the grout. On the other hand, increasing the density of the steel textiles from 4 to 8 cords/in reduced the axial stress in the cords and the strain of the grout.

3. The dense structure of the steel textiles comprising 8 cords/in impeded the impregnation of the steel cords into the grout and hence created weak surfaces that cracked at earlier stages. The chunks of grout that remained attached to the steel cords were of lower volume compared to that developed by the SRG coupons comprising steel textiles of 4 cords/in. Although these smaller chunks of grout provided a slight improvement to the tensile stress of the cords, this improvement was less than that observed for the case of the S4 steel textiles.

4. The evenly distributed micro cracks observed in most of the SRG coupons indicated that there was a good mechanical interlock between the twisted cords and the grout suggesting that both steel textiles can develop a good composite action.

Further research is needed to investigate different densities of the steel textiles, especially these with dense cord structure (cords density greater than 8 cords/in) to see if they compromise the mechanical interlock between the cords and the grout. Also, further studies are required to examine different types of grout matrices. In particular, these with low mechanical characteristics (ideal for masonry strengthening) to assess their role with the steel cords in the stress transfer mechanism.

Acknowledgment

The materials for this experiment (the steel textiles and mortar) were provided by Kerakoll S.p.A. (Sassuolo, MO, Italy). The first author would like to thank Shaqra University in Saudi Arabia and Saudi Arabian Cultural Bureau (SACB) in the UK for funding this part of his PhD research.

References

[1] De Santis, S. and de Felice, G., 2015. Tensile behaviour of mortar-based composites for externally bonded reinforcement systems. *Composites Part B: Engineering*, 68, pp.401-413.

[2] de Felice, G., D'Antino, T., De Santis, S., Meriggi, P. and Roscini, F., 2020. Lessons Learned on the Tensile and Bond Behavior of Fabric Reinforced Cementitious Matrix (FRCM) Composites. *Frontiers in Built Environment*, 6.

[3] de Felice G, De Santis S, Garmendia L et al. Mortar-based systems for externally bonded strengthening of masonry. Mater Struct. 2014;47(12):2021-2037.

[4] Fédération Internationale du Béton, Externally bonded FRP reinforcement for RC structures. Fib Bulletin 14, 2001, Lausanne, Switzerland.

[5] Carozzi, F., Bellini, A., D'Antino, T., de Felice, G., Focacci, F., Hojdys, Ł., Laghi, L., Lanoye, E., Micelli, F., Panizza, M. and Poggi, C., 2017. Experimental investigation of tensile and bond properties of Carbon-FRCM composites for strengthening masonry elements. *Composites Part B: Engineering*, 128, pp.100-119.

[6] Huang X, Birman V, Nanni A, Tunis G. Properties and potential for application of steel reinforced polymer and steel reinforced grout composites. Composites Part B: Engineering. 2005;36(1):73-82.

[7] Younis, A., Ebead, U. and Shrestha, K., 2019. Tensile characterization of multi-ply fabric-reinforced cementitious matrix strengthening systems. *Structural Concrete*, 21(2), pp.713-723.

[8] Arboleda, D., Carozzi, F., Nanni, A. and Poggi, C., 2016. Testing Procedures for the Uniaxial Tensile Characterization of Fabric-Reinforced Cementitious Matrix Composites. *Journal of Composites for Construction*, 20(3), p.04015063.

[9] Ebead, U., Shrestha, K., Afzal, M., El Refai, A. and Nanni, A., 2017. Effectiveness of Fabric-Reinforced Cementitious Matrix in Strengthening Reinforced Concrete Beams. *Journal of Composites for Construction*, 21(2), p.04016084.

[10] Donnini, J. and Corinaldesi, V., 2017. Mechanical characterization of different FRCM systems for structural reinforcement. *Construction and Building Materials*, 145, pp.565-575.

[11] D'Antino, T. and Papanicolaou, C., 2018. Comparison between different tensile test set-ups for the mechanical characterization of inorganic-matrix composites. *Construction and Building Materials*, 171, pp.140-151.

[12] Bilotta, A., Ceroni, F., Nigro, E. and Pecce, M., 2017. Experimental tests on FRCM strengthening systems for tuff masonry elements. *Construction and Building Materials*, 138, pp.114-133.

[13] Bilotta, A., Ceroni, F., Lignola, G. and Prota, A., 2017. Use of DIC technique for investigating the behaviour of FRCM materials for strengthening masonry elements. *Composites Part B: Engineering*, 129, pp.251-270.

[14] D'Antino, T., Calabrese, A. and Poggi, C., 2020. Experimental procedures for the mechanical characterization of composite reinforced mortar (CRM) systems for retrofitting of masonry structures. *Materials and Structures*, 53(4).

[15] Leone, M., Aiello, M., Balsamo, A., Carozzi, F., Ceroni, F., Corradi, M., Gams, M., Garbin, E., Gattesco, N., Krajewski, P., Mazzotti, C., Oliveira, D., Papanicolaou, C., Ranocchiai, G., Roscini, F. and Saenger, D., 2017. Glass fabric reinforced cementitious matrix: Tensile properties and bond performance on masonry substrate. *Composites Part B: Engineering*, 127, pp.196-214.

[16] Contamine, R., Si Larbi, A. and Hamelin, P., 2011. Contribution to direct tensile testing of textile reinforced concrete (TRC) composites. *Materials Science and Engineering: A*, 528(29-30), pp.8589-8598.

[17] Colombo, I., Magri, A., Zani, G., Colombo, M. and di Prisco, M., 2013. Erratum to: Textile Reinforced Concrete: experimental investigation on design parameters. *Materials and Structures*, 46(11), pp.1953-1971.

[18] Thermou, Georgia & Felice, Gianmarco & De Santis, Stefano & Alotaibi, Sultan & Roscini, Francesca & Hajirasouliha, Iman & Guadagnini, Maurizio. (2018) Mechanical characterization of multi-ply steel reinforced grout composites for the strengthening of concrete structures. CICE 2018. 9th International Conference on Fibre-Reinforced Polymer (FRP) Composites in Civil Engineering, 17-19 Jul 2018, Paris, France. IIFC , pp. 298-305.

[19] Mazzuca, S., Hadad, H., Ombres, L. and Nanni, A., 2019. Mechanical Characterization of Steel-Reinforced Grout for Strengthening of Existing Masonry and Concrete Structures. *Journal of Materials in Civil Engineering*, 31(5), p.04019037.

[20] De Santis, S., Ceroni, F., de Felice, G., Fagone, M., Ghiassi, B., Kwiecień, A., Lignola, G., Morganti, M., Santandrea, M., Valluzzi, M. and Viskovic, A., 2017. Round Robin Test on tensile and bond behaviour of Steel Reinforced Grout systems. *Composites Part B: Engineering*, 127, pp.100-120.

[21] De Santis, S. and de Felice, G., 2015. Steel reinforced grout systems for the strengthening of masonry structures. *Composite Structures*, 134, pp.533-548.

[22] Caggegi, C., Carozzi, F., De Santis, S., Fabbrocino, F., Focacci, F., Hojdys, Ł., Lanoye, E. and Zuccarino, L., 2017. Experimental analysis on tensile and bond properties of PBO and aramid fabric reinforced cementitious matrix for strengthening masonry structures. *Composites Part B: Engineering*, 127, pp.175-195.

[23] Mercedes, L., Gil, L. and Bernat-Maso, E., 2018. Mechanical performance of vegetal fabric reinforced cementitious matrix (FRCM) composites. *Construction and Building Materials*, 175, pp.161-173.

[24] Trochoutsou N, Di Benedetti M, Pilakoutas K, Guadagnini M. Mechanical Characterisation of Flax and Jute Textile-Reinforced Mortars. Constr Build Mater. 2021;271:121564.

[25] Ghiassi, B., Oliveira, D., Marques, V., Soares, E. and Maljaee, H., 2016. Multi-level characterization of steel reinforced mortars for strengthening of masonry structures. Materials & Design, 110, pp.903-913.

[26] De Santis, S., Carozzi, F., de Felice, G. and Poggi, C., 2017. Test methods for Textile Reinforced Mortar systems. *Composites Part B: Engineering*, 127, pp.121-132.

[27] RILEM Technical Committee 232-TDT (Wolfgang Brameshuber). Recommendation of RILEM TC 232-TDT: Test methods and design of textile reinforced concrete: Uniaxial tensile test: Test

method to determine the load bearing behavior of tensile specimens made of textile reinforced concrete. Mater Struct/Mater Construct. 2016;49(12):4923–4927.

[28] International Code Council. Acceptance criteria for masonry and concrete strengthening using fabric-reinforced cementitious matrix (FRCM) composite systems (AC434). Washington, DC: Interna- tional Code Council Evaluation Service, Inc., 2013

[29] EN 1015-11, Methods of test for mortar for masonry - Part 11: Determination of flexural and compressive strength of hardened mortar, European Committee for Standardization, 2007.

[30] Kerakoll S.p.a., "Steel bars and sheets for structural strengthening of reinforced concrete and masonry structures", 0075GeoSteelG600Code:E8652014/07, July 2014.

[31] Kerakoll S.p.a., "Repair and reinforcement of reinforced concrete and masonry", GeoSteelG1200Code:E10102017/05-EN, May 2017.

[32] Kerakoll S.p.a., "Mineral geo-mortars for monolithic repair and for structural strengthening of concrete", 00694GeoLite® Code:E7842014/07EN, June 2014.

[33] FIB (Federation Internationale du Beton), Fib Model Code for concrete structures 2010, 2013.

Chapter 4 Bond behaviour of RC substrates strengthened with multi-layers SRG systems

S. Alotaibi[1,2], G.E. Thermou[3], M. Guadanini[4], I. Hajirasouliha[4]

Abstract

This paper presents an experimental investigation to study the shear bond behaviour in SRG systems applied to concrete substrates. Four parameters were investigated including (1) the bond length (150, 200…add the values of the bond lengths testes), (2) the number of steel textile layers (1, 2, 3), (3) the density of the steel textile (1.57 and 3.15 cords/cm), and (4) the compressive strength of the concrete substrate (15 and 30 MPa). Three modes of failure were observed including (1) the tensile rupture of the steel cords, and debonding at (2) the textile-to-matrix interface and (3) the matrix-to-substrate interface. It was found that the bond length is responsible for increasing the axial stress in the cords and the slip of the loaded end of the SRG composite. It had also a significant effect in altering the mode of failure. Increasing the number of layers or the density of the steel textiles resulted in reducing the axial stress in the cords and consequently the slip of the composite. The mode of failure was also found to be altered when these two parameters were changed. Finally, the compressive strength of the substrate was found to be of insignificant effect on the bond performance as none of the observed modes of failure involved the substrate.

Keywords

Bond behaviour, bond performance; steel reinforced grout (SRG); fabric reinforced cementitious matrix (FRCM); textile reinforced mortar (TRM); shear bond test; multiple layer composites; digital image correlation (DIC).

4.1 Introduction

Since most of the disadvantages associated with the use of the FRP systems were related to the organic matrix used to impregnate the fibres (typically epoxy), the idea of replacing this organic matrix with an inorganic one such as grout or mortar has been introduced to the scientific community. The combination of fibres impregnated in grout or mortar has been subsequently know as Textile Reinforced Mortars (TRM) or Fabric Reinforced Cementitious Matrices (FRCM). Among the different fibres utilised in these systems, the use of steel has received special attention mainly due to its relatively low cost compared to other fibres. Also, steel as a traditional material that has been in the industry for many years has provided some confidence in the design stage. Inorganic matrices strengthened with steel (usually in the form of textiles) has been since known as Steel Reinforced Grout (SRG) systems [1-2].

Over the last few decades, the studies that have been conducted on the bond behaviour in FRCM and SRG systems have recognised the complexity of the stress transfer mechanisms and the occurrence of multiple failure modes for such systems [2-4]. As for SRG systems, several studies were conducted to investigate the bond behaviour on concrete [5-8] and masonry [2, 3, 9-13] substrates. Different parameters were investigated including the bond length, the bond width, the density of steel textile, the number of textile layers, the roughness of the substrate, the type of the matrix, and the strength of the substrate, the test setup, and the curing condition [see table 4.1]. The SRG composites, in these studies, were reported to fail in different modes including debonding at either the textile-to-matrix interface [5] or at the matrix-to-substrate interface [11]. Also, other modes of failure were reported including tensile rupture in cords [13] and slippage of textiles [14]. These modes of failure were observed for SRG systems applied to masonry and concrete substrates. The debonding at the matrix-to-substrate was reported to occur for SRG composites comprising matrices of high compressive strength applied to relatively weak masonry substrates [11]. This mode of failure was also reported for SRG composites of short bond length [11]. Slippage of cords was observed for SRG systems comprising stainless steel ropes and was attributed to their smooth surface which could not develop good interlocking with the grout [9]. It was also reported that SRG systems had an effective transfer length ranging from 150 mm to 300 mm [5, 7, 9]. Similar effective bond length was also reported for FRCM systems [15]. Most of the testing guidelines recommend a bond length in the range from 250 mm to 300 mm for the systems of inorganic-based matrices applied to masonry or concrete substrates [14, 16]. The use of multiple layers of the strengthening system is often recommended in some applications, such as the flexural strengthening of large span reinforced concrete beams [17]. To date, existing knowledge on the shear transfer mechanism developed along the multiple layers of the steel fabric and on the overall behaviour of multi-ply SRG composites is still very limited, despite the crucial role it plays on the effectiveness of externally bonded reinforcements.

To bridge this knowledge gap, this study was conducted to gain an improved understanding of the bond behaviour of multi-ply SRG systems applied to concrete substrates. In this experimental investigation, a total of 90 shear bond

tests were conducted on two groups of concrete blocks that had two different concrete batches. The first batch had a low compressive strength (L; 14 MPa), while the second had a medium compressive strength (M; 28 MPa). The first batch was designed to simulate the buildings that were built to old building codes while the second was representative of the modern-day buildings that have a normal concrete strength. The concrete substrates were strengthened with SRG composites that had different bond lengths (100 mm, 200 mm, 300 mm, and 400 mm), different densities of the steel textiles (4 and 8 cords/in), and different number of layers (1, 2, and 3 layers).

Table 4.1 *SRG shear bond parameters found in literature for concrete and masonry substrates*.

Parameter	**Concrete**	**Masonry**
Bond length (mm)	100-149 [5, 7, 8] 150-199 [7, 8] 200-249 [5, 7, 8] 250-299 [7] 300-349 [5, 7, 8] 350-399 [8] 400-450 [7]	50-99 [2, 18] 100-149 [18] 150-199 [2, 18] 200-249 [2, 18] 250-299 [18] 300-349 [18] 400-450 [2]
Bond width (mm)	50 [8] 100 [8]	40 [2] 50 [2]
Density of textile (g/m^2)	670 [8] 1200 [8] 2000 [8]	670 [9, 11] 1057 [9] 1086 [13] 1200 [13] 1500 [9] 2000 [11]
Number of layers	1 [8] 2 [8]	--
Surface treatment	Bush Hammered [8] Heavy sandblasted [8]	Sandblasted [2]
Type of matrix	--	Fibre-reinforced cement-based mortar [2, 3] Lime-based mortar [2, 9] Mineral mortar [11] Mineral-NHL mortar [3, 11] Geopolymer mortar [9] Pozzolan lime mortar [9]
Strength of substrate (N/mm^2)	13-25 [8] 40 [8]	Historic Brick [3] Tuff unit [3] 35.5 [11] 14.7 [11] 25.5 [11] 4.4 [11]
Test setup	--	Double lap [2] Single lap [2]
Curing condition	room temperature for 28 days only [8] Room temperature for 28 days and wet clothes each day [8]	--

4.2 Experimental programme

This study investigates different parameters of the bond behaviour of the SRG system applied to concrete substrates namely the bond length (including 100 mm, 200 mm, 300 mm, and 400 mm), the density of the steel textiles (including 4 and 8 cords/in), the number of the steel textile layers (including 1, 2, and 3 layers), and the strength of the concrete substrate (including low and medium compressive strengths). This latter parameter is only investigated for a bond length of 300 mm. A total of 90 plain concrete prims were cast. A typical concrete prism had a length of 500 mm and 150 mm square cross section. The labelling notation of the tested specimens is SB-A-B-C-D where SB denotes shear bond tests, A denotes the compressive strength of the concrete substrate (L; 14 N/mm^2 and M; 28 N/mm^2), B is the bond length in mm (100, 200, 300, and 400), and finally C indicates the density of the steel textiles (4; 4 cords/in and 8; 8 cords/in). The test results on series SB-L-300 and SB-M-300 are published in [18] and used herein for the purpose of comparison. Each tested series had at least 3 duplicate samples. The matrix of parameters for this study is provided in table 4.2.

4.2.1 Materials

The concrete prisms were cast using two different ready-mix concrete batches such that the first had a low compressive strength (L; 14 MPa) and the second had a medium compressive strength (M; 28 MPa). Specimens were kept wet after casting for the first 7 days and were then left in laboratory conditions for at least 28 days before testing.

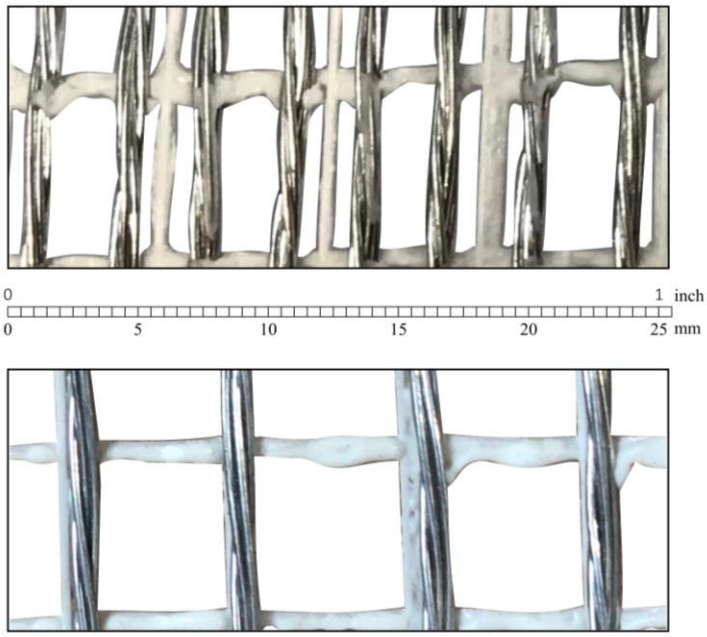

Figure 4.1 *Steel textiles of density 8 cords/in, S8 (top) and 4 cords/in, S4 (bottom).*

The steel textile used for SRG system is made of unidirectional ultra-high tensile strength steel (UHTSS) micro-cords, thermo-welded to a fibreglass micromesh. Each cord has a cross sectional area of 0.538 mm^2 and is obtained by joining 5 wires, 3 straight and 2 wrapped with a high torque angle to enhance the interlocking with the mortar (see Fig. 4.1). Wires have a cross sectional area of 0.11 mm^2 and are galvanized (coated with zinc) to improve their durability. Two different textiles were used for the strengthening of the beams. These two textiles had the same mechanical properties but were different in terms of cords density namely 4 cords/in (corresponds to 1.57 cords/cm, labelled as S4) and 8 cords/in (3.15 cords/cm; S8). The steel cords in S4 textile are evenly arranged such that the clear spacing between two cords is 5.45 mm, whereas, in S8 textile, cords are paired such that the clear spacing between two pairs is 2.28 mm. Table 4.3 provides detailed information on the mechanical properties of both steel textiles as defined by testing.

Table 4.2 *Details of the concrete prisms.*

	Serie	Substrate compressive strength	Steel textile density	No. of layers	Bond length
		N/mm2	cords/in		mm
1	SB-L-100-4-1	14	4	1	100
2	SB-L-100-4-2			2	
3	SB-L-100-4-3			3	
4	SB-L-100-8-1		8	1	
5	SB-L-100-8-2			2	
6	SB-L-100-8-3			3	
7	SB-L-200-4-1	14	4	1	200
8	SB-L-200-4-2			2	
9	SB-L-200-4-3			3	
10	SB-L-200-8-1		8	1	
11	SB-L-200-8-2			2	
12	SB-L-200-8-3			3	
13	SB-L-300-4-1	14	4	1	300
14	SB-L-300-4-2			2	
15	SB-L-300-4-3			3	
16	SB-L-300-8-1		8	1	
17	SB-L-300-8-2			2	
18	SB-L-300-8-3			3	
19	SB-M-300-4-1	28	4	1	300
20	SB-M-300-4-2			2	
21	SB-M-300-4-3			3	
22	SB-M-300-8-1		8	1	
23	SB-M-300-8-2			2	
24	SB-M-300-8-3			3	
25	SB-L-400-4-1	14	4	1	400
26	SB-L-400-4-2			2	
27	SB-L-400-4-3			3	
28	SB-L-400-8-1		8	1	
29	SB-L-400-8-2			2	
30	SB-L-400-8-3			3	

The matrix used to impregnate the steel textiles was a pre-mixed geopolymer mortar with a crystalline reaction geo-binder base. It had a compressive strength of 51 N/mm^2 and a tensile strength of 8 N/mm^2. The water-to-mortar powder mix ratio was 1:5.

Table 4.3 *The mechanical properties of steel textiles.*

	S4 N/mm2		S8 N/mm2
Number of cords	4		8
Cords density (cords/cm)	1.57		3.15
Surface mass density (g/m^2)	670		1300
Design thickness (mm)	0.084		0.169
Average tensile strength (N/mm^2)		3200	
Ultimate strain (%)		2.2	
Tensile modulus of elasticity (kN/mm^2)		186	

4.2.2 The application of the SRG system

The SRG composite was applied to either faces of the concrete block that was perpendicular to the casting face as it usually exhibits a better distribution of fine and coarse aggregates. A spacing of at least 50 mm between the edges of the SRG composite and that of the concrete block was maintained to avoid edge effects. All SRG composites had a typical width of 100 mm.

The concrete substrate (where the SRG composite is applied) was grinded by means of an electrical grinder to remove the thin smooth paste and expose the aggregate (Fig. 4.2). Prior to the application of the SRG composite, the grinded surface was cleaned from debris and dust and was kept wet for at least one day prior to the application to ensure that the water-to-cement ratio in the matrix is not compromised by any hydration processes that might take place in the substrate after the application of the SRG system.

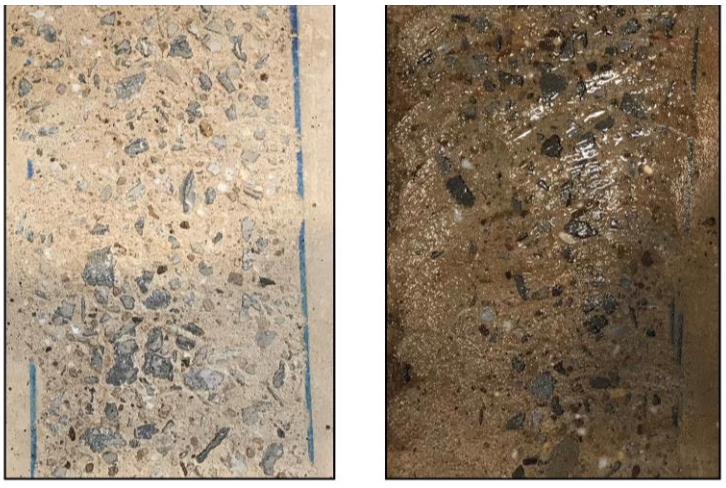

Figure 4.2 *Substrate surface (left) after grinding and (right) prior to application of the SRG system.*

To control the thickness of the SRG system, an acrylic mould designed for this purpose was used. After the mould was mounted on the specimen, a first layer of grout that had a thickness of 3 mm was applied. Then, the steel textile was placed on top of the layer and gently pressed by hand until it was fully impregnated in the grout. An additional 3 mm-thick layer of grout was then laid on top (see Fig. 4.3). This process was repeated more times for SRG composites with multiple layers and, in these cases, special attention was paid to ensure that the strips were aligned with each other. Also, it was made sure that the time of application was within the working time of the grout specified by the manufacturer. Finally, the specimens were covered with a hessian fabric, which was kept wet for at least 3 days to enhance the hydration process. The specimens were then left in laboratory conditions for at least 28 days before testing.

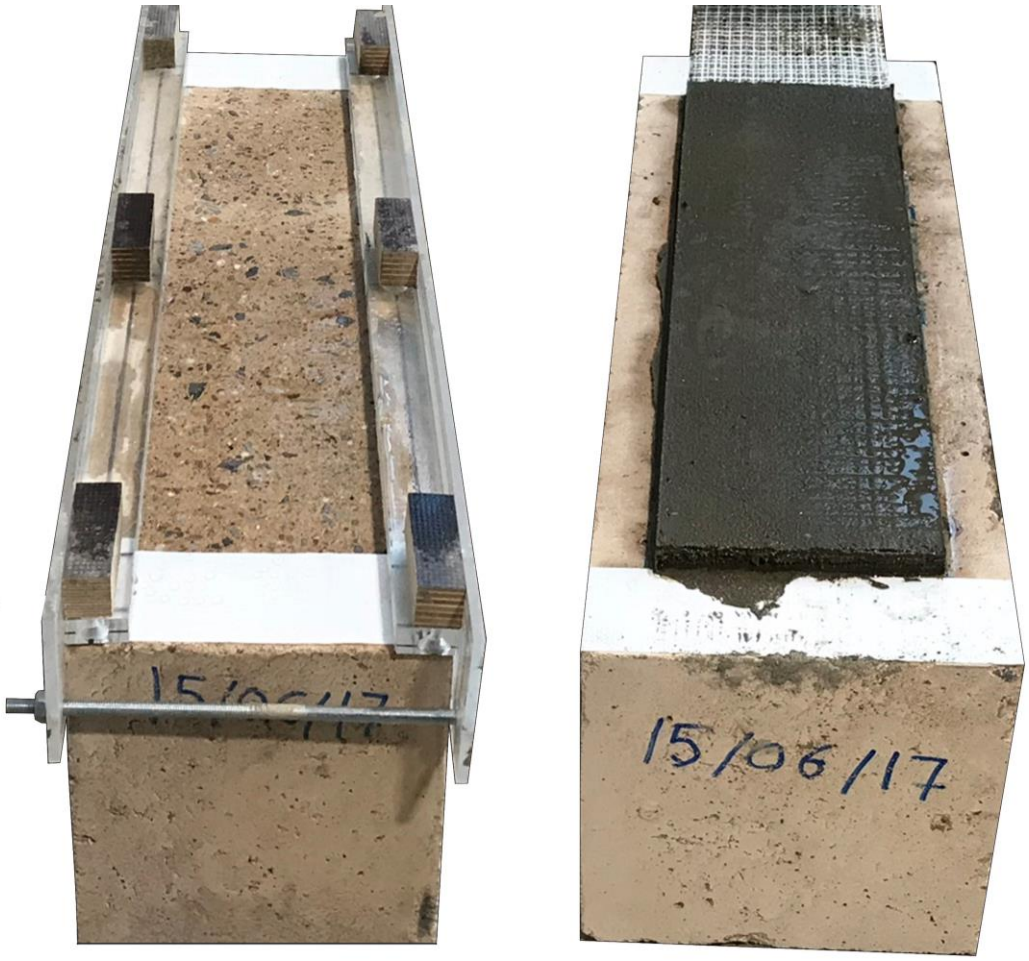

Figure 4.3 *The mould used to apply the SRG system (left) mounted on a typical specimen and (right) the specimen after the application of the SRG system.*

4.2.3 Test set-up and instrumentation

All specimens were tested in a direct single pull-out shear test configuration. A 200-kN hydraulic actuator was used to apply the pull-out load. All tests were carried out in displacement control protocol at a displacement rate of 0.01 mm/s. Fig. 4.4 provides a detailed schematic of the test setup. To grip the steel textile to the hydraulic actuator, the

dry end of the textile was sandwiched between perforated aluminium plates using a two-part epoxy adhesive. The holes in the aluminium plates will guarantee a uniform distribution of epoxy adhesive through the whole sandwich and hence preventing any possible textile-to-plate sliding in the gripping area. The aluminium plates were measuring 120 mm × 100 mm and had a thickness of 2 mm. Such a thickness would keep the total thickness of the sandwich (the thickness of the plates + the thickness of the adhesive layer) equal to that of the SRG composite. This latter step was to ensure that the composite is parallel to the gripping area. Any misalignment might introduce unfavourable stresses at the loaded end of the SRG composite. Any misalignment resulting from imperfections in the moulds and errors during SRG application was dealt with by the use of a self-adjustment steel plate with a hemispherical bolt (part 14 and 13, respectively in Fig. 4.4) such that the front of the specimen is reacting against the steel plate which was free to perform in-plane rotation as it had only one-point contact with the reaction frame through the hemispherical bolt. However, out-of-plane rotation was constrained by the means of a steel plate attached to the reaction frame preventing the back of the specimen from uplifting (part 1 in Fig. 4.4). The bed of the reaction frame (part 5 in Fig. 4.4) can be adjusted to a custom elevation by fastening/unfastening four bolts (part 6 in Fig. 4.4) through threaded openings in the reaction frame. This feature is to allow for adjusting the elevation of the concrete block prior to the test. On the other hand, the actuator was fitted with a specially designed gripping fixture. This elevation of the gripping fixture can also be adjusted by sliding it along a slotted plate (part 19 in Fig. 4.4). The sandwich was secured in place by means of four bolts driven by a click torque wrench against a steel plate above the sandwich. The high friction force generated by this mechanism will prevent any slippage that might occur between the sandwich and the gripping fixture or between different layers inside the sandwich. An extra measure was also taken to account for any possible slippage by using two L-shape steel plates (part 16 in Fig. 4.4) that was attached to the gripping fixture after inserting the sandwich. The function of these plates was to stop the back of the sandwich from slippage. A preloading cycle was then performed up to 2 kN to eliminate any slack in the unbonded textile and to trigger the self-adjustment mechanism.

Three properties were measured including the load, the slip of the SRG composite at the loaded end, and the slip of the steel cords. The load was directly measured from the integrated load cell. The slip of the composite was measured by a set of four LVDTs such that two were mounted to the sides of the concrete block while the other two were attached to the composite at the loaded end. All the LVDTs were reacting against a bracket that was attached to the top layer of the dry steel textile. Digital image correlation (DIC) system was also used to measure the slip of the composite. Finally, the slip of the cords was measured by attaching DIC targets to the far right and left cords of the dry textile in the vicinity of the loaded end. A detailed schematic of the instrumentation layout is presented in Fig. 4.5.

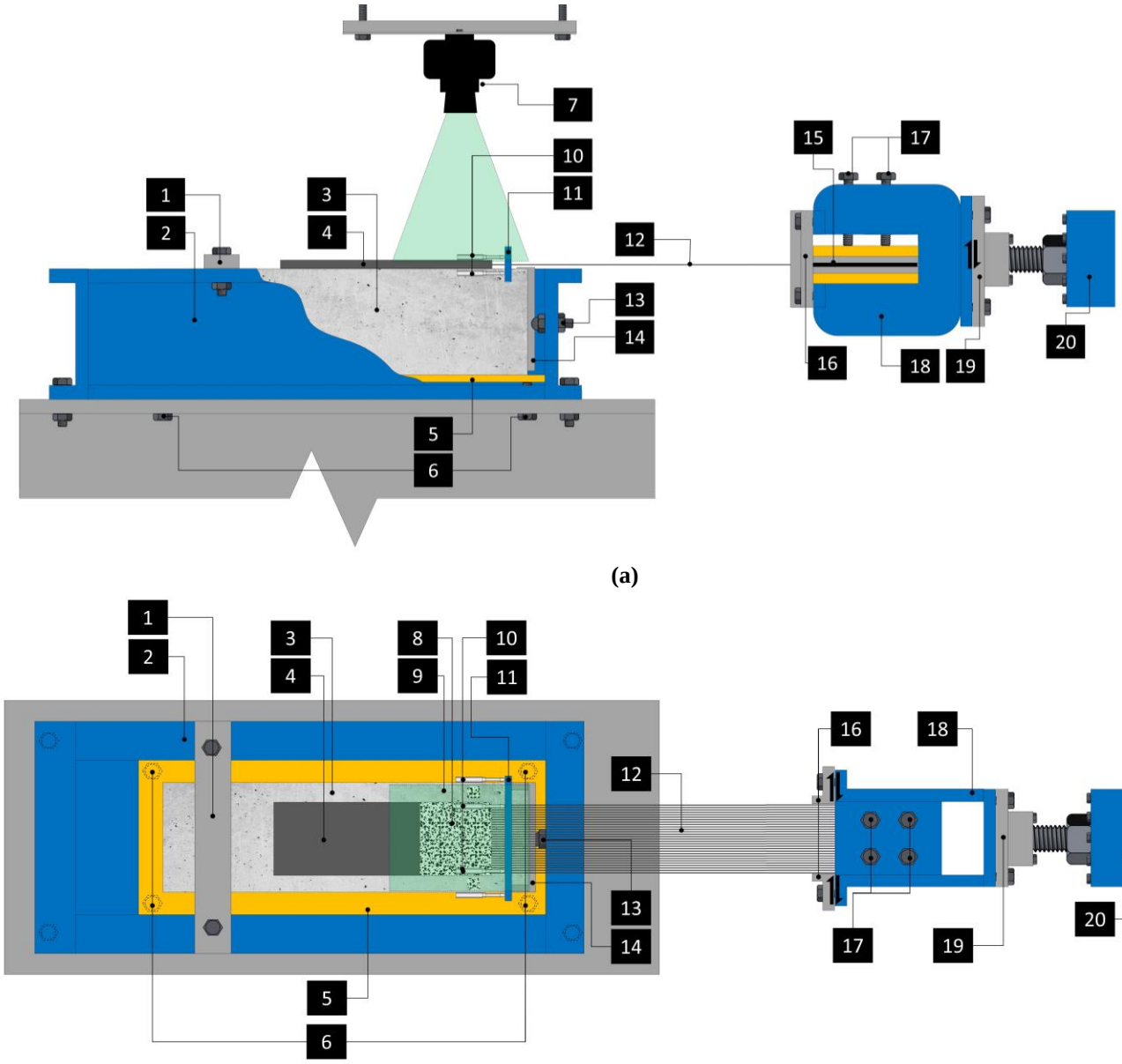

Legend

Part	Description	Part	Description
1	Steel plate to stop the back of the specimen from moving upwards because of the applied load	11	The reaction bracket for the LVDTs
2	Reaction frame: a steel frame to enclose the specimen	12	The dry steel fabric
3	concrete specimen	13	Self-adjustment hemispherical bolt
4	SRG composite	14	Self-adjustment steel plate
5	The bed of the reaction frame	15	SRP sandwich
6	Specimen-height adjustment bolts	16	Steel plates to prevent the sandwich from slippage
7	The camera for DIC system	17	Friction bolts to hold the sandwich in place
8	DIC speckle patterns	18	Grip fixture
9	Region of interest (ROI) for DIC camera	19	Grip fixture-elevation adjustment plate
10	The LVDTs measuring slip of SRG composite	20	Actuator load cell

Figure 4.4 *Detailed schematic (a) side view and (b) top view of the test setup.*

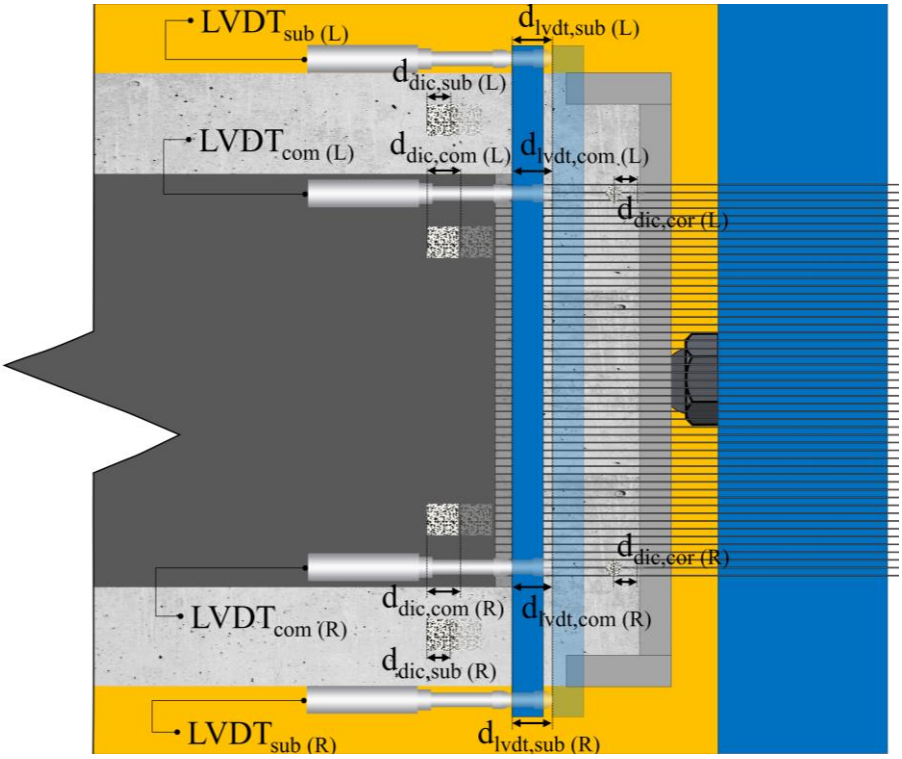

Figure 4.5 *The LVDT instrumentation layout.*

4.3 Results and discussion

Tables 4.4-4.8 provide the main results obtained from the shear bond tests. The key properties reported in the tables are the following:

- The ultimate load, P_u [kN], obtained directly from the load cell of the actuator.
- The ultimate axial stress in the steel cords, $f_{u,cords}$ [N/mm^2], obtained by dividing the maximum load, P_u, on the total area of the cords:

$$f_{u,cord} = \frac{P_u}{n\ x\ A_{cord}} \quad (1)$$

where n is the total number of cords in the SRG composite and A_{cord} is the cross-sectional area of a typical steel cord, equals to 0.538 mm^2.

- The maximum slip at the loaded end of the SRG composite, $s_{com,LVDT}$ [mm], measured by averaging the readings of the LVDTs mounted to the left and the right sides of the loaded end and was calculated as follows:

$$s_{com,LVDT} = \frac{\left(d_{lvdt,sub\ (L)} - d_{lvdt,com\ (L)}\right) + \left(d_{lvdt,sub\ (R)} - d_{lvdt,com\ (R)}\right)}{2} \quad (2)$$

where $d_{lvdt,sub\ (L)}$, $d_{lvdt,com\ (L)}$, $d_{lvdt,sub\ (R)}$, and $d_{lvdt,com\ (R)}$ are defined in Fig. 4.5.

- The maximum slip at the loaded end of the SRG composite, $s_{com,DIC}$ [mm], derived from DIC system, calculated as follows:

$$s_{com,DIC} = \frac{\left(d_{dic,com(L)} - d_{dic,sub(L)}\right) + \left(d_{dic,com(R)} - d_{dic,sub(R)}\right)}{2} \quad (3)$$

where $d_{dic,com(L)}$, $d_{dic,sub(L)}$, $d_{dic,com(R)}$, and $d_{dic,sub(R)}$ are defined in Fig. 4.5.

- The mode of failure classified according to TC Rilem 250 CSM [17] as shown in Fig. 4.6. Three modes of failure were observed including the debonding at the matrix-to-substrate interface (mode B), the debonding at the textile-to-matrix interface (mode C), and the tensile rupture of the cords (mode E1). Further discussion will be provided in the relevant section.

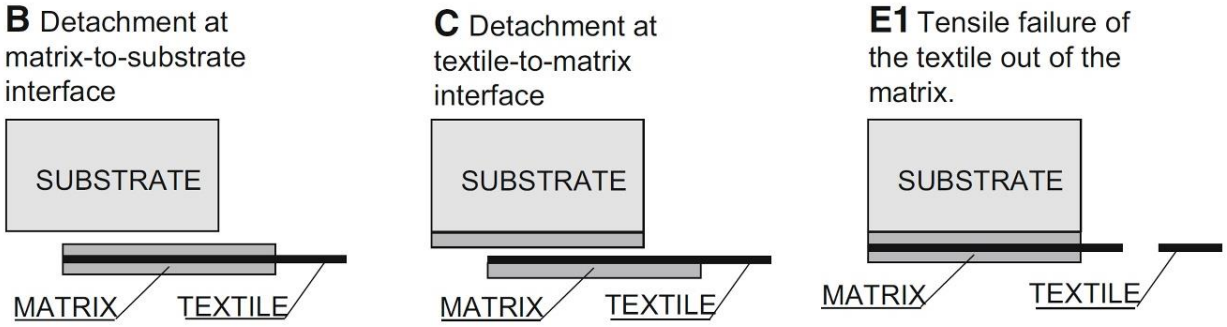

Figure 4.6 *Classification of different modes of failure according to TC RILEM 250 CSM [17].*

4.3.1 Stress-slip response

Figs. 4.7-4.10 presents the stress-slip response curves for all the tested series. Almost all tested specimens exhibited three distinct zones on stress-slip response curves. The first zone characterised an initial stiff branch corresponding to the elastic behaviour of the composite and was pronounced for the series comprising only one layer of steel textiles (series L-100-4-1, L-100-8-1, L-200-4-1, L-200-8-1, L-300-4-1, L-300-8-1, M-300-4-1, M-300-8-1, L-400-4-1, and L-400-8-1). The second stage characterising a less stiff behaviour was triggered by the initiation of transvers cracks in the SRG composite. This was followed by a final stage where no more cracks were formed, and the slip was increasing at a little gain in the axial stress. The last zone characterising a plateau segment of the stress-slip curve corresponds to the gradual progression of the debonding along the matrix-to-substrate interface (Mode B) or the matrix-to-textile interface (Mode C). The bond behaviour in the last zone is largely influenced by the bond length of the SRG composite. The last zone of the stress-slip curve was only observed for the SRG composites that had a bond length of 300 mm and 400 mm. However, the SRG composites comprising only one layer of S8 steel textile (series L-200-8-1) developed this plateau segment for a bond length of 200 mm contrary to their S4 textiles (series L-200-4-1) counterparts. This could be attributed to the improved stress distribution within the SRG composite as the stresses dissipated by S8 textiles were lower than that dissipated by their S4 textiles thanks to the

large number of cords in S8 textiles (31 cords) compared to their S4 counterparts (15 cords). The stress dissipation mechanism in S8 textiles prevented, or at least mitigated, localised stresses concentration at both interfaces and consequently postponed the debonding until the shear strength of the weakest interface was reached.

Table 4.4 *Results of shear bond tests for Series SB-L-1004.*

Group	Specimen	P_u kN	$f_{\mathrm{u,cord}}$ N/mm^2	$s_{com,LVDT}$ mm	$s_{com,DIC}$ mm	Mode of failure
SB-L-100-4-1	1	14.36	1779	0.58	0.41	B
	2	15.39	1907	0.31	0.47	B
	3	12.52	1551	0.37	0.44	B
	Average	14.09	1746	0.42	0.44	B
	St. dev.	1.45	180	0.14	0.03	
	CoV (%)	11	11	34	7	
SB-L-100-4-2	1	14.66	908	0.27	0.36	B
	2	17.71	1097	0.34	0.34	B
	3	13.02	807	0.26	0.29	B
	Average	15.13	937	0.29	0.33	B
	St. dev.	2.38	147	0.04	0.04	
	CoV (%)	16	16	14	13	
SB-L-100-4-3	1	17.99	743	0.21	0.25	B
	2	19.68	813	0.3	0.29	B
	3	20.82	860	0.49	0.40	B
	Average	19.5	805	0.33	0.31	B
	St. dev.	1.42	59	0.14	0.08	
	CoV (%)	8	8	43	26	
SB-L-100-8-1	1	14.63	877	0.49	0.44	C
	2	14.89	893	0.56	0.50	C
	3	17.73	1063	0.36	0.38	C
	Average	15.75	944	0.47	0.44	C
	St. dev.	1.72	103	0.1	0.06	
	CoV (%)	11	11	22	14	
SB-L-100-8-2	1	17.25	517	0.28	0.24	C
	2	18.38	551	0.41	0.44	B
	3	20.95	628	0.28	0.41	C
	Average	18.86	565	0.32	0.36	C
	St. dev.	1.9	57	0.08	0.11	
	CoV (%)	11	11	25	31	
SB-L-100-8-3	1	18.81	376	0.37	0.36	B
	2	21.61	432	0.24	0.29	B
	3*	-	-	-	-	
	Average	20.21	404	0.31	0.33	B
	St. dev.	1.98	40	0.09	0.05	
	CoV (%)	10	10	30	16	

Table 4.5 *Results of shear bond tests for Series SB-L-2004.*

Group	Specimen	P_u kN	$f_{u,cords}$ N/mm^2	$s_{com,LVDT}$ mm	$s_{com,DIC}$ mm	Mode of failure
SB-L-200-4-1	1	15.75	1952	0.88	0.68	B
	2	15.87	1967	0.55	0.63	B
	3	18.63	2309	1.06	0.94	B
	Average	16.75	2076	0.83	0.75	B
	St. dev.	1.63	202	0.26	0.17	
	CoV (%)	10	10	32	23	
SB-L-200-4-2	1	15.16	939	0.36	0.35	B
	2	18.14	1124	0.47	0.47	B
	3	16.46	1020	0.39	0.39	B
	Average	16.59	1028	0.41	0.40	B
	St. dev.	1.49	93	0.06	0.06	
	CoV (%)	9	10	15	15	
SB-L-200-4-3	1	14.89	615	0.18	0.30	B
	2	16.37	676	0.31	0.37	B
	3	15.47	639	0.27	0.35	B
	Average	15.58	643	0.25	0.34	B
	St. dev.	0.75	31	0.07	0.04	
	CoV (%)	5	5	28	12	
SB-L-200-8-1	1	15.28	916	1.29	0.71	C
	2	14.53	871	0.80	0.85	C
	3	12.63	757	0.54	0.57	C
	Average	14.15	848	0.88	0.71	C
	St. dev.	1.37	82	0.38	0.14	
	CoV (%)	10	10	44	20	
SB-L-200-8-2	1	18.11	543	0.54	0.45	C
	2	20.55	616	0.58	0.59	C
	3	19.18	575	0.53	0.46	B
	Average	19.28	578	0.55	0.50	C
	St. dev.	1.22	37	0.03	0.08	
	CoV (%)	7	7	6	16	
SB-L-200-8-3	1	17.51	350	0.50	0.45	B
	2	19.01	380	0.22	0.38	B
	3	19.71	394	0.22	0.31	B
	Average	18.74	375	0.31	0.38	B
	St. dev.	1.12	22	0.16	0.07	
	CoV (%)	6	6	52	19	

Table 4.6 *Results of shear bond tests for Series SB-L-3004.*

Group	Specimen	P_u kN	$f_{u,cords}$ N/mm^2	$s_{com,LVDT}$ mm	$s_{com,DIC}$ mm	Mode of failure
SB-L-300-4-1	1	17.27	2140	0.76	0.69	E1
	2	20.35	2522	2.11	1.22	E1
	3	18.36	2275	2.06	0.94	E1
	Average	18.66	2330	1.64	0.95	E1
	St. dev.	1.56	222	0.77	0.27	
	CoV (%)	9	10	47	29	
SB-L-300-4-2	1	13.90	861	1.09	0.91	B
	2	15.89	984	0.33	0.29	B
	3	20.88	1294	0.93	1.43	B
	Average	16.89	1046	0.78	0.88	B
	St. dev.	3.6	223	0.4	0.57	
	CoV (%)	22	22	52	65	
SB-L-300-4-3	1	15.82	653	0.48	0.14	B
	2	16.79	694	0.55	0.17	B
	3	16.35	675	0.27	0.15	B
	Average	16.32	674	0.43	0.15	B
	St. dev.	0.49	21	0.15	0.02	
	CoV (%)	4	4	35	14	
SB-L-300-8-1	1	15.81	979	0.33	0.20	C
	2	15.69	972	1.32	1.33	C
	3	15.42	955	1.10	1.12	B-C
	Average	15.64	969	0.92	0.88	C
	St. dev.	0.2	12	0.52	0.60	
	CoV (%)	2	2	57	69	
SB-L-300-8-2	1	26.34	816	0.60	0.51	B
	2	25.84	801	0.57	0.24	C
	3	26.84	832	0.39	0.80	B-C
	Average	26.34	816	0.52	0.52	C
	St. dev.	0.5	16	0.11	0.28	
	CoV (%)	2	2	22	54	
SB-L-300-8-3	1	27.32	564	0.71	0.18	B
	2	25.62	529	0.46	0.20	B
	3	32.48	671	0.45	0.42	B
	Average	28.47	588	0.54	0.27	B
	St. dev.	3.57	74	0.15	0.13	
	CoV (%)	13	13	28	49	

Table 4.7 *Results of shear bond tests for Series SB-M-3004.*

Group	Specimen	P_u kN	$f_{u,cords}$ N/mm^2	$s_{com,LVDT}$ mm	$s_{com,DIC}$ mm	Mode of failure
SB-M-300-4-1	1	20.56	2548	2.06	1.66	E1
	2	12.24	1516	0.78	0.26	B
	3	19.82	2456	2.89	2.57	E1
	Average	17.54	2173	1.91	1.50	E1
	St. dev.	4.6	571	1.06	1.16	
	CoV (%)	27	27	56	78	
SB-M-300-4-2	1	14.99	929	0.21	0.12	B
	2	24.83	1538	1.55	1.51	E1
	3	15.87	983	0.61	0.14	B
	Average	18.56	1150	0.79	0.59	B
	St. dev.	5.44	337	0.69	0.8	
	CoV (%)	30	30	88	136	
SB-M-300-4-3	1	20.72	856	1.23	0.43	B
	2	20.78	858	1.04	0.07	B
	3	20.08	829	0.42	0.68	B
	Average	20.53	848	0.90	0.39	B
	St. dev.	0.39	16	0.42	0.31	
	CoV (%)	2	2	47	80	
SB-M-300-8-1	1	14.76	915	1.22	N/A	C
	2	15.79	978	0.94	0.86	C
	3	15.98	990	0.84	0.75	C
	Average	15.51	961	1.00	0.81	C
	St. dev.	0.66	40	0.2	0.08	
	CoV (%)	5	5	20	10	
SB-M-300-8-2	1	27.48	851	1.43	N/A	C
	2	24.90	771	0.46	0.20	C
	3	23.19	719	0.56	N/A	B
	Average	25.19	780	0.82	0.20	C
	St. dev.	2.16	66	0.53		
	CoV (%)	9	9	65		
SB-M-300-8-3	1	32.54	672	1.59	0.54	C
	2	21.43	443	0.68	0.07	B
	3	23.97	495	0.27	0.08	B
	Average	25.98	537	0.85	0.23	B
	St. dev.	5.82	120	0.68	0.27	
	CoV (%)	23	23	80	118	

Table 4.8 *Results of shear bond tests for Series SB-L-4004.*

Group	Specimen	P_u kN	$f_{u,cords}$ N/mm^2	$s_{com,LVDT}$ Mm	$s_{com,DIC}$ mm	Mode of failure
SB-L-400-4-1	1	17.33	2148	1.72	0.52	E1
	2	18.17	2251	1.69	2.05	E1
	3	19.27	2388	1.96	1.06	E1
	Average	18.26	2262	1.79	1.21	E1
	St. dev.	0.97	120	0.15	0.78	
	CoV (%)	6	6	9	65	
SB-L-400-4-2	1	18.59	1152	0.88	1.09	B
	2	19.59	1214	1.16	1.17	B
	3	18.87	1169	0.90	1.03	B
	Average	19.02	1178	0.98	1.10	B
	St. dev.	0.52	32	0.16	0.07	
	CoV (%)	3	3	17	7	
SB-L-400-4-3	1	18.33	757	0.71	0.23	B
	2	17.16	709	0.88	0.24	B
	3	19.05	787	0.68	0.86	B
	Average	18.18	751	0.76	0.44	B
	St. dev.	0.95	39	0.11	0.36	
	CoV (%)	6	6	15	82	
SB-L-400-8-1	1	19.86	1191	0.99	0.76	C
	2	13.46	807	0.66	0.60	C
	3	14.19	851	0.89	0.87	C
	Average	15.84	950	0.85	0.74	C
	St. dev.	3.50	210	0.17	0.14	
	CoV (%)	23	23	20	19	
SB-L-400-8-2	1	21.65	648	1.13	0.58	C
	2	24.38	731	0.48	0.48	C
	3	25.28	758	0.65	0.56	B
	Average	23.77	712	0.75	0.54	C
	St. dev.	1.89	57	0.34	0.05	
	CoV (%)	8	9	46	10	
SB-L-400-8-3	1	23.47	469	0.65	0.51	B
	2	25.47	509	0.60	0.39	B
	3	35.17	703	1.06	0.42	B
	Average	28.04	560	0.77	0.44	B
	St. dev.	6.26	125	0.25	0.06	
	CoV (%)	23	23	33	14	

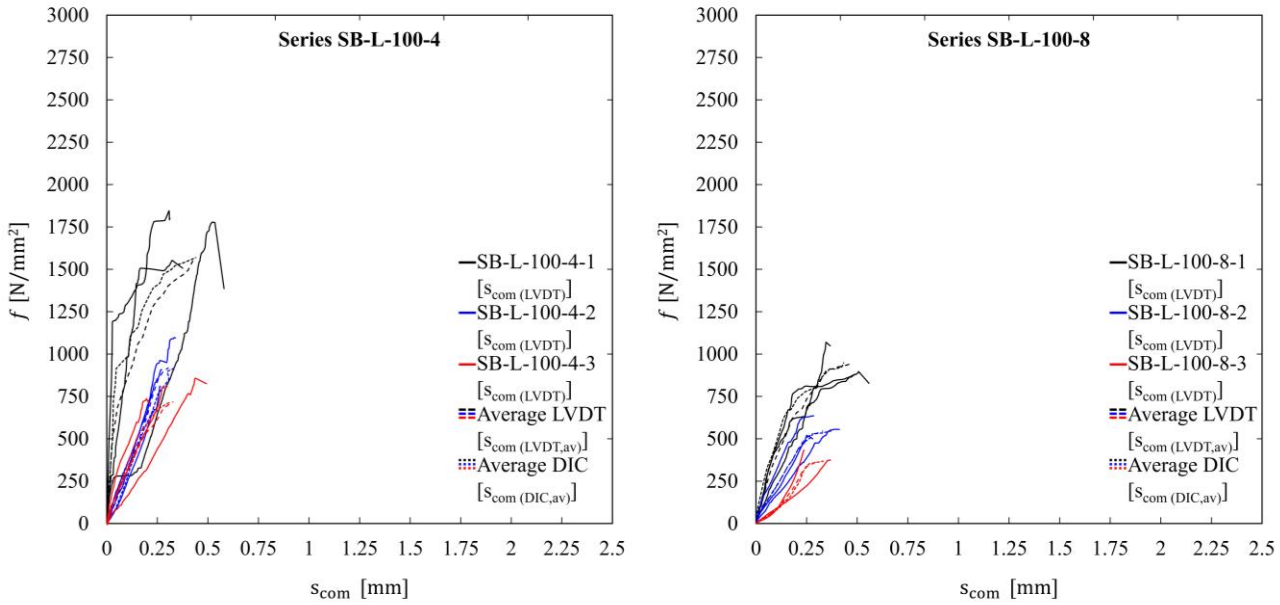

(a) **(b)**

Figure 4.7 *Stress-slip response curves for series SB-L-100-4 (a) and SB-L-100-8 (b)*

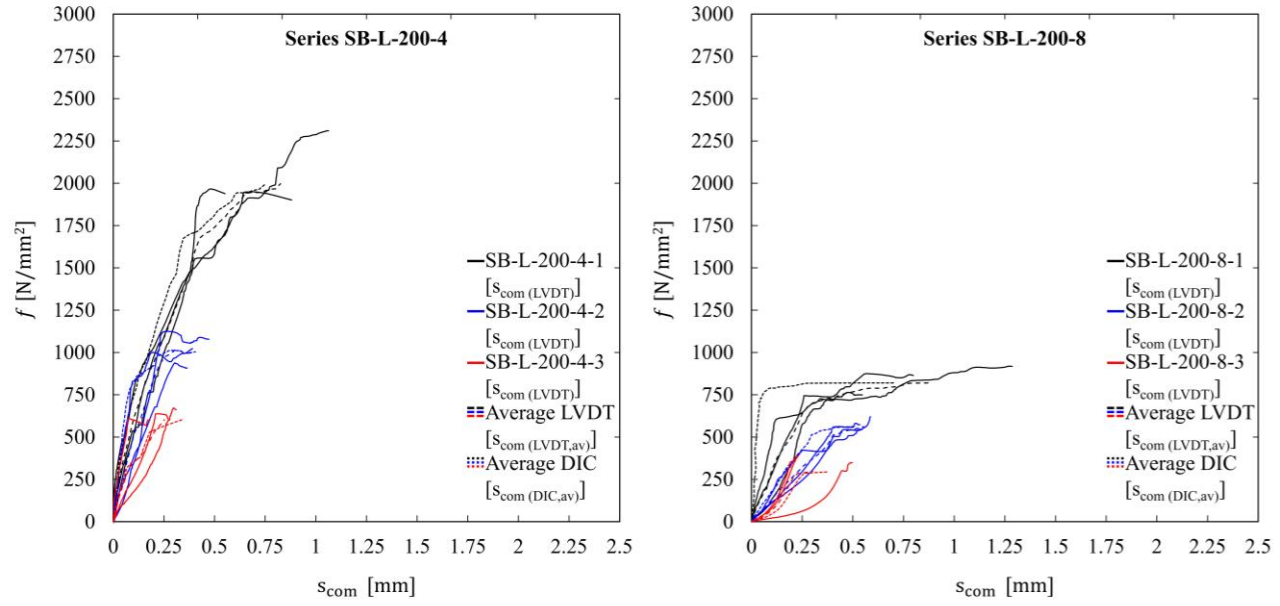

(a) **(b)**

Figure 4.8 *Stress-slip response curves for series SB-L-200-4 (a) and SB-L-200-8 (b).*

4.3.2 Failure mode and cracks behaviour

Three modes of failure were observed including the debonding at either the matrix-to-substrate interface (mode B), the textile-to-matrix interface (mode C), and the tensile rupture of the cords (E1). In the direct shear bond tests, the load is transferred from the actuator to the SRG composite through the tensile stresses developed at the cords. The tensile stresses are transferred from the cords to the surrounding grout via the developed bond stresses and

eventually to the substrate as shear stresses at the interface. Understanding the stress status with the SRG composite is crucial to understand different modes of failure. In general, the failure can occur at one of three areas including the cross section of the steel cord, the matrix-to-textile interface, and the matrix-to-substrate interface.

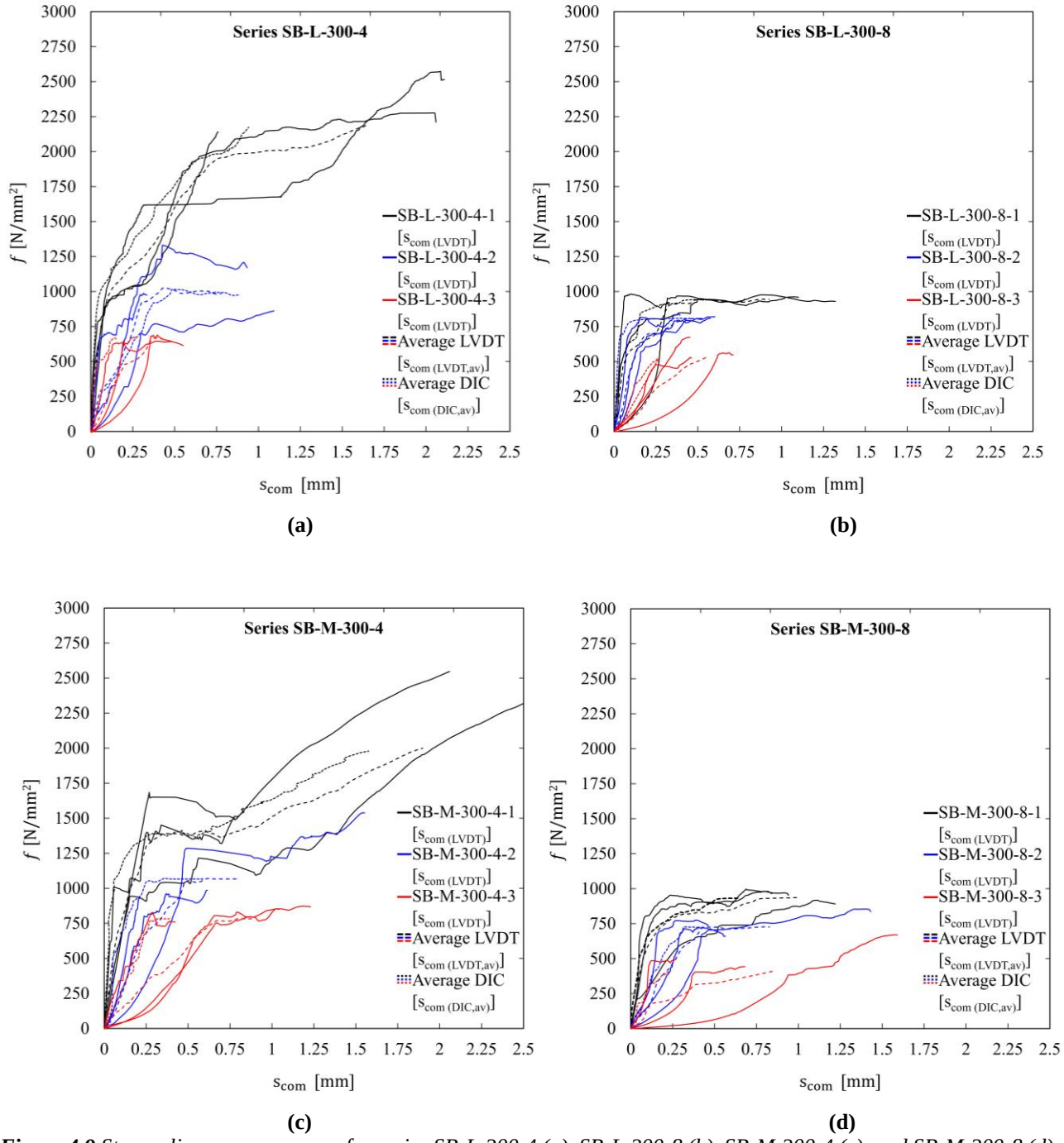

Figure 4.9 *Stress-slip response curves for series SB-L-300-4 (a), SB-L-300-8 (b), SB-M-300-4 (c), and SB-M-300-8 (d).*

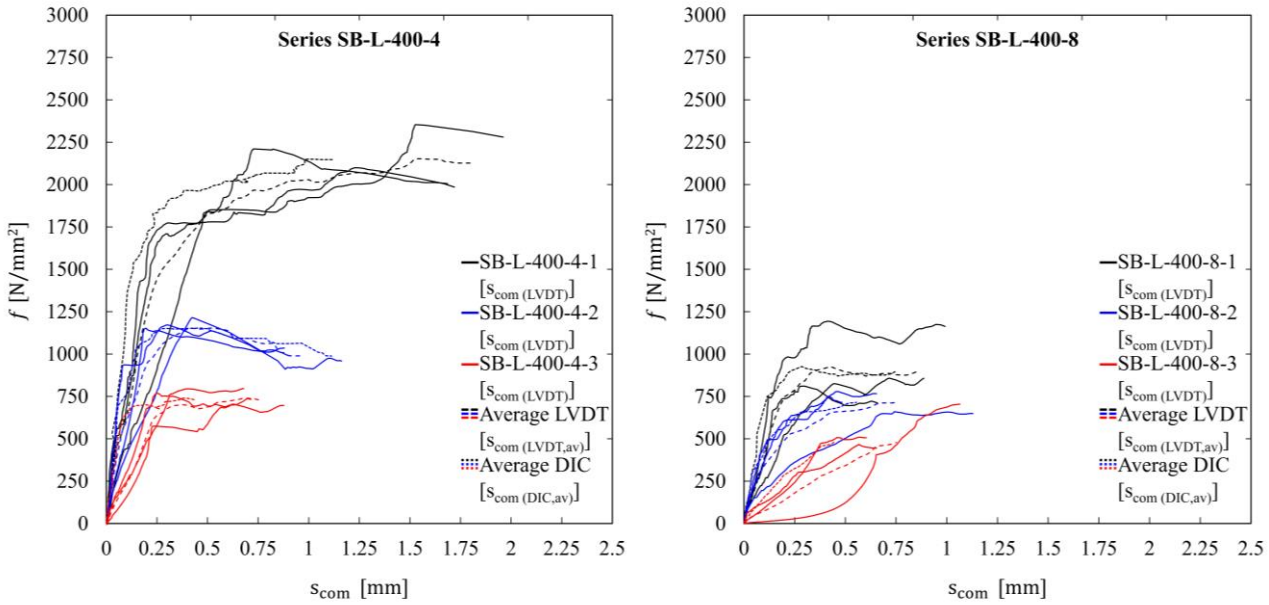

Figure 4.10 Stress-slip response curves for series SB-L-400-4 (a) and SB-L-400-8 (b).

When the applied stress reaches the breaking stress of the cord, tensile rupture occurs at the cross section of the cord (Mode E1). However, this mode of failure only occurs when the ultimate shear stress of both interfaces is higher than the applied shear stress. Indeed, this mode of failure was only observed for the SRG composites that has a smaller number of cords with longer bond lengths i.e., series L-300-4-1, M-300-4-1, and L-400-4-1.

On the other hand, when the ultimate shear stress of either interface is reached debonding will occur at the weakest interface. Apart from the specimens that failed by tensile rupture, it was generally observed that the specimens comprising S4 steel textiles almost failed by debonding at the matrix-to-substrate interface regardless of the number of layers, while the specimens strengthened with S8 textiles almost failed by debonding at the matrix-to-textile interface with the exception of these comprising three layers of textiles. It is worth noting that there are different parameters, beyond the scope of this study, that significantly influence the stress state within the composite e.g., the type and strength of the grout. Nevertheless, the parameters investigated in this study can provide a better understanding of the stress status within the SRG composite and how different mode of failure can be triggered.

The following paragraphs provide more detailed discussion about every mode of failure in terms of the nature and the causes.

1) Debonding at the interface between the bottom layer of the SRG matrix and the substrate (matrix-to-substrate interface), mode B (see Fig. 4.11). In this mode of failure, the SRG composites were fully detached from the concrete block and, in most cases, the SRG composites were almost intact. Almost 65 % of the tested specimens failed in this fashion. This mode of failure was mainly observed for:

- Specimens strengthened three layers of SRG composites (i.e., groups L-100-4-3, L-100-8-3, L-200-4-3, L-200-8-3, L-300-4-3, L-300-8-3, M-300-4-3, M-300-8-3, L-400-4-3, and L-400-8-3). These groups have the highest amount of reinforcement utilising either 45 or 93 cords for steel textiles S4 and S8, respectively. This relatively large number of cords cannot be driven to their breaking stress as it is way beyond the stress capacity of the interfaces between different layers of the SRG composite and between the composite and the substrate (it requires a theoretical tress of more than 140 GPa to break three layers of S4 textiles). Also, this large number of cords helped in developing a small and even dissipation of stresses inside the SRG composites which in turn prevented the formation of regions of localised stresses particularly at the interface between the textile and the grout often observed for S8 textiles. Now, the only interface that is prone to failure is that between the composite and the substrate and this explains why these groups failed at that interface.
- Specimens strengthened with two layers of S4 steel textile (i.e. groups L-100-4-2, L-200-4-2, L-300-4-2, M-300-4-2, L-400-4-2). These groups, as mentioned earlier, are unlikely to fail by textile rupture owing to their relatively large number of cords. Also, they are not prone to fail at the interface between the steel textile and the substrate as their layout allowed more grout to pass between cords and hence developing a better impregnation compared to their S8 textile counterparts. As a result, these groups had to fail at the weakest interface between the SRG composite and the substrate.
- Specimens strengthened with one layer of S4 steel textile for bond lengths 100 mm and 200 mm (i.e. L-100-4-1 and L-200-4-1). Although these groups had a relatively less number of cords (only 15 cords), they did not fail by rupture. The amount of stresses that was transferred at the interface between the SRG composite and the substrate was limited as the bond length was shorter than the effective bond length (> 250 mm). Since the interfaces inside the SRG composite, as already mentioned, were not critical, these groups failed at the interface at substrate level.

Figure 4.11 *Typical debonding at matrix-to-substrate interface (mode B) observed for most of the tested specimens.*

2) Debonding at the interface between the bottom layer of the SRG matrix and the steel textile (matrix-to-textile interface), mode C (see Fig. 4.12). This mode was observed for approximately 25 % of the tested specimens. It was mainly observed for specimens strengthened with one and two layers of S8 steel textile. The dense layout of S8 textiles hindered the full impregnation of grout between the cords and created regions of reduced volume of grout and stresses were dissipated through a less number of cords (compared to three layers of textiles) meaning higher stresses were transferred to the weakened regions of grout. All this was good grounds to cause the interface between the steel textile and the bottom layer of grout to be the weakest in the system and hence debonding was triggered at that interface.

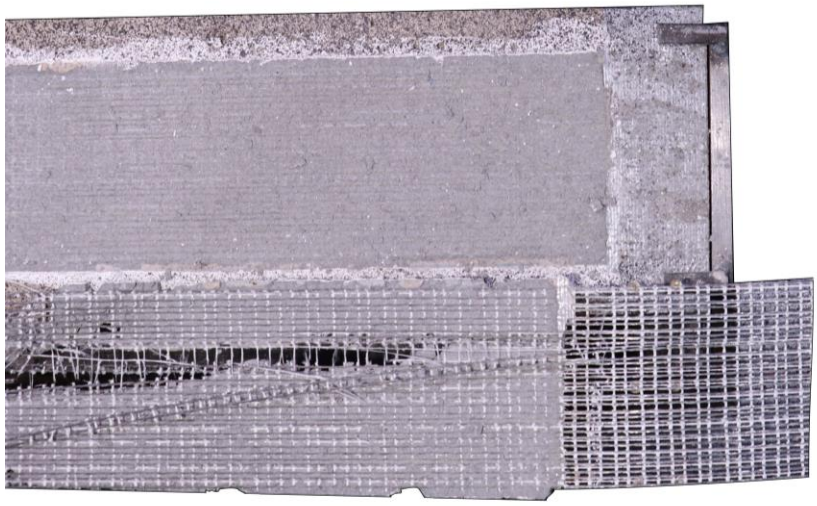

Figure 4.12 *Typical debonding at matrix-to-textile interface (mode C) observed for specimens strengthened with 1 or 2 layers of S8 textiles.*

3) Tensile rupture of steel textile outside the composite, mode E1 (see Fig. 4.13). This was observed for specimens strengthened with one layer of S4 steel textile for bond lengths 300 mm and 400 mm constituting almost 10 % of the tested specimens. When the bond length was longer than the effective bond length (> 250 mm), the interface between the SRG composite and the substrate could transfer more stresses and was no longer the weakest in the system. On the other hand, the interface between the steel textile and the grout is not prone to failure due to the good impregnation developed by the less dense textiles, S4. All this had to drive the cords to its ultimate tensile strength and to cause them to ultimately fail by rupture.

It is worth noting that for the SRG systems that had debonding at matrix-to-substrate interface, the utilization of the steel reinforcement was higher than the systems that failed by debonding at the matrix-to-textile interface. For instance, series SB-L-300-4-2, SB-M-300-4-2, and SB-L-400-4-2 failed by debonding at the matrix-to-substrate interface (mode B) at axial stress values in the steel cords of 1046 N/mm^2, 1150 N/mm^2, 1178 N/mm^2, respectively. On the other hand, their counterparts series SB-L-300-8-2, SB-M-300-8-2, and SB-L-400-8-2 failed by debonding at the matrix-to-textile interface (mode C) at less axial stress values (69 % on average).

4.3.3 Effective bond length

The load resisted by the specimen during the test is dissipated to the substrate as shear stresses along the matrix-to-substrate interface. Only a certain length of the composite is engaged in this stress transfer mechanism. When debonding initiates along the interface at the loaded end, this length shifts towards the back of the composite to satisfy stress conditions. This length is known in literature as “the effective bond length”.

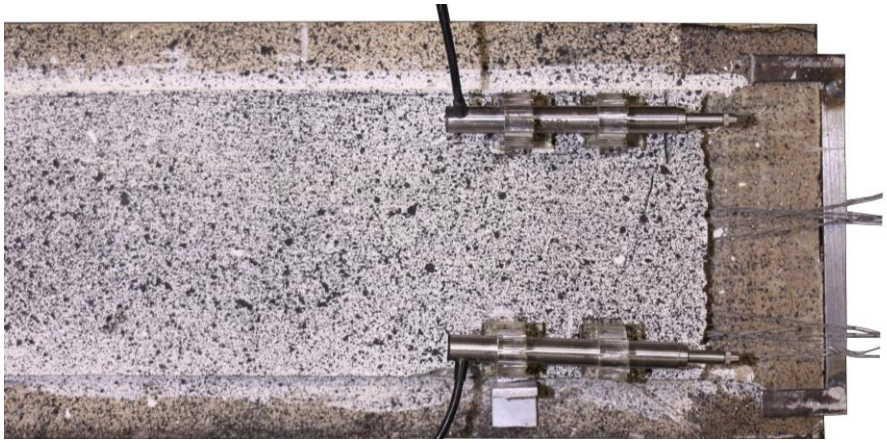

Figure 4.13 *Typical tensile rupture of cords (mode E1) observed for specimens strengthened with 1 layer of S4 textiles for bond lengths above 200mm.*

The stress-slip curves in Figs. 4.7-4.10 suggest that the effective bond length is insignificantly influenced by the density and the number of layers of the steel textiles. At a bond length of 200 mm, the plateau segment of the stress-slip curve was clearly developed for almost all series except the series comprising only one layer of the less denser steel textiles (i.e., series L-200-4-1). This latter could only develop this segment at a bond length of 300 mm. At the bond length of 400 mm, no further increase in axial stress was observed and the slip was increasing corresponding to the “shifting” mechanism. In general, the obtained data indicates that the effective bond length for the SRG strengthening systems lies between 200 mm and 300 mm.

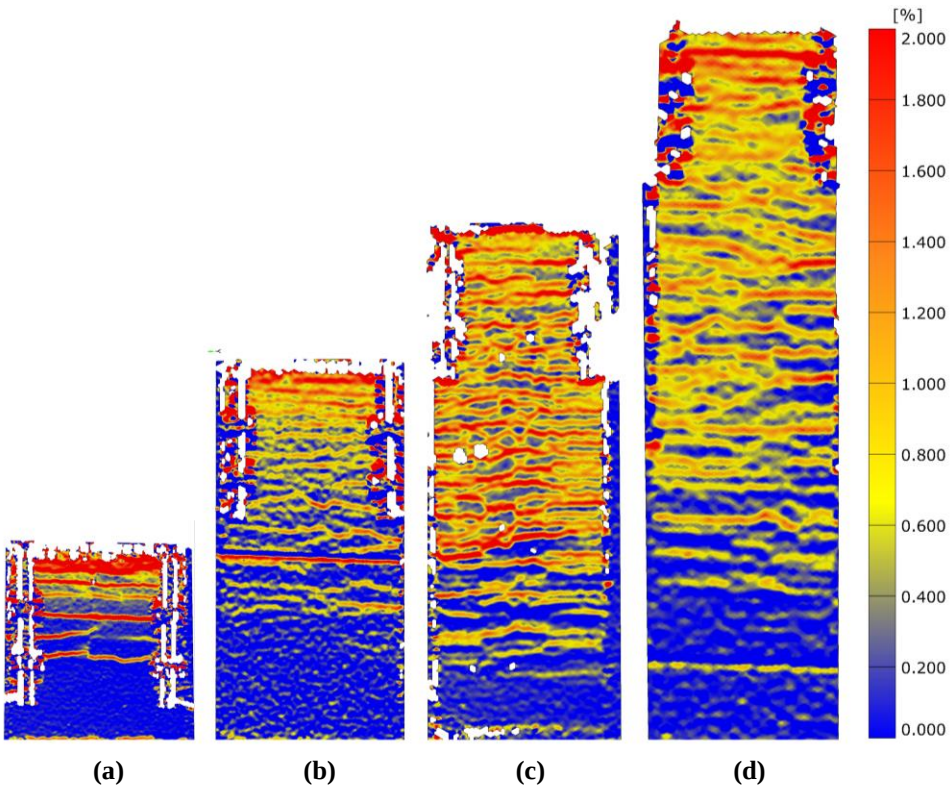

Figure 4.14 *Typical strain maps at failure for series L-100 (a), L-200 (b), L-300 and M-300 (c), and L-400 (d).*

The principle of the effective bond length was also confirmed by the strain maps obtained from the DIC system (Fig. 4.14). Almost all tested specimens developed transverse cracks at the loaded end on a certain length and these cracks were shifting backward as the test was progressing confirming that only a certain length of the composite is effectively engaged in the stress transfer mechanism.

4.3.4 Effect of the bond length

The bond length has a direct effect on the bond performance through influencing the shear strength of the matrix-to-substrate and textile-to-matrix interfaces through increasing the areas of interfaces. This enabled them to transfer more stresses to the substrate which, in turn, increased the axial stress in cords and affect the mode of failure. This is evident by the increase in the maximum axial stress observed for series L-200 compared to L-100 for the same steel textile and the same number of layers. For instance, group L-200-4-1 had an increase in the average maximum axial stress of approximately 19 % compared to their L-100-4-1 counterparts. This is almost true for all groups that had S4 textile. However, when S8 textiles were used the weakest link in the system was the textile-to-matrix interface and the matrix-to-substrate interface was no longer the critical one which made the bond length to seem of less significance for these groups. When the bond length was increased from 100 mm to 200 mm, specimens strengthen with relatively heavy steel textile reinforcement (all series except L-200-4-1) developed a plateau segment on stress-slip curves. Increasing the bond length from 200 mm to 300 mm enabled the SRG composites

strengthened with one layer of S4 textiles (series M-300-4-1 and L-300-4-1) to develop the effective bond length evident by the development of the last plateau segment on the stress-slip curve.

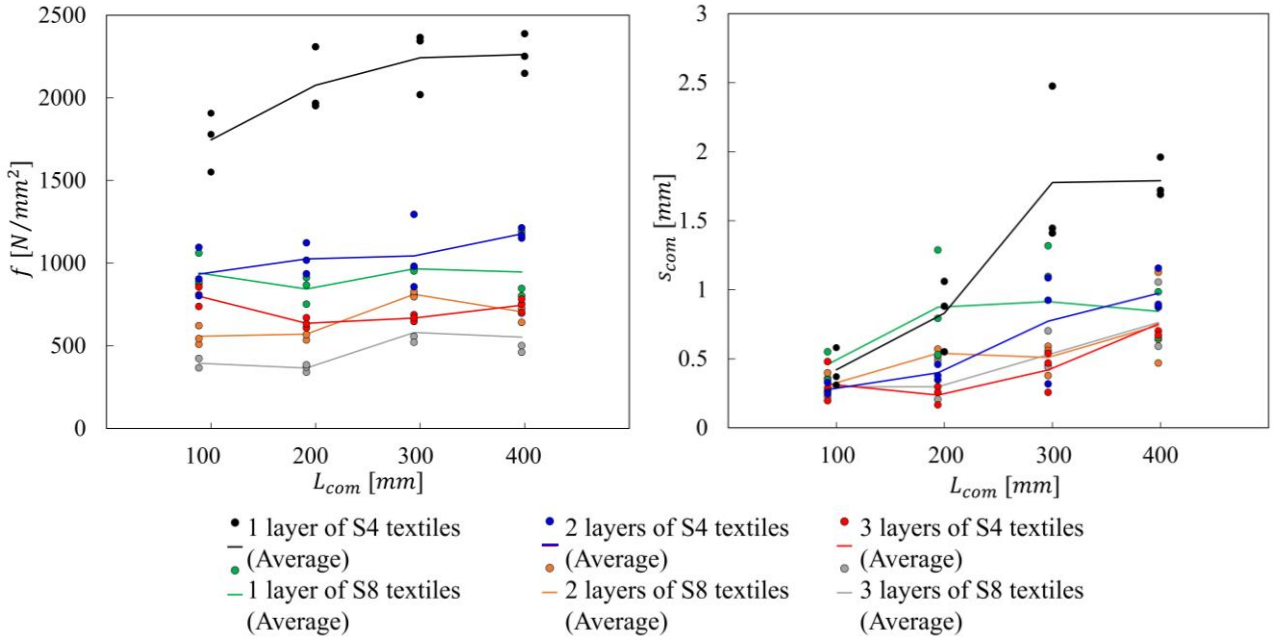

Figure 4.15 *The effect of the bond length on the maximum axial stress (left) and the maximum slip (right).*

Fig. 4.15 confirms that increasing the bond length seems to only significantly influences the specimens strengthened with the SRG composites comprising low reinforcement (S4-1). When specimens or strengthened with one layer of S8 textile or more layers of both textiles, the critical interface was no longer the matrix-to-substrate interface, and this made the bond length to seem of less significance. Although the area of the textile-to-matrix interface was also increased by increasing the bond length, however that interface was weakened by poor impregnation of the textiles.

4.3.5 Effect of the number of textile layers

Increasing the number of the textile layers resulted in a decrease in the maximum average axial stress of approximately 50 % and 65 % for specimens strengthened with two and three layers of S4 textile, respectively, compared to that strengthened with one layer of the same textile. While, increasing the number of layers of S8 textile led to a decrease in the maximum average axial stress of approximately 28 % and 48 % for two and three layers of textile, respectively, compared to one layer of the same textile. Similar percentages of decrease in the maximum slip at the loaded end of the SRG composites were also observed for both groups. The effect of increasing the number of layers is more pronounced for the transition from one to two layers of steel textiles. This was only observed for bond lengths more than 200 mm.

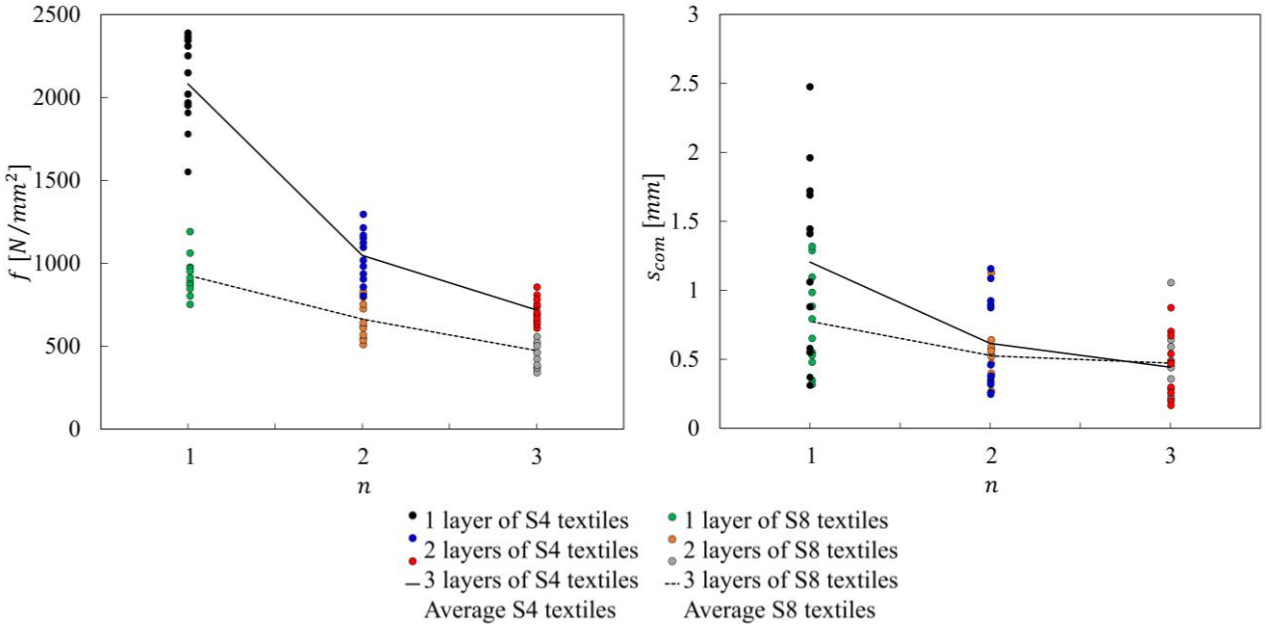

Figure 4.16 *The effect of the number of textile layers on the maximum axial stress (left) and the maximum slip (right).*

Doubling the number of layers caused the failure to occur at either the textile-to-matrix or matrix-to-substrate interfaces which already have a shear stress transfer limit that will trigger debonding once exceeded. These interfaces in composites of bond length shorter 300 mm could not develop enough anchorage stresses to cause rupture in the cords. Also, when the bond length was increases beyond 200 mm and the number of layers was doubled, the interfaces failed, again, to supply the right amount to break the cords. and this explains the reason of this alteration in the mode of failure when doubling the number of layers. Two and Three layers of both steel textiles had a comparable axial stress and slip with the latter being very close (see Fig. 4.16). This suggests that adding more than two layers of the SRG composites might not be effective.

4.3.6 Effect of the density of steel textile

Increasing the density of steel textile compromised the shear transfer quality of the textile-to-matrix interface. As explained earlier, grout layers could not develop a good impregnation when S8 steel textiles were used. The series comprising one and two layers of S8 textiles failed by debonding at the textile-to-matrix interface (mode C) regardless of bond length. However, when three layers of S8 textiles were used the mode of failure was altered to debonding at the matrix-to-substrate interface (mode B). This can be explained by the fact that the relatively large number of cords in composites comprising three layers of S8 textiles helped in reducing the amount of stresses dissipated at the textile-to-matrix interface and kept it below the ultimate shear stress of that interface and as a result debonding was driven to the weaker link which was the matrix-to-substrate interface. This principle, also, holds true for three layers of S4 steel textiles. All specimens strengthened with three layers of S4 textiles failed by debonding at textile-to-matrix interface (mode B). Indeed, this interface was the weakest among the three links

including the cords tensile strength and the matrix-to-substrate interface. The former required an axial stress much higher than both interfaces can afford to cause tensile rupture in the cords while the latter was strong due to the better impregnation achieved with the S4 textiles.

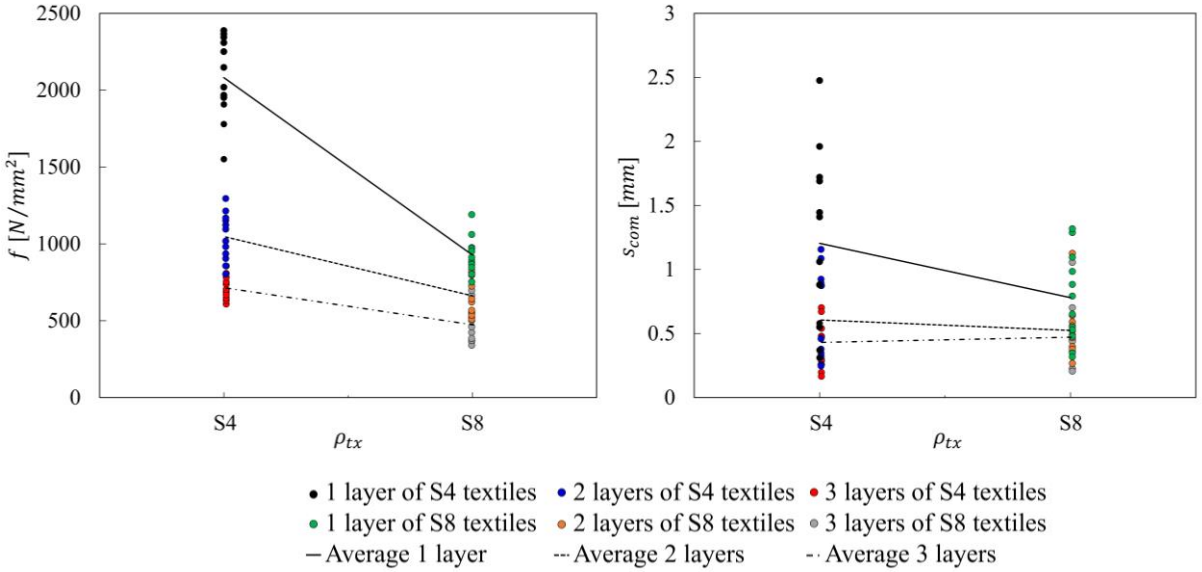

Figure 4.17 *The effect of the density of steel textile on the maximum axial stress (left) and the maximum slip (right).*

Fig. 4.17 presents graphs to visualise the effect of increasing the density of the steel textile from 4 to 8 cords/in in terms of the maximum average axial stress and the maximum slip. The influence is more significant for composites comprising only one layer of textiles.

4.3.7 Effect of the concrete compressive strength

Trend lines in Fig. 4.18 show that the effect of increasing the compressive strength of the substrate, $f_{c,sb}$, is insignificant. The fact that most of the tested specimens failed at matrix-to-substrate interface might seem contradictory to this finding. However, it should be realised that the debonding occurred at the interface between the SRG composite and the concrete substrate and did not involve the substrate. Debonding occurring at the interface is governed by the mechanical properties of that interface. The effect of concrete compressive strength is only pronounced when the debonding involves the concrete cover of the substrate which is typical for systems utilising epoxy resins such as FRP and SRP systems.

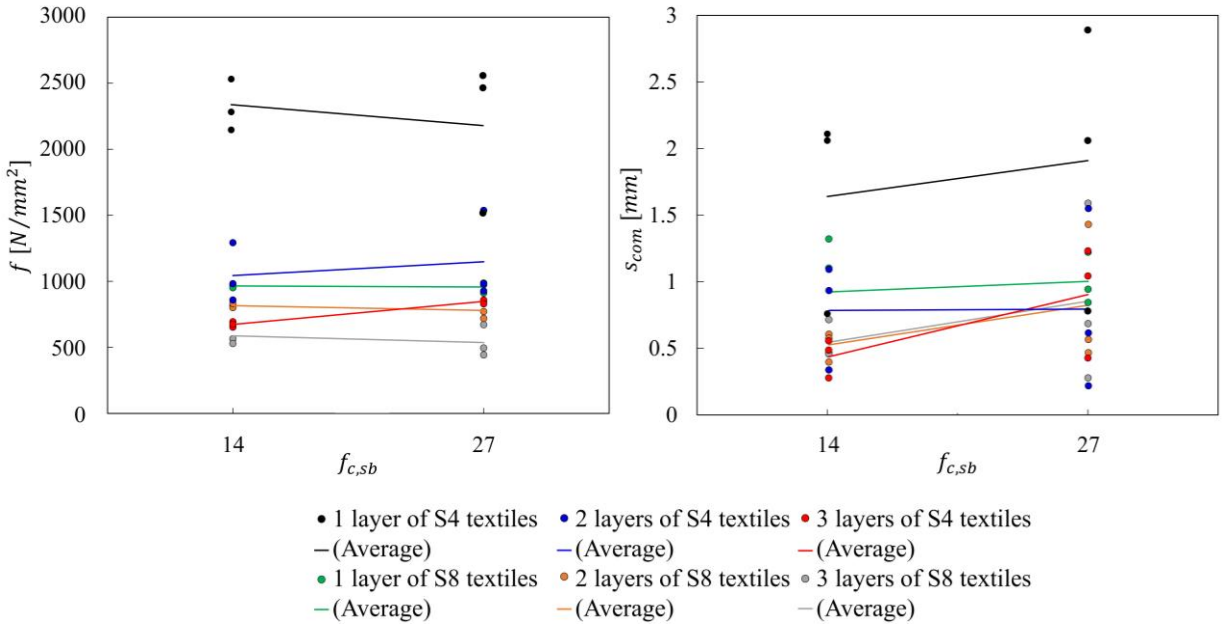

Figure 4.18 *The effect of the compressive strength of substrate on the maximum axial stress (left) and the maximum slip (right).*

4.4 Analytical Modelling

Different models were suggested for modelling the relationship between the interfacial shear stress and the relative slip between the substrate and the composite. Most of these models are originally developed for the FRP systems. Failure by debonding in the FRP system usually involves the substrate and hence the mechanical properties of the substrate are often involved in these models in terms of the compressive strength [19] or the tensile strength [20 and 21] of the concrete substrate. Contrary to the FRP systems, the involvement of the substrate in the debonding mechanism for the FRCM and the SRG systems is only insignificant. The FRP-bond models that do not account for the mechanical properties of the substrate seem to be more appropriate for modelling the shear stress in the inorganic-based systems.

The model developed in [22] for the interfacial bond stress in the FRP systems do not involve the mechanical properties of the substrate and hence it will be considered in this study to assess its validity for the SRG system. The model is expressed in the following form:

$$\tau\ (s)\ [N/mm^2] = E_{tx,II} \cdot t_{tx,1} \cdot A^2 \cdot B \cdot (e^{-B \cdot s} - e^{-2 \cdot B \cdot s}) \quad (4)$$

where $\tau\ (s)$ is the analytical interfacial shear stress at the matrix-to-substrate interface expressed as a function in the relative slip, s, between the composite and the substrate. $E_{tx,II}$ and $t_{tx,1}$ are the elastic modulus of and the thickness of the steel textiles, respectively. A and B are parameters for calibrating the shape of the curve and the peak value of the shear stress while s is the slip of the composite.

The analytical ultimate shear bond stress, $\tau_{u,an}$, and the corresponding slip, $s_{u,an}$, can be then calculated using the following equations:

$$\tau_{u,an}[N/mm^2] = \frac{E_{tx,II} \,.\, t_{tx,1} \,.\, B \,.\, A^2}{4} \tag{5}$$

$$s_{u,an}[mm] = \frac{0.693}{B} \tag{6}$$

The experimental interfacial shear stress, $\tau_{u,exp}$, was calculated by dividing the average ultimate applied load by the effective area of the composite. The effective area is defined by the effective bond length, L_{eff}, of the composite that is engaged in the shear stress transfer mechanism.

$$\tau_{u,exp}[N/mm^2] = \frac{P_{u,av}}{b_{com} \,.\, L_{eff}} \tag{7}$$

where b_{com} is the width of the composite and the value of L_{eff} depends on the length of the composite, L_{com} such that:

$$L_{com}[mm] = \begin{cases} L_{com}; & for\ L_f \leq L_{eff} \\ L_{eff}; & for\ L_f > L_{eff} \end{cases} \tag{8}$$

The corresponding experimental slip, $s_{u,exp}$, was taken as the average slip obtained from the LVDTs ($s_{com,LVDT}$).

Table 4.9 *The input parameters and the output values for the interfacial shear stress and the slip.*

Series	$E_{com,II}$ kN/mm^2	b_{com} mm	L_{com} mm	$t_{tx,1}$ mm	$P_{u,av}$ kN	A mm/mm	B 1/mm	R-squred[1]	$\tau_{u,an}$ N/mm^2	$\tau_{u,exp}$ N/mm^2	$\frac{\tau_{u,an}}{\tau_{u,exp}}$	$s_{u,an}$ mm	$s_{u,exp}$ mm	$\frac{s_{u,an}}{s_{u,exp}}$
SB-L-100-4-1				0.084	14.09	0.0129	1.8327	0.9452	1.19	1.41	0.84	0.38	0.42	0.90
SB-L-100-4-2	186	100	100	0.168	15.13	0.0099	1.7873	0.851	1.37	1.51	0.91	0.39	0.29	1.34
SB-L-100-4-3				0.252	19.5	0.0092	1.7381	0.9253	1.72	1.95	0.88	0.40	0.33	1.21
SB-L-100-8-1				0.168	15.75	0.0107	1.5905	0.9383	1.42	1.58	0.90	0.44	0.47	0.94
SB-L-100-8-2	186	100	100	0.338	18.86	0.0087	1.5603	0.9255	1.86	1.89	0.98	0.44	0.32	1.38
SB-L-100-8-3				0.507	20.21	0.0065	1.679	0.7595	1.67	2.02	0.83	0.41	0.31	1.32
SB-L-200-4-1				0.084	16.75	0.0155	0.8439	0.9398	0.79	0.84	0.94	0.82	0.83	0.99
SB-L-200-4-2	186	100	200	0.168	16.59	0.0079	1.6923	0.9632	0.83	0.83	1.00	0.41	0.41	1.00
SB-L-200-4-3				0.252	15.58	0.0042	2.9966	0.9402	0.62	0.78	0.79	0.23	0.25	0.92
SB-L-200-8-1				0.168	14.15	0.0089	1.0571	0.9712	0.65	0.71	0.92	0.66	0.88	0.75
SB-L-200-8-2	186	100	200	0.338	19.28	0.0097	0.7136	0.9415	1.06	0.96	1.10	0.97	0.55	1.76
SB-L-200-8-3				0.507	18.74	0.0075	0.8	0.8003	1.06	0.94	1.13	0.87	0.31	2.81
SB-L-300-4-1				0.084	18.66	0.0151	0.6231	0.9143	0.55	0.62	0.89	1.11	1.64	0.68
SB-L-300-4-2	186	100	300	0.168	16.89	0.0078	1.1371	0.9463	0.54	0.56	0.96	0.61	0.78	0.78
SB-L-300-4-3				0.252	16.32	0.0074	0.9528	0.9441	0.61	0.54	1.13	0.73	0.43	1.7
SB-L-300-8-1				0.168	15.64	0.0075	1.1955	0.9379	0.53	0.52	1.02	0.58	0.92	0.63
SB-L-300-8-2	186	100	300	0.338	26.34	0.0065	1.3276	0.901	0.88	0.88	1.00	0.52	0.52	1.00
SB-L-300-8-3				0.507	28.47	0.0049	1.2333	0.7628	0.70	0.95	0.74	0.56	0.54	1.04
SB-L-400-4-1				0.084	18.26	0.0142	0.7554	0.9085	0.59	0.61	0.97	0.92	1.79	0.51
SB-L-400-4-2	186	100	300[2]	0.168	19.02	0.0076	1.4156	0.9369	0.64	0.63	1.02	0.49	0.98	0.5
SB-L-400-4-3				0.252	18.18	0.0064	1.2453	0.9423	0.6	0.61	0.98	0.56	0.76	0.74
SB-L-400-8-1				0.168	15.84	0.0073	1.23	0.9499	0.51	0.53	0.96	0.56	0.85	0.66
SB-L-400-8-2	186	100	300[2]	0.338	23.77	0.006	1.3062	0.9519	0.74	0.79	0.94	0.53	0.75	0.71
SB-L-400-8-3				0.507	28.04	0.0044	1.2657	0.7897	0.58	0.93	0.62	0.55	0.77	0.71

[1] Pseudo R- Squared value for nonlinear regression analysis obtained from NCSS statistical software.

[2] For $L_f > L_{f,effective}$; $L_f = L_{f,effective}$.

Table 4.9 provides the key data of the analytical analysis. The value of E_{tx} can be determined from the direct tensile tests on the dry steel textiles for different number of layers. However, the difference between the values of E_{tx} for different number of layers is only marginal, hence a value of 186 kN/mm^2 will be adopted for the analytical modelling. The width of the composite, b_{com} , is constant for all the testes SRG composites and is equal to 100 mm. The effective bond length, L_{eff}, was taken equal to 250 mm. The thickness of the steel textiles (t_{tx}) is calculated using the following expression:

$$t_{tx}[mm] = n \,.\, t_{tx,1} \tag{9}$$

where n is the number of the steel textile layers and $t_{tx,1}$ is the equivalent thickness for one layers of the steel textiles and is equal to 0.084 mm or 0.168 for the steel textile of 4 cords/in or 8 cords/in, respectively.

Nonlinear regression analysis was then performed to determine the values of the calibration parameters *A* and *B* for each series after several iterations in NCSS software.

Figs. 4.19-4.22 presents the bond-slip curves obtained from the experimental data (solid lines) and from the analytical model in Equation 4 (dashed lines). In general, the model seems able to capture the experimental response when the bond length is equal or larger than 200 mm except for the specimens that were strengthened with three layers of the steel textiles regardless of the density of the steel textiles. These specimens always exhibited a stiff initial behaviour and eventually failed in a brittle manner without developing a decreasing branch. The model is based on the assumption that the tested specimen will undergo an initial elastic stage represented by the ascending segment of the curve and when the ultimate shear bond stress of the interface is reached, debonding will initiate at the loaded end and an equivalent length of the composite will be engaged near the free end to satisfy the stress state in the system and this process will repeat until there is no sufficient length near the free end can replace the deboned length at the loaded end.

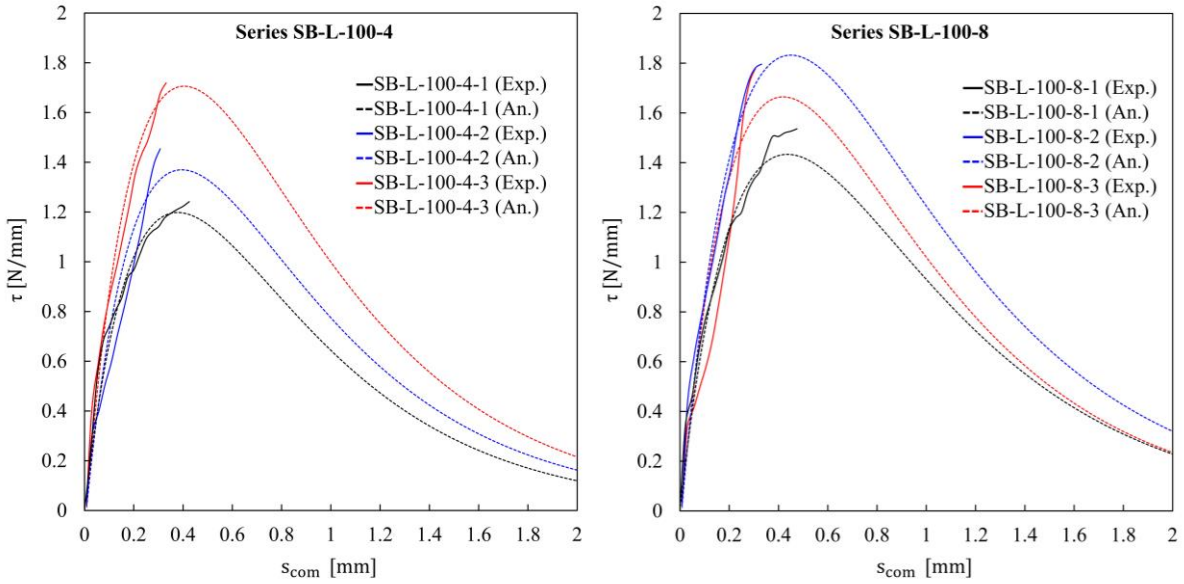

(a) **(b)**

Figure 4.19 *The analytical bond-slip relationship modelling for (a) series SB-L-100-4 and (b) series SB-L-100-84.*

When this condition is reached, the composite will then be fully detached, and any further loading will be solely resisted by the frictions between the substrate and the debonded composite. The process of shifting the engaged area of the composite (defined by the effective bond length) towards the free end and the associated friction is represented in the model by the post-peak segment on bond-slip curve. Specimens with short bond length or heavily reinforced will not always exhibit the post-peak behaviour as they usually fail in a sudden and brittle mode, and this explains why the model fails to capture such specimens.

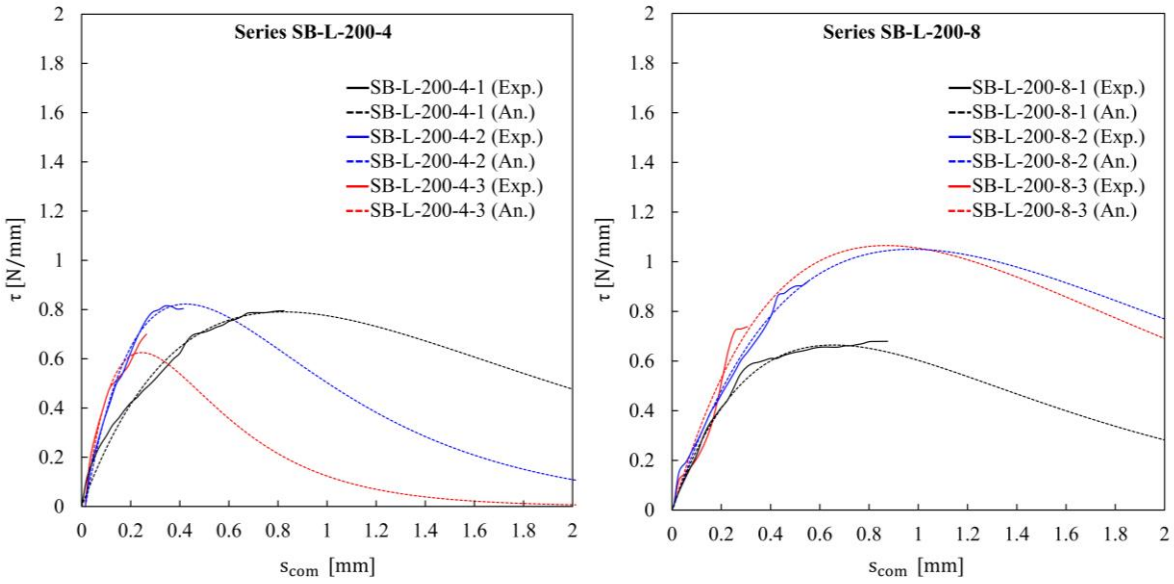

(a) **(b)**

Figure 4.20 *The analytical bond-slip relationship modelling for (a) series SB-L-200-4 and (b) series SB-L-200-8.*

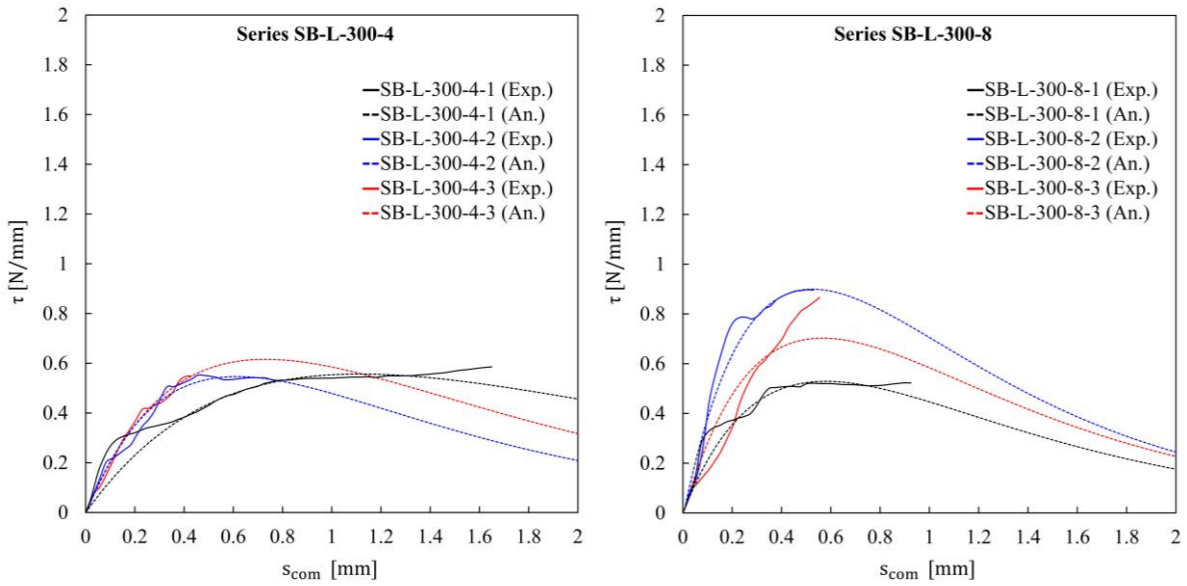

(a) **(b)**

Figure 4.21 *The analytical bond-slip relationship modelling for (a) series SB-L-300-4 and (b) series SB-L-300-8.*

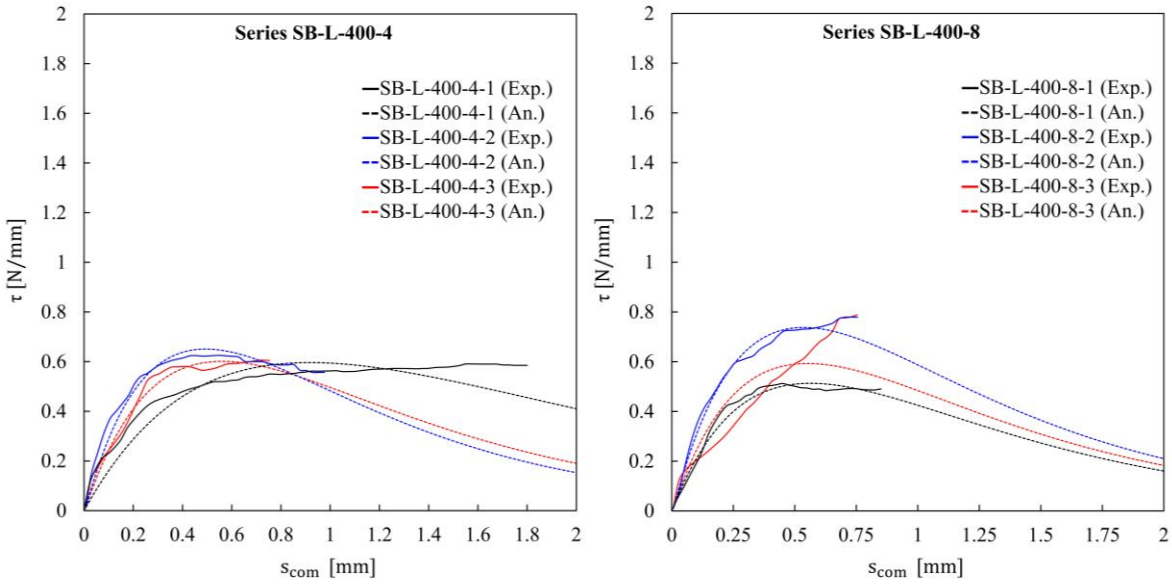

(a) **(b)**

Figure 4.22 *The analytical bond-slip relationship modelling for (a) series SB-L-400-4 and (b) series SB-L-400-8.*

4.5 Conclusions

A total of 90 shear bond tests were conducted on concrete substrates. Four parameters were investigated including the compressive strength of the substrate, the bond length of the SRG composite, the density of the steel textile, and the number of textile layers. The following can be concluded in this experimental investigation:

- Almost all tested specimens exhibited a three-stage stress-slip response such that the first branch was stiff and linear corresponding to the elastic behaviour of the composite followed by another branch of reduced stiffness as the cracks initiated and the last branch representing the process of stress transfer mechanism where the effective bond length was shifting towards the end of the composite. This last branch was developed for the SRG composites that had a bond length more than the effective bond length.
- Although the composite reinforcement ratio was found to insignificantly affect the bond length, the effective bond length of the SRG system can be considered to lie between is between 200 mm and 300 mm.
- Three modes of failure were identified including the tensile rupture of cords observed for the SRG composites comprising only one layer of S4 textiles for bond length more than 200 mm, the debonding at the textile-to-matrix interface which occurred for the series that had one and two layers of S8 textiles regardless of the bond length and the compressive strength of the substrate, and finally the debonding at the matrix-to-substrate interface observed for the SRG composites strengthened with two and three layers of S4 textile and three layers of S8 textiles regardless of the bond length and the compressive strength of the substrate. This latter mode was also observed for the SRG composites comprising one layer of S4 textiles for bond length less than 300 mm.
- The bond length influences the bond performance through increasing the areas of contact at both the textile-to-matrix and the matrix-to-substrate interfaces and hence allowed these interfaces to transfer more stresses to the substrate which in turn resulted in increasing the axial stress in the cords and consequently the slip at the loaded end of the SRG composite. This was only pronounced for the SRG composites comprising only one layer of S4 textiles. Increasing the bond length beyond the effective bond length will only contribute to increasing the slip (the plateau segment of the curve in the last zone of stress-slip curve) while the load will not gain any increase compared to that developed by the SRG composites that have a bond length equal to the effective bond length.
- Increasing the number of textile layers resulted in a decrease in the axial stress in cords and the slip and was significant for the transition from one to two layers. On the other hand, the effect in terms of stress and slip for the transition from two to three layers of textile was less significant suggesting that increasing the number of layers beyond two layers might not be effective.
- Increasing the density of the steel textiles significantly decreased the axial stress and slip in the SRG composites that had one layer of textiles. This effect was less significant for more layers. The use of the denser textiles hindered the full impregnation of grout at the textile-to-matrix interface and created weak regions that triggered the debonding at that interface.
- The compressive strength of the substrate was insignificant in terms of the axial stress and slip. Also, the mode of failure was not affected by the strength of the substrate. This was attributed to the fact that the

debonding at the matrix-to-substrate did not involve the substrate and hence it was not governed by the mechanical characteristics if the substrate.

- An analytical modelling based on the bond-slip model proposed in [22] was carried out. The model provides a good correlation for specimens with bond length of 200 mm or larger. However, the model could not fully capture the specimens strengthened with three layers of the steel textiles irrespective of the bond length and the density of the steel textiles as they always fail in a sudden and a brittle manner.

Acknowledgment

The materials for this experiment (the steel textiles and mortar) were provided by Kerakoll S.p.A. (Sassuolo, MO, Italy). The first author would like to thank Shaqra University in Saudi Arabia and Saudi Arabian Cultural Bureau (SACB) in the UK for funding this part of his PhD research.

References

1. X. Huang, V. Birman, A. Nanni, G. Tunis. Properties and potential for application of steel reinforced polymer and steel reinforced grout composites. Compos B Eng 2005; 36 (1): 73-82.

2. G. de Felice, S. De Santis, L. Garmendia, B. Ghiassi, P. Larrinaga, P.B. Lourenço, D.V. Oliveira, F. Paolacci, C.G., Papanicolaou. Mortar-based systems for externally bonded strengthening of masonry. Mater Struct 2014; 47(12): 2021-2037.

3. L. Ascione, G. de Felice, S. De Santis. A qualification method for externally bonded Fibre Reinforced Cementitious Matrix (FRCM) strengthening systems. Compos B Eng 2015; 78: 497-506.

4. J. Donnini, V. Corinaldesi, A. Nanni. Mechanical properties of FRCM using carbon fabrics with different coating treatments. Compos B Eng 2016; 88: 220-228.

5. M. Matana, A. Nanni, L.R. Dharani, P. Silva, G. Tunis. Bond Performance of steel reinforced polymer and steel reinforced grout. In: Proceedings of BBFS Conference. Hong Kong, December, 2005.

6. E. Stievanin, F. Da Porto, M. Panizza, E. Garbin, C. Modena. Bond characterization between historical concrete substrate and SRG/SRP strengthening systems. In: Proceedings of SEMC Conference. Cape Town, September, 2013.

7. F. Bencardino, A. Condello, A. F. Ashour. Single-lap shear bond tests on Steel Reinforced Geopolymeric Matrix-concrete joints. Compos B Eng 2017; 110: 62-71.

8. F. Ascione, M. Lamberti, A. Napoli, R. Realfonzo. Experimental bond behavior of Steel Reinforced Grout systems for strengthening concrete elements. Constr Build Mater 2020; 232: 105-117.

9. S. De Santis, F. Ceroni, G. de Felice, M. Fagone, B. Ghiassi, A. Kwiecień, G. Lignola, M. Morganti, M. Santandrea, M. Valluzzi, A. Viskovic. Round Robin Test on tensile and bond behaviour of Steel Reinforced Grout systems. Compos B Eng 2017b: 127: 100-120.

10. A. Razavizadeh, B. Ghiassi, D. V. Oliveira. Bond behaviour of SRG-strengthened masonry units: Testing and numerical modelling. Constr Build Mater 2014; 64: 387-397.

11. S. De Santis, G. de Felice. Steel reinforced grout systems for the strengthening of masonry structures. Compos Struct 2015; 134: 533-548.

12. S. De Santis. Bond behaviour of Steel Reinforced Grout for the extrados strengthening of masonry vaults. Constr Build Mater 2017; 150: 367-382.

13. A. Bilotta, F. Ceroni, E. Nigro, M. Pecce. Experimental tests on FRCM strengthening systems for tuff masonry elements. Constr Build Mater 2017; 138: 114-133.

14. S. De Santis, F. Carozzi, G. de Felice, C. Poggi. Test methods for Textile Reinforced Mortar systems. Compos B Eng 2017; 127: 121-132.

15. G. de Felice, G., D'Antino, A., De Santis, S., Meriggi, P., Roscini, F. Lessons learned on the tensile and bond behaviour of Fabric Reinforced Cementitious Matrix (FRCM) composites. Frontiers in Built Environment 2020; 6.

16. G. de Felice G, Aiello MA, Caggegi C, Ceroni F, De Santis S, Garbin E, Gattesco N, Hojdys Ł, Krajewski P, Kwiecień A, Leone M, Lignola GP, Mazzotti C, Oliveira D, Papanicolaou C, Poggi C, Triantafillou T, Valluzzi MR, Viskovic A. Recommendation of RILEM TC 250-CSM: Test method for Textile Reinforced Mortar to substrate bond characterization. Mater Struct 2018; 51 (4).

17. A. Napoli, R. Realfonzo. Reinforced concrete beams strengthened with SRP/SRG systems: Experimental investigation. Constr Build Mater 2015; 93: 654-677.

18. G. Thermou, S. De Santis, G. de Felice, S. Alotaibi, F. Roscini, I. Hajirasouliha, M. Guadagnini. Bond Behaviour of Multi-Ply Steel Reinforced Grout Composites. Constr Build Mater [under review]19. J. Chen and J. Teng. Anchorage Strength Models for FRP and Steel Plates Bonded to Concrete. Journal of Structural Engineering 2001;127(7):784-791.

20. Lu X, Teng J, Ye L, Jiang J. Bond–slip models for FRP sheets/plates bonded to concrete. Eng Struct. 2005;27(6):920-937.

21. Neubauer U, Rostasy F. Design aspects of concrete structures strengthened with externally bonded CFRP plates. In: 7Th Int. Conf. On Struct. Edinburgh: ECS Publications; 1997:109–118.

22. Dai J, Ueda T, Sato Y. Development of the Nonlinear Bond Stress–Slip Model of Fiber Reinforced Plastics Sheet–Concrete Interfaces with a Simple Method. Journal of Composites for Construction. 2005;9(1):52-62.

Chapter 5 Flexural Behaviour of RC Beams Strengthened with Steel Reinforced Grout Systems

Sultan Alotaibi[1,2*], Georgia Thermou[3], Iman Hajirasoulah[1], Maurizio Guadanini[1]

[1] *Department of Civil and Structural Engineering, The University of Sheffield, Sheffield, UK*

[2] *Department of Civil Engineering, Shaqra University, Dawadmi, Saudi Arabia*

[3] *Department of Civil and Structural Engineering, The University of Nottingham, Nottingham, UK*

** Corresponding author. E-mail: salguery@su.edu.sa*

Abstract

This paper presents the results of an experimental investigation on the flexural behaviour of reinforced concrete (RC) beams strengthened with Steel Reinforced Grout (SRG) systems. Four-point bending tests were performed on six full-scale beams which were strengthened with SRG systems of different textile density (4 and 8 cords/in) and number of layers (1 and 2 layers). One of the beams was provided with an anchorage system. All beams were instrumented with a set of LVDTs to measure deflection and slip of the SRG composite and a set of strain gauges to obtain the strain in the internal reinforcement. Digital Image Correlation (DIC) system was used to obtain crack patterns and strain maps. Test results showed that all the tested beams developed a trilinear load-deflection response. In general, the strengthened beams exhibited a stiffer response up to the yielding of the steel rebars ~~in the first two stages on the load-deflection curves~~. The use of the steel textiles of low density (4 cords/in) enabled the SRG composite to develop a better impregnation with the grout and resulted in full exploitation of the textiles as they eventually failed by tensile rupture regardless of the number of the textile layers. On the other hand, the use of high-density steel textiles (8 cords/in) compromised the bond between the textile and the matrix and developed interlaminar shearing at textile-matrix interface for the beam strengthened with a single layer of the textile, while the beam strengthened with two layers ultimately failed by end debonding of the SRG composites. The SRG composite provided an enhancement to the load carrying capacity in the range from 10 % to 28 %, while the deflection was marginally increased.

Keywords:

Flexural Strengthening;;RC beams; Steel Reinforced Grout(SRG); Bending Tests; Digital Image Correlation (DIC).

5.1 Introduction

In general, the use of Fibre Reinforced Polymer composites (FRPs) in the strengthening sector has been discouraged by a number of disadvantages including high cost in terms of materials and labour, low performance under elevated temperatures, toxic nature of epoxy, lack of reversibility, and lack of vapour permeability [1-2]. These disadvantages were primarily associated with the organic matrix used to impregnate the fibres (typically epoxy). To address some of these issues, Fabric Reinforced Cementitious Matrices (FRCM) composites have been introduced as a replacement for the FRP system. Inorganic matrices (e.g., grout) were used in FRCM composites as an impregnation medium instead of the organic ones. Although these inorganic matrices were not as efficient as the organic ones in terms of the mechanical bond to the fibres, they have shown a set of advantages, including compatibility with the substrate, ease of application, and improved performance under elevated temperatures, not to mention their relatively low cost [2-3]. Among these FRCM systems, the use of the steel textiles has recently received special attention from the scientific community mainly due to its relatively low cast compared to other fibre textiles and its good mechanical properties. The use of steel textile to reinforce the composite is known as SRP (Steel Reinforced Polymer) with organic composites or SRG (Steel Reinforced Grout) with inorganic ones.

Knowledge on the performance of FRCM composites in different applications is well established in the scientific community [e.g., 4-11]. SRP systems are also investigated in several studies available in the literature [e.g., 12-15]. As for the system under investigation (SRG system), different aspects of this system were studied including tensile behaviour [e.g., 16], bond behaviour to masonry [e.g., 17-19] and to concrete [e.g., 20-21], confinement applications [e.g., 22-26], strengthening of RC beams for shear [27-28] and for flexure [e.g., 5, 12-13, 29-35]. While these studies in general demonstrated the good performance of FRCM systems compared to the use of FRPs, they were mainly limited to the application of one layer of external reinforcement. Also, the bond behaviour of these FRCM composites was mainly devoted to masonry substrates. The use of only one layer of external reinforcement will not always be sufficient to meet the new upgrading requirements, particularly when strengthening large flexural members with limited width. In this case multiple layers of external reinforcement might be considered. As for FRCM systems, slippage and debonding of multiple layers of reinforcement is reported in the literature [7, 10, 31, 36]. The use of steel textile of relatively high-density cords is also shown to trigger interlaminar debonding at textile-matrix interface [30 and 33].

The beams strengthened with the SRP and SRG systems generally exhibit a trilinear load-deflection curve, which includes a branch characterising the elastic response of the beam up to the formation of the cracks followed by an almost-linear branch describing elastic response of the internal reinforcement up to the yielding of the steel rebars, and finally a significant drop in the stiffness of the RC beam [13, 33]. The use of strengthening systems comprising steel textiles (SRP and SRG) generally improved the flexural capacity of the strengthened RC beams [13]. Furthermore, the global behaviour in terms of strength and deformability of the beams strengthened with steel textiles was found not to be affected by the utilised matrix (epoxy adhesive vs grout) [12]. However, the beams strengthened with the SRP systems exhibited more deflection ductility than their SRG counterparts [13]. Also, the beams strengthened with both systems (i.e., SRP and SRG) exhibited vertical cracks corresponding to a critical diagonal crack in the substrate [12].

The use of the SRG system was reported to improve to the flexural capacity of the strengthened RC beams. A total increase in the ultimate capacity in the range from 20 % to 40 % was reported [2, 13, 33] compared to a reference beam (i.e., un-strengthened beam). However, an improvement of 100 % in the flexural capacity was also reported for prestressed-concrete beams [12]. It was also observed that the use of the SRG systems was able to increase the load at which the internal steel rebars reach yielding. An increase by15 %-21 % of the yield load with respect to the reference beam was reported [30]. On the other hand, the use of the SRP systems significantly improved the flexural capacity of the strengthened RC beams. A strength increase of almost the double was observed for the strengthened specimens with respect to the un-strengthened specimens with the presence of anchorage system [13, 14]. However, without the anchorage system, the improvement to the flexural capacity was reduced to only 75 % compared to the control specimens [13]. It is worth mentioning that not all the SRP systems developed such high percentages in terms of improvement to the flexural capacity as some of the beams strengthened with SRP systems developed an enhancement in the flexural capacity of only 30 % [2, 34].

As for the mode of failure, the beams strengthened with systems made of steel fabrics in general did not develop any cohesive debonding (i.e., debonding involving a thick layer of the substrate).This was mainly attributed to the lower axial stiffness of the steel textile compared to the other FRP systems, where cohesive debonding is often observed [12]. However, the engagement of the concrete substrate is more pronounced in the SRP systems compared to the SRG system. This was evident by the mode of failure as the beams strengthened with SRP systems failed by end debonding with chunks of the concrete substrate, while their SRG counterparts failed at the interface between the SRG composite and the substrate without involving the latter [15]. Also, debonding at the matrix-to-textile interface (interfacial debonding) was observed for some RC beams strengthened with the SRG system [30, 33]. However, this mode of failure was associated with use of steel textile of high-density cords as they hindered the full impregnation of the textiles within the grout and created a weak interface prone to debonding. It was, also, reported that the beams strengthened with steel textiles irrespective of the matrix used (i.e., epoxy vs grout)

experienced debonding at the matrix-to-substrate interface that initiated at a location away from the composite end (intermediate debonding)[13]. However, when the U-anchorage system was provided, the mode of failure was altered from intermediate debonding to end debonding with either slippage (for the beams strengthened with the SRG systems) or rupture of the textiles (for the beams strengthened with the SRP systems) [13]. In fact, the presences of an anchorage system helped in achieving full exploitation of the steel textiles in the SRP systems [13]. The efficiency of different anchorage systems (e.g., nail anchors) has been also investigated in the past. However, the beams strengthened with the SRG composites with this system did not gain a significant improvement in terms of the structural performance [15].

This study presents an experimental investigation of the flexural behaviour of six full-scale RC beams strengthened with SRG system. Three parameters are investigated including the density of steel textile (4 and 8 cords/in), the number of layers of steel textile (1 and 2), and the influence of the anchorage system. The main aim of this study is to build a better understanding of the flexural performance and the failure mechanism of RC beams that are strengthened with different steel textile and different number of layers. Furthermore, this study explores the mechanism of stress transfer in the RC beams strengthened with multiple layers of the textiles and how the density of the textile can affect that mechanism. For the first time, the efficiency of single and multi-layer SRG systems is compared for flexural strengthening of full-scale elements using the same amount of reinforcement. This is important from optimisation perspectives, as the use of a single-layered SRG system can save additional costs in terms of material (grout between different layers) and the associated labour cost. The results are then used to provide practical design recommendations for more efficient design of SRG systems, especially when more than one layer of textile is required.

5.2 Experimental Programme

A total of six beams were tested in four-point bending test under displacement control. using the typical cross section of 250 mm ×150 mm (see Fig. 5.1). All the specimens had the span length of 2500 mm, with the same constant-moment and shear spans equal to 768 mm and 766 mm, respectively (see Fig. 5.2). The shear span ratio a/d was equal to 3.07 to avoid any shear-governed modes of failure (shear-compression and shear-tension modes). Each beam was reinforced with two 12 mm diameter rebars and two 10 mm diameter rebars as tensile and compression internal reinforcement, respectively. The shear links were 8 mm steel bars spaced at 138 mm centre-to-centre with a total concrete cover of 12 mm. A schematic illustration of the geometry and reinforcement detailing of a typical beam is provided in Figs. 5.1-5.2.

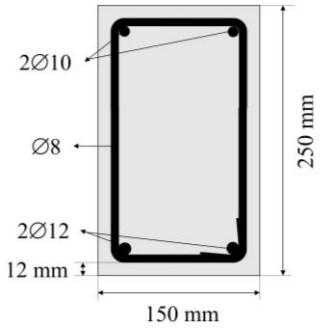

Figure 5.1 *Typical cross section of a beam specimen.*

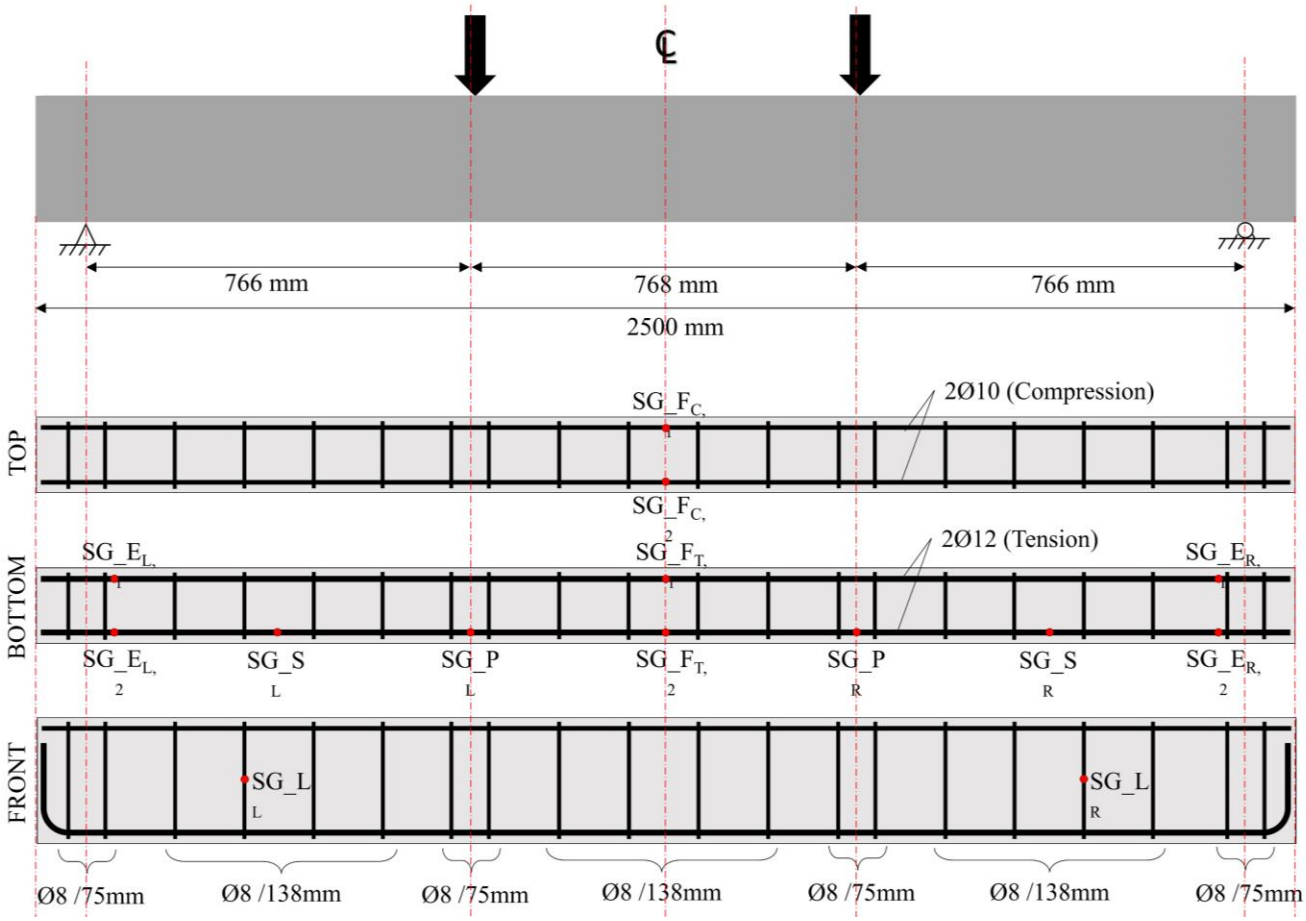

Figure 5.2 *Detailing of internal reinforcement and the layout of strain gauges for a typical beam.*

Different SRG strengthening layouts were applied to five beams, while the last beam served as the control specimen. One of the SRG strengthened beams was used as a reference beam for comparison with the various strengthening SRG configurations. The strengthened beams were labelled following the notation "B-SX-Y", in which "B" denotes beam, "SX" denotes the density of steel textile ("S4" for steel textile of 4 cords/in and "S8" for steel textile of 8 cords/in), "Y" denotes the number of steel textile layers (1 or 2). The control beam was named as "B-REF", while

the reference beam which was strengthened with one layer of a S8 textile was labelled as "B-S8-1-REF". Table 5.1 provides details of the internal and external reinforcement for each beam.

Table 5.1 *Internal and external reinforcement details.*

Beam	Internal reinforcement			External reinforcement		
	Tension	Compression	Shear	Textile density (cord/in)	Number of layers	Anchorage
B-REF	Ø12	Ø10	Ø8	N/A	N/A	N/A
B-S8-1-REF				8	1	Both ends
B-S4-1				4	1	One end
B-S4-2				4	2	One end
B-S8-1				8	1	One end
B-S8-2				8	2	One end

5.2.1 Materials

All beam specimens were cast with one ready-mix concrete batch that had a mean cubic (150 mm edge) compressive strength of 38 MPa at 28 days. The beams were kept wet after casting for the first 7 days and were then left in laboratory conditions for at least 28 days before testing.

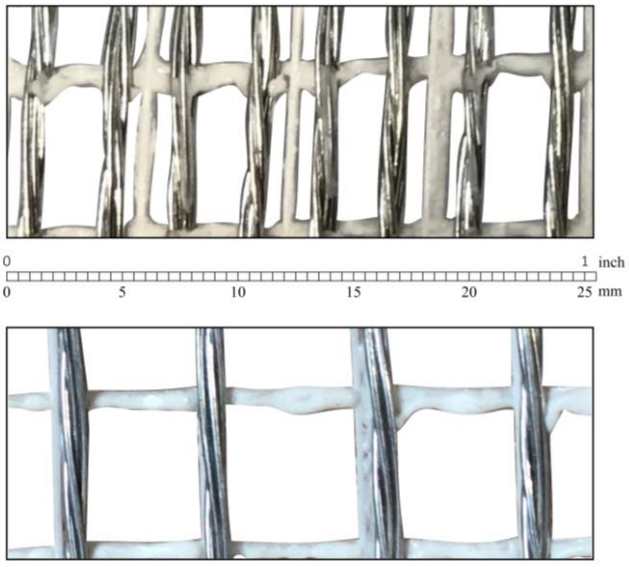

Figure 5.3 *Steel textile of densities 8 cords/in (above) and 4 cords/in (below).*

The mechanical properties of flexural and shear internal reinforcement are presented in Table 5.2. It includes the average yield stress and the corresponding strain and the average ultimate stress and the corresponding strain.

The steel textile used for SRG system is made of unidirectional ultra-high tensile strength steel (UHTSS) micro-cords, thermo-welded to a fibreglass micromesh. Each cord has a cross sectional area of 0.538 mm^2 and is obtained

by joining 5 wires, 3 straight and 2 wrapped with a high torque angle to enhance the interlocking with the mortar. Wires have a cross sectional area of 0.11 mm^2 and are galvanized (coated with zinc) to improve their durability. As shown in Fig. 5.3, two different textiles were used for the strengthening of the beams. These two textiles had the same mechanical properties but were different in terms of cords density namely 4 cords/in (1.57 cords/cm, labelled as S4) and 8 cords/in (3.15 cords/cm, labelled as S8). The steel cords in S4 textile are evenly arranged such that the clear spacing between two cords is 5.45 mm, whereas, in S8 textile, the cords are paired such that the clear spacing between two pairs is 2.28 mm (see Fig. 5.3). Table 5.3 provides detailed information on the mechanical properties of both steel textiles.

The matrix used to manufacture SRG system was a pre-mixed geopolymer mortar with a crystalline reaction geo-binder base. It had a compressive strength of 51 N/mm^2, tensile strength of 8 N/mm^2 and Young's modulus of 22 kN/mm^2. The water-to-mortar powder mix ratio was 1:5.

Table 5.2 *The mechanical properties of the reinforcing rebar.*

Rebar	Yield stress N/mm^2	Yield strain	Ultimate stress N/mm^2	Ultimate strain
Ø12	524	0.0025	637	0.117
Ø10	559	0.0025	652	0.109
Ø8	540	0.0027	664	0.091

Table 5.3 *The mechanical properties of steel textiles according to the manufacturer.*

Property	S4 N/mm2	S8 N/mm2
Number of cords	4	8
Cords density (cords/cm)	1.57	3.15
Surface mass density (g/m^2)	670	1300
Design thickness (mm)	0.084	0.169
Average tensile strength (N/mm^2)	3200	
Ultimate strain (%)	1.5	
Tensile modulus of elasticity (kN/mm^2)	186	

5.2.2 Application of the SRG system

Prior to the application of SRG composite, the substrate (i.e., the tension face of the beam) was grinded by means of an electrical angle grinder to remove the smooth layer of paste and expose aggregate for a better bond between the composite and the beam (see Fig. 5.4(a)). The grinded surface was then cleaned from debris and dust and was kept wet for at least one day prior to the installation of SRG system. This latter step was to ensure that the water-to-cement ratio in the matrix is not compromised by any hydration process that might takes place within the substrate after the application of the composite. For the strengthened specimens, the SRG system was applied to the bottom

of the beam (tension face) by means of a specially designed acrylic mould to control the thickness of the SRG composite (see Fig. 5.4(b)). After the application of the first layer of grout, the steel fabric was placed on top of the layer and gently pressed by hand until it was fully impregnated in the mortar. An additional layer of grout was then laid on the top of the steel textile as shown in Fig. 5.4(c). This process was repeated once more for SRG composites with two layers of steel textile. Special attention was paid to ensure that the textile layers were aligned with each other. It was also ensured that the installation time for the SRG composite was within the working time of the mortar. This is crucial as it ensures the homogeneity between the layers of a single SRG composite. Each layer of grout had a thickness of 3 mm, which was controlled by the acrylic moulds. Finally, the strengthened beams were covered with a hessian fabric, and were then kept wet for three days to enhance the hydration process.

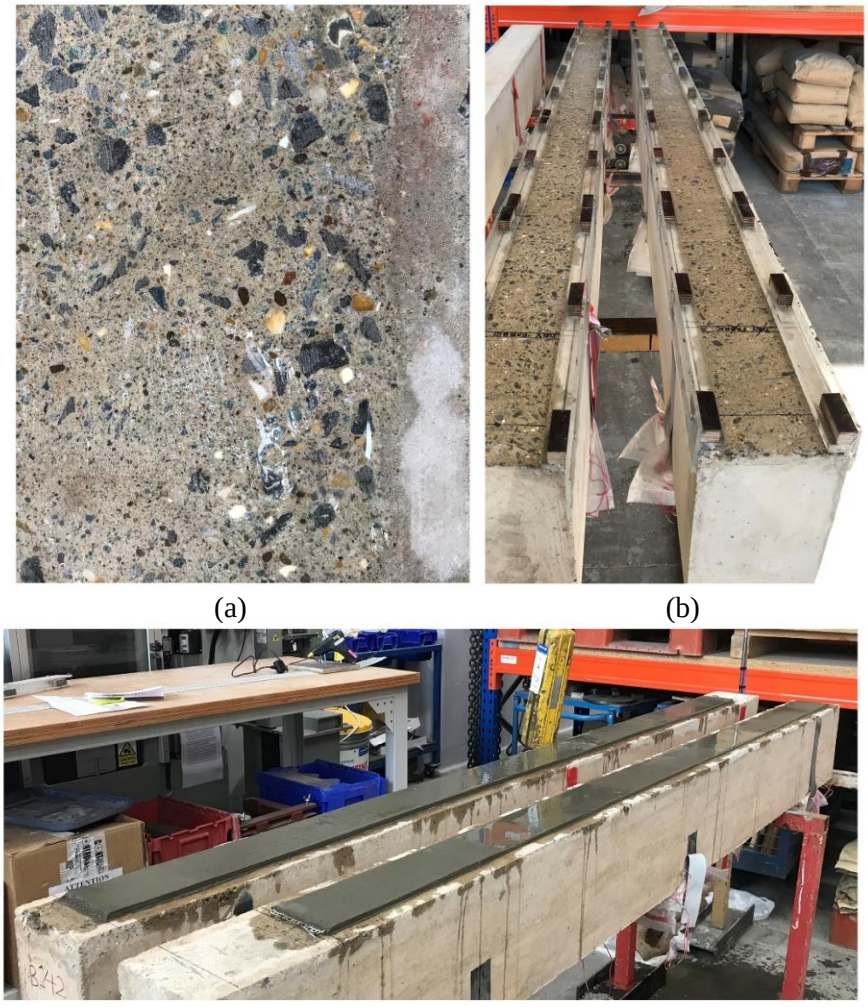

Figure 5.4 *(a) Substrate after grinding, (b) Acrylic moulds mounted on beams prior to the application of SRG composite, and (c) SRG composite applied to the beams.*

The strengthening layout for the strengthened specimens is presented in Fig. 5.5. The width of the SRG composite strip was 100 mm for all the strengthened beams. The SRG strip was not applied to the full width of the bottom of

the beam (150 mm) to avoid edge effects and exhibit a better distribution of fine and coarse aggregates. All the strengthened beams had SRG composites of a total length of 2250 mm. The SRG composite in reference beam B-S8-1-REF was extended beyond the support at the controlled side of the beam, while on the observed side it was terminated 50 mm before the support. The dry steel textile was extended beyond the support and was sandwiched between two aluminium plates and impregnated in a two-part epoxy to provide anchorage to the SRG composite. The aluminium plates were also attached to the beam by mean of the same two-part epoxy adhesive. The rest of the strengthened beams (i.e., B-S4-1, B-S4-2, B-S8-1, and B-S8-2) had the same strengthening layout as beam B-S8-1-REF, however the steel textile was also terminated 40 mm off the support leaving a bare steel textile of 10 mm extending outside the composite to monitor the slippage (see Fig. 5.6).

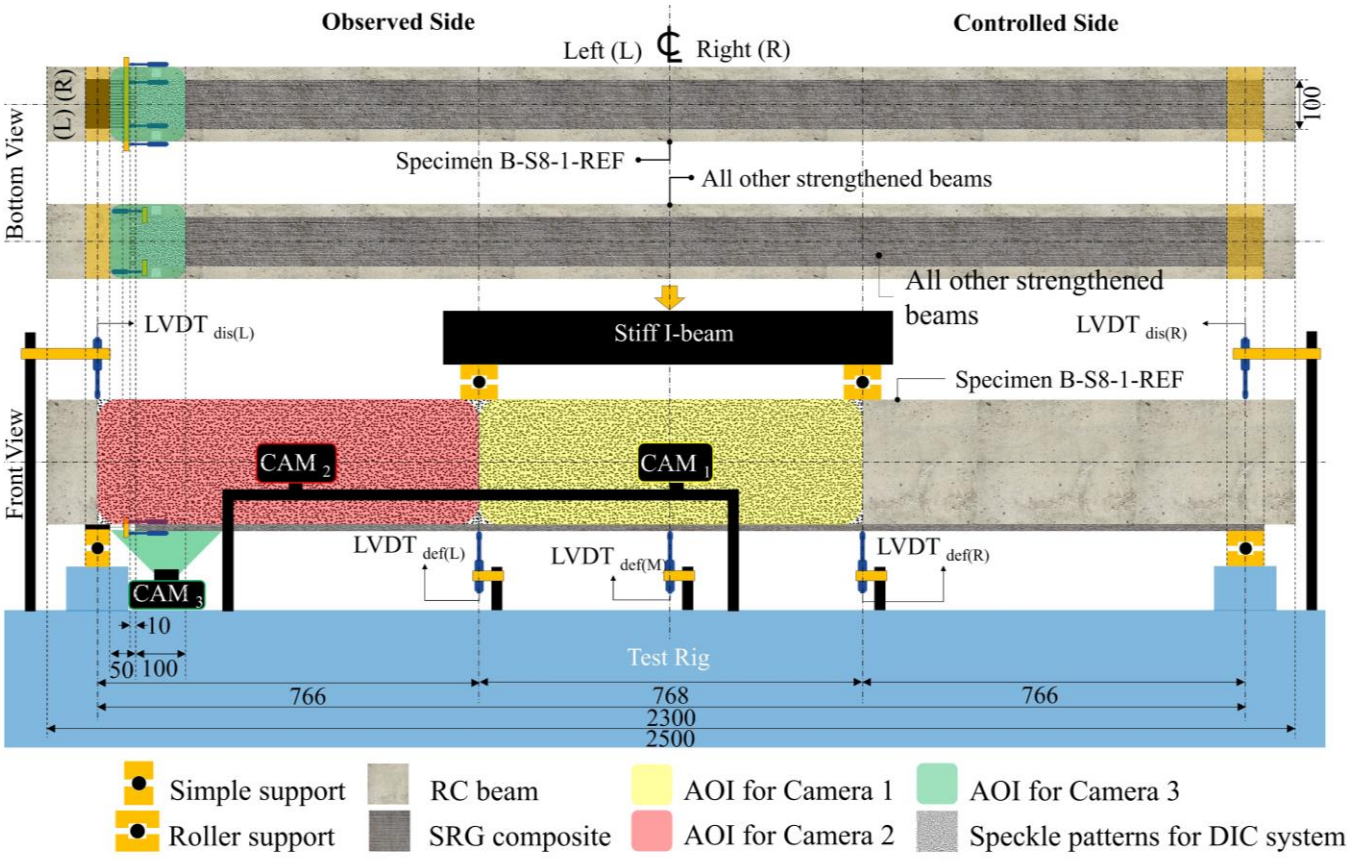

Figure 5.5 *The test set up and instrumentation of LVDTs and DIC system.*

5.2.3 Test set-up and instrumentation

All beams were tested under a four-point bending test protocol. The displacement-controlled load was applied at rate of 0.60 mm/min. The load was transferred from the actuator to the specimen through a stiff I-beam which was in contact with the specimen on two roller supports (see Fig. 5.5). The RC beam was reacting against another two rollers and fixed supports transferring the load to the test rig. A preloading cycle up to 25 kN was performed to

make sure the setup arrangement is working as planned. The first loading cycle was followed by a second unloading cycle and the beams were finally loaded to failure.

Fig. 5.6 provides a schematic presentation of the LVDTs setup for the SRG composite. All beams were instrumented with five LVDTs to measure deflection and displacement of the beams at midspan, under the load points, and at the supports of each beam. To measure the slip of the free end of the SRG composite (at the observed side of the beam, see Fig. 5.6) in beam B-S8-1-REF, a set of four LVDTs were used. Two of the LVDTs were attached to substrate while the other two were attached to the composite. All the LVDTs were reacting against a bracket that was glued to the bare steel fabric. The rest of the strengthened beams were instrumented with only two LVDTs to measure the slip of the SRG composite such that both were attached to the substrate and were reacting against two brackets that were attached to the sides of the free end of the composite.

Figure 5.6 *The bare part of the steel textile at the free end of the SRG composite.*

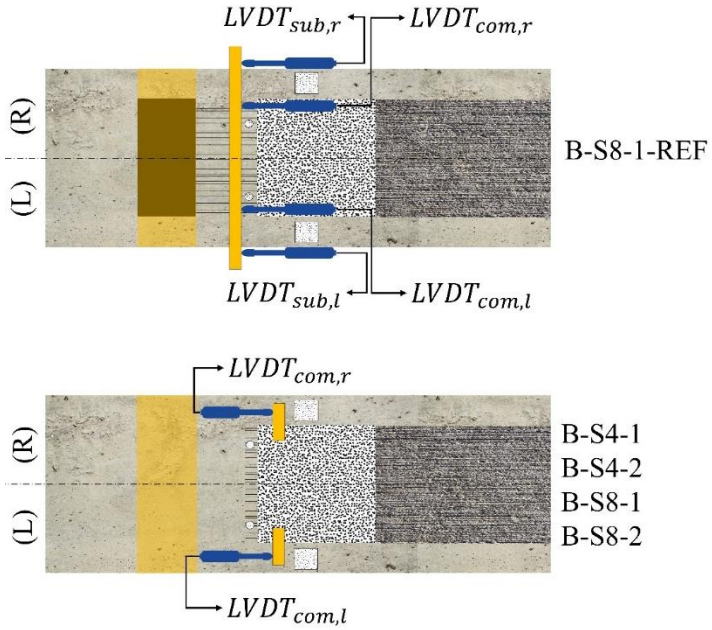

Figure 5.7 *Details of the LVDT instrumentation at the end of the SRG composite.*

A set of fourteen strain gauges were glued to the internal rebars to measure strain at different location on the internal reinforcement including the tensile and compression reinforcement and the shear links at the middle of the shear span. Furthermore, the strain was measured in the tensile rebars at positions corresponding the concentrated loads including the supports and the point loads. The details of the locations of these strain gauges are presented in Fig. 5.2.

Digital Image Correlation (DIC) system was used to capture strain maps and crack patterns for three Areas Of Interest (AOI) including the flexural span, the shear span of the observed side of the beam, and the free end of the SRG composite. These areas are defined by referring to the colour of the hatched areas in Fig. 5.5. Three digital cameras were used to capture still images of the AOIs. Cameras 1 and 2 were positioned in front of the beam to capture still images of the flexural (yellow area in Fig. 5.5) and shear (red area in Fig. 5.5) spans, respectively. On the other hand, camera 3 was positioned beneath the monitored side of the beam (the green area in Fig. 5.5) to capture images of the monitored end of the SRG composite.

5.3 Results and Discussion

Table 5.4 summarises the results obtained from four-point bending tests for all the beams. The table includes the following results:

1. The load at which the internal reinforcement reached yielding, F_y , and the corresponding deflection at midspan, δ_y. The yield load, F_y, is defined as the point on the load-deflection curve at which the slope experiences a significant change.
2. The ultimate load at either crushing of concrete or failure of the SRG system by either tensile rupture of the steel textiles or debonding, F_u and the corresponding deflection at midspan, δ_u.
3. The increase in the yield load with respect to the reference beam, $F_{y/}\, F_{y,control}$.
4. The increase in the ultimate load with respect to the reference beam, $F_{u/}\, F_{u,control}$.
5. The displacement ductility index of the strengthened beams, $\mu_\delta = \delta_u/\delta_y$.
6. The mode of failure. Five modes of failure were observed including crushing of concrete after the yielding of the internal reinforcement (A), rupture of the steel textile (B), slippage of cords (C), debonding at textile-matrix interface (D), and debonding at substrate-matrix interface (E).

Table 4 *The results of four-point bending tests*

Specimen	F_y (kN)	F_u (kN)	$F_{y/}\, F_{y,control}$	$F_{u/}\, F_{u,control}$	δ_y (mm)	δ_u (mm)	μ_δ	Failure mode
B-REF	63	69	1	1	11.57	58.19	5.03	A
B-S8-1-REF	71	86	1.13	1.25	13.93	58.51	4.20	D

B-S4-1	65	76	1.03	1.10	14.24	59.04	2.80	B
B-S4-2	69	89	1.09	1.29	13.73	60.36	3.45	B
B-S8-1	71	84	1.13	1.22	13.06	58.13	3.20	B+C+D
B-S8-2	77	88	1.22	1.28	15.47	62.68	1.44	E

5.3.1 Load-deflection response

The load-midspan deflection curves and the deflection profile at yield and ultimate loads for all tested beams are plotted in Figs. 5.8-5.9. All the tested beams exhibited a flexural response characterising three distinct stages. The first stage (stage 1) is represented by the segment of the curve up until the formation of cracks and it characterises the elastic behaviour of the beam. The second branch of the curve up until the drastic change in slope describes the second stage (stage 2) characterising a semi-linear flexural behaviour that ended as soon as the flexural internal tension reinforcement yielded. The last segment of the curve represents the third stage (stage 3) characterising a significant drop in stiffness where the midspan deflection increases at a little gain in the load until the failure of the beam.

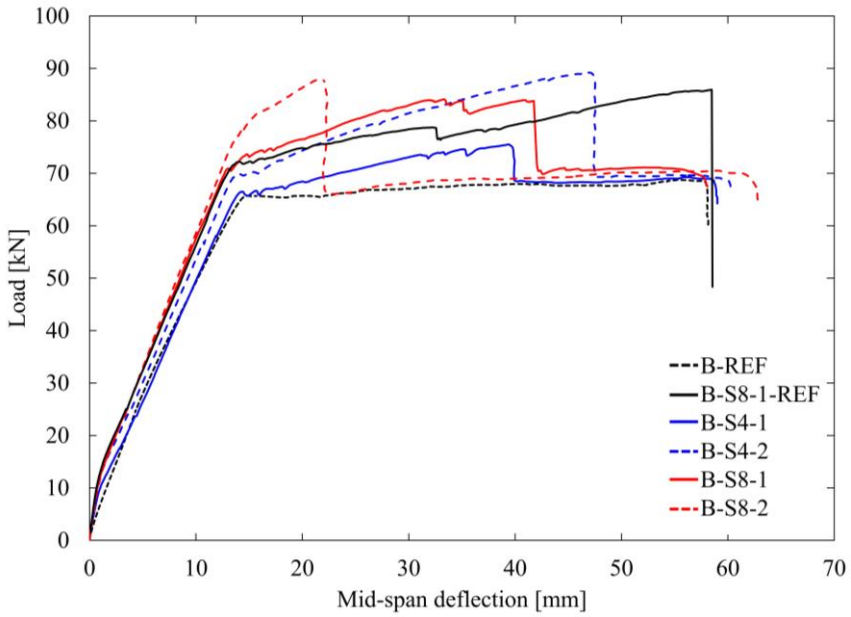

Figure 5.8 *The Load-deflection curves for tested beams.*

Beam B-REF (un-strengthened control beam) and beam B-S4-1 had an elastic behaviour ending at an approximate cracking load of 9 kN and 12 kN, respectively. The rest of the tested beams (i.e., B-S8-1-REF, B-S8-1, B-S8-2, and B-S4-2) had a stiffer elastic behaviour compared to beams B-REF and B-S4-1. The formation of flexural cracks for this group occurred at a load of approximately 17 kN. This initial stiffer behaviour is due to the contribution of SRG

systems of higher stiffness. Beams with low amount of external reinforcement (i.e., B-S4-1) developed a less stiff initial behaviour compared to the rest of the strengthened beams.

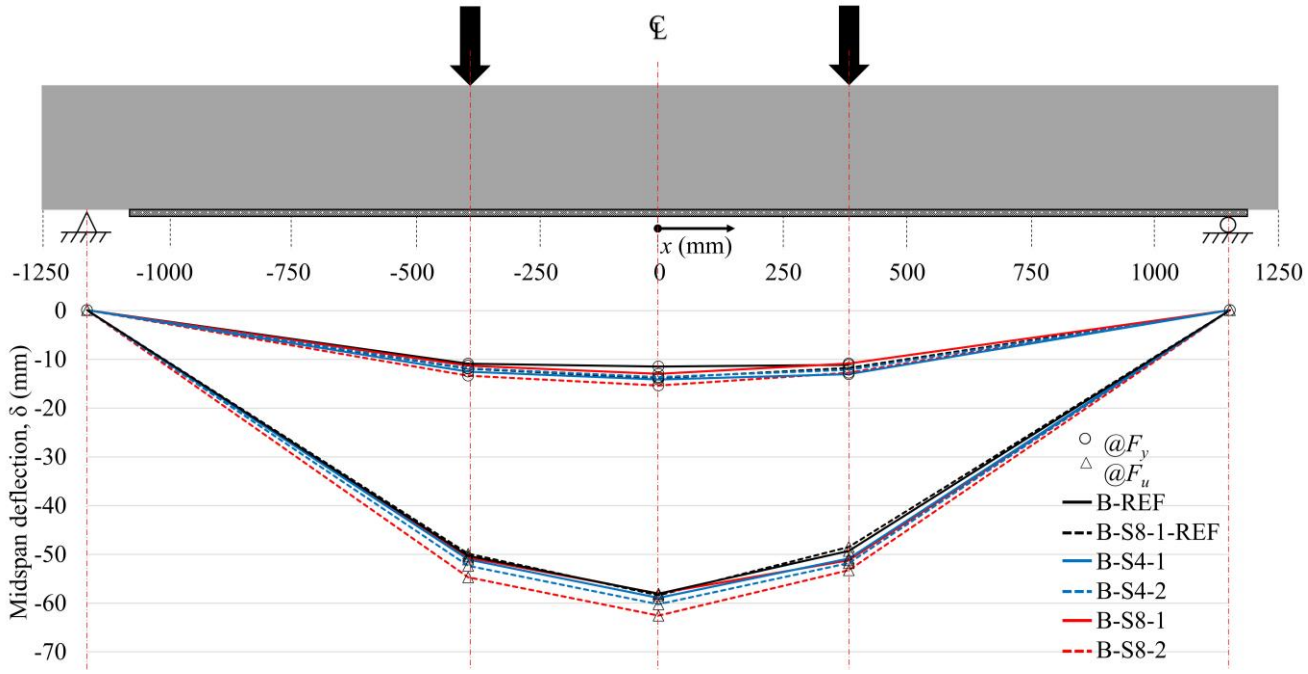

Figure 5.9 *The deflection profile for tested beams at yield and ultimate loads.*

The above trend was also observed for the second branch of the load-deflection curve where the composites of high amount of steel reinforcement attained a higher stiffness, however, the yielding of the internal reinforcement occurred at different load values. The yielding of internal reinforcement for beams B-REF and B-S4-1 occurred at a load of approximately 63 kN and 65 kN, respectively, while beam B-S4-2 attained a slightly higher yielding load of 69 kN. Beams B-S8-1-REF and B-S8-1 (both had one layer of S8 steel textile) developed a similar yielding load of approximately 71 kN. The highest yielding load was experienced by beam B-S8-2, which had the highest amount of composite reinforcement (two layers of S8 steel textile).

The tested beams behaved quite differently in the last branch of the load-deflection curve. The reference beam B-REF experienced a drastic change in the stiffness at no significant increase in the applied load until the failure of the beam . Beam B-S4-1 developed a relatively higher slope compared to that of B-REF and experienced some drops in the curve corresponding to the initiation and propagation of cracks in the composite. After the SRG composite failed in beam B-S4-1 by textile rupture at an approximate load of 76 kN, the beam just resembled the behaviour of B-REF in the last stage up to the point of failure. The strengthened reference beam, B-S8-1-REF, exhibited a reduction in stiffness after the yielding of the steel rebars (i.e., stage 3). However, the stiffness of Beam B-S8-1-REF in stage 3 was higher than that which was developed by beam B-REF in the same stage. There was a dramatic decline in the load-deflection curve at a load of approximately 79 kN corresponding to the propagation of

a major interlaminar crack (i.e., at textile- matrix interface), however, the curve resumed the ascending trend at the same stiffness prior to the drop until it reached its ultimate load at approximately 86 kN. Comparing beams B-S8-1-REF and B-S8-1 which had the same steel textiles and the same number of layers, it was observed that they behaved quite similarly in terms of yield load, stiffness, and the attained ultimate load. However, beam B-S8-1 experienced a major drop in the third branch of the load-deflection curve at a deflection of approximately 42 mm corresponding to the slippage of steel cords within the SRG composite. This was however prevented in beam B-S8-1-REF due to the anchorage system implemented in that beam. The beams that had two layers of SRG composite (i.e., B-S4-2 and B-S8-2) behaved quite differently based on the density of steel textile used in the SRG composite. Beam B-S4-2, which was strengthened with two layers of S4 textile, attained its peak load corresponding to a higher deflection (approximately 47 mm) before the failure of the SRG system. On the contrary, the beam B-S8-2, which was strengthened with two layers of S8 steel textile, attained its peak load at a deflection value of approximately 47 % of that developed by B-S4-2. Beam B-S8-2 had the highest amount of SRG reinforcement and developed the highest stiffness among all the tested beams. This beam specimen failed due to debonding at an ultimate load of approximately 88 kN. The beams strengthened with the same amount of reinforcement but with different number of layers (i.e., B-S4-2 and B-S8-1) exhibited a similar flexural behaviour. However, the mode of failure was different as B-S4-2 failed by tensile rupture of the steel textile at a load of 89 kN, while B-S8-1 failed by debonding at the matrix-to-textile interface at a load of 88 kN. This can be attributed to the poor penetration of the grout within the steel textile which was often observed for the textiles with high density of cords.

The increase in the yield load of the strengthened beams with respect to that of the reference beam B-REF ranged from 3 % to 22 %. Beam B-S4-1 improved the yield load as little as 3 %, whereas beam B-S8-2 provided an increase in the yield load of approximately 22 %. The beams that had the same amount of reinforcement (i.e., Beam B-S8-1-REF, B-S8-1 and B-S4-2)) exhibited an increased yield load compared to the reference beam by a very close percentages (in the range 9 %-13 %).

The load values attained by all the strengthened beams at the failure of the SRG system were in the range from 76 kN to 89 kN. The $F_{uf}/ F_{u,control}$ ratio for these specimens ranged from 1.10 to 1.29. Beam B-S4-2 developed the highest ratio among all the strengthened beams mainly due to the improved impregnation between the grout and the relatively low-density steel textile. This mechanical interlock prevented the interlaminar shear at textile-matrix interface and led to the full exploitation of the textile as it eventually failed by the rupture of the textile. Again, beams strengthened with equal amount of reinforcement exhibited comparable $F_{uf}/ F_{u,control}$ ratios regardless of the number of steel textile layers and the presence of the anchorage system. However, the anchorage system in beam B-S8-1-REF significantly influenced the displacement ductility ratio of the beam, which was equal to 4.20. Beam B-S4-2 developed the highest displacement ductility ratio of 3.45 after beam B-S8-1-REF. Beams with the same (B-S8-1) or higher (B-S8-2) amount of the external reinforcement could not attain such a displacement ductility

ratio because of the interruption of debonding which was prevented in beam B-S8-1-REF by the action of the anchorage system.

5.3.2 Crack pattern

Fig. 5.10 presents crack patterns and strain maps at yield and ultimate loads for all the tested beams at the flexural and shear spans of the monitored side of the beams obtained from the DIC system. It was observed that all the tested beams developed comparable crack patterns. The beams had typical vertical flexural cracks in the flexural span and typical inclined cracks in the shear span. The first crack was developed in the beginning of stage 2 and the process of cracks initiation and propagation continued up until the yielding of the steel rebars. After this stage, no new cracks were formed but the existing cracks were still propagating. The average crack spacing for all the tested beams was approximately 137 mm which corresponds to the shear links that was spaced at 138 mm. The SRG composite in all the strengthened beams also developed small and evenly distributed transverse cracks, which in most cases corresponded to the cracks in the substrate.

5.3.3 Failure modes

Beam B-REF had the typical failure of concrete crushing at the compression zone after the yielding of the internal reinforcement (see Fig. 5.11). On the other hand, beam B-S8-1-REF developed an interfacial crack that first initiated at substrate-matrix interface at the middle of the beam and then propagated diagonally to the textile-matrix interface (interlaminar shearing as shown in Fig. 5.12(a)). This interfacial crack progressively progressed to both ends of the beam. However, the SRG system did not collapse and remained functioning due to the anchorage system and the beam ultimately failed by concrete crushing (see Fig. 5.12(b)). Both beams B-S4-1 and B-S4-2 failed by rupture of steel textile at their midspan (as shown in Figs. 5.13-5.14).

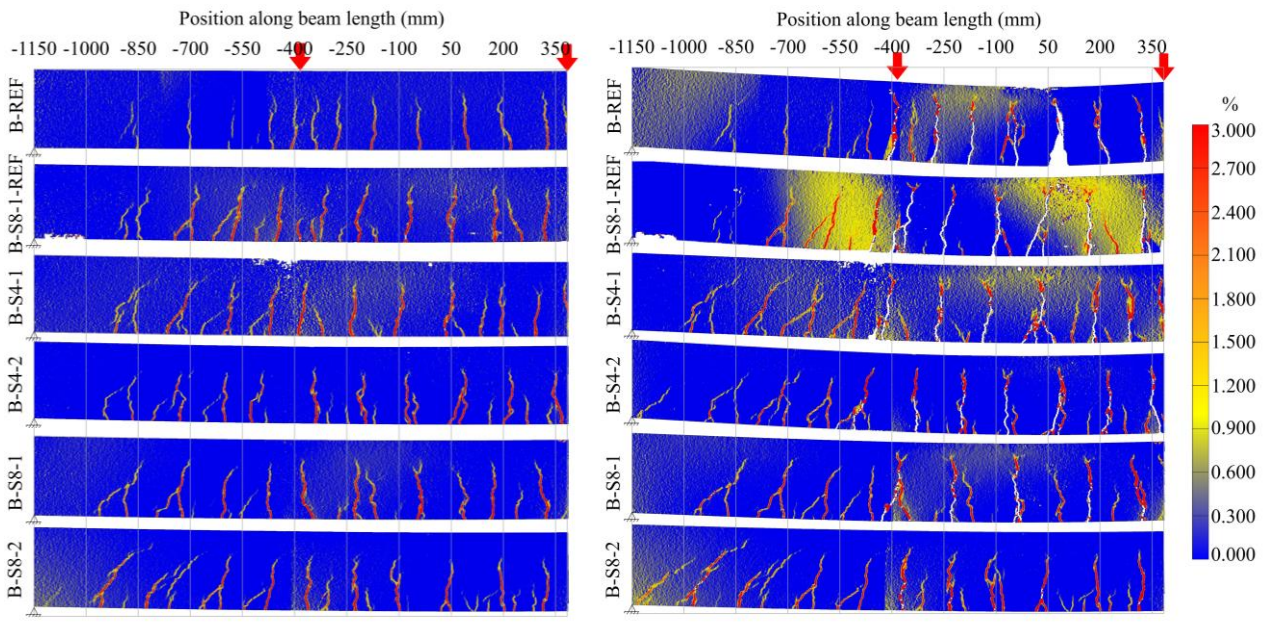

Figure 5.10 *The crack patterns at (a) yield load, and (b) at ultimate load.*

The beams strengthened with the low-density steel textile (S4) prevented the occurrence of debonding at both substrate-matrix and textile-matrix interfaces regardless of the number of textile layers. This behaviour is attributed to the improved mechanical interlock between the grout and the steel textile enhanced by the larger spacings between the steel cords which enabled the grout to achieve a better impregnation. Beams strengthened with S4 steel textiles exhibited transverse cracks in the thickness of the SRG composite sometimes corresponding to the cracks in the substrate (i.e., diagonal cracks in the shear span as shown in Fig. 5.15). However, these cracks did not propagate in the longitudinal directions (i.e., at the textile-matrix interface).

Figure 5.11 *The mode of failure for control beam B-REF (crushing of concrete after the yielding of internal reinforcement).*

Beam B-S8-1 developed a major crack at the far left of the constant-moment region near to the controlled end. This crack initiated at the substrate-matrix interface and then had a diagonal branch that eventually propagated as textile-matrix crack towards the controlled end of the beam (see Fig. 5.16). At a deflection of approximately 42 mm, a set of 21 cords slipped inside the SRG composite, which was evident by the first drop on the load-deflection curve and confirmed by the DIC system (see Fig. 5.17), followed by the rupture of the remaining steel cords. Beam B-S8-2 developed a crack at substrate-matrix interface near the monitored end. This crack initiated at the tip of a diagonal shear crack that was approximately 100 mm off the end of the SRG composite and progressively propagated towards the end of the composite and caused the SRG composite to detach from the substrate over that length (i.e., 100 mm). This was then progressively shifted towards the anchored end with a rather slow progression rate until almost half of the composite detached from the beam (see Fig. 5.18).

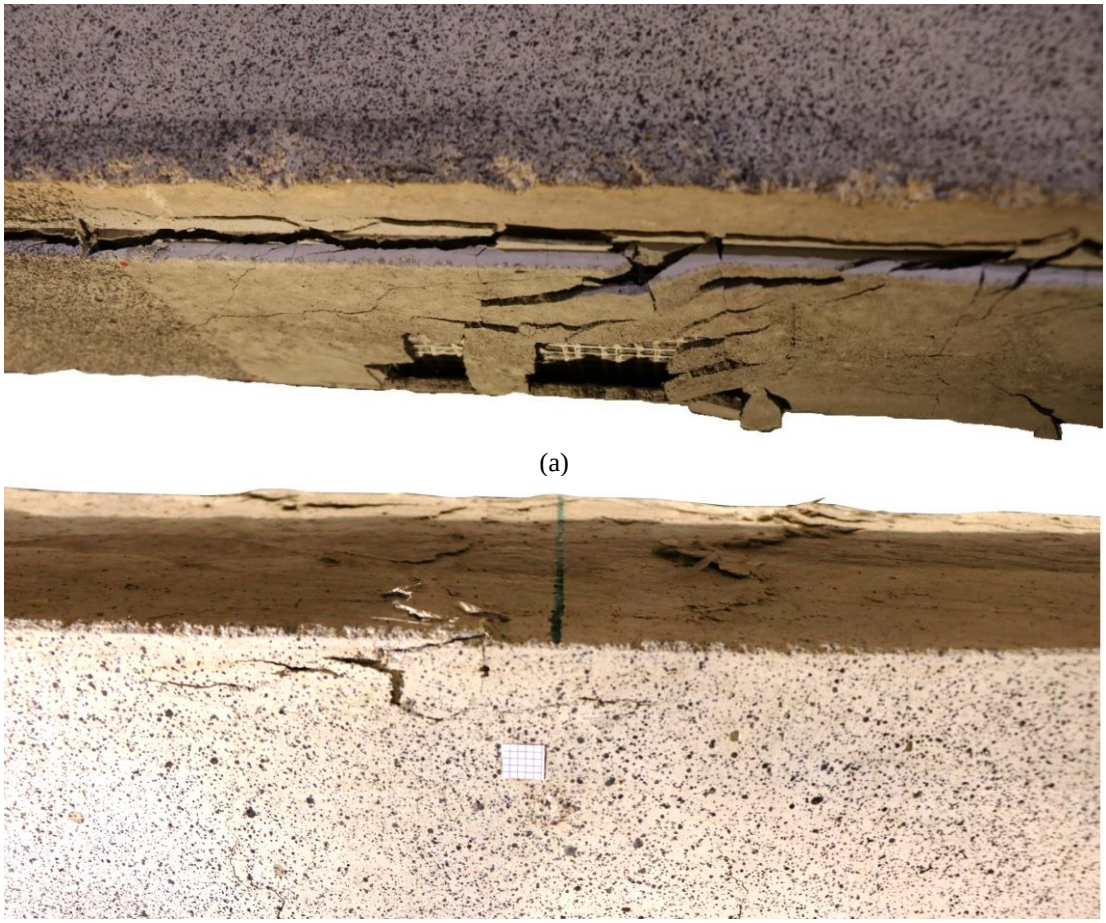

(a)

(b)

Figure 5.12 *The mode of failure for beam B-S8-1-REF (a) interlaminar shearing near the support and (b) eventual failure by concrete crushing at midspan.*

Figure 5.13 *The mode of failure for beam B-S4-1 (rupture of steel textile).*

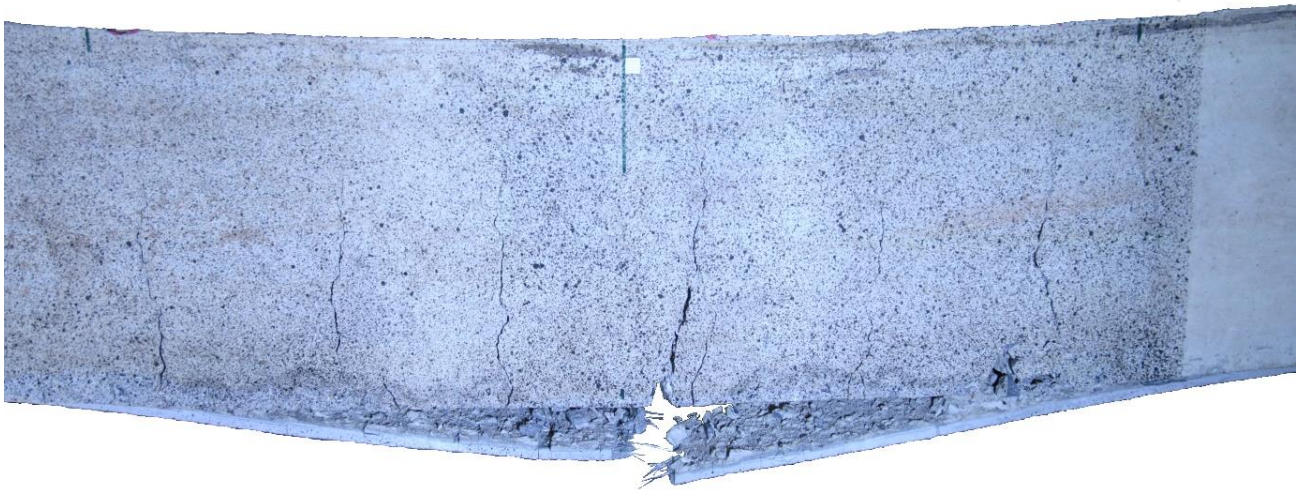

Figure 5.14 *The mode of failure for beam B-S4-2 (rupture of steel textile).*

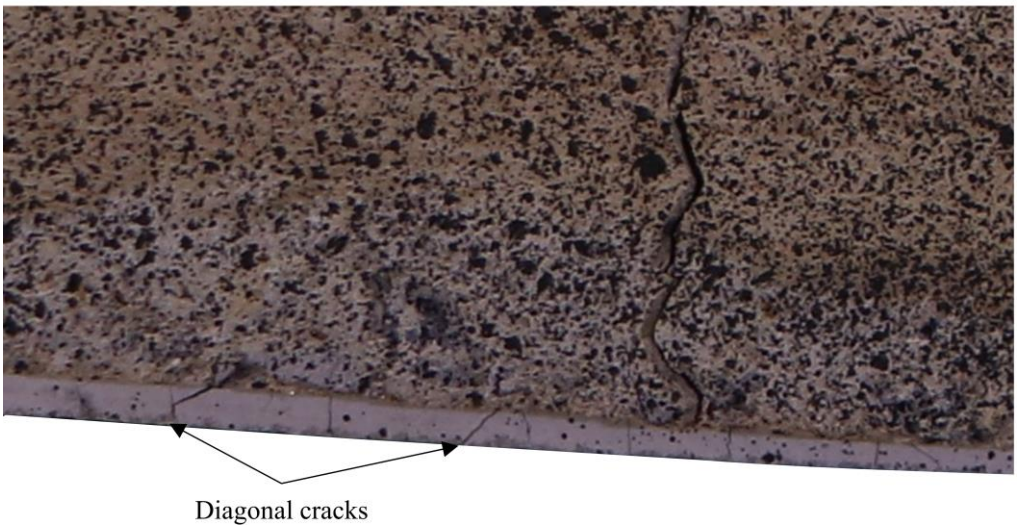

Figure 5.15 *A close image of beam B-S4-2 showing the diagonal cracks throughout the thickness of the composite*.

It is worth noting that beam B-S8-2 had no interfacial cracks in the SRG composite and the debonding was solely observed on the substrate-matrix interface. The relatively high stiffness of beam B-S8-2 resulted in the premature debonding of the SRG, which initiated as end-anchorage debonding and subsequently propagated towards the opposite support in a brittle manner. However, the use of one or two layers of the light density steel fabric (S4 steel textiles), or one layer of the medium density fabric (S8 steel textiles), enabled the full mobilisation of the SRG mechanical properties and promoted flexural failures governed by yielding of the internal steel reinforcement followed by rupture of the externally bonded steel fabric.

(a)

(b)

Figure 5.16 *(a) The mode of failure for beam B-S8-1 (Slippage of steel textile) and (b) close image of the SRG composite at the middle of the beam.*

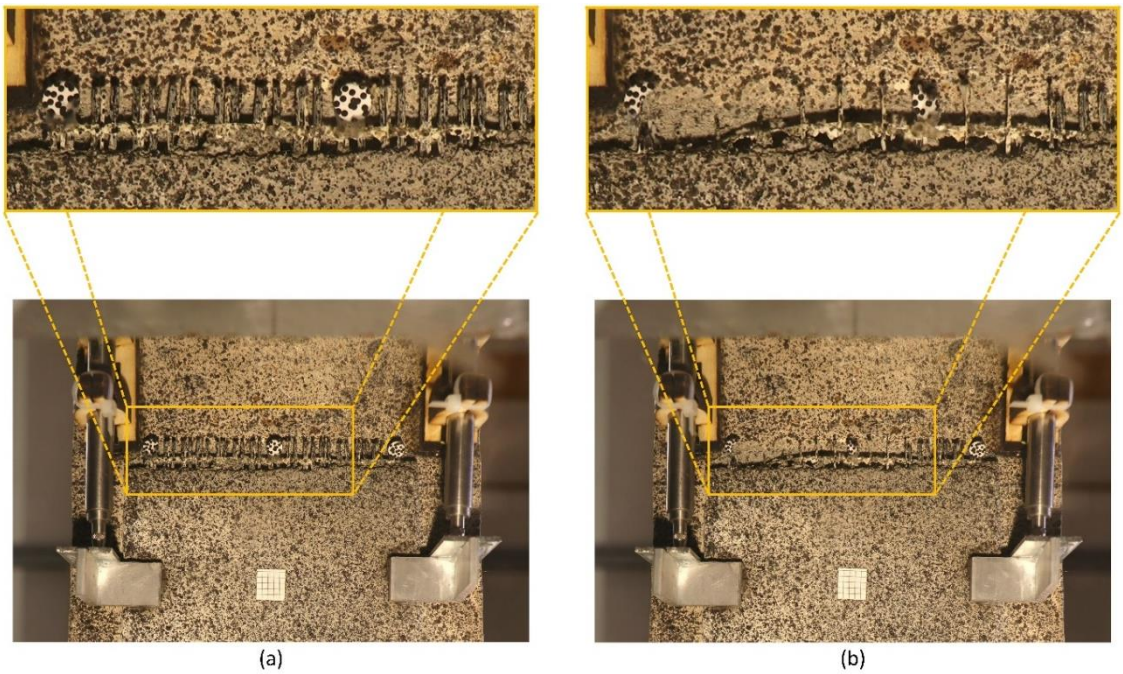

Figure 5.17 *The slippage of steel cords in beam B-S8-1. The frame (a) just before the slippage and (b) after the slippage.*

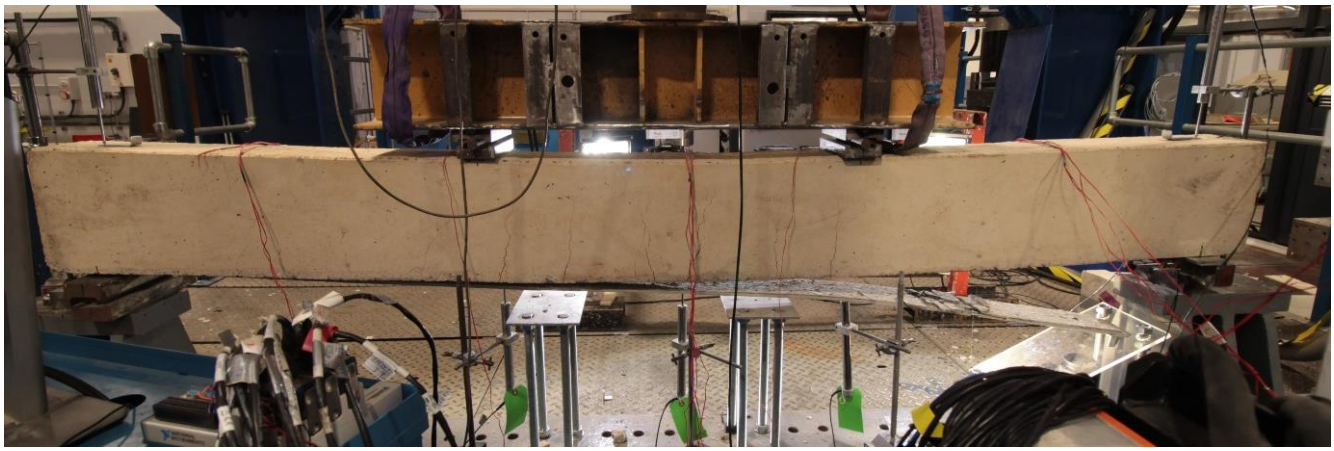

Figure 5.18 *The mode of failure for beam B-S8-2 (End debonding of SRG composite- Right).*

5.3.4 Strain distribution

The strain values in the internal steel rebars for all the tested beams are plotted in the Figs. 5.19-5.21. It should be mentioned that the data acquisition system had a malfunction and caused the strain gauges in beam B-REF to stop recording at a load of approximately 55 kN. All beams exhibited comparable strains at all points except those at the tension rebars at midspan and under the loading points. The average strain in the tension reinforcement at midspan ranged from of 3×10^3 με to 4×10^3 με. However, the strain at midspan of tension rebars at the failure of the SRG system seems to have an increasing trend. The beam strengthened with two layers of S4 steel textile (B-S4-2) only experienced a reduction in the strain of the tension reinforcement of almost 19 % compared to that of the beam strengthened with only one layer of S4 textile (B-S4-1). On the other hand, the beam strengthened with two layers of S8 steel textile (B-S8-2) developed a strain at the midspan of the flexural reinforcement of approximately 52 % less than that for the beam strengthened with two layers of S8 textile (B-S8-2). It confirms that the beams strengthened with SRG composites of high stiffness (by doubling the number of layers or the amount of the external reinforcement) tend to experience a reduction in the strain of in the internal reinforcement. This can be attributed to the poor penetration of the grout within the steel textile as discussed before. The beam strengthened with one layer of S8 steel textile with anchorage (B-S8-1-REF) had a midspan strain at SRG failure comparable to that of B-S8-1 which had the same amount of external reinforcement suggesting that the anchorage system does not affect the strain of the internal reinforcement.

5.3.5 Slip of SRG composite

The slip values of the observed end of the SRG composite corresponding to yield and SRG failure loads obtained from DIC system and LVDTs for strengthened beams are plotted in Fig. 5.22. The results demonstrate a good agreement between the DIC estimated values with the corresponding LVDT measurements for all the tested specimens. In general, beams strengthened with only one layer of SRG composites of both S4 and S8 steel textiles exhibited a reduced slip compared to that of the beams strengthened with two layers of the same steel textiles at

both yield and failure loading points. However, beam B-S8-2 showed a slip value (0.33 mm) less than that of beam B-S8-1 (0.55 mm) due to the interruption of debonding in the latter beam. Thinner composites (one layer) tend to match the deflection of the beam hence developing less stress, and consequently less slip, on the end of the composite contrary to stiffer composites (two layers).

This analogy is also valid for describing the debonding of beam B-S8-2 where the SRG composite reached a point it is no longer able to match the deflection of the beam (at approximately 22 mm) owing to its high stiffness. This in return increased the peeling stresses at the end of the SRG composite and triggered the debonding. Although the SRG composite in beams B-S8-2 and B-S4-2 had the same thickness (approximately 9 mm) yet the SRG composite in beam B-S4-2 failed at a slip value greater than that of beam B-S8-2. This can be explained by the fact that the SRG composite in beam B-S4-2 had less reinforcement (30 cords) than that for beam B-S8-2 (62 cords) and this contributed to the higher stiffness of the latter composite. Beam B-S8-1-REF and beam B-S8-1 are typical in terms of the SRG strengthening system and this explains the similarities in the slip values at both yield and SRG failure loads for these beams. This also suggests that the anchorage system did not provide much improvement to the slip of the composite.

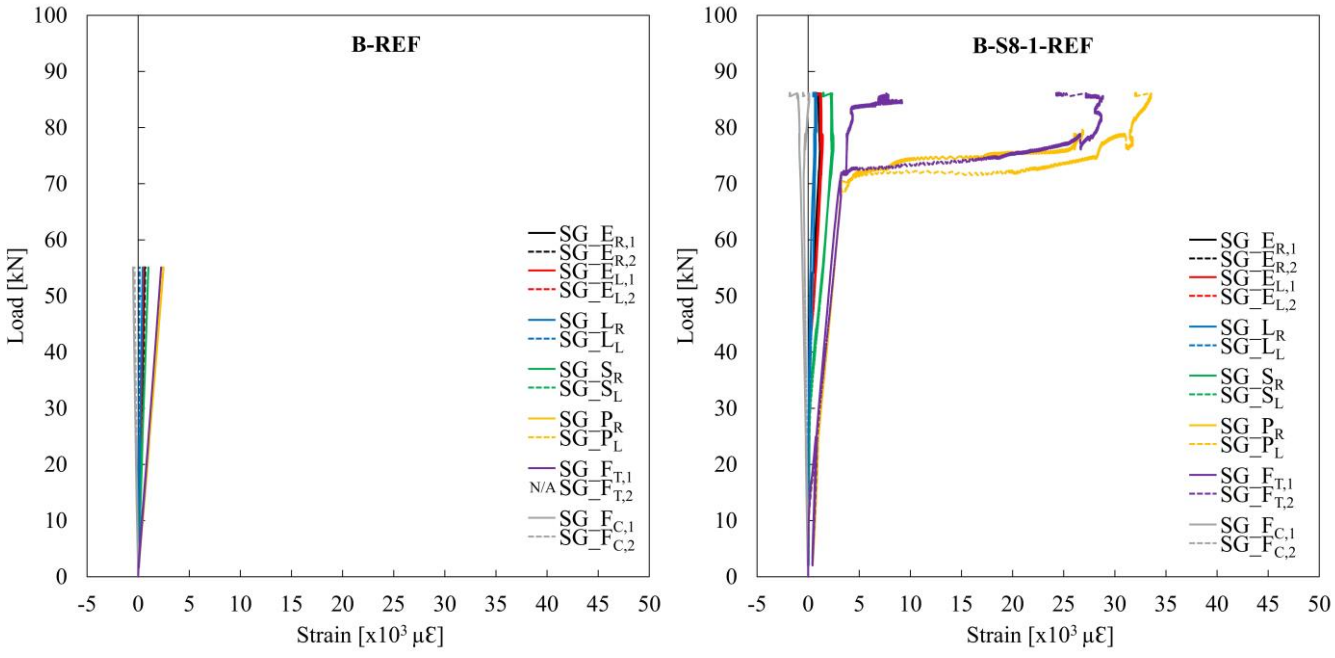

(a) (b)

Figure 5.19 *The load vs the average strain of the tension internal reinforcement at midspan for (a) beam B-REF, and (b) beam B-S8-1-REF.*

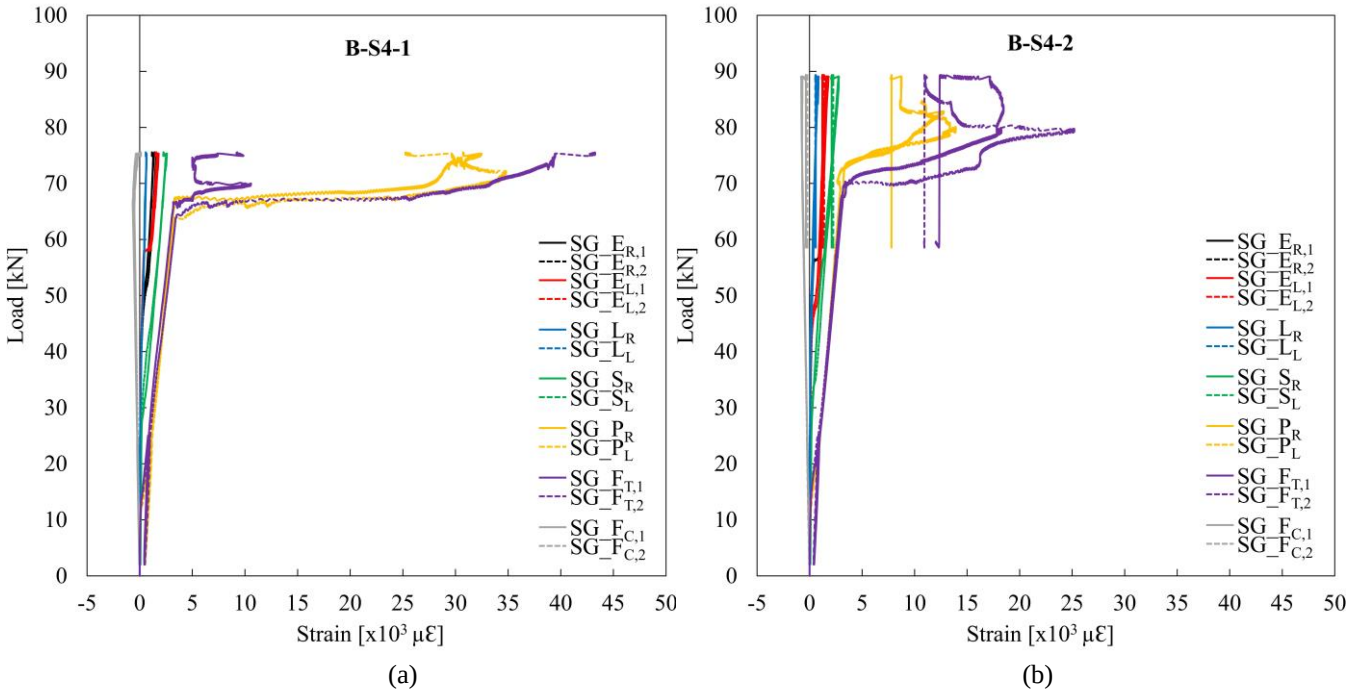

(a) (b)

Figure 5.20 *The load vs the average strain of the tension internal reinforcement at midspan for (a) beam B-S4-1, and (b) beam B-S4-1-2.*

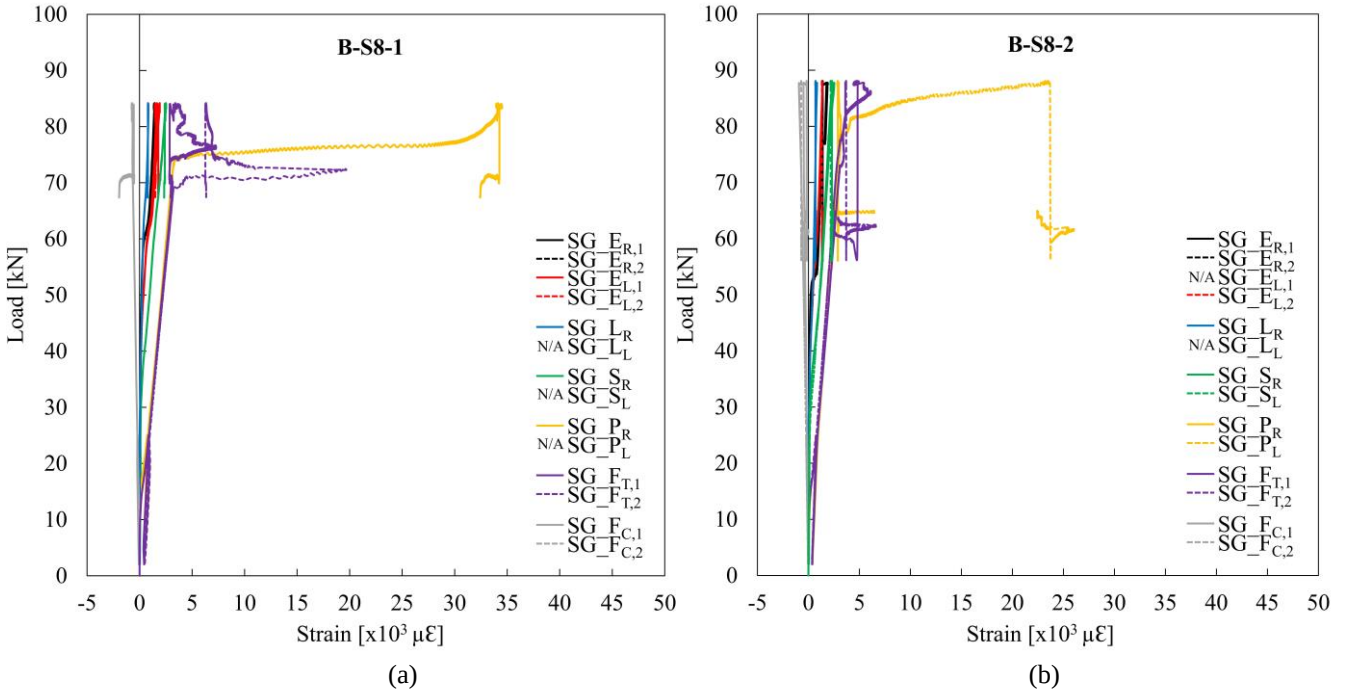

(a) (b)

Figure 5.21 *The load vs the average strain of the tension internal reinforcement at midspan for (a) beam B-S8-1, and (b) beam B-S8-2.*

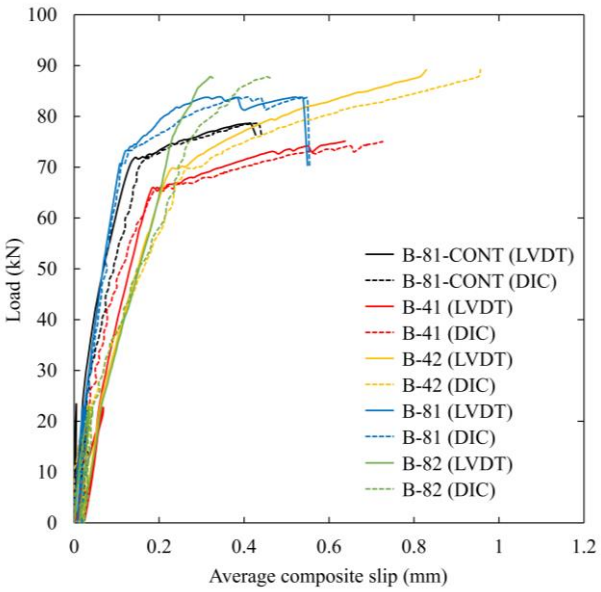

Figure 5.22 *The load vs the average slip at the free end of the SRG composite for all strengthened beams obtained from LVDTs and DIC system.*

5.3.6 The Effect of the Key Design parameters

This sections investigates the effect of the key design parameters used in this study on the efficiency of SRG beam flexural strengthening. A comparison is made between the flexural behaviour of the beams strengthened with different steel textiles but for the same number of layers (i.e., B-S4-1 vs. B-S8-1 and between B-S4-2 vs. B-S8-2). Furthermore, another comparison is made between the beams strengthened with different number of layers but for the same density of steel textile (i.e., B-S4-1 vs. B-S4-2 and between B-S8-1 vs. B-S8-2). The effect of changing the number of layers for the same amount of external reinforcement (i.e., B-S4-2 vs. B-S8-1) is also compared. Figs. 5.23-5.24 provide information, for the sake of comparison, between the beams strengthened with different densities and different number of layers of the steel textiles in terms of the load at yield and at the failure of the SRG system, the corresponding midspan deflections, the average slip at the end of the SRG composite, s_{ave}, and the average strain in the tension reinforcement at midspan, $\varepsilon_{FT,ave}$. It is worth noting that the midspan deflection and the average strain corresponding to the yield load seem to have no trend as they were comparable for all the beams under consideration. It is also worth mentioning that the interruption of debonding in beam B-S8-2 made a break in some of the increasing trends.

- Effect of textile density: Increasing the density of the steel textile from S4 to S8 textiles (for beams strengthened with only one layer) slightly increased the load at the yield and at the failure of the SRG by 9 % and 10 %, respectively. The increase in the midspan deflection at the failure of the SRG system was rather insignificant. The average slip at yield and the average strain at the failure of the SRG system were reduced, on average by approximately 45 %, while the slip at the failure of the SRG system was reduced

by only 14 %. In the case of the beams strengthened with two layers of steel textile, increasing the density of the textile from S4 to S8 textiles had no influence on the load at the yield and the failure of the SRG system, whereas the midspan deflection was reduced by approximately 50 % due to debonding. The average slip at yield load was increased by only 9 %. However, at the failure of the SRG system, both the average slip and the average strain were decreased by approximately 65 % on average.

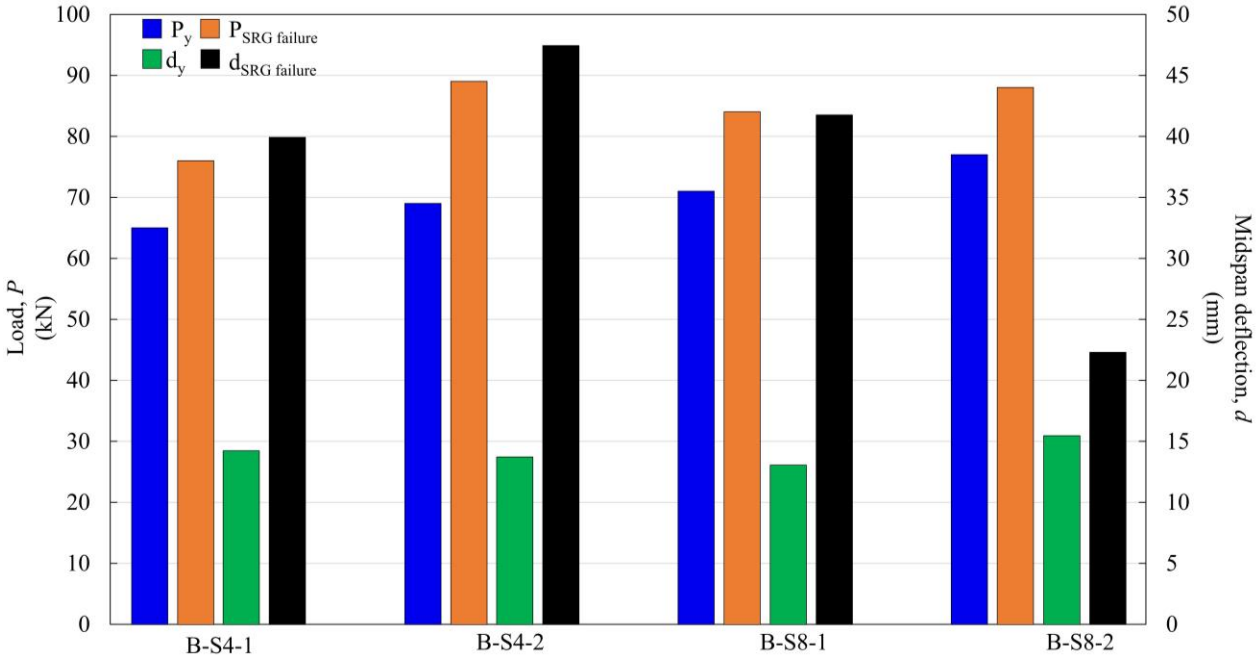

Figure 5.23 *The load at yield and the load at the failure of the SRG system and the corresponding midspan deflection for the beams with different densities and layers of steel textile.*

- Effect of the number of layers: Increasing the number of layers (from 1 to 2 layers) for steel textile S4 slightly increased the yield load by 6 % while the load at the failure of the SRG system and the corresponding midspan deflection was increased by approximately 18 % on average. The average slip at the yield and at the failure of the SRG system was increased by approximately 22 % and 30 %, respectively, while the average strain at the failure of the SRG system was reduced by approximately 19 %. On the other hand, doubling the number of layers for S8 steel textile resulted in increasing the average slip at yield by more than double. However, the average slip, average strain, and the midspan deflection at the failure of the SRG system was, on average, reduced by approximately 46 % mainly due to debonding. The load at yield and at the failure of the SRG system was insignificantly increased by approximately 8 % and 5 %, respectively.
- It is worth noting that increasing the number of the steel textile layers has no influence on the penetration of the grout within the textile contrary to the density of the steel textile, where increasing the number of cords per unit length of the textile contributes towards hindering the grout from achieving a better

impregnation with the steel textile. The penetration process is significantly influenced by the distance between the steel cords. The distance between the cords on two successive layers is far greater than that between any adjacent cords on the same textile, hence the density of the textile is more critical to that process from the number of layers.

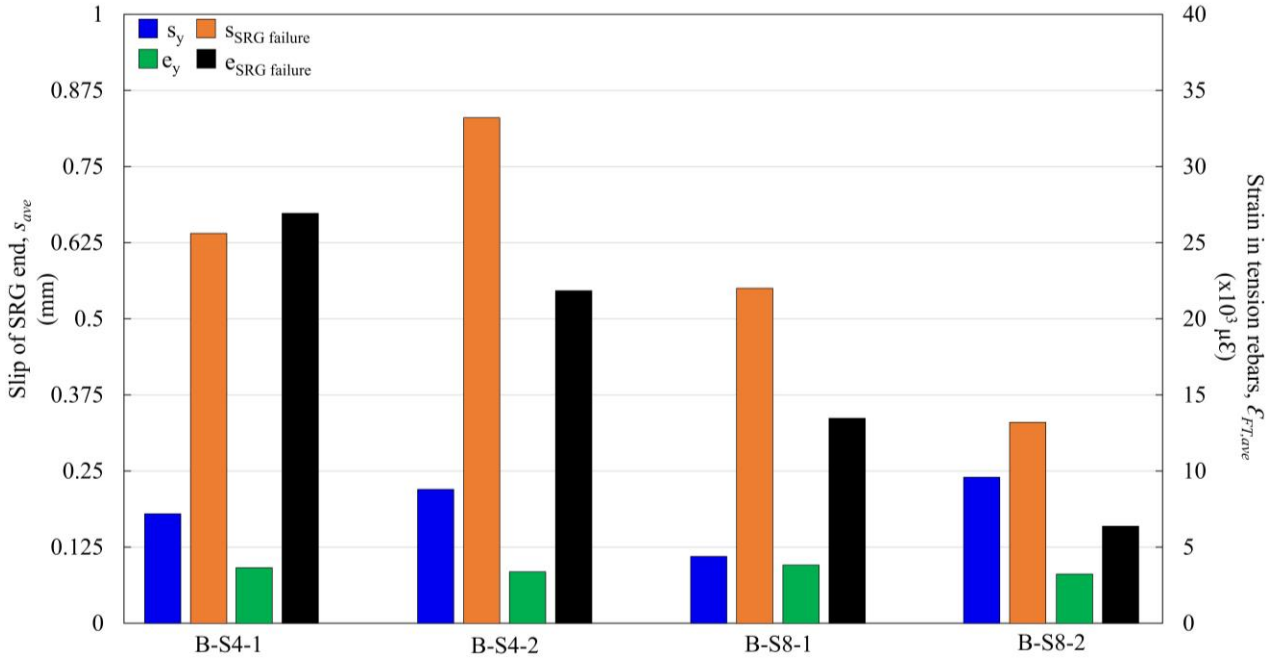

Figure 5.24 *The average slip at the end of the SRG composite and the average strain in the internal tension rebars at midspan corresponding to the loads at yield and at failure*.

- Finally, the comparison between the beams that had the same amount of external reinforcement but different number of layers (i.e., B-S4-2 and B-S8-1) reveals that using two layers of the same reinforcement (B-S4-2) doubled the average slip at yield and increased the average slip and strain at the failure of the SRG system by more than half compared to that of only one layer (B-S8-1). However, the load values at the yield and at the failure of the SRG system were marginally affected, whereas the midspan deflection at the failure of the SRG system was decreased by approximately 12 %.

5.4 Analytical Modelling

The debonding phenomenon often disrupts the full utilisation of the external strengthening system, in particular, composites with multiple layers of reinforcement. The classical cross section analysis of beams with external strengthening systems is based on the assumption that the bond between the composite and the substrate is perfect, hence it does not account for debonding failure, let alone predicting the strain at debonding.

To address this issue, few guidelines attempted to provide some models for predicting the strain of the external reinforcement at debonding mainly for the FPR systems. For instance, CNR-DT 200 R1 [36] provides the following formulation to estimate the design strain of the external reinforcement, ε_{fd}:

$$\varepsilon_{fd}^{CNR} = \frac{f_{sd}}{E_{tx}} = \frac{k_q}{E_f} \cdot \sqrt{\frac{E_{tx}}{t_{tx,1}} \cdot 2 \cdot k_b \cdot k_{G,2} \cdot \sqrt{f_{c,sb} \cdot f_{t,sb}}} \quad (1)$$

such that:

$$\varepsilon_{fd}^{CNR} \leq \frac{\eta_a \cdot \varepsilon_{u,tx}}{\gamma_f} \quad (2)$$

where:

f_{sd} is the strength of the external reinforcement at debonding;

E_{tx} is the elastic modulus of the external reinforcement (=$E_{tx,II}$);

$t_{tx,1}$ is the equivalent thickness of the external reinforcement;

k_q is a coefficient to account for load distribution (equal to 1); $k_{G,2}$ is a corrective factor calibrated against experimental results (equal to 0.10 mm); $f_{c,sb}$ and $f_{t,sb}$ are the mean value of concrete compressive and tensile strength, respectively; $\varepsilon_{u,tx}$ is the ultimate tensile strain of the external reinforcement; γ_f is a partial safety factor ranging from 1.20 to 1.50 for systems sensitive to debonding;

and

k_b is a geometrical corrective factor based on the ratio between the width of the composite (b_{com}) and that of the beam (b_{sb}). This factor can be calculated using the following relationship:

$$k_p = \sqrt{\frac{2-b_f/b}{1+b_f/b}} \geq 1 \quad (3)$$

η_a used in Eq. (2) is an environmental conversion factor. The value of this factor is only given in CNR for different FRP systems under different exposure conditions. Under external exposure conditions, the value η_a equals 0.65, 0.75, and 0.85 for glass, aramid, and carbon FRP systems, respectively. The value of this factor is not established yet for the FRCM systems, however, it is most likely to fall below 0.65 considering the brittle nature of inorganic matrices used in the FRCM system when compared to epoxy adhesives.

ACI 440.2R [37] provide the following expression for the estimation of the design strain the external reinforcement:

$$\varepsilon_{fd}^{ACI\ 440} = 0.41 \cdot \sqrt{\frac{f_{c,sub}}{n \cdot E_{tx} \cdot t_{tx,1}}} \quad (4)$$

Such that:

$$\varepsilon_{fd}^{ACI} \leq C_E \,.\, \varepsilon_{fu} \quad (5)$$

where:

n is the number of external reinforcement layers, and

C_E is an environmental conversion factor. ACI 440 [37] provides values for $C_E$factor based on the utilised reinforcement material and exposure conditions comparable to those suggested in CNR-DT 200 [36].

The ACI committee report 549 [38] suggests the following design tensile strain for FRCM systems used for strengthening RC members:

$$\varepsilon_{fd}^{ACI\ 549} = \varepsilon_{fu} - 1\,STD \leq 0.012 \quad (6)$$

The beams strengthened with two layers of FRCM strengthening system will have a lower design tensile strain as doubling the number of the external reinforcement layers will result in increasing the thickness of the composite (t_f) which is inversely proportional to the design strain in Eqs. (1) and (4).

It is worth noting that the above mentioned guidelines do not consider the presence of anchorage system which can greatly affect the level of the tensile strain of the external reinforcement. Providing anchorage to the strengthening system can prevent debonding and help the external reinforcement to attain higher tensile strains, resulting in overconservative predictions of the design strain values provided by these guidelines. On the other hand, owing to the fact that these formulations are originally developed for FRP systems, different modes of failure apart from debonding are not considered including slippage of the reinforcement within the matrix and interlaminar shearing failure, which are common for the FRCM systems.

In Table 5.5, the design strain of the steel textile is calculated for each strengthened beam according to the previously introduced guidelines. The obtained design values are then compared against the strain at failure (debonding or rupture of the textiles) obtained from the experimental data. In general, the values of the design strain are shown to be overconservative. However, the suggested design strain values for beam B-S8-2 are higher than the debonding strain of that beam with the exception of CNR-DT 200 [36] guideline which suggested a design value very close to the debonding strain. Both ACI 440 [37] and ACI 549 [38] provide a design strain value considerably higher to the strain at debonding in beam B-S8-2 of approximately 121 % and 193 %, respectively. This highlights the need to develop more accurate design equations for flexural strengthening using SRG systems. However, more experimental test data would be required to obtain reliable results.

Table 5.~~4~~5 *Values for the design strain in the strengthening system suggested in CNR and ACI guidelines*.

Beam	CNR-DT 200 [a]		ACI 440 [a]		ACI 549	Analytical [b]	Error		
	ε_{fd}^{CNR}	$\eta_a \cdot \varepsilon_{fu}/\gamma_f$ [a]	$\varepsilon_{fd}^{ACI\ 440}$	$C_E \cdot \varepsilon_{fu}$	$\varepsilon_{fd}^{ACI\ 549}$	ε_{fu}^{An}	$\frac{\varepsilon_{fd,min}^{CNR}}{\varepsilon_{fu}^{An}}$	$\frac{\varepsilon_{fd,min}^{ACI\ 440}}{\varepsilon_{fu}^{An}}$	$\frac{\varepsilon_{fd,min}^{ACI\ 549}}{\varepsilon_{fu}^{An}}$
	Eq. (1)	Eq. (2)	Eq. (4)	Eq. (5)	Eq. (6)				
	%	%	%	%		%	%	%	%
B-S4-1	1.14	0.62	2.02	0.75	1.2	1.31	47.33	57.25	91.60
B-S4-2	0.81	0.62	1.43	0.75	1.2	1.34	46.27	55.97	89.55
B-S8-1	0.81	0.62	1.42	0.75	1.2	1.04	59.62	72.12	115.38
B-S8-2	0.57	0.62	1.00	0.75	1.2	0.62	91.94	120.97	193.55

[a] Factors η_a, γ_f, C_E were assumed equal to 0.50, 1.20, and 0.50, respectively.

[b] Strain values were obtained from cross section analysis.

5.5 Summary and Conclusions

This study aimed to investigate the flexural behaviour of RC beams strengthened with steel reinforced grout (SRG) systems. Six full scale RC beams were tested in four-point bending configuration. Five beams were strengthened using SRG system with different arrangements, while the last beam was used as a benchmark. Three key parameters were investigated including the density of steel textile (4 and 8 cords/in steel textile), the number of steel textile layers (one and two layers), and the presence of anchorage system. Based on the presented results, the following conclusions can be drawn:

- All tested beams exhibited a flexural response characterising three distinct stages including a linear elastic stage up to the formation of cracks followed by semi-linear flexural behaviour that ended by the yielding of the internal reinforcement and finally a stage characterised by a significant drop in stiffness.
- The beams with low amount of external reinforcement developed a less stiff behaviour in the first two stages compared to the rest of the strengthened beams.
- The beams strengthened with identical SRG composites (e.g. B-S8-1-REF and B-S8-1) or SRG composites having the same amount of reinforcement (e.g. B-S4-2 and B-S8-1) developed a comparable load-deflection behaviour.
- Regardless of the adopted strengthening configuration, all tested beams developed a similar crack pattern. The average crack spacing was 137 mm which corresponds to the spacing between the shear links. The SRG composite also developed small and evenly distrusted transvers cracks which in most cases corresponded to the cracks developed in the beam.
- The beams strengthened with composites of relatively high stiffness (B-S8-2) resulted in the premature debonding of the SRG, which initiated as end-anchorage debonding and subsequently propagated towards the opposite support in a brittle manner. In contrast, the use of SRG composites of low stiffness enabled the full mobilisation of the SRG mechanical properties and promoted flexural failures governed by yielding of the internal steel reinforcement followed by rupture of the externally bonded steel fabric.

- Increasing the density of the steel textile, regardless of the number of layers, insignificantly increased the load at yield and at the failure of the SRG. However, the average stain in the internal flexural reinforcement was significantly reduced at the failure of the SRG system. This also holds true when altering the number of layers from 1 to 2 layers regardless of the density of the steel textile.
- The use of two layers of the low-density steel textiles instead of one layer of the denser textile enabled a better impregnation of the grout through the cords and prevented interlaminar shearing and hence led to a full exploitation of the textile.
- The ultimate strain value in the external reinforcement was compared with the design values suggested by three international guidelines including CNR-DT 200, ACI 440, and ACI 549. It was found that these guidelines are in general overconservative in terms of the value of design strain for the external reinforcement (by up to 193 %). However, the design strain values for beam that failed by debonding were close or higher than the strain at debonding.

Acknowledgment

The materials for this experiment (the steel textiles and mortar) were provided by Kerakoll S.p.A. (Sassuolo, MO, Italy). The first author would like to thank Shaqra University in Saudi Arabia and Saudi Arabian Cultural Bureau (SACB) in the UK for funding this part of his PhD research.

References

[1] Matana M, Nanni A, Dharani L.R, Silva P, Tunis G. Bond Performance of steel reinforced polymer and steel reinforced grout. In: Proceedings of BBFS Conference. Hong Kong, December, 2005.

[2] Huang X, Birman V, Nanni A, Tunis G. Properties and potential for application of steel reinforced polymer and steel reinforced grout composites. Composites Part B: Engineering. 2005;36(1):73-82.

[3] de Felice G, De Santis S, Garmendia L, Ghiassi B, Larrinaga P, Lourenço P et al. Mortar-based systems for externally bonded strengthening of masonry. Materials and Structures. 2014;47(12):2021-2037.

[4] Babaeidarabad S, Loreto G, Nanni A. Flexural Strengthening of RC Beams with an Externally Bonded Fabric-Reinforced Cementitious Matrix. Journal of Composites for Construction. 2014;18(5):04014009.

[5] Bencardino, F. & Ombres, L. Structural Performance of RC Beams Strengthened by SRG and FRCM System. IABSE Symposium Report. 97. 38-45.

[6] D'Ambrisi A, Focacci F. Flexural Strengthening of RC Beams with Cement-Based Composites. Journal of Composites for Construction. 2011;15(5):707-720.

[7] Ebead U, Shrestha K, Afzal M, El Refai A, Nanni A. Effectiveness of Fabric-Reinforced Cementitious Matrix in Strengthening Reinforced Concrete Beams. Journal of Composites for Construction. 2017;21(2):04016084.

[8] Elsanadedy H, Almusallam T, Alsayed S, Al-Salloum Y. Flexural strengthening of RC beams using textile reinforced mortar – Experimental and numerical study. Composite Structures. 2013;97:40-55.

[9] Jabr A, El Ragaby A, Ghrib F. Flexural Strengthening of RC Beams Using Glass-FRCM. Proceedings, Annual Conference - Canadian Society for Civil Engineering 3 (2016): 2047-057.

[10] Ombres L. Debonding analysis of reinforced concrete beams strengthened with fibre reinforced cementitious mortar. Engineering Fracture Mechanics. 2012;81:94-109.

[11] Raoof S, Koutas L, Bournas D. Textile-reinforced mortar (TRM) versus fibre-reinforced polymers (FRP) in flexural strengthening of RC beams. Construction and Building Materials. 2017;151:279-291.

[12] Balsamo A, Nardone F, Iovinella I, Ceroni F, Pecce M. Flexural strengthening of concrete beams with EB-FRP, SRP and SRCM: Experimental investigation. Composites Part B: Engineering. 2013;46:91-101.

[13] Bencardino F, Condello A. Structural behaviour of RC beams externally strengthened in flexure with SRG and SRP systems. International Journal of Structural Engineering. 2014;5(4):346.

[14] Mitolidis G, Salonikios T, Kappos A. Tests on RC Beams Strengthened at the Span with Externally Bonded Polymers Reinforced with Carbon or Steel Fibers. Journal of Composites for Construction. 2012;16(5):551-562.

[15] Prota A, Yong Tan K, Nanni A, Pecce M, Manfredi G. Performance of Shallow Reinforced Concrete Beams with Externally Bonded Steel-Reinforced Polymer. ACI Structural Journal. 2006;103(2):163-170.

[16] Alotaibi S, Thermou G, Hajirasouliha I, Guadagnini M. Tensile behaviour of multi-ply steel-reinforced grout (SRG) composites. Proceedings of the 7th International Conference on Computational Methods in Structural Dynamics and Earthquake Engineering. 2019: 1138-145.

[17] Baietti G, D'Antino T, Carloni C. Some Key Aspects in the Mechanics of Stress Transfer Between SRG and Masonry. Applied Sciences. 2020;10(20):7303.

[18] Bencardino F, Nisticò M, Verre S. Experimental Investigation and Numerical Analysis of Bond Behavior in SRG-Strengthened Masonry Prisms Using UHTSS and Stainless-Steel Fibers. Fibers. 2020;8(2):8.

[19] Santandrea M, Focacci F, Mazzotti C, Ubertini F, Carloni C. Determination of the interfacial cohesive material law for SRG composites bonded to a masonry substrate. Engineering Failure Analysis. 2020;111:104322.

[20] Alotaibi S, Thermou G, Hajirasouliha I, Guadagnini M. Bond Behaviour of Multi-layer Steel Reinforced Grout (Srg) Strengthening Systems to Concrete. Proceedings of the 9th Biennial Conference on Advanced Composites in Construction. 2019: 171-77.

[21] Thermou G, De Santis S, de Felice G, Alotaibi S, Roscini F, Hajirasouliha I et al. Bond behaviour of multi-ply steel reinforced grout composites. Construction and Building Materials. 2021;305:124750.

[22] Ombres L, Verre S. Numerical Analysis of the Structural Response of Masonry Columns Confined with SRG (Steel Reinforced Grout). IMEKO International Conference on Metrology for Archaeology and Cultural Heritage. 2017: 718-22.

[23] Salsavilca J, Yacila J, Tarque N, Camata G. Experimental and analytical bond behaviour of masonry strengthened with steel reinforced grout (SRG). Construction and Building Materials. 2020;238:117635.

[24] Thermou G, Katakalos K, Manos G. Influence of the Loading Rate on the Axial Compressive Behavior of Concrete Specimens Confined with SRG Jackets. Proceedings of the 4th International Conference on Computational Methods in Structural Dynamics and Earthquake Engineering. 2013: 1107-122.

[25] Thermou G, Katakalos K, Manos G. Experimental investigation of substandard RC columns confined with SRG jackets under compression. Composite Structures. 2018;184:56-65.

[26] Yacila J, Salsavilca J, Tarque N, Camata G. Experimental assessment of confined masonry walls retrofitted with SRG under lateral cyclic loads. Engineering Structures. 2019;199:109555.

[27] Thermou G, Papanikolaou V, Lioupis C, Hajirasouliha I. Steel-Reinforced Grout (SRG) strengthening of shear-critical RC beams. Construction and Building Materials. 2019;216:68-83.

[28] Wakjira T, Ebead U. Experimental and analytical study on strengthening of reinforced concrete T-beams in shear using steel reinforced grout (SRG). Composites Part B: Engineering. 2019;177:107368.

[29] Da Porto F, Stievanin E, Gabin E, Valluzzi M. SRG Application for Structural Strengthening of RC Beams. American Concrete Institute, ACI Special Publication. 2012:119-32.

[30] Sneed L, Verre S, Carloni C, Ombres L. Flexural behavior of RC beams strengthened with steel-FRCM composite. Engineering Structures. 2016;127:686-699.

[31] Ombres L. Flexural analysis of reinforced concrete beams strengthened with a cement based high strength composite material. Composite Structures. 2011;94(1):143-155.

[32] Ombres L, Verre S. Flexural Behaviour of SRG (steel Reinforcing Grout)-strengthened Reinforced Concrete Beams. Proceedings of the 9th International Conference on Fibre-Reinforced Polymer (FRP) Composites in Civil Engineering, 2018: 581-88.

[33] Ombres L, Verre S. Flexural Strengthening of RC Beams with Steel-Reinforced Grout: Experimental and Numerical Investigation. Journal of Composites for Construction. 2019;23(5):04019035.

[34] Papakonstantinou C, Katakalos K. Flexural behavior of reinforced concrete beams strengthened with a hybrid inorganic matrix - steel fiber retrofit system. Structural Engineering and Mechanics. 2009;31(5):567-585.

[35] Petracca M, Camata G, Carloni C, Napoli A, Realfonzo R, Casadei P. Numerical Analysis of RC Beams Strengthened with SRG. American Concrete Institute, ACI Special Publication, 2018;324:6.1-6.12.

[36] CNR DT 200. Guide for the design and construction of externally bonded FRP systems for strengthening existing structures. Rome, Italy: National Research Council, Advisory Committee on Technical Regulations for Constructions; July 2004.

[37] ACI Committee 440.2R. Guide for the design and construction of externally bonded FRP systems for strengthening concrete structures. ACI 440.2R-02. Farmington Hills, MI, USA: American Concrete Institute; 2002.

[38] ACI Committee 549.4R. Guide to Design and Construction of Externally Bonded Fabric-Reinforced Cementitious Matrix (FRCM) Systems for Repair and Strengthening Concrete and Masonry Structures. ACI 549.4R-13. Farmington Hills, MI, USA: American Concrete Institute; 2013.

Chapter 6 Analytical Modelling

6.1 Introduction

The debonding load in the external strengthening system is a crucial design parameter. Debonding phenomena can interrupt the full exploitation of the strengthening system and often occur at a strain level well before the ultimate strain of the fibres is reached. Hence, a significant amount of research has been carried out to provide a reliable estimation of the debonding load. The debonding phenomena in the inorganic-based strengthening composites (FRCM and SRG systems) is more complicated than the FRP systems as it can occur at different interfaces including the matrix-to-substrate and matrix-to-textiles interfaces. The state of stress and strain in the external strengthening system at debonding is a crucial design parameter as the design strain needs to be limited to the strain at debonding after introducing the proper safety factor. Although measuring the strain at fibre/cord level is far complicated in these systems, there were several attempts to obtain the strain from gauges directly attached to the fibres embedded in the matrix. However, these gauges, in most cases, suffered from premature debonding from the fibre surface due-to high shear stresses implied by the mechanical interlocking provided by the encompassing matrix. In some other studies, the strain gauges were attached to the external layer of the matrix. However, the strains obtained from these gauges cannot be considered reliable due to the slippage of the fibres and the cracking of the matrix. In some different cases, the strain gauges were mounted to the internal steel rebars and the strain in fibres was computed from the classical cross section analysis with the assumption of perfect bond and plane cross section [1].

Although the bond behaviour in the FRP systems is not identical to that of the FRCM and the SRG systems due to the fact that the matrices used in these systems are different (epoxy vs grout), however the principle of stress transfer mechanism is the same. In fact, the parameters that govern the debonding in these systems are associated with either the substrate or the matrix. Understanding how these different parameters are formulated in the existing FRP bond models is important in the process of modelling the bond behaviour in the SRG systems. The existing shear bond models for the FRP systems can be categorised into the following three categories [2]:

1. Models based on simple assumptions e.g., Brosens and van Gemert 1997, Chaallal et al. (1998), and Khalifa et al. (1998).
2. Models based on fracture mechanics approach e.g., Holzenkämpfer (1994), Täljsten (1994), Yuan and Wu (1999), Yuan et al. (2001), and Neubauer and Rostásy (1997).

3. Empirical models based on regression of experimental data e.g. Hiroyuki and Wu (1997), Tanaka (1996), and Maeda et al. (1997).

Table 6.1 provides different models for estimating the debonding load in the FRP systems. Most of the models are expressed as functions in different geometrical and mechanical properties of either the substrate or the composite or both. The compressive ($f_{c,sb}$) and the tensile ($f_{t,sb}$) strengths of the substrate were often considered since the common mode of failure for the FRP system is the cohesive debonding within the substrate. The geometrical properties were also considered often as a ratio between the width of the FRP plate to the width of the substrate (b_{com}/b_{sb}). The axial stiffness of the FRP plate ($E_{com} \cdot t_{com}$) was also a significant parameter for estimating the debonding load in the FRP systems. The ratio between the bond length (L_{com}) to the effective bond length (L_{com}) was also considered in few models. To assess the adoptability of these FRP models to the SRG system, an evaluation on specific models will be conducted in the following section to decide whether any of these models can adopted to the SRG system.

6.2 Evaluation of the applicability of existing FRP shear bond models

Eleven FRP models were considered to assess their applicability to the SRG systems including Neubauer and Rostásy [3], Serbescu et al. [4], Holzenkämpfer [5], Yang [6], Izumo [7], Chen and Teng [8], Fib 19 [9], TR55 [10], CNR -DT 200 [11], and SIA 166 [12]. Table 6.2 provides the input parameters for the constituent materials including the substrate, the textile, the matrix, and the composite. Since many existing models have different symbols for the same property, the properties of each material were given a distinct subscript according to the following notations:

- Substrate-related parameters [subscripted as “sb”] including the width of the substrate (b_{sb}), and the compressive ($f_{c,sb}$) and the tensile ($f_{t,sb}$) strengths.
- Textile-related parameters [subscripted as “tx”] including the number of the steel cords (n_{cords}), the equivalent thickness of one layer of the textile ($t_{tx,1}$) and the area of the steel textile (A_{tx}).
- Matrix-related parameters [subscripted as “mx”] including the compressive ($f_{c,mx}$) and the tensile ($f_{t,mx}$) strengths.
- Composite-related parameters [subscripted as “com”] including the number of the steel textile layers (n), the overall thickness of the composite (t_{com}), the reinforcement ratio (ρ_{com}), the bond length (L_{com}), the bond width (b_{com}), and the modulus of elasticity (E_{com}) obtained from the direct tensile tests on the SRG composite coupons [Chapter 3].

The above-introduced symbols will be used herein to refer to the corresponding property. The compressive strength ($f_{c,sb}$) refers to the cubic strength at 28 days. When the tensile strength is not specified, the expression provided by the Model Code 2010 [13] and Eurocode 2 [14] was used to calculate its value:

$$f_{t,sb} = 0.30 \cdot {f_{c,sb}}^{2/3} \quad (1)$$

the equivalent thickness of the textile ($t_{tx,1}$) refers to the thickness of a single layer of the textile. It can be calculated using Eq. (2):

$$t_{tx,1} = \frac{A_{tx,1}}{b_{com}} = \frac{n_{cords} \cdot A_{cord}}{b_{com}} \quad (2)$$

where $A_{tx,1}$ is the area of a single layer of the steel textile which equals the number of the steel cords in a single layer ($n_{cords,1}$) multiplied by the area of the cord (A_{cord}). b_{com} refers to the width of the SRG composite.

The modulus of elasticity (E_{com}) refers to that average elastic modulus from the elastic zone (II, $E_{com} = E_{com,II}$) on the stress-strain curve for the direct tensile tests of the coupons. This was derived for different number of the layers of the steel textiles. However, the variations between the values of (E_{com}) for different layers was marginal and hence the elastic modulus of a single layer can be assumed to represent multiple layers.

The reinforcement ratio (ρ_{com}) was calculated using the following formulation:

$$\rho_{com} = \frac{A_{tx}}{A_{com}} = \frac{n_{cords} \cdot A_{cord}}{b_{com} \cdot t_{com}} = \frac{n \cdot t_{tx,1}}{t_{com}} \quad (3)$$

Table 6.3 reports the experimental ultimate load of the shear bond tests for all series and the predictions of different models. In general, the coefficient of variation between the experimental and the predicted ultimate load was high and was ranging from 23 % to 53 %. Some of the models could provide an acceptable estimate of the ultimate load for only certain series (e.g., Serbescu et al and Chen and Teng for series M-300-8, Neubauer for series L-300-8 and series L-400-8, and Holzenkämpfer for series L-400-4). However, none of the evaluated models was able to capture the overall behaviour of the SRG system.. This is not surprising as these models were generally developed for FRP systems which utilises epoxy matrices that have different mechanical properties compared to grout matrices in SRG systems. The complex behaviour of the SRG system under investigation requires the development of a conditional model comprising different expressions for different conditions. The conditions for each expression should be based on the key parameters that have a direct impact on the bond behaviour. The accuracy of these models in predicting the debonding load in the SRG system is plotted in Figs. 6.1-6.5.

Table 6.1 *The parameters governing the FRP bond models.*

Reference	Model	Substrate			Composite			
		b_{sb}	$f_{c,sb}$	$f_{t,sb}$	t_{com}	b_{com}	L_{com}	E_{com}
Sato [15]	$P_u = 2.68 \times 10^{-5} \cdot (f_c')^{0.2} E_p t_p \cdot 1.89 \cdot (E_p t_p)^{0.4} \cdot (b_p + 7.4)$		✓		✓	✓		✓
JCI [16]	$P_u = 0.93 \cdot (f_c')^{0.44} \cdot 0.125 \cdot (E_p t_p)^{0.57} \cdot b_p$		✓		✓	✓		✓
Yang [6]	$P_u = \left(0.5 + 0.08 \cdot \sqrt{\frac{0.01 \cdot E_p \cdot t_p}{f_t}}\right) \cdot b_p \cdot 100 \cdot 0.5 \cdot f_t$			✓	✓	✓		
Izumo [17]	$P_u = \begin{cases} (3.8 \cdot f_c'^{0.67} + 15.2) \cdot L \cdot E_p \cdot b_p \cdot t_p & For\ CFRP \\ (3.4 \cdot f_c'^{0.67} + 69) \cdot L \cdot E_p \cdot b_p \cdot t_p & For\ AFRP \end{cases}$		✓		✓	✓	✓	✓
Chen and Teng [11]	$P_u = 0.427 \cdot \beta_p \cdot \beta_L \cdot \sqrt{f_c'} \cdot \sqrt{\frac{E_p \cdot t_p}{\sqrt{f_c'}}}$	✓	✓		✓	✓	✓	✓
Holzenkämpfer [5]	$P_u = \begin{cases} 0.78 b_p \sqrt{2(c_f k_p^2 f_{ctm}) E_p t_p} & L \geq L_e \\ 0.78 b_p \sqrt{2(c_f k_p^2 f_{ctm}) E_p t_p}\ \frac{L}{L_e}(2 - \frac{L}{L_e}) & L < L_e \end{cases}$	✓		✓	✓	✓	✓	✓
Neubauer and Rostásy [3]	$P_u = \begin{cases} 0.64 k_p b_p \sqrt{E_p t_p f_{ctm}} & L \geq L_e \\ 0.64 k_p b_p \sqrt{E_p t_p f_{ctm}}\ \frac{L}{L_e}(2 - \frac{L}{L_e}) & L < L_e \end{cases}$	✓		✓	✓	✓	✓	✓
Brosens and van Gemert [18]	$P_u = 0.5 b_p L f_{ctm}$			✓		✓	✓	

Table 6.1 *Continued*

Reference	Model (original notations)	Substrate			Composite			
		b_{sb}	$f_{c,sb}$	$f_{t,sb}$	t_{com}	b_{com}	L_{com}	E_{com}
fib 19 [9]	$F_{fb} = \begin{cases} 0.25 \cdot \sqrt{\frac{2-b_f/b}{1+b_f/b}} \cdot 1 \cdot b_f \cdot \sqrt{2 \cdot E_f \cdot t_f \cdot {f_{cm}}^{2/3}} & l_b \geq l_e \\ 0.25 \cdot \sqrt{\frac{2-b_f/b}{1+b_f/b}} \cdot \frac{l_b}{l_e}\left(2-\frac{l_b}{l_e}\right) \cdot b_f \cdot \sqrt{2 \cdot E_f \cdot t_f \cdot {f_{cm}}^{2/3}} & l_b < l_e \end{cases}$	✓	✓		✓	✓		✓
TR 55 [10]	$P_{max} = 0.5 \cdot 1.06 \cdot \sqrt{\frac{2-b_f/b_c}{1+b_f/400}} \cdot b_f \cdot \sqrt{E_f t_f f_{ctk}}$	✓		✓	✓	✓		✓
CNR -DT 200 [11]	$P_{max} = b_f \cdot \sqrt{2 \cdot E_f \cdot t_f \cdot 0.03 \cdot \sqrt{\frac{2-b_f/b_c}{1+b_f/400}} \cdot \sqrt{f_{ck} \cdot f_{ctm}}}$	✓	✓	✓	✓	✓		✓
SIA 166 [12]	$P_{max} = 0.5 \cdot b_f \cdot \sqrt{E_f t_f f_{ctH}}$			✓	✓			✓
CIDAR [19]	$P_{max} = 0.427 \cdot \sqrt{\frac{2-b_f/b_c}{1+b_f/b_c}} \cdot b_f \cdot \sqrt{E_f t_f \sqrt{f_c}}$	✓	✓		✓	✓		✓
Serbescu et al [4]	$P_{max} = \frac{2}{3}\beta k_{bf}\left(0.8\sqrt{f_{cu}}\right)\left(\sqrt{\frac{E_f t_f}{2.8 f_{ctm}}}\right) b_f$	✓	✓	✓	✓	✓		✓

Table 6.2 *Input parameters for the analytical modelling.*

Series	Substrate (sb)			Textile (tx)			Matrix (mx)		SRG composite (com)					
	b_{sb} mm	$f_{c,sb}$ N/mm^2	$f_{t,sb}$ N/mm^2	n_{cords}	$t_{tx,1}$ mm	A_{tx} mm^2	$f_{c,mx}$ kN/mm^2	$f_{t,mx}$ kN/mm^2	b_{com} mm	n	t_{com} mm	ρ_{com}	L_{com} mm	E_{com} kN/mm^2
SB-L-100-4-1	150	14	1.74	15	0.084	8.07	51	4.13	100	1	6	0.013	100	157
SB-L-100-4-2				30	0.084	16.14				2	9	0.018	100	160
SB-L-100-4-3				45	0.084	24.21				3	12	0.020	100	161
SB-L-100-8-1				31	0.169	16.68				1	6	0.028	100	169
SB-L-100-8-2				62	0.169	33.36				2	9	0.037	100	170
SB-L-100-8-3				93	0.169	50.03				3	12	0.042	100	166
SB-L-200-4-1				15	0.084	8.07				1	6	0.013	200	157
SB-L-200-4-2				30	0.084	16.14				2	9	0.018	200	160
SB-L-200-4-3				45	0.084	24.21				3	12	0.020	200	161
SB-L-200-8-1				31	0.169	16.68				1	6	0.028	200	169
SB-L-200-8-2				62	0.169	33.36				2	9	0.037	200	170
SB-L-200-8-3				93	0.169	50.03				3	12	0.042	200	166
SB-L-300-4-1				15	0.084	8.07				1	6	0.013	300	157
SB-L-300-4-2				30	0.084	16.14				2	9	0.018	300	160
SB-L-300-4-3				45	0.084	24.21				3	12	0.020	300	161
SB-L-300-8-1				31	0.169	16.68				1	6	0.028	300	169
SB-L-300-8-2				62	0.169	33.36				2	9	0.037	300	170
SB-L-300-8-3				93	0.169	50.03				3	12	0.042	300	166
SB-M-300-4-1		28	2.77	15	0.084	8.07				1	6	0.013	300	157
SB-M-300-4-2				30	0.084	16.14				2	9	0.018	300	160
SB-M-300-4-3				45	0.084	24.21				3	12	0.020	300	161
SB-M-300-8-1				31	0.169	16.68				1	6	0.028	300	169
SB-M-300-8-2				62	0.169	33.36				2	9	0.037	300	170
SB-M-300-8-3				93	0.169	50.03				3	12	0.042	300	166
SB-L-400-4-1		14	1.74	15	0.084	8.07				1	6	0.013	400	157
SB-L-400-4-2				30	0.084	16.14				2	9	0.018	400	160
SB-L-400-4-3				45	0.084	24.21				3	12	0.020	400	161
SB-L-400-8-1				31	0.169	16.68				1	6	0.028	400	169
SB-L-400-8-2				62	0.169	33.36				2	9	0.037	400	170
SB-L-400-8-3				93	0.169	50.03				3	12	0.042	400	166

Table 6.3 *Output data for existing models.*

Series	Experimental	Neubauer		Serbescu		Holzenkämpfer		Yang		Izumo (CFRP)		Izumo (AFRP)		Chen and Teng	
	$P_{u,ex}$	$P_{u,th}$	$\frac{P_{u,ex}}{P_{u,th}}$	$P_{u,th}$	$\frac{P_{u,ex}}{P_{u,th}}$	$P_{u,th}$	$\frac{P_{u,ex}}{P_{u,th}}$	$P_{u,th}$	$\frac{P_{u,ex}}{P_{u,th}}$	$P_{u,th}$	$\frac{P_{u,ex}}{P_{u,th}}$	$P_{u,th}$	$\frac{P_{u,ex}}{P_{u,th}}$	$P_{u,th}$	$\frac{P_{u,ex}}{P_{u,th}}$
	kN	kN		kN		kN		kN		kN		kN		kN	
SB-L-100-4-1	14.09	8.04	1.75	9.63	1.46	12.66	1.11	4.56	3.09	5.76	2.45	13.67	1.03	5.38	2.62
SB-L-100-4-2	15.13	11.09	1.36	13.27	1.14	12.34	1.23	4.64	3.26	5.48	2.76	13.00	1.16	7.42	2.04
SB-L-100-4-3	19.50	13.86	1.41	16.58	1.18	12.59	1.55	4.71	4.14	5.70	3.42	13.52	1.44	9.27	2.10
SB-L-100-8-1	15.75	11.13	1.42	13.31	1.18	17.51	0.90	4.64	3.39	11.02	1.43	26.15	0.60	7.45	2.12
SB-L-100-8-2	18.86	15.74	1.20	18.83	1.00	17.51	1.08	4.76	3.96	11.02	1.71	26.15	0.72	10.53	1.79
SB-L-100-8-3	20.21	19.27	1.05	23.06	0.88	17.51	1.15	4.85	4.16	11.02	1.83	26.15	0.77	12.90	1.57
SB-L-200-4-1	16.75	12.07	1.39	9.63	1.74	18.99	0.88	4.56	3.67	11.52	1.45	27.34	0.61	8.71	1.92
SB-L-200-4-2	16.59	16.64	1.00	13.27	1.25	18.51	0.90	4.64	3.57	10.95	1.51	25.99	0.64	12.01	1.38
SB-L-200-4-3	15.58	20.79	0.75	16.58	0.94	18.88	0.83	4.71	3.31	11.39	1.37	27.04	0.58	15.01	1.04
SB-L-200-8-1	14.15	16.69	0.85	13.31	1.06	26.26	0.54	4.64	3.05	22.04	0.64	52.30	0.27	12.05	1.17
SB-L-200-8-2	19.28	23.60	0.82	18.83	1.02	26.26	0.73	4.76	4.05	22.04	0.87	52.30	0.37	17.04	1.13
SB-L-200-8-3	18.74	28.91	0.65	23.06	0.81	26.26	0.71	4.85	3.86	22.04	0.85	52.30	0.36	20.87	0.90
SB-L-300-4-1	18.66	12.57	1.48	9.63	1.94	19.78	0.94	4.56	4.09	14.40	1.30	34.17	0.55	9.16	2.04
SB-L-300-4-2	16.89	17.33	0.97	13.27	1.27	19.28	0.88	4.64	3.64	13.69	1.23	32.49	0.52	12.63	1.34
SB-L-300-4-3	16.32	21.65	0.75	16.58	0.98	19.67	0.83	4.71	3.46	14.24	1.15	33.80	0.48	15.78	1.03
SB-L-300-8-1	15.64	17.39	0.90	13.31	1.17	27.35	0.57	4.64	3.37	27.54	0.57	65.37	0.24	12.67	1.23
SB-L-300-8-2	26.34	24.59	1.07	18.83	1.40	27.35	0.96	4.76	5.53	27.54	0.96	65.37	0.40	17.92	1.47
SB-L-300-8-3	28.47	30.11	0.95	23.06	1.23	27.35	1.04	4.85	5.87	27.54	1.03	65.37	0.44	21.94	1.30
SB-M-300-4-1	17.54	15.84	1.11	10.81	1.62	24.92	0.70	7.18	2.44	19.46	0.90	38.70	0.45	10.89	1.61
SB-M-300-4-2	18.56	21.84	0.85	14.90	1.25	24.30	0.76	7.28	2.55	18.50	1.00	36.80	0.50	15.02	1.24
SB-M-300-4-3	20.53	27.28	0.75	18.61	1.10	24.78	0.83	7.36	2.79	19.24	1.07	38.28	0.54	18.76	1.09
SB-M-300-8-1	15.51	21.90	0.71	14.94	1.04	34.46	0.45	7.28	2.13	37.22	0.42	74.03	0.21	15.07	1.03
SB-M-300-8-2	25.19	30.98	0.81	21.14	1.19	34.46	0.73	7.43	3.39	37.22	0.68	74.03	0.34	21.31	1.18
SB-M-300-8-3	25.98	37.94	0.68	25.89	1.00	34.46	0.75	7.54	3.45	37.22	0.70	74.03	0.35	26.09	1.00
SB-L-400-4-1	18.26	12.57	1.45	9.63	1.90	19.78	0.92	4.56	4.00	14.40	1.27	34.17	0.53	9.16	1.99
SB-L-400-4-2	19.02	17.33	1.10	13.27	1.43	19.28	0.99	4.64	4.10	13.69	1.39	32.49	0.59	12.63	1.51
SB-L-400-4-3	18.18	21.65	0.84	16.58	1.10	19.67	0.92	4.71	3.86	14.24	1.28	33.80	0.54	15.78	1.15
SB-L-400-8-1	15.84	17.39	0.91	13.31	1.19	27.35	0.58	4.64	3.41	27.54	0.58	65.37	0.24	12.67	1.25
SB-L-400-8-2	23.77	24.59	0.97	18.83	1.26	27.35	0.87	4.76	4.99	27.54	0.86	65.37	0.36	17.92	1.33
SB-L-400-8-3	28.04	30.11	0.93	23.06	1.22	27.35	1.03	4.85	5.78	27.54	1.02	65.37	0.43	21.94	1.28
Average			1.03		1.24		0.88		3.75		1.26		0.55		1.47
SD			0.29		0.28		0.23		0.89		0.67		0.28		0.43
CoV (%)			28		23		26		24		53		50		30

Table 6.3 *Continued*

Series	Experimental		Fib 19		TR55		CNR -DT 200		SIA 166		Proposed			
	$P_{u,ex}$	MoF_{ex}	$P_{u,th}$	$\frac{P_{u,ex}}{P_{u,th}}$	$P_{u,th}$	$\frac{P_{u,ex}}{P_{u,th}}$	$P_{u,th}$	$\frac{P_{u,ex}}{P_{u,th}}$	$P_{u,th}$	$\frac{P_{u,ex}}{P_{u,th}}$	$P_{u,th}$	$\frac{P_{u,ex}}{P_{u,th}}$	MoF_{th}	$\frac{MoF_{ex}}{MoF_{th}}$ [1]
	kN		kN		kN		kN		kN		kN			
SB-L-100-4-1	14.09	B	6.98	2.02	8.96	1.57	6.86	2.05	8.18	1.72	16.37	0.86	B	1
SB-L-100-4-2	15.13	B	9.63	1.57	12.35	1.22	9.46	1.60	11.29	1.34	15.96	0.95	B	1
SB-L-100-4-3	19.50	B	12.03	1.62	15.43	1.26	11.82	1.65	14.10	1.38	16.28	1.20	B	1
SB-L-100-8-1	15.75	C	9.66	1.63	12.39	1.27	9.49	1.66	11.32	1.39	15.67	1.00	C	1
SB-L-100-8-2	18.86	C	13.66	1.38	17.52	1.08	13.42	1.41	16.01	1.18	18.64	1.01	C	1
SB-L-100-8-3	20.21	B	16.73	1.21	21.46	0.94	16.43	1.23	19.60	1.03	19.24	1.05	B	1
SB-L-200-4-1	16.75	B	10.47	1.60	8.96	1.87	6.86	2.44	8.18	2.05	16.37	1.02	B	1
SB-L-200-4-2	16.59	B	14.44	1.15	12.35	1.34	9.46	1.75	11.29	1.47	15.96	1.04	B	1
SB-L-200-4-3	15.58	B	18.04	0.86	15.43	1.01	11.82	1.32	14.10	1.11	16.28	0.96	B	1
SB-L-200-8-1	14.15	C	14.49	0.98	12.39	1.14	9.49	1.49	11.32	1.25	15.67	0.90	C	1
SB-L-200-8-2	19.28	C	20.49	0.94	17.52	1.10	13.42	1.44	16.01	1.20	18.64	1.03	C	1
SB-L-200-8-3	18.74	B	25.09	0.75	21.46	0.87	16.43	1.14	19.60	0.96	19.24	0.97	B	1
SB-L-300-4-1	18.66	E1	10.91	1.71	8.96	2.08	6.86	2.72	8.18	2.28	18.23	1.02	E1	1
SB-L-300-4-2	16.89	B	15.05	1.12	12.35	1.37	9.46	1.79	11.29	1.50	18.35	0.92	B	1
SB-L-300-4-3	16.32	B	18.80	0.87	15.43	1.06	11.82	1.38	14.10	1.16	18.72	0.87	B	1
SB-L-300-8-1	15.64	C	15.09	1.04	12.39	1.26	9.49	1.65	11.32	1.38	15.67	1.00	C	1
SB-L-300-8-2	26.34	C	21.34	1.23	17.52	1.50	13.42	1.96	16.01	1.65	25.46	1.03	C	1
SB-L-300-8-3	28.47	B	26.14	1.09	21.46	1.33	16.43	1.73	19.60	1.45	28.30	1.01	B	1
SB-M-300-4-1	17.54	E1	13.75	1.28	11.29	1.55	9.16	1.92	10.31	1.70	18.23	0.96	E1	1
SB-M-300-4-2	18.56	B	18.96	0.98	15.57	1.19	12.63	1.47	14.22	1.31	23.12	0.80	B	1
SB-M-300-4-3	20.53	B	23.68	0.87	19.44	1.06	15.77	1.30	17.76	1.16	23.58	0.87	B	1
SB-M-300-8-1	15.51	C	19.01	0.82	15.61	0.99	12.66	1.22	14.26	1.09	15.67	0.99	C	1
SB-M-300-8-2	25.19	C	26.89	0.94	22.08	1.14	17.91	1.41	20.17	1.25	25.46	0.99	C	1
SB-M-300-8-3	25.98	B	32.93	0.79	27.04	0.96	21.93	1.18	24.70	1.05	33.82	0.77	B	1
SB-L-400-4-1	18.26	E1	10.91	1.67	8.96	2.04	6.86	2.66	8.18	2.23	18.23	1.00	E1	1
SB-L-400-4-2	19.02	B	15.05	1.26	12.35	1.54	9.46	2.01	11.29	1.69	18.35	1.04	B	1
SB-L-400-4-3	18.18	B	18.80	0.97	15.43	1.18	11.82	1.54	14.10	1.29	18.72	0.97	B	1
SB-L-400-8-1	15.84	C	15.09	1.05	12.39	1.28	9.49	1.67	11.32	1.40	15.67	1.01	C	1
SB-L-400-8-2	23.77	C	21.34	1.11	17.52	1.36	13.42	1.77	16.01	1.48	25.46	0.93	C	1
SB-L-400-8-3	28.04	B	26.14	1.07	21.46	1.31	16.43	1.71	19.60	1.43	28.30	0.99	C	0
Average				1.19		1.30		1.68		1.42		0.98		0.97
SD				0.33		0.31		0.41		0.33		0.09		0.19
CoV (%)				28		24		24		24		9		19

.[1] $For\ MoF_{ex} = MoF_{th}, MoF_{ex}/MoF_{th} = 1, otherwisw\ 0$

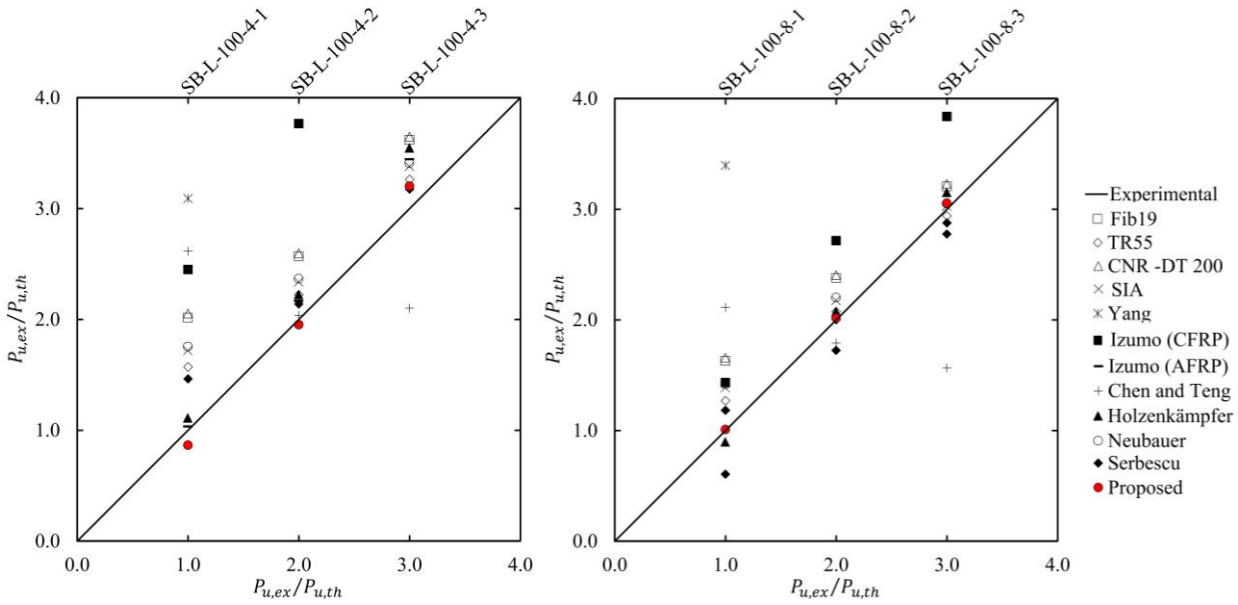

Figure 6.1 *The accuracy of different models in predicting the debonding load in the SRG system for series L-100-4 (left) and series L-100-8 (right).*

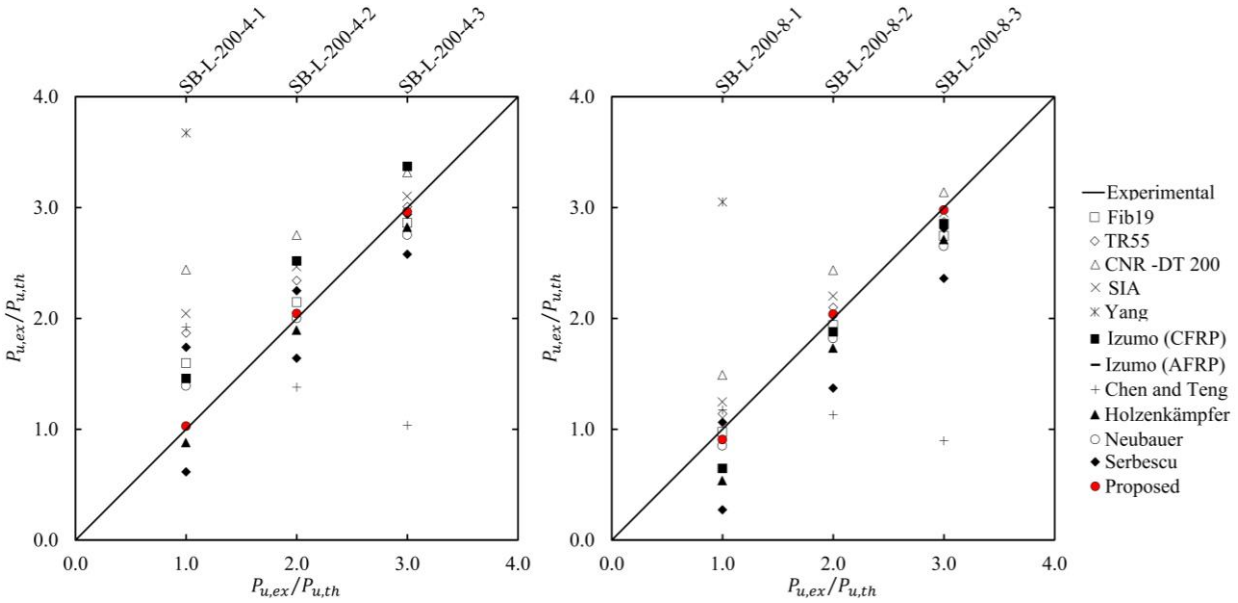

Figure 6.2 *The accuracy of different models in predicting the debonding load in the SRG system for series L-200-4 (left) and series L-200-8 (right).*

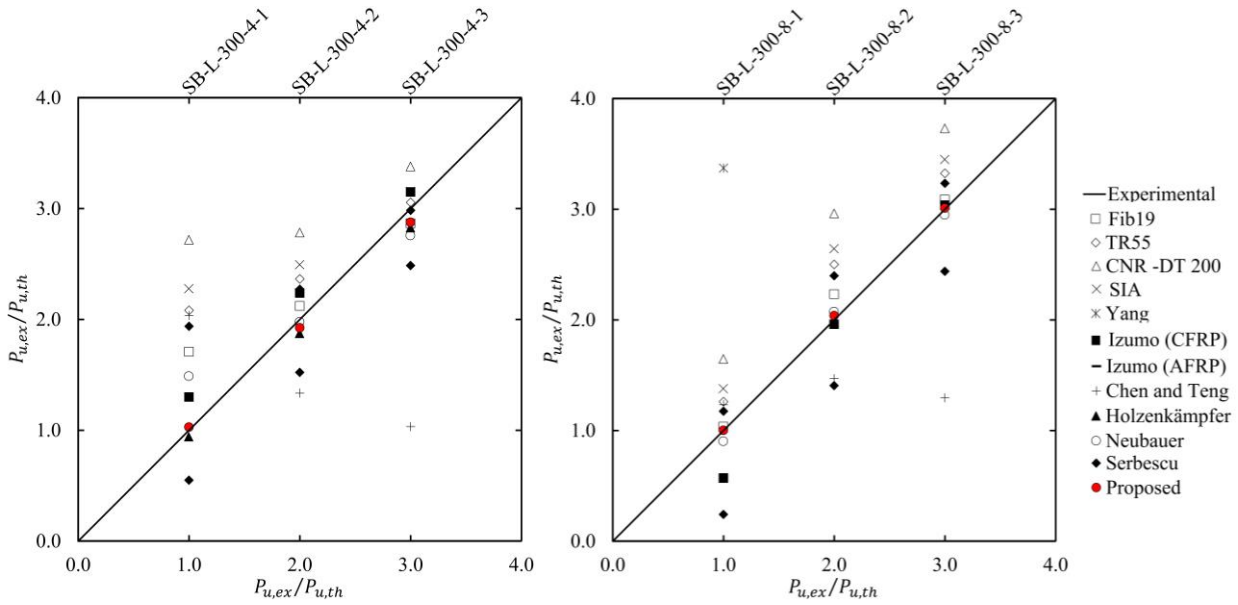

Figure 6.3 *The accuracy of different models in predicting the debonding load in the SRG system for series L-300-4 (left) and series L-300-8 (right).*

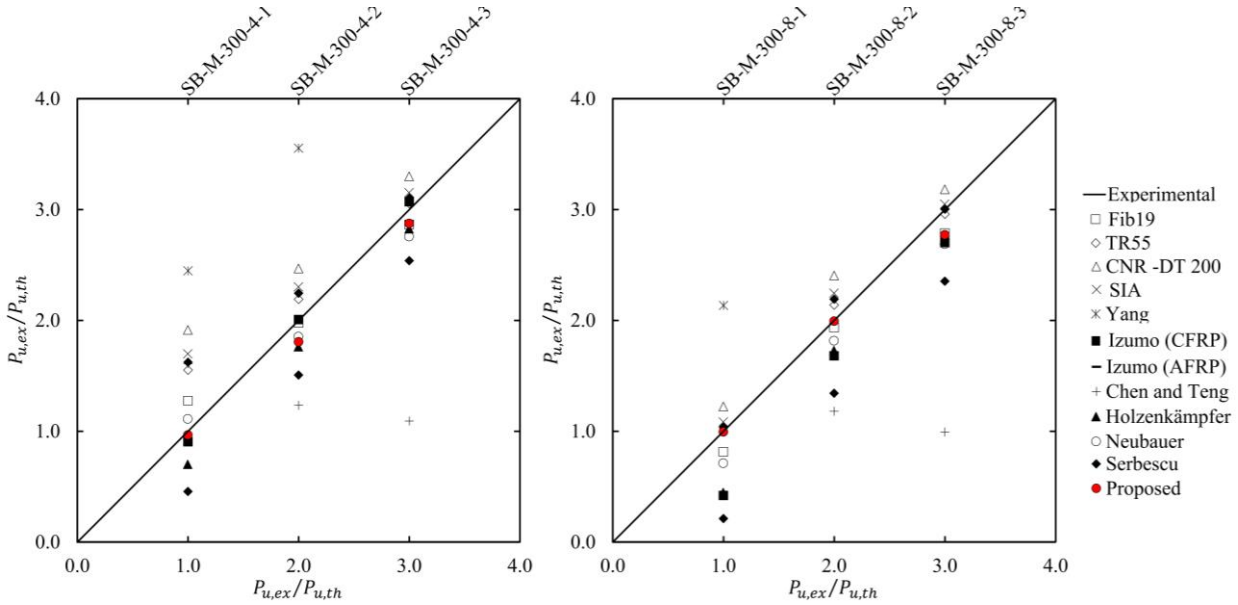

Figure 6.4 *The accuracy of different models in predicting the debonding load in the SRG system for series M-300-4 (left) and series M-300-8 (right).*

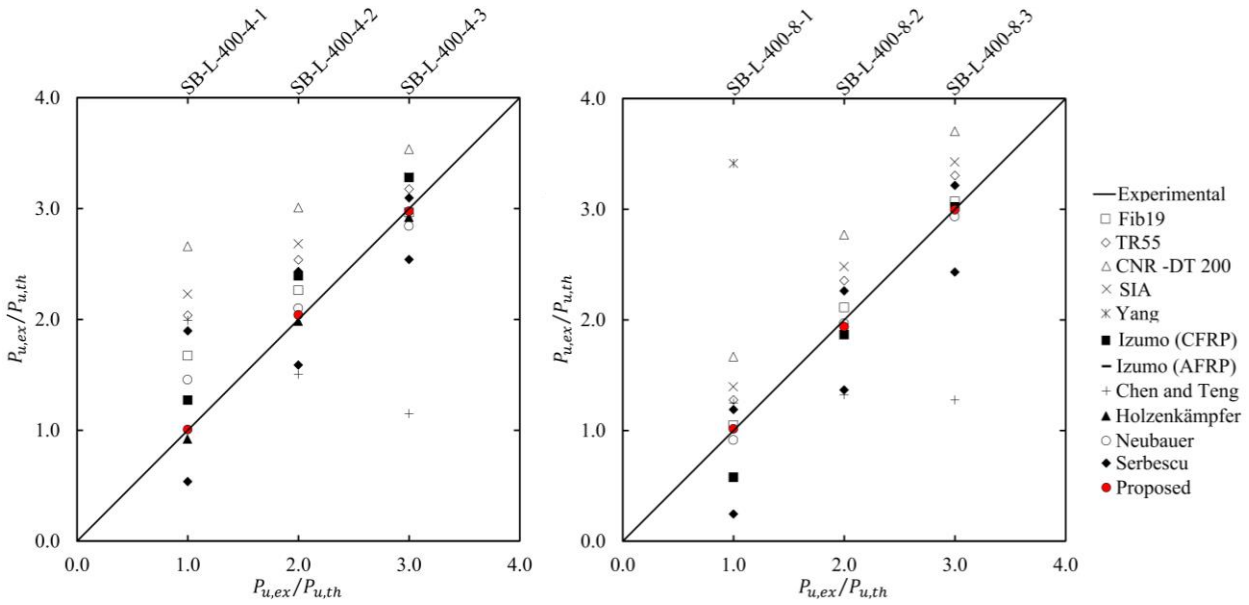

Figure 6.5 *The accuracy of different models in predicting the debonding load in the SRG system for series L-400-4 (left) and series 4-100-8 (right).*

6.3 Estimating the failure load in the SRG system

6.3.1 Shear bond tests

Two key properties were found to largely influence the shear bond behaviour in the second experimental programme including the bond length and the composite reinforcement ratio. This latter is a function of the density of the steel textiles, the thickness of the SRG composites, and the number of the textile layers. Direct shear bond tests confirmed the following statements:

- The behaviour of the SRG composites with a short bond length (100 mm) is rather complex. This short length could not provide the sufficient anchorage force that would enable the composite to develop a complete bond response.
- The behaviour of the tested specimens comprising SRG composites with bond length of 300 mm and 400 mm is different to that of the specimens with a bond length of 100 mm and 200 mm regardless of the reinforcement ratio. This indicates that the effective bond length lies between 200 and 300 mm. An effective bond length of 250 mm will be considered in the next calculations.
- For SRG composites with reinforcement ratios equal or less than 0.02, increasing the number of the steel textile layers did not provide much improvement to the load capacity. On the other hand, the SRG composites with reinforcement ratios greater than 0.02 exhibited a slight improvement in the load capacity for bond lengths less than the effective bond length. This improvement was sound for bond length greater than the effective bond length.

- For reinforcement ratios equal or below 0.02, the governed mode of failure was debonding at the matrix-to-substrate interface. However, the series comprising one layer of the steel textiles experienced tensile rupture of the textile for bond lengths greater than 200 mm. Furthermore, debonding at the matrix-to-textile interface was not observed for series with low reinforcement ratio.
- Debonding at the matrix-to-textile interface was the dominant mode of failure for the series with reinforcement ratios greater than 0.02. However, the use of three layers of the steel textile layer always altered the mode of failure to debonding at the matrix-to-substrate interface.

In fact, this complex behaviour requires a conditional model to capture the effect of different parameters. The key parameters that will define the conditions of that model would be the reinforcement ratio and the effective bond length. Since failure can occur at three different sections including the cross section of the steel cords (i.e., tensile rupture of the textiles), the surface between the substrate and the composite (i.e., debonding at the matrix-to-substrate interface), and the surface/surfaces between the matrix and the steel textile (i.e., debonding at the matrix-to-substrate interface). Each mode of failure requires a unique model to predict the load that would cause the failure at that surface. The mechanical properties of the materials at the interface would define the right model to predict the failure load.

The philosophy of the proposed model is based on the assumption that the failure in the SRG system will occur at the weakest section. In other words, the section with the least resistance to the applied load. A check must be conducted to determine the section of the minimum capacity. However, not all sections need to be checked as for reinforcement ratio below 0.02 debonding at the matrix-to-textile was not observed. The SRG systems comprising textiles of low reinforcement ratios must be checked against the debonding at the matrix-to-substrate interface and the tensile strength of the textiles such that the section that can develop the least load would determine the maximum load that can be resisted by the SRG system.

On the other hand, when the reinforcement ratio is greater than 0.02, the dominant mode of failure would be the debonding at the matrix-to-textile interface. However, these systems with high reinforcement ratio can also experience a debonding at the matrix-to-substrate interface (common for three layers) and this require the designer to do a check on that interface. The maximum load that can be attained by the SRG systems with high reinforcement ratios is governed by debonding at either the matrix-to-textile interface (being the dominant) or the matrix-to-substrate interface.

The proposed model for bond tests

Two expressions are proposed to calculate the maximum load that can be resisted by the interface including the debonding load at the matrix-to-substrate interface ($P_{deb,1}$) and the debonding load at the matrix-to-textile interface ($P_{deb,2}$):

$$P_{deb,1} = \alpha \cdot \beta \cdot b_{com} \cdot \sqrt{f_{t,sb} \cdot E_{com} \cdot t_{tx,1}} \quad (4)$$

$$P_{deb,2} = \varphi \cdot \xi \cdot b_{com} \cdot \sqrt{f_{t,mx} \cdot E_{com} \cdot t_{tx,1}} \quad (5)$$

where E_{com} is the elastic modulus of the SRG composite in the third zone on the stress-strain curve. E_{com} is very close to the elastic modulus of the steel textile (E_{com}), hence this latter can be used instead of E_{com} in Eq. (1) and (2). $t_{tx,1}$ is the equivalent thickness of the textile (1 layer), $f_{t,mx}$ and $f_{t,sb}$ are the tensile strength of the matrix and the substrate respectively. b_{com} is the width of the SRG composite.

α is a coefficient calibrated against the experimental data and is expressed by the following expression:

$$\alpha = \begin{cases} 1 & \text{for } \rho_f > 0.02 \text{ and } L_{com} < L_e \\ 1.15 & \text{for } \rho_f > 0.02 \text{ and } L_{com} \geq L_e \\ 0.85 & \text{for } \rho_f \leq 0.02 \text{ and } L_{com} < L_e \\ 1.25 & \text{for } \rho_f \leq 0.02 \text{ and } L_{com} \geq L_e \end{cases} \quad (6)$$

β is a coefficient to account for the influence of the bond length as a ratio to the effective bond length according to the following equation:

$$\beta = \begin{cases} \frac{L_{com}}{L_e}\left(2 - \frac{L_{com}}{L_e}\right) & \text{for } \rho_f > 0.02 \text{ and } L_{com} < L_e \\ 1 & \text{for } \rho_f > 0.02 \text{ and } L_{com} \geq L_e \\ \frac{L_{com}}{L_e}\left(2 - \frac{L_{com}}{L_e}\right) & \text{for } \rho_f \leq 0.02 \text{ and } L_{com} < L_e \\ 1 & \text{for } \rho_f \leq 0.02 \text{ and } L_{com} \geq L_e \end{cases} \quad (7)$$

φ is a coefficient calibrated against the experimental data and is equal to 0.45.

ξ is a coefficient to account for the effect of the number of the steel textile layers and is given by the following conditional expression:

$$\xi = \begin{cases} n^{0.25} & \text{for } \rho_f > 0.02 \text{ and } L_{com} < L_e \\ n^{0.70} & \text{for } \rho_f > 0.02 \text{ and } L_{com} \geq L_e \end{cases} \quad (8)$$

where n is the number of the textile layers and L_{com} and L_e are the bond length and the effective bond length, respectively.

The check for the tensile failure of the steel textile is needed when the reinforcement ratio is less than or equal to 0.02. The theoretical load that can cause a rupture to the external reinforcement can be calculated using the following expression:

$$P_{rup} = \zeta \cdot A_{tx} \cdot f_{u,tx} \qquad \text{for } \rho_f \leq 0.02 \tag{9}$$

where A_{tx} is the total area of the steel textile and $f_{u,tx}$ is the ultimate tensile strength that can be resisted by the textile.

The value of ζ for direct shear bond tests can be determined by equating the theoretical rupture load to the experimental load for the specimens that experienced rupture of the steel textiles. The following expression can be written:

$$P_{rup} = \zeta \cdot A_{tx} \cdot \sigma_{f,u} = P_{u,exp} \tag{10}$$

Solving for ζ

$$\zeta = \frac{P_{u,exp}}{A_{tx} \cdot \sigma_{f,u}} \tag{11}$$

Three series in direct shear bond tests experienced failure by tensile rupture of textiles including SB-L-300-4-1, SB-M-300-4-1, and SB-L-400-4-1. Considering the average ultimate load for the three, the value of ζ can be determined from Eq. (11) to be equal to 0.75.

The estimated maximum load and the mode of failure obtained from the proposed model is reported in Table 6.3. The model was able to capture the behaviour of the SRG system for different reinforcement ratios and different bond lengths. The estimated values of the maximum load only yielded a coefficient of variation (CoV) of only 9 %. Also, the model provided a reliable tool for estimating the mode of failure for each tested series. Out of 30 modes, the model predicted 29 modes matching the experimental failure mode. Fig. 6.6 provides a design flowchart for estimating the value and the mode of failure.

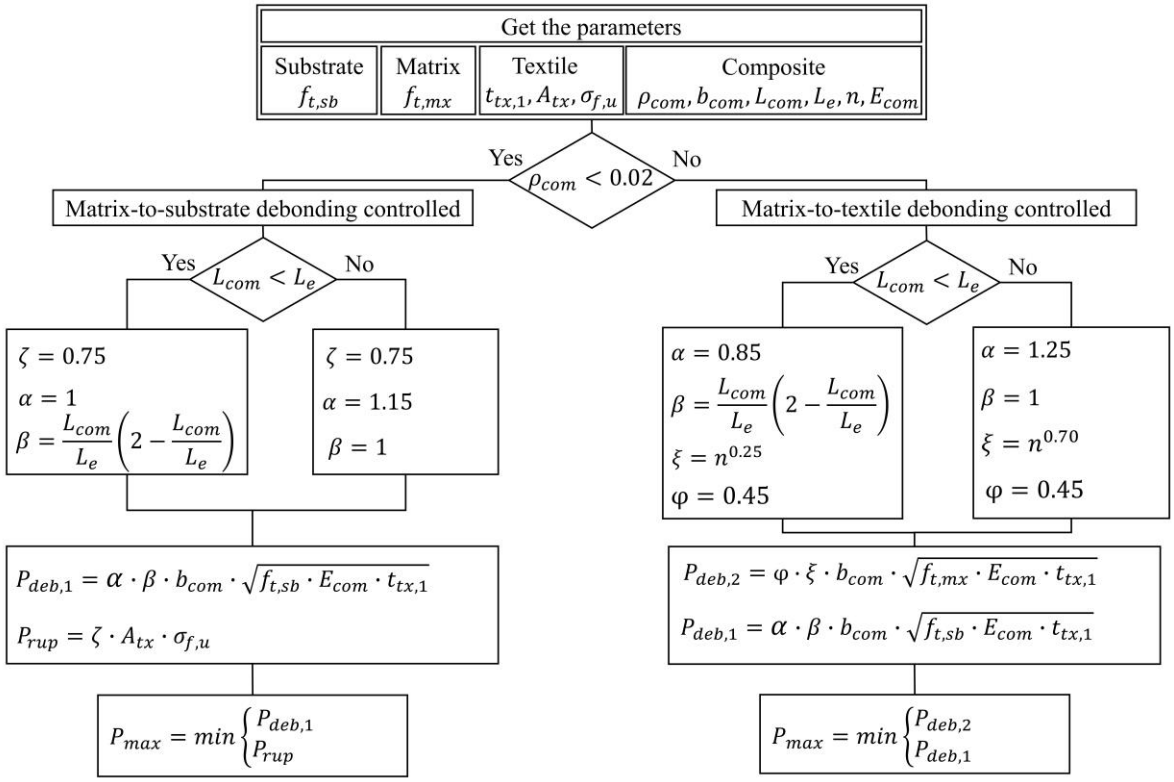

Figure 6.6 *The design flow chart for estimating the load and mode of failure*.

6.3.2 Beam tests

The failure mechanism in beam tests is similar to that of shear bond tests since the geometrical and mechanical properties that influence the failure load and mode are the same for both tests. The combination of the SRG composite and the tension face of the RC beam (i.e., the substrate) can be theoretically considered as a system in a shear bond test. The applied load in beam tests will translate to internal force that act on the cross section of the beam [see Fig. 6.7].

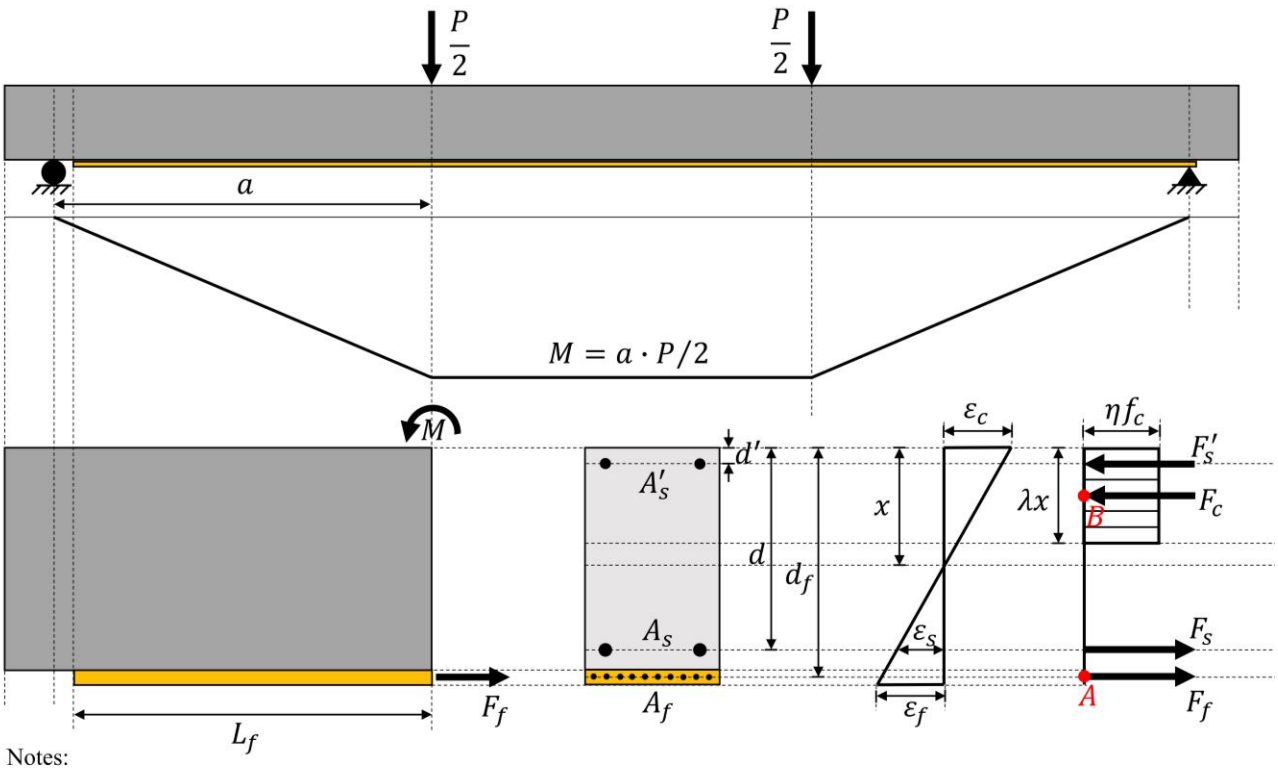

Notes:
Dimensions are Exaggerated
Notations of EC2 are adopted
$\varepsilon_c, \varepsilon_s$, and ε_f are the strains in concrete, steel, and fibres, respectively.

Figure 6.7 *Internal forces in a typical strengthened RC beam.*

The prediction of the ultimate load in beam tests

The internal force (F_f) acting upon the SRG composite in a strengthened beam (see Fig. 6.7) is equivalent to that force acting upon the composite in shear bond tests. The load and mode of failure in shear bond tests can be predicted following the procedure presented in the previous section. Hence, when the properties of the SRG composite and the substrate are known, the failure load of the SRG composite can be predicted (see Fig. 6.6). The weakest surface in the SRG system will govern the mode of failure in the strengthened beam such that:

$$F_f = \min\{P_{rup}, P_{deb,1}, P_{deb,2}\} \quad (12)$$

Once (F_f) is predicted, the neutral axis, the moment acting upon the cross section, and the ultimate load can also be calculated. The neutral axis can be calculated by equating the moments at points A and B in Fig. 6.7 such that:

$$M_A = M_B \quad (13)$$

$$M_A = F_s' \cdot (d_f - d') + F_c \cdot \left(d_f - \frac{\lambda x}{2}\right) - F_s \cdot (d_f - d) \quad (14)$$

$$M_B = F_f \cdot \left(d_f - \frac{\lambda x}{2}\right) + F_s \cdot \left(d - \frac{\lambda x}{2}\right) + F_s' \cdot \left(\frac{\lambda x}{2} - d'\right) \quad (15)$$

where

$$F_s' = A_s' \cdot f_y' \quad (16)$$

$$F_c = \eta f_c \cdot \lambda x \cdot b_{sb} \quad (17)$$

$$F_s = A_s \cdot f_y \quad (18)$$

F_s', F_c, and F_s are the internal forces in the compression reinforcement, the concrete block, and the tensile reinforcement, respectively. d_f, d', d, a, and b_{sb} are the effective length of the external reinforcement, the compression rebars, the tensile rebars, the shear span, and the width of beam, respectively (see Fig. 6.7). A_s' and A_s are the cross-sectional areas of the compression and the tensile reinforcement, respectively. f_y and f_c are the yield strength of the tensile rebars and the cubic compressive strength of the concrete ($f_c = f_{c,sb}$). λ is a factor defining the effective height of the compression zone equal to 0.80, while η is a factor defining the effective strength of the concrete equal to unity. Bi-linear stress-strain relation was assumed for the compression zone according to Eurocode 2 [14].

Substituting Eqs. 14-15 into Eq. 13 and solving for x:

$$x = \frac{\frac{\lambda}{2}\left(2\eta f_c b_{sb} d_f + F_f + A_s f_y - A_s' f_y'\right) \pm \sqrt{\left[\frac{-\lambda}{2}\left(2\eta f_c b_{sb} d_f + F_f + A_s f_y - A_s' f_y'\right)\right]^2 - 2\eta f_c b_{sb} d_f \lambda^2 \left(F_f + A_s f_y - A_s' f_y'\right)}}{\eta f_c b_{sb} \lambda^2} \quad (19)$$

The moment acting upon the cross section can now be calculated from Eq. 14 or Eq. 15. The ultimate theoretical load which the strengthened beam can develop can be calculated from the following equation:

$$P_{u,an} = \frac{2M}{a} \quad (20)$$

6.4 Validation of the proposed procedure for estimating the ultimate load

The proposed procedure (introduced in the previous section) for calculating the ultimate load for the RC beams strengthened with the SRG system was validated against two sources. The first source is the experimental data obtained from the bending tests conducted on the strengthened beams (see Chapter 5), while the second source is the available experiments on the flexutal behviour of RC beams strengthened with the SRG system. Although the latter is very limited in literature, however, few studies were considered for this task. These studies are namely Naploi & Realfonzo [20], Ombrees & Verre [21], and Bencardino & Condello [22].

Table 6.6 summaries the key properties for the experiments that were considered for the validation process. These properties were used to predict the failure load and mode for the SRG system, and this load was used

for calculating the ultimate capacity of the strengthened beams. The geometrical properties include the width of the SRG composite, b_{com}, the spear span, a, and the equivalent thickness of one layer of the textile, $t_{tx,1}$. The properties d_f, d', and d are the effective length of the SRG composite, the compression rebars, and the tensile rebars, respectively. ρ_{com} is the SRG reinforcement ratio defined in Eq. 3, while A_{tx}, A_s, and A'_s are the cross-sectional areas of the steel textiles, the compression rebars, and the tensile rebars, respectively. On the other hand, the mechanical properties were provided including f_y, $f_{u,tx}$, $f_{t,sb}$, and $f_{t,mx}$ which denote the yield strength of the tensile rebars, the ultimate stress of the steel textile, the tensile strength of the substrate and the matrix, respectively. When the tensile strength was not reported in the considered studies, Eq.1 was used to estimate its value. Finally, the elastic modulus, E_{tx}, of the steel textile was also provided.

Table 6.7 provides the outputs of the analytical modelling including the calibration factors for bond tests α, β, φ, ξ, and ζ. It also reports the failure load associated with the three theoretical modes of failure including the the rupture load, P_{rup}, the debonding load at the matrix-to-substrate interface, $P_{deb,1}$, and the debonding load at the matrix-to-textile interface, $P_{deb,2}$. The minimum value of these theoretical modes should govern the failure mechanism in the tested beam. The value represents the internal force, the debonding load at the matrix-to-substrate interface, F_f, acting upon the SRG composite. The corresponding moment, M, and ultimate analytical load, $P_{u.an}$, were then calculated for each beam. The ratio between the experimental ultimate load, $P_{u.ex}$, and the analytical and experimental modes of failure were reported.

As it can be seen in Table 6.7, the predicted values for the failure load in the strengthened beams were very close to the experimental load values. The average value of the ratios between the experimental and the analytical load, $P_{u.ex}/P_{u.an}$, was 1.01 with a standard deviation and coefficient of variation of 0.08 and 8, respectively. The coefficient of determination, R^2, of the proposed model had a value of 99.4 %. Furthermore, the experimental modes of failure for 93 % of the tested beams in the validation database were captured by the model. It is worth noting that the beams that experienced textile slippage in the failure mechanism were not considered when calculating the accuracy of the model in capturing the mode of failure as the model is only capable of predicting textile rupture and debonding but not slippage. Fig. 6.8 provides a graph showing the accuracy of the proposed procedure for predicting the failure load in the RC beams strengthened with SRG system for all tested beams.

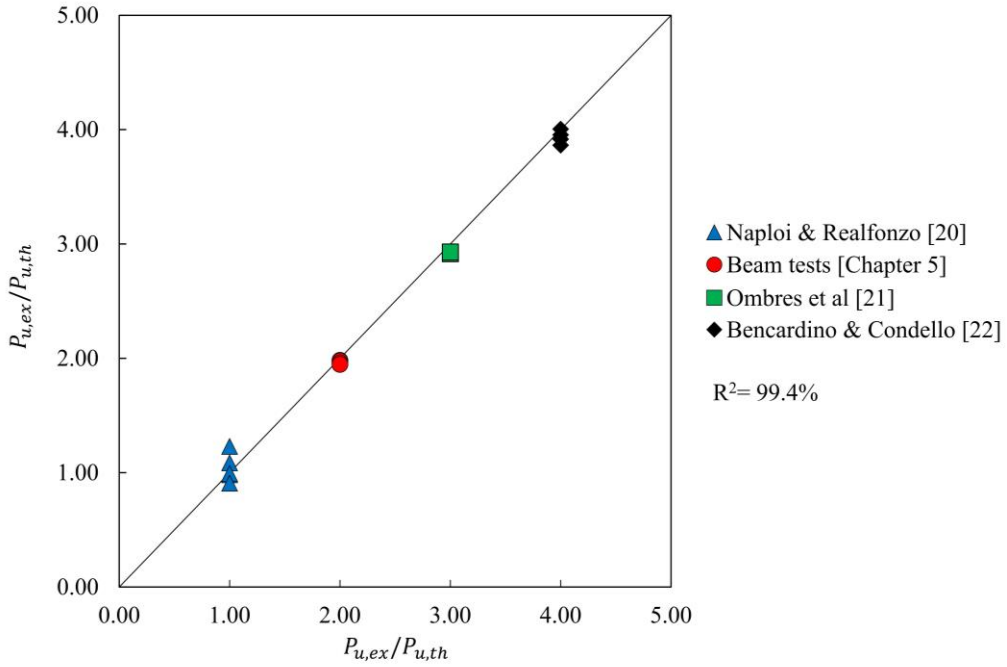

6.8 *The accuracy of the proposed procedure in predicting the failure load for SRG-strengthened beams.*

Table 6.6 *The key inputs for the experiments used for the calibration of the proposed model.*

Ref.	Beam	b_{com}	a	$t_{tx,1}$	d	d'	d_f	ρ_{com}	A_{tx}	A_s	A'_s	f_y	$f_{u,tx}$	$f_{t,sb}$	$f_{t,mx}$	E_{tx}
		mm						%	mm^2			N/mm^2				kN/mm^2
Ch.5	B-S4-1	100	766	0.084	224	25	253.0	1.3	8.0	226	157	524	2900	3.39	4.13	190
	B-S4-2						254.5	1.8	16.1							
	B-S8-1			0.169			253.0	2.8	16.7							
	B-S8-2						254.5	3.7	33.4							
[20]	SRG-1LD	200	1220	0.084	167	33	205.0	0.8	16.7	393	157	460	2800	2.08	4.34	190
	SRG-2LD						207.5	1.1	33.4							
	SRG-1MD			0.254			205.0	2.5	50.6							
	SRG-1MD-B						205.0		50.6							
	SRG-1MD-A						205.0		50.6							
	SRG-2MD						207.5	3.4	101.1							
[21]	B-1L B-1L-1A B-1L-2A	70	1600	0.169	268	32	305.0	1.7	11.8	226	226	474	3000	2.20	3.72	190
[22]	A-EB	100	900	0.24	206	42	255.0	2.4	24.0	226	100	367	1470	1.70	3.80	74
	A-IRS															
	B-EB	150	1500		354		405.0		36.0	402		492				
	B-IRS															

Table 6.7 *The predictions of the proposed model of the failure load for the existing experiments on RC beams.*

Ref.	Beam	α	β	φ	ξ	ζ	P_{rup}	$P_{deb,1}$	$P_{deb,2}$	F_f	M	$P_{u,th}$	$P_{u,ex}$	$\frac{P_{u,ex}}{P_{u,th}}$	Mode of failure *	
							kN	kN	kN	kN	kN.m	kN	kN		Thermotical	Experimental
Chapter 3	B-S4-1	2.23	1.00	1.00	1.00	0.88	21.4	52.0	26.4	21.4	29.6	77.3	76.0	0.98	B	B
	B-S4-2	2.23			1.62		42.9	52.0	42.9	42.9	34.9	91.0	89.0	0.98	B	B
	B-S8-1	1.39			1.00		43.0	45.9	37.4	37.4	33.5	87.4	84.0	0.96	D	B+C+D
	B-S8-2	1.39			1.62		86.0	45.9	60.7	45.9	35.6	92.9	88.0	0.95	E	E
[20]	SRG-1LD	2.23	1.00	1.00	1.00	0.88	41.4	81.4	52.8	41.4	34.7	56.9	61.8	1.09	B	B
	SRG-2LD	2.23			1.62		82.8	81.4	85.7	81.4	42.2	69.2	68.7	0.99	E	E
	SRG-1MD	1.39			1.00		124.4	88.0	91.5	88.0	43.2	70.8	69.5	0.98	E	E
	SRG-1MD-B	1.39			1.00		124.4	88.0	91.5	88.0	43.2	70.8	70.2	0.99	E	E
	SRG-1MD-A	1.39			1.00		124.4	88.0	91.5	88.0	43.2	70.8	64.3	0.91	E	E
	SRG-2MD	1.39			1.62		248.9	88.0	148.7	88.0	43.4	71.2	87.6	1.23	E	E
[21]	B-1L	2.23	1.00	1.00	1.00	0.88	31.1	41.5	24.3	24.3	32.6	40.8	37.5	0.92	D	D
	B-1L-1A												37.3	0.92	D	D
	B-1L-2A												37.9	0.93	D	D
[22]	A-EB	1.39	1.00	1.00	1.00	0.88	40.5	27.6	29.6	27.6	21.2	47.2	43.2	0.92	E	E
	A-IRS												47.4	1.00	E	C
	B-EB						60.8	41.4	44.5	41.4	77.7	103.6	89.5	0.86	E	E
	B-IRS												99.0	0.95	E	D

*B: Rupture of the steel textile, C: Slippage of cords, D: Debonding at textile-matrix interface, and E: Debonding at substrate-matrix interface.

6.5 Conclusions

The evaluation of the existing model for estimating the debonding load in the FRP systems indicated that some of these models were able to predict the bond behaviour in the SRG systems for certain parameters. However, the overal behaviour of the SRG system could not captured for the parameters investigated in the experimental progeramme. An analytical model was propesed which was based on the assumption that the SRG composites with low reinforcement ratios (less than or equal to 0.02) are governed by either the tensile rupture of the steel textiles or the debonding at the matrix-to-substrate interface with latter being the dominant mode of failure. On the other hand, the SRG composites with high reinforcement ratios are governed by the debonding at the matrix-to-textile interface. However, increasing the number of the textile layers was found to alter the mode of failure to debonding at the matrix-to-substrate interface. The suggested model has three expressions to account for the three modes of failure such that the SRG systems with low reinforcement ratios must be checked against the tensile rupture of the steel textiles and the debonding at the matrix-to-substrate interface, while those with high reinforcement ratios need to be checked against both modes of debonding. Different coefficients were introduced to account for the effect of the bond length and the number of the textile layers. Also, the expressions have calibration factors to account for the differences between bond and beam tests. The proposed model for the shear bond tests can be utilised to predict the failure load in the strengthened RC beams. This was based on the approach that the internal force acting upon the SRG composite in the strengthened beam can be equated with force acting on the composite in shear bond tests. When this latter can be predicted from the proposed model, the moment capacity of the beam can be calculated.

References

[1] F. Bencardino, C. Carloni, A. Condello, F. Focacci, A. Napoli and R. Realfonzo, "Flexural behaviour of RC members strengthened with FRCM: State-of-the-art and predictive formulas", *Composites Part B: Engineering*, vol. 148, pp. 132-148, 2018.

[2] J. Chen and J. Teng, "Anchorage Strength Models for FRP and Steel Plates Bonded to Concrete", *Journal of Structural Engineering*, vol. 127, no. 7, pp. 784-791, 2001.

[3] Neubauer U, Rostasy F., “Design aspects of concrete structures strengthened with externally bonded CFRP plates”, In: 7Th Int. Conf. On Struct. Edinburgh: ECS Publications; 1997:109–118.

[4] A. Serbescu, M. Guadagnini and K. Pilakoutas, "Standardised double-shear test for determining bond of FRP to concrete and corresponding model development", *Composites Part B: Engineering*, vol. 55, pp. 277-297, 2013. Available: 10.1016/j.compositesb.2013.06.019.

[5] Holzenkämpfer, O. (1994). ‘‘Ingenieurmodelle des verbundes geklebter bewehrung für betonbauteile.’’ Dissertation, TU Braunschweig (in German).

[6] Yang, Z.J., Chen, J.F., and Proverbs, D. 2003. Finite element modelling of concrete cover separation failure in FRP plated RC beams, Construction and Building Materi 17(1): 3-13.

[7] Izumo, K., Saeki, N., Fukao, M., and Horiguchi, T. 1999. Bond behavior and strength between fiber sheets and concrete. Transactions of the Japan Concrete Institute, 21: 423-430.

[8] Chen, J.F., and Teng J.G. 2001. Anchorage strength model for FRP and steel plates attached to concrete. Journal of Structural Engineering, ASCE, 127(7):784-791.

[9] E. fib Working Group and S. Matthys, “Externally applied FRP reinforcement for concrete structures,” vol. 90. International Federation for Structural Concrete, 2019.

[10] TR55. Concrete Society Technical Report 55, “Design guidance for strengthening concrete structures using fibre composite materials”. The Concrete Society, Crowthorne (UK); 2000.

[11] CNR-DT 200. Guidelines for design, execution and control of strengthening interventions by means of fibre-reinforced composites materials, reinforced concrete and prestressed concrete structures, masonry structures. CNR – DT 200/2004. National Research Council, Advisory Committee on Technical Regulations for Constructions, Rome; 2004.

[12] SIA166. Klebebewehrungen (Externally bonded reinforcement). Schweizerischer Ingenieur und Architektenverein SIA; 2003 [in German].

[13] FIB (Federation Internationale du Beton), Fib Model Code for concrete structures 2010, 2013.

[14] British Standards Institution. Eurocode 2: Design of Concrete Structures: British Standard. London: BSi, 2008.

[15] Sato, Y., Ueda, T., Kakuta, Y., and Tanaka, T. 1996. Shear reinforcing effect of carbon fibre sheet attached to side of reinforced concrete beams. Proceedings of the 2nd International Conference on Advanced Composite Materials in Bridges and Structures, Montreal, Canada, 11-14 August, 1996, El-Badry (ed.), CSCE, p 621-627.

[16] JCI (Japanese Concrete Institute). 2003. Technical Report of Technical Committee on Retrofit Technology. Proceedings of the International Symposium on Latest Achievement of Technology and Research on Retrofitting Concrete Structures. Kyoto, Japan, 2003, pp. 4-42.

[17] Izumo, K., Saeki, N., Fukao, M., and Horiguchi, T. 1999. Bond behavior and strength between fiber sheets and concrete. Transactions of the Japan Concrete Institute, 21: 423-430.

[18] Brosens, K., and Van Gemert, D. 1997. Anchoring stresses between concrete and carbon fibre reinforced laminates, Non-Metallic (FRP) Reinforcement for Concrete Structures, Proceedings of the 3rd International Symposium, Sapporo, Japan, pp. 271-278.

[19] CIDAR. Design Guideline for RC structures retrofitted with FRP and metal plates: beams and slabs DRAFT 3. Centre for Infrastructure Diagnosis, Assessment and Rehabilitation, Standards Australia; 2006.

[20] A. Napoli and R. Realfonzo, "Reinforced concrete beams strengthened with SRP/SRG systems: Experimental investigation", *Construction and Building Materials*, vol. 93, pp. 654-677, 2015.

[21] Ombres L, Verre S. Flexural Strengthening of RC Beams with Steel-Reinforced Grout: Experimental and Numerical Investigation. Journal of Composites for Construction. 2019;23(5):04019035.

[22] F. Bencardino and A. Condello, "Eco-friendly external strengthening system for existing reinforced concrete beams", *Composites Part B: Engineering*, vol. 93, pp. 163-173, 2016.

Chapter 7 Conclusions

This thesis investigated the flexural behaviour of RC beams externally strengthened with the SRG composites. Also, the tensile and shear bond behaviour of multiple layers of these composites were studied as understanding these aspects was crucial to understand the flexural behaviour of structural members strengthened with these composites.. The theoretical part of the thesis involved an up-to-date literature review that explored the effort that has been made in the scientific community regarding the use of the inorganic-based composites including the FRCM and SRG systems. The theoretical part, also, included an analytical modelling of the data obtained from the experimental programmes. This latter was divided into three programmes. The first experimental programme comprised the direct tensile tests conducted on the dry single steel cords, dry steel textiles, and the SRG composite coupons. The aim of this programme was to get a better understand of the tensile behaviour of the SRG composites made of different steel textile densities and different number of layers. While the second programme involved the shear bond tests conducted on concrete prisms strengthened with different combinations of the SRG composites to gain insight into the bond behaviour associated with use of multiple layers of these composites comprising different steel textiles. Finally, the last experimental programme was conducted to understand the flexural behaviour of full-scale RC beams strengthened with SRG composites that had different number of layers and different densities of steel textiles. The following section highlights the general conclusions drawn from the experimental programmes and the analytical modelling.

7.1 General conclusions

•

• The SRG coupons exhibited a three-zone stress-strain behaviour. The first zone had a stiff behaviour characterising the contribution of the grout, while the second zone described the process of cracks initiation and propagation. The end of this latter process led to the last stage where the applied load was mainly resisted by the steel textile only with a slight contribution of the grout (tension stiffening).

• The SRG coupons, compared to the dry textiles, developed a stiffer initial behaviour due to the contribution of the grout. Also, they developed a slightly higher axial stress due to the tension stiffening effect of the grout.

• Increasing the number of the steel textile layers enhanced the axial stress in the cords and the strain of the grout. However, this enhancement was sound for the transition from one to two layers of the steel textiles. The increased thickness of the SRG coupons comprising more layers helped the cords to attain higher axial loads as the chunks of grout providing tension stiffening were larger in volume compared to that for the SRG coupons comprising only one layer of the steel textiles. Also, the increased cross sections in the SRG coupons of multiple

layers required higher energy to propagate cracks throughout the section and hence resulted in increasing the strain of the grout.

- Increasing the density of the steel textiles from 4 to 8 cords/in reduced the axial stress in the cords and the strain of the grout. The dense structure of the steel textiles comprising 8 cords/in impeded the impregnation of the steel cords into the grout and hence created weak surfaces that cracked at earlier stages. The chunks of grout that remained attached to the steel cords were of lower volume compared to that developed by the SRG coupons comprising steel textiles of 4 cords/in. Although these smaller chunks of grout provided a slight improvement to the tensile stress of the cords, this improvement was less than that observed for the case of the S4 steel textiles.

- The evenly distributed micro cracks observed in most of the SRG coupons indicated that there was a good mechanical interlock between the twisted cords and the grout suggesting that both steel textiles can develop a good composite action.

-

- Almost all tested shear bond specimens exhibited a three-stage stress-slip response such that the first branch was stiff and linear corresponding to the elastic behaviour of the composite followed by another branch of reduced stiffness as the cracks initiated and the last branch representing the process of stress transfer mechanism where the effective bond length was shifting towards the end of the composite. This last branch was developed for the SRG composites that had a bond length more than the effective bond length.

- The effective bond length of the SRG strengthening system in shear bond tests was found to lie between a bond length of 200 mm and 300 mm.

- Three modes of failure in shear bond tests were identified including the tensile rupture of cords observed for the SRG composites comprising only one layer of S4 textiles for bond length more than 200 mm, the debonding at the textile-to-matrix interface which occurred for the series that had one and two layers of S8 textiles regardless of the bond length and the compressive strength of the substrate, and finally the debonding at the matrix-to-substrate interface observed for the SRG composites strengthened with two and three layers of S4 textile and three layers of S8 textiles regardless of the bond length and the compressive strength of the substrate. This latter mode was also observed for the SRG composites comprising one layer of S4 textiles for bond length less than 300 mm.

- The bond length influences the bond performance through increasing the areas of contact at both the textile-to-matrix and the matrix-to-substrate interfaces and hence allowed these interfaces to transfer more stresses to the substrate which in turn resulted in increasing the axial stress in the cords and consequently the slip at the loaded end of the SRG composite. This was only pronounced for the SRG composites comprising only one layer of S4 textiles. Increasing the bond length beyond the effective bond length will only contribute to increasing the slip (the

plateau segment of the curve in the last zone of stress-slip curve) while the load will not gain any increase compared to that developed by the SRG composites that have a bond length equal to the effective bond length.

- Increasing the number of textile layers resulted in a decrease in the axial stress in cords and the slip and was significant for the transition from one to two layers. On the other hand, the effect in terms of stress and slip for the transition from two to three layers of textile was less significant suggesting that increasing the number of layers beyond two layers might not be effective.

- Increasing the density of the steel textiles significantly decreased the axial stress and slip in the SRG composites that had one layer of textiles. This effect was less significant for more layers. The use of the denser textiles hindered the full impregnation of grout at the textile-to-matrix interface and created weak regions that triggered the debonding at that interface.

- The compressive strength of the substrate was insignificant in terms of the axial stress and slip. Also, the mode of failure was not affected by the strength of the substrate. This was attributed to the fact that the debonding at the matrix-to-substrate did not involve the substrate and hence it was not governed by the mechanical characteristics if the substrate.

- The utilisation of the SRG reinforcement was considerably higher (31 % on average) for the SRG systems that failed by debonding at the matrix-to-substrate interface than the SRG systems that failed by debonding at the matrix-to-textile interface.

-

- All tested beams exhibited a flexural response characterising three distinct stages including a linear elastic stage up to the formation of cracks followed by semi-linear flexural behaviour that ended by the yielding of the internal reinforcement and finally a stage characterised by a significant drop in stiffness.

- The beams with low amount of external reinforcement developed a less stiff behaviour in the first two stages compared to the rest of the strengthened beams.

- The beams strengthened with identical SRG composites (e.g. B-S8-1-REF and B-S8-1) or SRG composites having the same amount of reinforcement (e.g. B-S4-2 and B-S8-1) developed a comparable load-deflection behaviour.

- Regardless of the strengthening system, all tested beams developed a similar crack pattern. The average crack spacing was 137 mm corresponding to that of the shear reinforcement. The SRG composite also developed small and evenly distrusted transverse cracks which in most cases corresponded to the cracks in the beam.

- The beams strengthened with composites of relatively high stiffness (B-S8-2) resulted in the premature debonding of the SRG, which initiated as end-anchorage debonding and subsequently propagated towards the opposite support in a brittle manner, whereases the use of SRG composites of low stiffness enabled the full mobilisation of the SRG mechanical properties and promoted flexural failures governed by yielding of the internal steel reinforcement followed by rupture of the externally bonded steel fabric.

- Increasing the density of the steel textile, regardless of the number of layers, insignificantly increased the load at yield and at the failure of the SRG. However, the average stain in the internal flexural reinforcement was significantly reduced at the failure of the SRG system. This also holds true when altering the number of layers from 1 to 2 layers regardless of the density of the steel textile.

- The use of two layers of the low-density steel textiles instead of one layer of the denser textile enabled a better impregnation of the grout through the cords and prevented interlaminar shearing and hence let to a full exploitation of the textile.

- The applicability of some of the existing FRP bond models were evaluated for the SRG system. Although some of these models have shown a good prediction of the debonding load, however, they could not capture all the parameters investigated in the experimental programmes.

- The proposed model for predicting the debonding load and mode in shear bond tests was able to capture the behaviour of the SRG system and the debonding load was predicted with a coefficient of variation of only 9 %. Furthermore, the predicated failure mode matched the experimental mode for 29 tests out of 30 tests (97 %).

- The proposed model for shear bond tests was utilised to calculate the failure load in the strengthened RC beams. The proposed procedure for calculating the failure load in the strengthened beams had a coefficient of determination of 99.4 %, while its accuracy in predicting the mode of failure was 93 %.

7.2 Design recommendations and guidelines

7.2.1 The design philosophy

The design philosophy is to use an SRG system that can deliver the target strength increase in the RC beam (after applying the proper safety factor). The designer should also consider utilising the highest possible percentage of the SRG system when strengthening an RC beam. In other words, the SRG system should be designed to fail by the tensile rupture of the steel textiles after the yielding of the internal steel rebars. However, this is not always the case, especially when strengthening RC beams that demand a high upgrading requirement. In such a case, the full utilisation of the external SRG system cannot be achieved as debonding at either the matrix-to-substrate or the matrix-to-textile interfaces is more likely to occur. When the SRG system is prone to failure by debonding, then the

SRG system should be designed to fail by the debonding at the matrix-to-substrate interface. This latter mode of failure can utilise the SRG reinforcement to an extent greater than that observed for the debonding at the matrix-to-textile interface. The following bullet points provide a general guideline to design an SRG system for the strengthening of RC beams:

- The designer can satisfy the upgrading requirements by adjusting two parameters, the first is the density of the steel textile and the second is the number of the layers of the steel textile.
- The designer should first attempt to increase the number of layers to satisfy the strengthening requirements. However, when the target upgrade requires the use of an SRG system that has more than three layers, the designer should consider increasing the density of the steel textiles.
- If increasing the number and density of the steel textile layers cannot satisfy the upgrade requirements, then it is recommended to introduce an anchorage mechanism to the SRG system or to consider using different strengthening schemes other than the SRG system. The details of the anchorage system cannot be provided at this stage as it was out of the scope of this work. Further discussion about the anchorage system is provided in the future work section.

The first step in designing an SRG strengthening system is to obtain the target strength increase in terms of bending moment, M_t. The designer should then choose a trial SRG system (in terms of density of the steel textiles and the number of layers) considering the above guidelines to calculate the moment capacity of the strengthened beam, M_s. If the chosen SRG system cannot develop the target moment, then another SRG system should be considered by altering the parameters (i.e., the density of the textiles and the number of the layers) and iterate until the developed moment, M_s, is equal to the target moment, M_t, or in close proximity. Table 7.1 provides a step-by-step guideline for this process.

7.2.2 Choices of the materials for the SRG systems

The SRG system is a composite of two materials the steel textile and the grout. Different steel textiles are available in the market varying in the structure, the coating, and the strength of cords. The structure of the steel cords can be made be joining straight or twisted filaments. These steel filaments undergo a chemical treatment to inhibit corrosion by coating them by different corrosion inhibitors e.g., brass or zinc. Also, the strength of the steel filaments can be tailored to specific applications. The steel textiles of low tensile strength are usually considered for strengthening low-strength substrates e.g., masonry structures. Although the experimental programmes in this thesis was based on the use of twisted zinc-coated high-strength steel cords, however, the following recommendations can be made:

- The use of steel textiles of twisted filaments is highly recommended. The twisted cords provide a very good mechanical interlocking mechanism with the surrounding matrix. This would in turn mobilise greater portions of the grout in stress transfer mechanism and provide higher strength increase to the overall system. This was evident in the experimental programmes conducted in this thesis and was also reported in literature.
- The coating system only impacts the long-term durability and should not have an impact on the structural behaviour. The designer should choose a steel textile with any coating system as long as it satisfies the durability requirements.
- The findings of this research and the suggested models are intended to be used with RC beams. Concrete substrates are usually of higher compressive strength compared to masonry elements; hence the designer is recommended to choose a high-strength steel textile. Using steel textiles of low strength is usually recommended for the strengthening of masonry elements which is out of the scope of research.

Table 7.1 Design guidelines for the use of the SRG systems for flexural strengthening of RC beams.

			Unit	Symbol	Equation
A.	Get the target capacity of the beam after strengthening		N.mm	M_t	--
B.	Get the geometrical and mechanical properties of the beam				
	B.1	The span of the beam	mm	L	--
	B.2	The height of the cross section	mm	h	--
	B.3	The width of the cross section	mm	b_{sb}	--
	B.4	The concrete cover	mm	c	--
	B.5	The number tensile reinforcement rebars	--	N_s	--
	B.6	The diameter of the tensile reinforcement rebars	mm	$\emptyset_s$	--
	B.7	The number compression reinforcement rebars	--	N'	--
	B.8	The diameter of the compression reinforcement rebars	mm	$\emptyset'$	--
	B.9	The diameter of the shear links	mm	$\emptyset_l$	--
	B.10	The area of the tensile reinforcement	mm^2	A_s	$A_s = \frac{\pi N_s \emptyset_s{}^2}{4}$
	B.11	The area of the compression reinforcement	mm^2	A'_s	$A'_s = \frac{\pi N' \emptyset'^2}{4}$
	B.12	The effective depth of the tensile reinforcement	mm	d	$d = h - (\frac{\emptyset_s}{2} + \emptyset_l + c)$
	B.13	The yield strength of the tensile reinforcement	N/ mm^2	f_y	--
	B.14	The yield strength of the compression reinforcement	N/ mm^2	f'_y	--
	B.15	The compressive strength of the concrete	N/ mm^2	$f_{c,sb}$	--
	B.16	The tensile strength of the concrete	N/ mm^2	$f_{t,sb}$	If not given, use this equation: $f_{t,sb} = 0.30 \cdot f_{c,sb}{}^{2/3}$
C.	Choose an SRG system and get the following parameters				
	C.1	The density of the steel textile	cord/mm	ρ_{tx}	--
	C.2	The width of the SRG composite	mm	b_{com}	Set $b_{com} = b_{sb}$
	C.3	The area of a single cord	mm^2	A_{cord}	--
	C.4	The number of steel textile layers	--	n	--

Table 7.1 (continued)

			Unit	Symbol	Equation
	C.5	The thickness of a single grout layer	mm	t_{layer}	--
	C.6	The Elastic modulus of the steel textile	N/ mm^2	E_{tx}	--
	C.7	The equivalent thickness of the steel textile for 1 layer	mm	$t_{tx,1}$	$t_{tx,1} = \rho_{tx} A_{cord}$
	C.6	The total area of steel textiles	mm^2	A_{tx}	$A_{tx} = n t_{tx,1} b_{com}$
	C.7	The overall thickness of the SRG composite	mm	t_{com}	$t_{com} = t_{layer}(n+1)$
	C.8	The effective depth of the SRG composite	mm	d_f	$d_f = h + \frac{t_{com}}{2}$
D.	Calculate the depth of the neutral axis for the strengthened beam		mm	x	Use Eq. 18 (P160), with $\lambda = 0.80$ and $\eta = 1$
E.	Get the maximum load of the chosen SRG system		N	P_{max}	Use the flowchart in Fig. 6.6 (P158)
F.	Get the internal force acting upon the SRG system in the		N	F_f	Set $F_f = P_{max}$
G.	Calculate moment capacity of the strengthened beam		N.mm	M_s	$M_s = \phi \left[F_f \left(d_f - \frac{\lambda x}{2} \right) + A_s f_y \left(d - \frac{\lambda x}{2} \right) + A'_s f'_y \left(\frac{\lambda x}{2} - d' \right) \right]$ ϕ is a safety factor
H.	If the calculated moment of the strengthened beam is equal to or close enough to the target moment, use the chosen SRG system. Otherwise change the parameters of the SRG composite (C.1-C.5) and repeat calculations until the equation to the right is satisfied.				$M_s \cong M_t$

7.3 Further work

Although this work was conducted to understand the mechanical and bond behaviour of the SRG system and ultimately the flexural performance of the RC beams strengthened with this system, however, this research was governed by the available steel textiles in the market. These textiles are produced in different steel materials and different cord structure and densities. For instance, some steel textiles available in the market are made of stainless steel. Also, these textiles can be made of cords that have straight filaments or twisted ones. Furthermore, the way the filaments are twisted can be different e.g., some cords are made of three straight filaments and two twisted ones (3X2), while other are made of twelve straight filaments and one twisted around (12X1). Also, the density of the steel textiles in the market are ranging from 4-23 cord/in. The experimental programme of this thesis was conducted on galvanised steel textiles that had cord densities of 4 and 8 cord/in with 3X2 cord structure. The proposed models for estimating the failure load in the shear bond and beam tests was calibrated against the experimental programme and available data in the literature. Although the calibration database consisted of SRG systems that had different parameters in terms of cord material and density, however, it did not cover all the SRG systems in the market. For example, the database had only steel textiles with densities 4, 8, and 12 cord/in that were made of 3X2 filaments. In fact, calibrating the proposed models against all the SRG systems available in the market is far too difficult to be accomplished within this research for two considerations: one, the limitations on the experimental programme; and two, the limited data on the use of different SRG systems.

Although the findings of the second experimental programme on the shear bond tests (Chapter 4) indicated that using more than two layers of the SRG system might not effective, however, the effect of adding three layers to the RC beams was not investigated due to a range of constrains including finance, time, and availability of space and technical support. Strengthening RC beams with SRG systems that have more than one layer needs further investigation as it might develop a bond behaviour different to that observed for shear bond tests due to different nature of both setups including the loading mechanism and the bond length which is often longer in beam tests.

Also, the use of anchorage systems for the SRG composite was not fully investigated in this study. In fact, this topic is too huge to be fully addressed within a single work. It largely affects the mode of failure in the strengthened RC beams and consequently the bond and flexural behaviour. Further studies are needed to better understand how introducing an anchorage system can affect the response of the strengthened RC beams.

Having all this said, further work is needed to fully understand how different manufacturing parameters of these systems can influence the bond and flexural behaviour of the strengthened beams in terms of the cords material, density, and filament structure. The proposed models need a further calibration once additional data is available on the different SRG systems available in the market.

Appendix A Mechanical Characterisation of Multi-ply SRG Composites for the Strengthening of Concrete Structures

MECHANICAL CHARACTERIZATION OF MULTI-PLY STEEL REINFORCED GROUT COMPOSITES FOR THE STRENGTHENING OF CONCRETE STRUCTURES

Georgia E. Thermou[1,2], Gianmarco de Felice[3], Stefano De Santis[3], Sultan Alotaibi[1], Francesca Roscini[3], Iman Hajirasouliha[1], Maurizio Guadagnini[1]

[1]The University of Sheffield, Civil and Structural Engineering Department, Sir Frederick Mappin Building Mappin Street, Sheffield, S1 3JD, UK (corresponding author: g.thermou@sheffield.ac.uk); [2]Aristotle University of Thessaloniki, Civil Engineering Department, 54124, Thessaloniki, Greece (on leave); [3]Roma Tre University, Department of Engineering, Via Vito Volterra 62, 00146 Rome, Italy

ABSTRACT

The use of externally bonded Steel-Reinforced Grout (SRG) composites, comprising Ultra High Tensile Strength Steel (UHTSS) textiles embedded in an inorganic mortar matrix, has been shown to provide an effective and cost-efficient solution for the repair and strengthening of existing structures. Although several studies have been carried out in the last decade to investigate the SRG-to-concrete bond behaviour, most of the existing literature examines the use of systems with a single layer of steel textile and only limited information is available on multi-ply SRG composites, which are often required for applications to large structural elements. This paper presents the preliminary results of an experimental study on SRG systems comprising multiple layers of galvanized UHTSS textiles within a geopolymer mortar. The investigation comprises three stages: 1) direct tensile tests on SRG coupons to characterize the tensile properties of the composite system; 2) lap-splice tests (for overlap length ranging from 100 mm to 300 mm) to develop an improved understanding of the textile-to-textile load transfer capacity; 3) single-lap bond tests to examine the effect on bond behaviour of number of steel textile plies (one, two or three) and steel cord density (4 and 8 cord/in) on concrete substrates. Digital Image Correlation (DIC) was used to obtain full-field displacement measurements and map crack development.

KEYWORDS

New composite materials, systems and strengthening techniques; Experimental study; Bond and interfacial stresses; Bond and interfacial stresses; Steel-Reinforced Grout (SRG); Digital Image Correlation (DIC)

INTRODUCTION

With the passing of the years, structures become deficient during or after their working life as a result of seismic events, changes in codes and in use, continuous deterioration caused by ageing and environmental induced degradation (e.g. De Santis et al. 2017b). In those cases that demolition is not an option due to either the prohibited cost or the cultural and historical significance of the structure, retrofitting is the only solution. Depending on the objectives of retrofitting and the level of intervention, global as well as local intervention methods could be selected (e.g. Thermou et al. 2012).

In the past three decades, the use of Fibre Reinforced Polymers (FRPs) has emerged as one of the most popular local strengthening methods. However, FRPs have shown some drawbacks including high cost, poor fire resistance, lack of vapour permeability, toxic nature of epoxy, incompatibility of resins and substrate, and poor reversibility (e.g. Matana et al. 2005; Huang et al. 2005). Since many of these drawbacks are mainly associated with the use of organic matrix as the bonding material, a new generation of composite systems, named either Fabric Reinforced Cementitious Matrix (FRCM) of Textile Reinforced Mortar (TRM) systems, has been developed where inorganic matrix is used instead (e.g. Huang et al. 2005; Papanicolaou et al. 2008; de Felice et al. 2014).

Experimental studies on the bond behaviour of various FRCM systems have identified the complexity entailed in the shear transfer mechanisms. The failure modes observed in the inorganic-based composite systems are related to the bond strength developed between the composite and the substrate (de Felice et al. 2014; Ascione et al. 2015) as well as to the adhesion between the fabric and the matrix (Donnini et al. 2016).

In case of the Steel-Reinforced Grout (SRG) system, studies on bond behaviour have been conducted for both concrete (Matana et al. 2005; Stievanin et al. 2013; Bencardino et al. 2017) and masonry (de Felice et al. 2014; Razavizadeh et al. 2014; De Santis and de Felice 2015; Ascione et al. 2015; De Santis 2017; De Santis et al. 2017b; Bilotta et al. 2017) substrates. Different parameters were considered in these investigations including bond length (e.g. Matana et al. 2005; De Santis 2017), fabric density (e.g. De Santis et al. 2017b; Bilotta et al. 2017), surface preparation (de Felice et al. 2014; Matana et al. 2005), matrix strength (e.g. Ascione et al. 2015), substrate strength (e.g. De Santis and de Felice 2015) and substrate curvature (e.g. De Santis 2017).

As expected, the bond behaviour of SRGs is quite similar to that of the other FRCMs due to the presence of the inorganic matrix. For the SRG system, the failure modes observed are related to debonding at fabric-matrix interface (e.g. Matana et al. 2005), debonding at substrate-matrix interface with or within a thin layer of substrate (cohesive failure in substrate) (e.g. De Santis and de Felice 2015), detachment of the composite from the substrate (e.g. De Santis and de Felice 2015), slippage of fabric out of the matrix (De Santis et al. 2017) and fabric rupture (tensile failure) (e.g. Bilotta et al. 2017). De Santis and de Felice (2015) attributed the debonding at substrate-matrix interface to the high strength of the matrix applied on a relatively weak substrate. Detachment of the composite from the substrate is mainly associated with short bond (anchorage) lengths. Slippage of fabric out of the matrix is attributed in (De Santis et al. 2017b) to the poor interlocking between the grout and the smooth surface of stainless steel cords and ropes.

Some of the above-mentioned studies suggested an effective bond length ranging from 150 to 300 mm (Matana et al. 2005; De Santis et al. 2017b, Bencardino et al. 2017). The suggested effective bond length on concrete substrates was higher than that on masonry substrates. This might be attributed to the variation in terms of mechanical (e.g. strength) and physical (e.g. porosity) properties between masonry and concrete. The fact that failure in SRG system generally occurs at fabric-matrix interface led to the conclusion that high level of surface preparation other than cleaning may not be required (Matana et al. 2005). All the previous studies related to the bond behaviour of SRG systems focused on the study of single-layered SRG systems.

SRG can be used effectively as externally bonded reinforcement for the flexural strengthening of RC beams and multiple layers of fabric may be required, depending on the target level of performance (Napoli and Realfonzo

2015). To date, there is very limited knowledge on the shear transfer mechanism developed along the multiple layers of the steel fabric and the overall mechanical behaviour of multi-ply SRG composites. This study aims to bridge the gap and build a better understanding of the bond behaviour of multi-ply SRG composites applied to concrete substrates. The tensile behaviour of SRG composite is studied to assess the influence of cracking and the contribution of the grout to the overall composite behaviour (i.e. tension stiffening effect). The stress transfer between different layers of fabric is investigated through lap-splice tests. In a future stage of the study, single-lap shear bond tests will be carried out on multi-ply SRG composites comprising one, two, and three layers of steel fabric of two different densities (4 and 8 cords/in).

EXPERIMENTAL PROGRAMME

MATERIALS

The textile utilized in this study is made of unidirectional Ultra-High Tensile Strength Steel (UHTSS) micro-cords, fixed to a fibreglass micromesh to facilitate installation. Each cord has a diameter of 0.9 mm and is obtained by joining 5 filaments, 3 straight and 2 wrapped with a high torque angle to enhance the interlocking with the mortar (Fig. 1a). Cords have a cross sectional area of 0.11 mm^2 and are coated with zinc (galvanized) to provide protection against rusting. Two different fabrics were tested, having density of 4 cords/in (1.57 cords/cm; S4) and 8 cords/in (3.15 cords/cm; S8). In the lower density textile (S4), cords are evenly arranged such that the clear spacing between each two cords is 5.45 mm while cords in the latter (S8) are paired such that the clear spacing between each two pairs is 4.55 mm (Fig. 1b). The design thickness of the textiles is 0.169 mm and 0.084 mm and their surface mass density is 1330 and 670 g/m^2 for S8 and S4 respectively. The UHTSS textiles were embedded in a mineral geo-mortar with a crystalline reaction geo-binder base. The mechanical characteristics of the grout according to the manufacturer's datasheet (evaluated at 28 days) including compressive strength, tensile strength, and adhesion bond strength are 55 MPa, 10 MPa, and 2 MPa respectively. Grout was mixed with water at a water-to-cement ratio of 1:5.

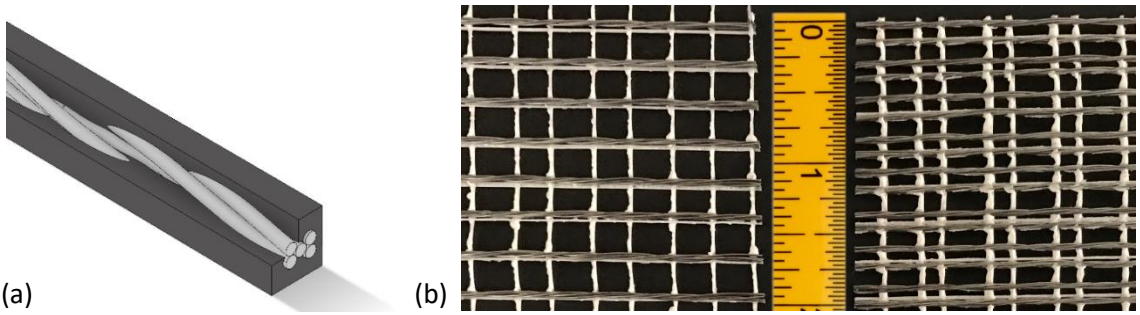

Figure 1. *Schematic representation of a single cord embedded in the grout matrix (a) and photographs of the 4 cords/in (left) and 8 cords/in (right) textiles (b)*

LAP-SPLICE TESTS

DIRECT TENSILE TESTS

Direct tensile tests were carried out on prismatic specimens (coupons) with 600mm total length, 50mm width and 10mm thickness, comprising a textile strip comprising either 8 cords (in the case of S4 textile) or 16 cords (S8). Coupons were manufactured in Perspex moulds, kept wet for the first 48h, then demoulded and placed in water for 26 days and, finally, stored in the laboratory for at least 7 days before testing. Tests were performed with a 500kN

hydraulic universal testing machine under displacement control at 0.01mm/s rate. The specimens were clamped in the wedges of the machine with sufficient gripping pressure to avoid slippage. In order to ensure a proper load transfer and avoid the crushing of the mortar matrix in the gripping areas, the ends of the specimens were wrapped with glass fibre reinforced polymer (GFRP) (De Santis et al. 2017a). The load was recorded by an integrated load cell. Stress (f) was derived by dividing the load by the cross sectional area of the steel textile, equal to 4.27mm^2 for S4 and to 8.54mm^2 for S8. Displacements were recorded by two linear potentiometers and the strain (ε) was derived as the mean of the displacements recorded by the transducers divided by their gage length (200mm). Digital image correlation (DIC) was also used and images were taken at 5s intervals during test execution with a digital camera mounted on a stiff frame at a distance of 1.1m from the specimen ensuring the parallelism between the surface of the specimen and the sensor. All images were post-processed to derive the displacement field on the whole surface of the coupon. Two points were selected, one in the upper portion and one in the lower portion of the coupon, each of which was in the middle between two cracks, and the strain was calculated as their relative displacement divided by the initial distance (Tekieli et al. 2017). Eight specimens with S4 and eight with S8 were tested. The stress-strain response curves, plotted in Figure 1, exhibit a first linear stage in which the mortar is uncracked, a second stage in which the crack pattern progressively develops, and, finally, a third stage, in which no new cracks appear and failure is attained by the nearly-simultaneous rupture of the steel cords. Such a three-stage behaviour has already been observed on similar SRG composites comprising high-strength cement or geopolymer mortars (De Santis et al. 2017b). The mean values of peak stress (f_t), corresponding strain (ε_t), and tensile modulus of elasticity in the uncracked stage (E_I) and in the cracked stage (E_t) are summarised in Table 1, along with the corresponding coefficient of variation (in round brackets).

***Table 2**. Results of direct tensile tests and lap-splice tests: mean values (coefficients of variation in round brackets)*

Textile	L' [mm]	Series	f_t [N/mm^2]	ε_t [%]	E_I [kN/mm^2]	E_t [kN/mm^2]	s_p [mm]
S4	0 [(a)]	S4-000	3062.1 (1.7%)	2.06 (4.3%)	1713.2 (5.5%)	177.9	–
	100	S4-100	2394.0 (12.2%)	–	–	–	1.14
	200	S4-200	2769.9 (5.2%)	–	–	–	2.05
	300	S4-300	2795.5 (3.8%) [(b)]	–	–	–	2.39
S8	0 [(a)]	S8-000	3014.7 (2.5%)	2.29 (6.4%)	1688.1	172.9	–
	100	S8-100	988.8 (12.2%)	–	–	–	0.41
	200	S8-200	1193.0 (5.3%)	–	–	–	1.02
	300	S8-300	1139.6 (5.4%)	–	–	–	1.33

[(a)] Direct tensile tests (no overlap); [(b)]One specimen failed by tensile rupture of the steel cords.

LAP-SPLICE TESTS

Lap-splice tests were carried out to investigate the textile-to-textile load transfer capacity, which is a key transfer mechanism in multi-ply externally bonded SRG reinforcements and can be limited by the development of interlaminar shear failure between textile layers. Since no attempts of running lap-splice tests on SRG composites have been made so far, the ASTM standard D7616 (ASTM 2017) developed for FRPs was followed. The specimens were similar to those subjected to direct tensile tests. They had 600mm total length, 50mm width and 12mm thickness, were manufactured in the same moulds and underwent the same curing process. In this case, however, the textile strip was not continuous. Two layers were placed on one side, 6mm spaced, and one layer was placed, on the other side, in the middle between them, with an overlap length (L') of 100mm, 200mm or 300mm (Figure 2). The spacing between the plies at the overlap was 3mm. The symmetry with respect to the thickness prevented the occurrence of parasitic bending moments caused by eccentricities during test execution. During manufacturing, particular care was paid to ensure that the textile strips were aligned, that their spacing was constant, and that an adequate amount of mortar passed through the voids between the cords. The ends of the coupons were wrapped

with GFRP and tests were performed with the same protocol of direct tensile tests. Five specimens nominally identical were manufactured and tested for each value of L', for a total of 15 specimens for S4 and 15 for S8.

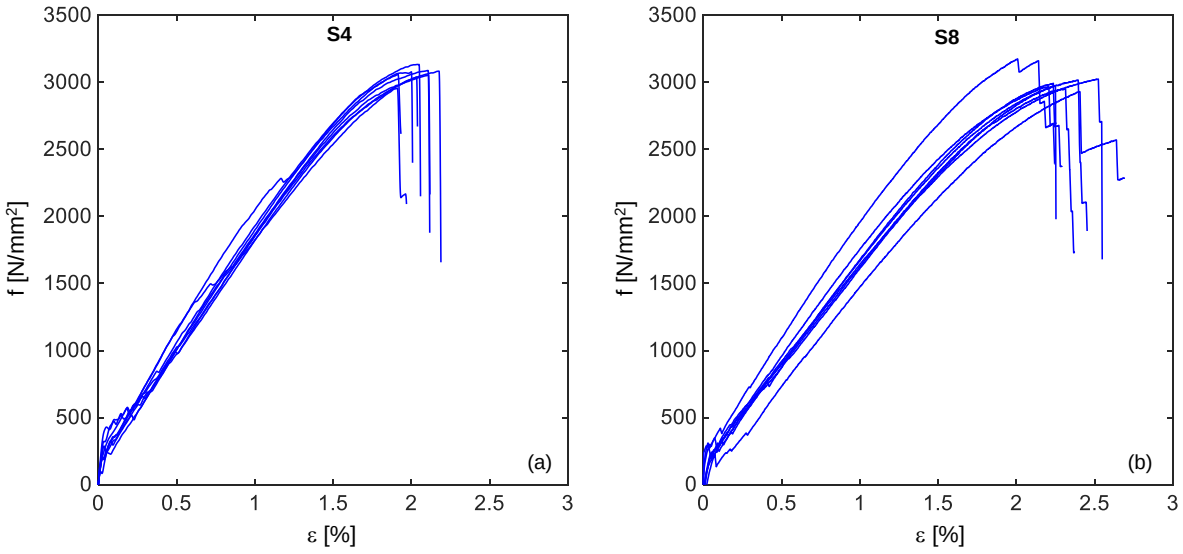

Figure 2. *Stress-strain response curves of direct tensile tests on SRG coupons comprising S4 (a) and S8 (b) textiles*

In the initial phase of the test, the specimens were uncracked. Then, a first (main) transversal crack formed at the end of the overlap, on the side of the single textile layer. From this moment on, the width of this crack increased with the increase of the applied load and other cracks progressively appeared on the portion of the coupon comprising one ply of textile (Figure 3a), whereas the surface of the other portion remained uncracked. A longitudinal crack also appeared, and progressively extended, in the thickness of the coupon along the overlap (Figure 3b). In all specimens, failure occurred by the relative sliding of the textile layers, with the only exception of specimen with S4 textile and 300mm overlap length, in which the cords fractured. Figure 4 shows the stress-slip response curves, the stress (f) being referred to one ply of textile and the slip (s) being the relative displacement between the two portions of coupon separated by the main crack. The slip was measured with DIC using two points that were selected after the end of the test, on the two sides of the main crack. It is worth noting that this would have been unfeasible with conventional measurement devices (displacement transducers) since the crack pattern was unknown a priori. At the attainment of the peak stress, a brittle failure occurred with the shortest overlap length (L'=100mm), whereas a stress quasi-stabilization was observed with L'=200mm and L'=300mm, indicating that the effective transfer length was exceeded. In this case, the increase of slip was associated with the portion of overlap involved in the load transfer process progressively shifting away from the main crack. The values of peak stress (f_t) attained in lap-splice tests are shown in Figure 5 together with those of direct tensile tests, and are also listed in Table 1 together with the ultimate slip (s_u). With S4 textile, the maximum stress resulted similar to the tensile strength with L'=200mm and L'=300mm, suggesting that the effective transfer length is comprised between 100mm and 200mm. It should be considered that the peak stress in lap-splice tests might be expected to be lower than that of direct tensile tests (in this case, by 9% on average) due to unavoidable misalignments and to the different clamping conditions of the textile on one side (at the overlap), which may cause uneven stress distribution amongst the cords. Much lower stress (on average 37-39% of the tensile strength) was attained in lap-splice tests with S8, due to its higher density, which resulted in a lower amount of mortar matrix passing through the cords.

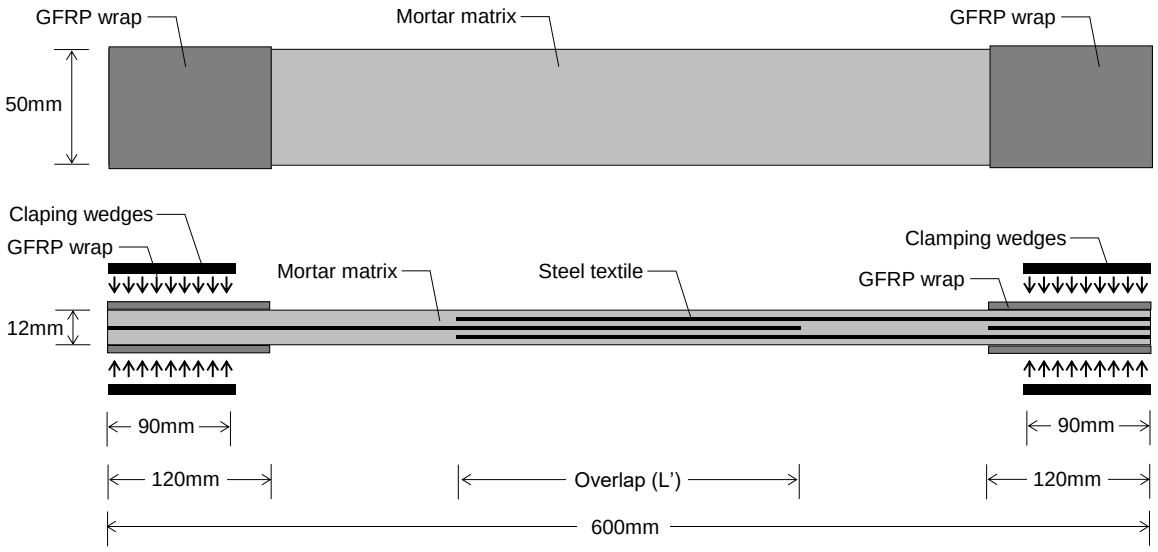

Figure 3. *Top and side view of SRG specimens manufactured for lap-splice tests*

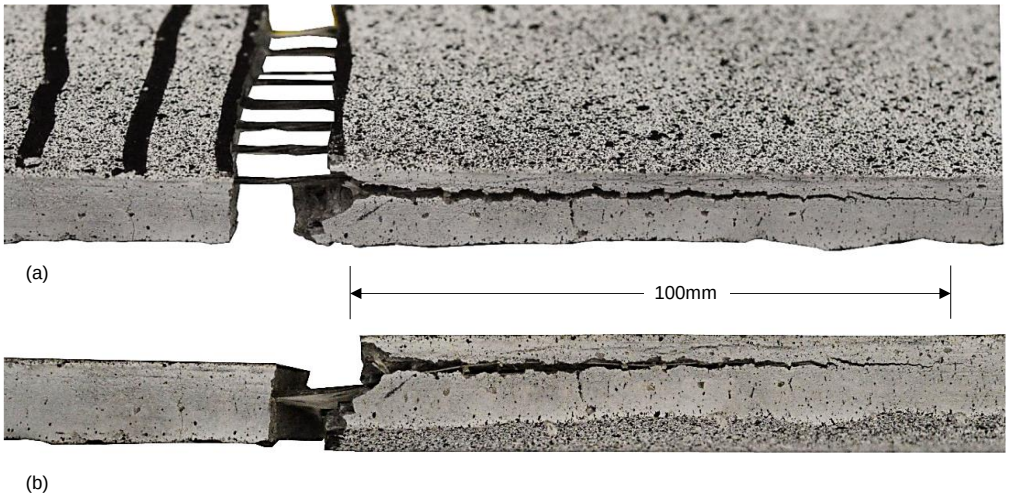

Figure 4. *Typical crack pattern observed in lap-splice tests (S4-100-02 specimen)*

BOND SHEAR TESTS

SPECIMENS DETAILS AND PREPARATION

A set of 24 unreinforced concrete prisms were cast for the single-lap shear bond tests. The typical concrete prism has a square cross section of 150 mm and a length of 500 mm. The compressive strength($f_{cm,cube}$)of the concrete prisms used for the single-lap shear bond tests was evaluated by testing six cubes at 28 days and the average value was 27.2 MPa. The concrete substrate was ground to remove the smooth layer and to expose the aggregates (Figure 6a). After the concrete surface was cleaned from the dust, it was saturated with water. Then, the first layer of grout was applied over a length of 300 mm and a width of 100 mm. The SRG composite was terminated 50 mm to the edge of concrete block (the loaded end) to avoid edge-effects. The thickness of the grout layer was kept to approximately 3 mm by using specially designed moulds (Figure 6b). The steel fabric was then placed and gently pressed to ensure good impregnation with grout. Another layer of grout having the same thickness (3 mm) was then

applied. This process was repeated for multiple layers. In case of two and three layers, attention was paid to ensure a good alignment between fabric layers. Moulds were removed two days after casting. Then, the specimens were carefully moved and kept in laboratory conditions for at least 28 days. At the far end of the dry steel fabric (gripping area), the steel cords were encapsulated in a two-component epoxy and sandwiched between aluminium plates. For multiple layers, the spacing between different layers of fabric was kept to 3 mm by using similar aluminium plates.

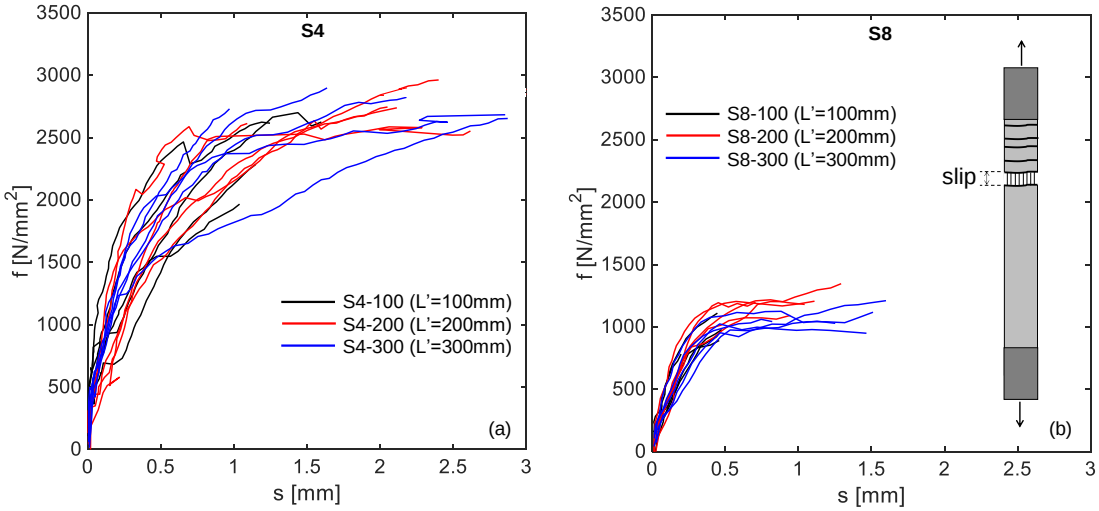

Figure 5. *Stress-slip response curves of lap-splice tests on SRG specimens comprising S4 (a) and S8 (b) textiles*

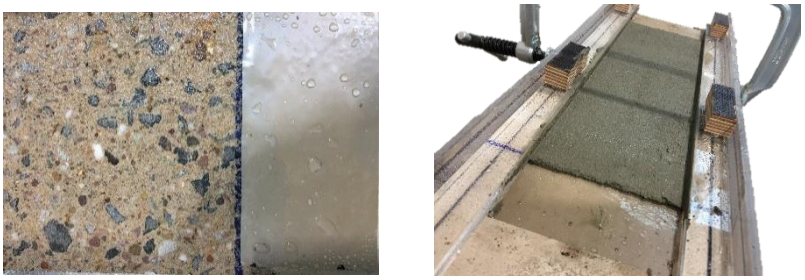

Figure 6. *Substrate after preparation (a) and mortar layer and mould used to control the thickness of the SRG (b)*

TEST SETUP

The direct single-lap shear bond test setup will be adopted in this phase of testing (Fig. 7). The potential misalignment between the actuator and the SRG composite will be mitigated by: 1) adjusting the position of the specimen within the reaction frame by means of a levelling plate, three levelling bolts and one stabilizer bolt; 2) selecting a free length of the dry fabric that is long enough (400mm) to limit the effect of its inclination. DIC will be used to measure the strain in the composite and gain detail insights into slip, cracking pattern and strain distribution.

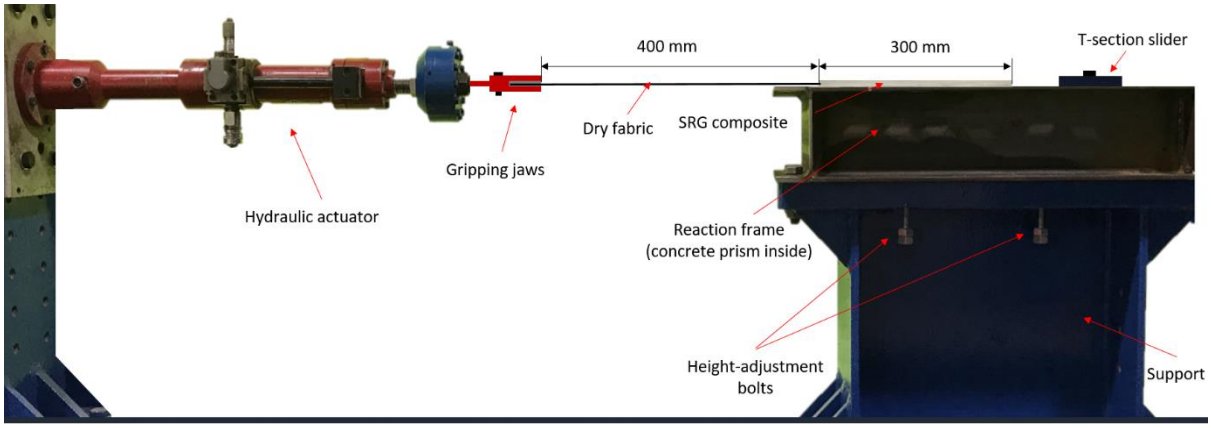

Figure 7. *Experimental setup for direct single-lap shear bond tests*

CONCLUSIONS

This paper presented some preliminary results of an experimental study on SRG systems comprising multiple layers of galvanized UHTSS textiles within a geopolymer mortar. The mechanical properties of the SRG system such as the mean values of peak stress and strain, and tensile modulus of elasticity in the uncracked and in the cracked stage were defined by direct tensile tests. Lap-splice tests were carried out and conclusions were drawn about the textile-to-textile load transfer capacity. It was observed that rupture of the steel cords occurred only in the specimens with S4 textile and 300mm overlap length. In all other cases failure occurred by relative sliding of the textile layers. In the case of S4 textile specimens, the effective transfer length was found to be between 100mm and 200mm. The shortest overlap length (L'=100mm) led to brittle failure at the attainment of the peak stress, whereas for the higher overlap lengths examined (L'=200mm and L'=300mm) a quasi-stabilization was observed. This implies that the increase of slip was associated with the portion of overlap involved in the load transfer process progressively shifting away from the main crack. A third phase of testing is currently underway to examine the effect on SRG-to-concrete bond behaviour of a number of steel textile plies and steel cord density.

ACKNOWLEDGMENTS

Kerakoll S.p.A. is kindly acknowledged for providing the materials. The first author wishes to acknowledge the financial support provided by the European Union's Horizon 2020 research and innovation programme under the Marie Skłodowska-Curie grant agreement No 700863. G. de Felice, S. De Santis and F. Roscini acknowledge the Italian Ministry for Foreign Affairs for cofounding this study within the Research Projects "Composites with inorganic matrix for sustainable strengthening of architectural heritage" Affairs (Year 2017, Grant N. PGR00234).

REFERENCES

A. Bilotta, F. Ceroni, E. Nigro, M. Pecce (2017). "Experimental tests on FRCM strengthening systems for tuff masonry elements", Construction and Building Materials, 138, 114-133

A. Razavizadeh, B. Ghiassi, D. V. Oliveira (2014). "Bond behaviour of SRG-strengthened masonry units: Testing and numerical modelling", Construction and Building Materials, 64, 387-397

ASTM (2017). "Standard Test Method for Determining Apparent Overlap Splice Shear Strength Properties of Wet Lay-Up Fiber-Reinforced Polymer Matrix Composites Used for Strengthening Civil Structures", D7616M - 11

E. Stievanin, F. Da Porto, M. Panizza, E. Garbin, C. Modena (2013). "Bond characterization between historical concrete substrate and SRG/SRP strengthening systems", Proceedings of 5th Int. Conference on Structural Engineering, Mechanics and ComputationSEMC2013, Cape Town, South Africa

F. Bencardino, A. Condello, A. F. Ashour (2017). "Single-lap shear bond tests on Steel Reinforced Geopolymeric Matrix-concrete joints", Composites Part B: Engineering, 110, 62-71

G.E. Thermou, S.J. Pantazopoulou, A.S. Elnashai (2012). "Global interventions for seismic upgrading of substandard RC buildings", Journal of Structural Engineering, ASCE, 138(3), 387-401.

G. de Felice, S. De Santis, L. Garmendia, B. Ghiassi, P. Larrinaga, P.B. Lourenço, D.V. Oliveira, F. Paolacci, C.G., Papanicolaou (2014) "Mortar-based systems for externally bonded strengthening of masonry. Materials and Structures", 47(12), 2021-2037.

J. Donnini, V. Corinaldesi, A. Nanni (2016). "Mechanical properties of FRCM using carbon fabrics with different coating treatments", Composites Part B: Engineering, 88, 220-228

L. Ascione, G. de Felice, S. De Santis (2015). "A qualification method for externally bonded Fibre Reinforced Cementitious Matrix(FRCM) strengthening systems", Composites Part B: Engineering, 78, 497-506

M. Matana, A. Nanni, L.R. Dharani, P. Silva, G. Tunis (2005). "Bond Performance of steel reinforced polymer and steel reinforced grout", Proceedings Int. Symp. On bond behaviour of FRP in structures (BBFS), Hong Kong, China

M. Tekieli, S. De Santis, G. de Felice, A. Kwiecień, F. Roscini (2017). "Application of Digital Image Correlation to composite reinforcements testing", Composite Structures, 160, 670-688.

S. De Santis (2017). "Bond behaviour of Steel Reinforced Grout for the extrados strengthening of masonry vaults", Construction and Building Materials, 150, 367-382

S. De Santis, F. Carozzi, G. de Felice, C. Poggi (2017a). "Test methods for Textile Reinforced Mortar systems", Composites Part B: Engineering, 127, 121-132.

S. De Santis, F. Ceroni, G. de Felice, M. Fagone, B. Ghiassi, A. Kwiecień, G. Lignola, M. Morganti, M. Santandrea, M. Valluzzi, A. Viskovic (2017b). "Round Robin Test on tensile and bond behaviour of Steel Reinforced Grout systems", Composites Part B: Engineering, 127, 100-120

S. De Santis, G. de Felice (2015). "Steel reinforced grout systems for the strengthening of masonry structures", Composite Structures, 134, 533-548

X. Huang, V. Birman, A. Nanni, G. Tunis (2005). "Properties and potential for application of steel reinforced polymer and steel reinforced grout composites", Composites Part B Engineering, 36 (1), 73-82

C.G. Papanicolaou, T.C. Trinantafillou, M. Papathanasiou, K. Karlos (2008). "Textile reinforced mortar (TRM) versus FRP as strengthening material of URM walls: out- of- plane cyclic loading", *Materials and Structures*, 41, 1, 143-157.

A. Napoli, R. Realfonzo (2015) "Reinforced concrete beams strengthened with SRP/SRG systems: Experimental investigation" Construction and Building Materials, 93, 654-677.

Appendix B Tensile Behaviour of Multi-ply SRG composites

COMPDYN 2019
7th ECCOMAS Thematic Conference on
Computational Methods in Structural Dynamics and Earthquake Engineering
M. Papadrakakis, M. Fragiadakis (eds.)
Crete, Greece, 24–26 June 2019

TENSILE BEHAVIOUR OF MULTI-PLY STEEL- REINFORCED GROUT (SRG) COMPOSITES

Sultan S. Alotaibi[1,2], **Georgia E. Thermou**[3], **Iman Hajirasouliha**[4], **Maurizio Guadagnini**[4]

[1] PhD student, The University of Sheffield, Civil and Structural Engineering Department, Sir Frederick Mappin Building Mappin Street, Sheffield, S1 3JD, UK

[2]Shaqra University, Civil Engineering Department, 17441, Al Duwadimi, Saudi Arabia;

ssalotaibi1@sheffield.ac.uk

[3] Assistant Professor, University of Nottingham, Civil Engineering Department, B76 Coates Building, Nottingham, NG7 2RD, UK

[4] Senior lecturer, The University of Sheffield, Civil and Structural Engineering Department, Sir Frederick Mappin Building Mappin Street, Sheffield, S1 3JD, UK

ABSTRACT

Steel Reinforced Grout (SRG) composites consist of Ultra High Tensile Strength Steel (UHTSS) fabrics embedded in an inorganic mortar matrix. The use of SRG for the repair and retrofitting of deficient structures has emerged as a novel technique in the last few years. This paper discusses the results of a comprehensive experimental study on the tensile behaviour of multi-ply SRG composites. A total of 24 direct tensile tests were conducted on SRG coupons to assess the influence of the fabric's layout and architecture on cracking and overall tensile behaviour. Two main parameters were investigated, including the number of fabric layers (1, 2, and 3 layers) and the density of the steel fabric (4 and 8 cords/in). It was found that, although the grout contribution is significant up until failure regardless of the number of layers, the ultimate strength of the composite is generally governed by the ultimate strength of the fabric. The large amount of densely distributed cracks that developed throughout the length of the coupons suggests that a good bond could develop between the fabric and the grout, possibly as a result of the geometry of the twisted cords and the development of good mechanical interlock.

KEYWORDS: Composite Materials; Steel-Reinforced Grout (SRG); Bond Behaviour; Seismic Retrofitting; Tensile Tests; Digital Image Correlation (DIC)

INTRODUCTION

Different strengthening systems have been used for repair and strengthening of existing structures. Externally bonded reinforcement (EBR) system is one of the most widely used techniques as it provides significant improvement to the structural member in terms of strength, mass and stiffness. Among EBR systems are Fibre Reinforced Polymers (FRPs) which consist of textiles impregnated in epoxy-based composites. This latter system, however, was reported to have some disadvantages associated with fire performance and durability. To address these issues, an inorganic-based system has been proposed which is a composite made of textiles embedded in an inorganic matrix. This innovative system has shown many promising advantages including better material compatibility and vapour permeability, better performances at high temperatures, and lower cost and time of installation [1].

Different acronyms are used to describe this system including Textile Reinforced Mortar (TRM), Fibre Reinforced Cementitious Matrices (FRCM), and Steel Reinforced Grout (SRG). This latter acronym is exclusive for inorganic-based composites with only steel textiles while FRCM and TRM include steel or other textiles e.g. carbon. A considerable amount of literature has been published on organic-based composites (i.e. FRP) contrary to inorganic-based systems (e.g. SRG) due to the novelty of SRG system. Debonding is a common failure mode in SRG composites when used as EBR for flexural members. This establishes the fact that understanding tensile behaviour for such systems is fundamental.

For large structural members, one layer of reinforcement might not be sufficient to achieve the desired flexural capacity and hence more than one layer should be considered. This paper investigates the tensile behaviour of multiple layers of two different textiles. Twenty-four direct tensile tests have been conducted on SRG coupons. Two parameters were considered including the number of steel reinforcement layer (one, two, and three layers) and the density of cords within a textile (four and eight cords/in).

Few studies were devoted to understanding tensile behaviour of SRG composite. Different parameters were considered including textile density [1, 2, 4-8], ageing [2], and matrix type [3-5]. It seems that the tensile behaviour of SRG system strengthened with multi-ply steel has not yet been investigated which is often required for strengthening large structural members.

EXPERIMENTAL PROGRAMME

A total of twenty-four coupons of SRG composite were manufactured (four identical coupons for each parameter of study). Coupons were cast in a mould made of acrylic glass. Each coupon was cast individually i.e. not cut out of a wider sheet of composite. Each coupon measures 600 mm x 50 mm. The thickness of each coupon is 6, 9, and 12 mm for coupons of one, two, and three layers of steel textile respectively [Figure 1a].

Two steel textiles were used in this experiment with the same mechanical properties but varying in cords density including 4 and 8 cords/in. The textile is made of unidirectional ultra-high strength galvanized steel cords fixed to a non-structural fibre-glass mesh. Each cord is made of three straight filaments and two twisted along the other three. Each cord has an area of 0.538 mm^2 and a tensile breaking load of more than 1500 N. The equivalent thickness of the textile is approximately 0.084 mm and 0.169 mm for textiles of 4 and 8 cord/in respectively. The mechanical properties (found in the manufacturer's data sheet) for both textiles, including tensile strength, elastic modulus, and strain at failure are 2800 MPa, 190 GPa, and 1.5%, respectively. The matrix is a polymer-modified cement mortar reinforced with microfibers to enhance hydration and mitigate shrinkage [1]. The mortar was mixed using a water-to-cement ratio of 1/5.

Each coupon was cast by applying a first layer of grout with a thickness of approximately 3 mm. Immediately after applying the first layer, the steel textile was placed on top and gently pressed to ensure a good impregnation

with the grout. An additional layer of grout was applied with the same thickness as the first layer. This process was repeated for coupons with two and three layers of steel textiles. Coupons were left to cure in a mist room for the first 28 days and were then placed in a laboratory condition until the day of testing.

The coupon specimens are given the notation DT-DX-LY-Z, where DT indicates direct tensile tests, DX indicates textile density including 4 cord/in (X=4) and 8 cord/in (X=8), LY indicates number of layers of steel textile including one layer (Y=1), two layers (Y=2), and three layers (Y=3), and finally Z is to differentiate between identical samples. Four identical coupons for each series were fabricated and tested, i.e. Z=1, 2, 3, and 4.

Coupons were tested in a universal testing machine at a loading rate of 0.01 mm/s. Tensile load was applied to the coupon by clamping both ends in between the jaws of the machine. To prevent local damage, the ends of the coupon were impregnated in a two-part epoxy and sandwiched between two aluminium plates measuring 100mm x 50mm.

The load was acquired from the load cell of the testing machine while average and local strain was derived by means of extensometers and Digital Image Correlation (DIC). The extensometer was placed on one side of the specimen to measure the relative displacement between two rods attached to the two ends of the composite [Figure 1a]. DIC speckles were painted on the front face of the coupon and images were captured during the test at 5 seconds intervals. A light source was pointed towards the front face of the coupon to achieve the right contrast. It should be noted, however, that the data acquired from DIC system is not presented in this paper. An image of the general setup is shown in Figure 1b.

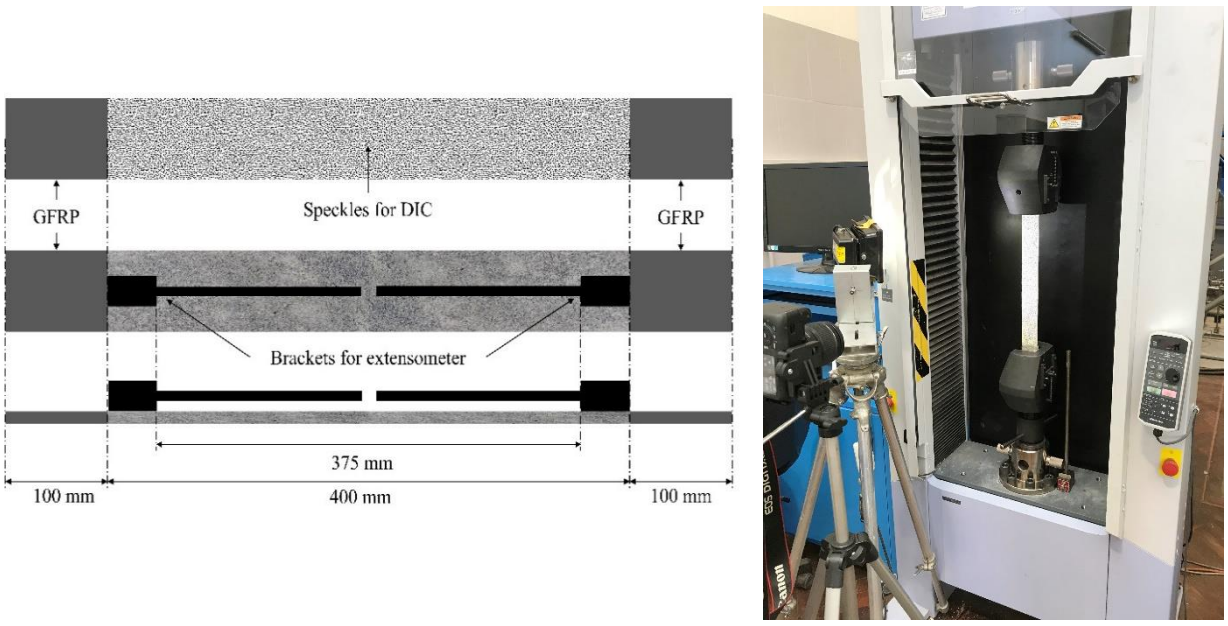

(a) (b)

Figure 1. *(a) Geometry and instrumentation of coupon (b) Test setup*

RESULTS AND DISCUSSION

The results of direct tensile tests are given in Table 1. Maximum stress, strain at maximum stress, and modulus of elasticity for Zone 3 (see below) are given in the table. The maximum stress was calculated by dividing the maximum load by the cross-sectional area of the steel cords. This latter was calculated by multiplying the cross-sectional area of one cord by the total number of cords for each series. The stress-strain envelops and average curves for all series are presented in Figure 2.

Table 1. *Direct tensile test results*

Series	Specimen	F_{max} (kN)	σ_{max} (MPa)	ε_{max} (%)	E (GPa)
DT-D4-L1	DT-D4-L1-1	11.42	3032.4	N/A	N/A
	DT-D4-L1-2	8.83	2344.67	N/A	N/A
	DT-D4-L1-3	9.38	2490.71	1.53	171
	DT-D4-L1-4	11.11	2950.08	1.87	147
	Average	**10.19**	**2704.47**	**1.7**	**159**
	CV (%)	**12.5**	**12.51**	**14.15**	**11**
DT-D4-L2	DT-D4-L2-1	20.17	2677.91	1.7	146
	DT-D4-L2-2	21.43	2845.2	1.87	155
	DT-D4-L2-3	22.67	3009.83	2.03	142
	DT-D4-L2-4	20.06	2663.31	1.6	Undetectable
	Average	**21.09**	**2799.07**	**1.8**	**148**
	CV (%)	**5.82**	**5.83**	**10.54**	**5**
DT-D4-L3	DT-D4-L3-1	31.52	2789.88	1.78	153
	DT-D4-L3-2	32.58	2883.7	N/A	157
	DT-D4-L3-3	31.63	2799.62	1.71	159
	DT-D4-L3-4	41.95	3713.05	1.77	Undetectable
	Average	**34.42**	**3046.57**	**1.76**	**157**
	CV (%)	**14.65**	**14.65**	**2.16**	**2**
DT-D8-L1	DT-D8-L1-1	22.21	2752.17	1.89	134
	DT-D8-L1-2	14.84	1838.91	N/A	Undetectable
	DT-D8-L1-3	19.83	2457.25	1.58	156
	DT-D8-L1-4	18.61	2306.08	1.36	Undetectable
	Average	**18.88**	**2338.61**	**1.61**	**145**
	CV (%)	**16.3**	**16.3**	**16.54**	**11**
DT-D8-L2	DT-D8-L2-1	43.58	2700.13	1.88	144
	DT-D8-L2-2	42.1	2608.43	N/A	Undetectable
	DT-D8-L2-3	41.43	2566.92	1.79	141
	DT-D8-L2-4	43.02	2665.43	1.81	140
	Average	**42.54**	**2635.23**	**1.83**	**142**
	CV (%)	**2.25**	**2.25**	**2.59**	**2**
DT-D8-L3	DT-D8-L3-1	64.95	2682.78	1.78	152
	DT-D8-L3-2	67.81	2800.91	2.08	138
	DT-D8-L3-3	63.97	2642.3	1.77	149
	DT-D8-L3-4	64.83	2677.82	2.19	Undetectable
	Average	**65.39**	**2700.96**	**1.96**	**142**
	CV (%)	**2.56**	**2.56**	**10.86**	**6**

Almost all specimens showed three distinct zones behaviour. Un-cracked specimen (Zone 1), cracks initiation and propagation (Zone 2) and finally crack widening (Zone 3). In Zone 1 the contribution of grout is dominant, while Zone 2 can be seen as a transition zone in which the stress is progressively transferred to the steel cords. In Zone 3, load is mostly resisted by the steel cords yet the grout is still contributing through tension stiffening between cracked sections. A similar three-zone behaviour is reported in [e.g. 3 and 8].

In terms of maximum stress, an ascending trend can be identified. Increasing the number of textile layers seems to slightly increase the stress that can be developed in the steel textile. An increase of approximately 3.5 % and 12.6% was observed for series DT-D4-L2 (2 layers) and DT-D4-L3 (3 layers), respectively, when compared to DT-D4-L1 (1 layer). On the other hand, coupons with two and three layers of medium-density textile are characterised by an increase, in ultimate stress of 12.7% and 15.5%, respectively, compared to the one-layer counterpart. A similar trend was also observed for strain, although at a lower rate.

Stress-strain diagrams clearly show that, regardless of the number of layers, the grout contribution is significant up until failure and the ultimate strength of the composite is generally governed by the ultimate strength of the textile.

The formation of large amount of evenly distributed micro cracks suggests good composite action between the steel cords and the polymer-modified matrix. This indeed indicates that good bond was developed between the fabric and the grout, largely as a result of the geometry of the twisted cords and the development of good mechanical interlock. The cracks were barely noticeable by naked eyes and could only be detected after image processing in DIC software. However, some coupons had a noticeable single crack at either top, bottom, or both ends as a result of local stresses at the clamping area [e.g., Figure 3a, 3b]. No crushing was noticed at ends thanks to the GFRP wrapping at the edges. Slippage of cords within the grout was not observed.

All tested specimens failed explosively expelling debris of grout fragments [e.g., Figure 3e], with larger amounts of energy being released for multiple layers of the denser steel textile. A quasi-simultaneous rupture of cords was observed for almost all coupons either at middle or at one end [e.g., Figure 3d, 3f]. However, early rupture of cords was observed for few coupons at a load of approximately 0.85 F_{max}. This can be as a result of unavoidable misalignment of the steel cords or layers during the manufacturing process.

CONCLUSION

The aim of the present study was to examine the tensile behaviour of multi-ply steel-reinforced grout composites. Two parameters were investigated including steel textile density (4 and 8 cord/in) and number of textile layers (1, 2, and 3). A total of 24 direct tensile tests were conducted on SRG coupons. A tensile behaviour characterised by three distinct zones was observed for almost all specimens, with the first zone being governed by the grout, the second zone corresponding to the stress being transferred to the steel cords, and finally the last zone where the steel is governing. Although the grout contribution is significant up until failure regardless of the number of layers, the ultimate strength of the composite is generally governed by the ultimate strength of the fabric. The large amount of densely distributed cracks that developed throughout the length of the coupons suggests that a good bond develops between the textile and the grout, largely as a result of the geometry of the twisted cords and the development of good mechanical interlock. It was also found that increasing the number of textile layers slightly increase the stress in the reinforcement. The coupons failed by either rupture of the cords at one end or at the middle; in both cases, however, it was nearly simultaneous and explosive.

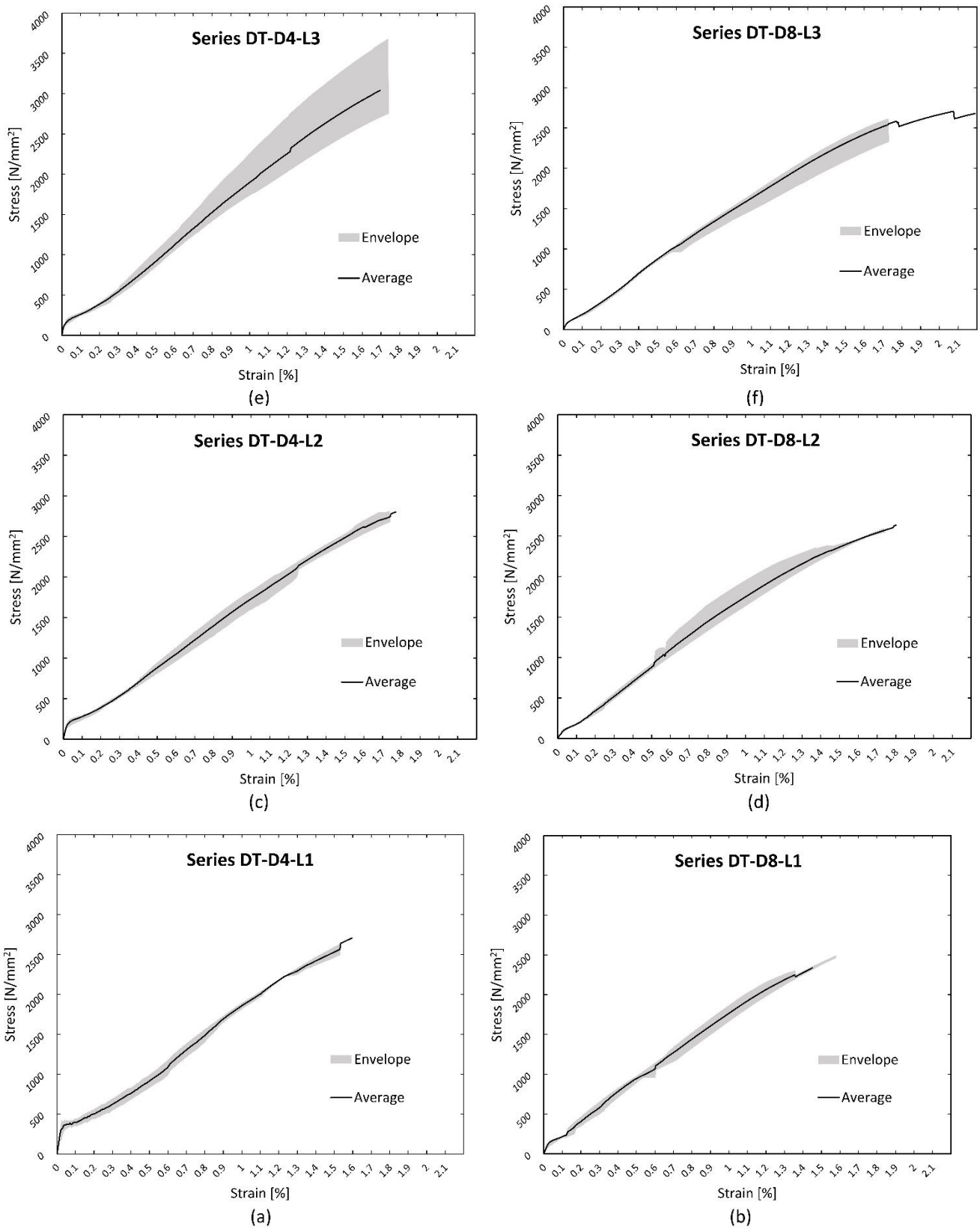

Figure 2. *Envelope stress-strain and average curves for (a) Series DT-D4-L1, (b) Series DT-D8-L1, (c) Series DT-D4-L2, (d) DT-D8-L2, (e) Series DT-D4-L3 Series, and (f) Series DT-D8-L3*

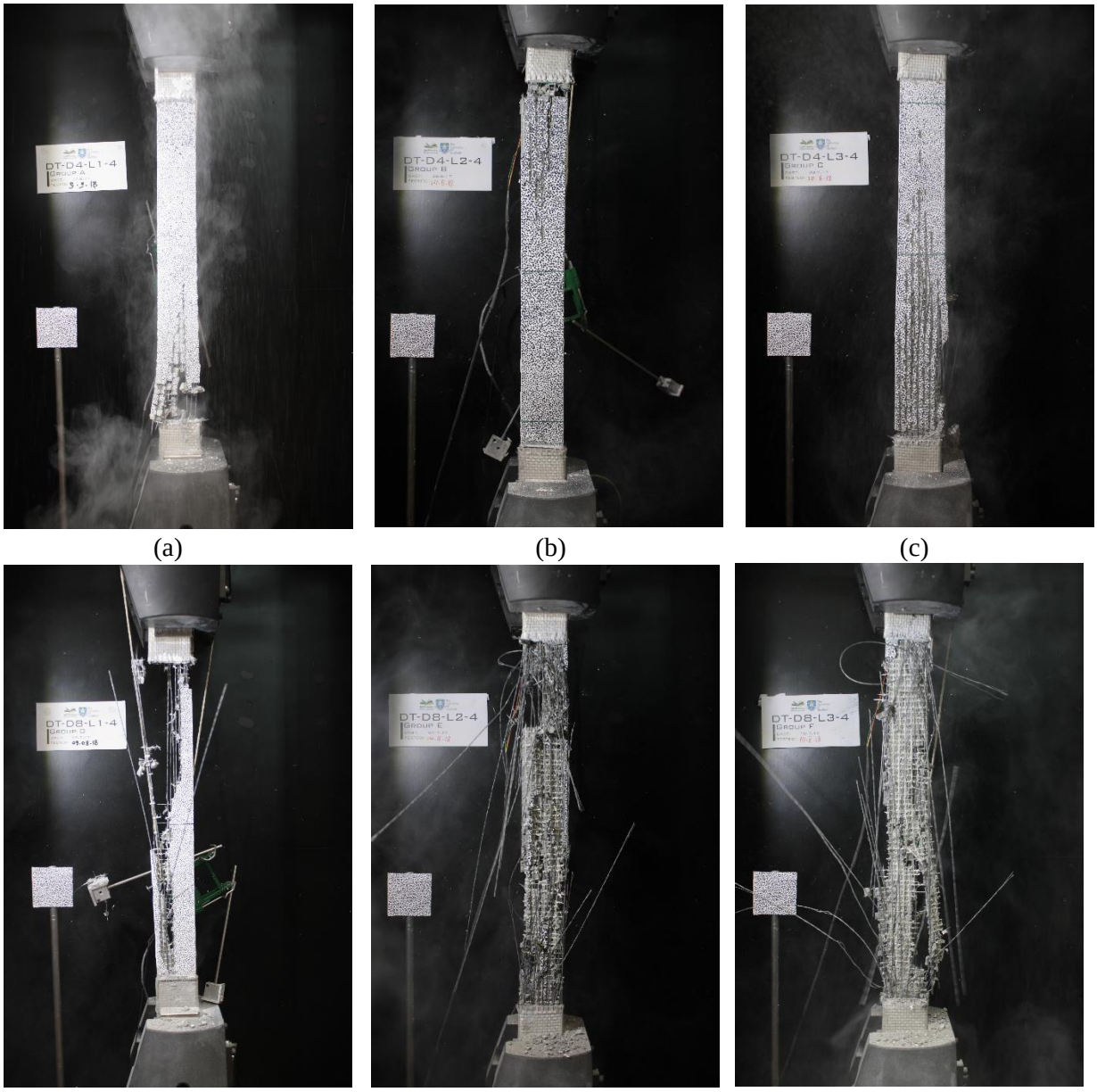

(a) (b) (c)

(d) (e) (f)

Figure 3. *Failure mode of different specimens from (a) Series DT-D4-L1, (b) Series DT-D4-L2, (c) Series DT-D4-L3, (d) Series DT-D8-L1, (e) Series DT-D8-L2, and (f) Series DT-D8-L3*

ACKNOWLEDGEMENT

The materials (steel textiles and cement) for this experiment were provided by Kerakoll S.p.A.. The first author would like to thank the Saudi Arabian Cultural Bureau (UK) and Shaqra University (Saudi Arabia) for sponsoring his PhD research.

REFERENCES

[1] S. De Santis and G. de Felice, Tensile behaviour of mortar-based composites for externally bonded reinforcement systems. *Composites Part B: Engineering*, **68**, 401-413, 2015.

[2] S. De Santis and G. de Felice, Steel reinforced grout systems for the strengthening of masonry structures. *Composite Structures*, **134**, 533-548, 2015.

[3] B. Ghiassi, D. V. Oliveira, V. Marques, E. Soares, and H. Maljaee, Multi-level characterization of steel reinforced mortars for strengthening of masonry structures. *Materials & Design*, **110**, 903-913, 2016.

[4] A. Bilotta, F. Ceroni, E. Nigro, and M. Pecce, Experimental tests on FRCM strengthening systems for tuff masonry elements. *Construction and Building Materials*, **138**, 114-133, 2017.

[5] S. De Santis, F. Ceroni, G. de Felice, M. Fagone, B. Ghiassi, A. Kwiecień, G. P. Lignola, M. Morganti, M. Santandrea, M. R. Valluzzi, and A. Viskovic, Round Robin Test on tensile and bond behaviour of Steel Reinforced Grout systems. *Composites Part B: Engineering*, **127**, 100-120, 2017.

[6] A. Bilotta, F. Ceroni, G. P. Lignola, and A. Prota, Use of DIC technique for investigating the behaviour of FRCM materials for strengthening masonry elements. *Composites Part B: Engineering*, **129**, 251-270, 2017.

[7] T. D'Antino and C. Papanicolaou, Mechanical characterization of textile reinforced inorganic-matrix composites. *Composites Part B: Engineering*, **127**, 78-91, 2017.

[8] G. Thermou, G. de Felice, S. De Santis, S. Alotaibi, F. Roscini, I. Hajirasouliha, M. Guadagnini, Mechanical characterization of multi-ply steel reinforced grout composites for the strengthening of concrete structures. *9th International Conference on Fibre-Reinforced Polymer (FRP) Composites in Civil Engineering (CICE 2018)*, France, Paris, July 17-19, 2018.

Appendix C Bond Behaviour of Multi-layer SRG Strengthening Systems to Concrete

ADVANCED COMPOSITES IN CONSTRUCTION 2019

BOND BEHAVIOUR OF MULTI-LAYER SRG STRENGHTENING SYSTEMS TO CONCRETE

S. Alotaibi[1,2], G.Thermou[3],I. Hajirasouliha[1], M. Guadagnini[1]

[1]*The University of Sheffield, Civil and Structural Engineering Department, Sir Frederick Mappin Building Mappin Street, Sheffield, S1 3JD, UK (corresponding author: ssalotaibi1@sheffield.ac.uk);*

[2] *Shaqra University, Civil Engineering Department, 17441, Al Duwadimi, Saudi Arabia (PhD student);*

[3]*University of Nottingham, Civil Engineering Department, B76 Coates Building, Nottingham, NG7 2RD, UK*

Abstract

Steel Reinforced Grout (SRG) composites are characterised by a good fire performance and compatibility with concrete substrates and can provide an efficient and cost-effective alternative to conventional Fibre Reinforced Polymer (FRP) composite systems. Although, SRG composites with multiple layers are often required to strengthen large structural members, most of the available studies only deal with SRG composites comprising a single layer of steel fabric. This study aims to develop a better understanding of the bond performance of multi-layer SRG composites to concrete. A set of 18 single-lap shear bond tests are conducted on different SRG systems bonded to concrete prisms of low compressive strength (14 MPa). Two main design parameters are considered in this study, including the number of the steel fabric layers (1, 2, and 3) and the density of the steel fabric (4 and 8 cords/in). Digital Image Correlation (DIC) is used to obtain full-field displacement measurements and examine crack initiation and development. It is found that, although the composites with one layer of medium-density steel fabrics tend to fail at the fabric-matrix interface due to the high localised stresses, the use of multiple layers can lead to a more uniform distribution of stresses within the composite and promote debonding at the substrate-composite interface. The results presented in this paper will assist in developing more efficient bond-slip models for SRG systems.

Keywords

Composite materials; Strengthening; Retrofitting; Experimental study; Bond and interfacial stresses; Shear transfer; Steel-Reinforced Grout (SRG); Digital Image Correlation (DIC)

Introduction

Although Fibre Reinforced Polymers (FRPs) are widely used for the strengthening of substandard structures, they still suffer from some disadvantages including low performance in fire, limited applicability on wet surfaces, and relatively high cost. The efforts to eliminate, or at least mitigate, these disadvantages led to the development of a new generation of strengthening composites, namely Fibre Reinforced Cementitious Matrices (FRCMs) and Steel Reinforced Grout composites (SRGs).

SRG is a composite made of high strength unidirectional steel cords fixed to a non-structural glass fibre mesh and embedded in a grout matrix. Previous studies have investigated the feasibility of using SRG composite systems to enhance flexural performance of RC beams [e.g., 1] and the axial capacity of RC columns [e.g., 2, 3].

The influence of different parameters on the bond behaviour of SRG composites to masonry [4] and concrete [5,6] substrates has been examined in previous studies, including the type of steel cord (galvanized and stainless steel cords), the density of cords (4, 5, and 8 cord/in), and the type of matrix (lime-based, geopolymer, lime and pozzolan-based, and fibre-reinforced matrices). Different bond lengths were also investigated ranging from 100 to 400 mm.

Understanding the bond behaviour of strengthening systems is crucial as, in the majority of practical applications, debonding is the governing mode of failure and can significantly limit their efficiency. Although some strengthening applications require the use of more than one layer of reinforcement, as is the case for larger structural members, the bond behaviour of multi-layer SRG composites has not yet been investigated.

The work presented in this paper is part of a larger study aiming at assessing the influence of critical parameters on the bond behaviour of SRG systems, including type of steel fabrics, number of layers, bond length and concrete strength. This paper presents the preliminary results of a study on the bond behaviour of single and multi-layer SRG composites applied to low strength concrete substrates. Eighteen single-lap shear bond tests were carried out as part of this study on different composite systems comprising one, two and three layers of steel fabrics with density of 4 and 8 cord/in.

Experimental Programme

A total of 18 plain concrete prisms were cast. Each prism had a cross section of 150 mm x 150 mm and a length of 500mm. The SRG system used in this experiment consisted of two types of steel fabrics and a single inorganic matrix. Both steel fabrics had the same mechanical characteristics but different number of high strength steel cords, resulting in two different fabric densities (4 and 8 cord/in). The steel fabric is made of unidirectional cords fixed to a glass fibre mesh. Each cord consists of five twisted Ultra High Tensile Strength Steel (UHTSS) wires [Figure 1a]. As per manufacturer data sheet, the steel cord has a tensile breaking load, tensile strength, elastic modulus, and strain at breaking load of 1500 N, 2800 MPa, 190 GPa, and 1.5 %, respectively. The equivalent thickness of low-density (i.e., 4 cord/in) and medium density (i.e. 8 cord/in) steel fabrics is 0.084 mm and 0.169 mm, respectively. The matrix was made by mixing a polymer-modified cement with water at a mixing ratio of 1/5. The 28-day average compressive strength of concrete prisms was 14 MPa.

The notation SB-LXY was used to identify different test series, where SB denotes shear bond tests, L denotes low compressive strength substrate, X indicates the density of the fabric (X=4 and 8 for steel fabrics of 4 and 8 cord/in, respectively), and finally Y is the number of layers of steel fabric (Y=1, 2 and 3 for one, two and three layers of steel fabrics, respectively). Three identical specimens were constructed for each test series.

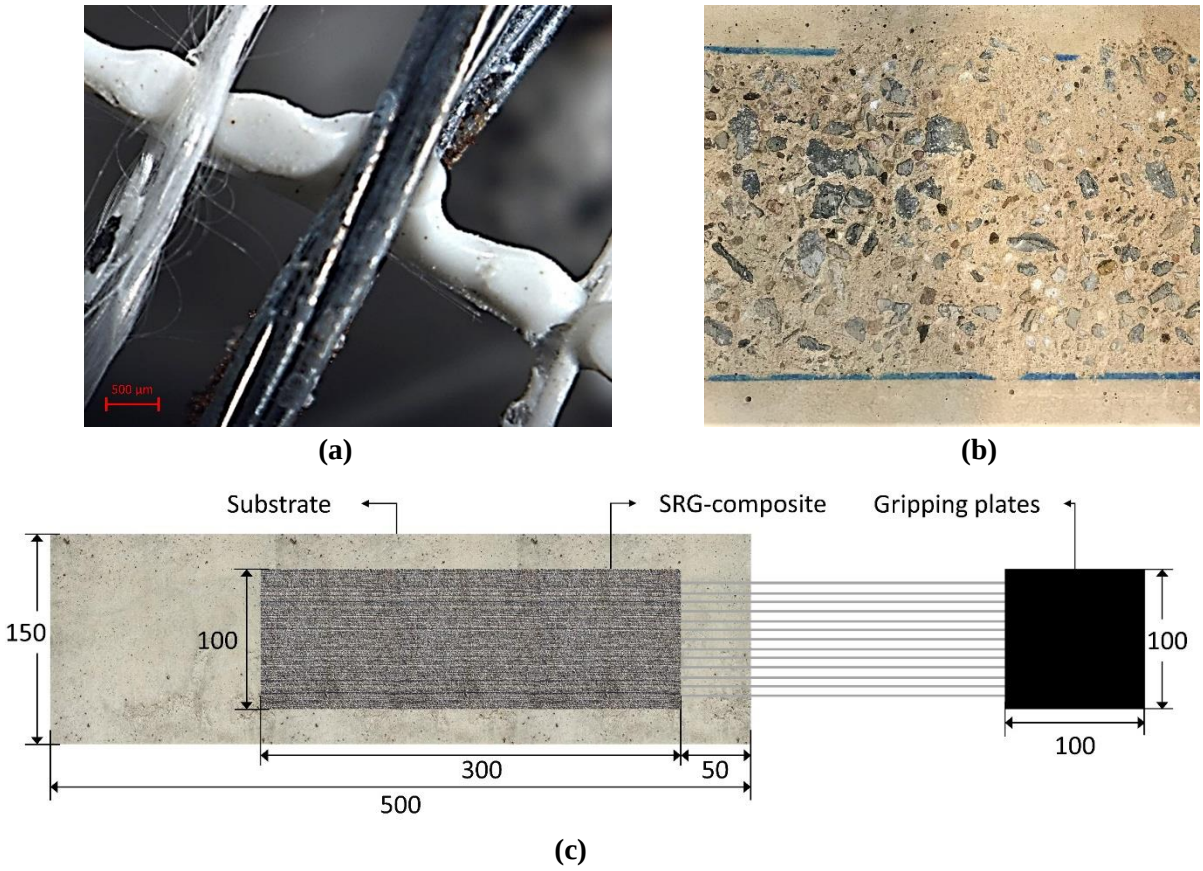

Figure 1 *(a) microscopic image showing the structure of a cord fixed to a fibre glass mesh (b) the surface of the substrate after grinding (c) schematic of the test specimen*

An area of 300 mm x 100 mm of the concrete prism was grinded prior to the application of the SRG system by means of an electrical grinder [Figure 1b]. The bonded length of the SRG composite started 50 mm from the face of the prism to avoid the edge effect at the loaded end [Figure 1c]. Specially designed acrylic moulds were used to apply the SRG composite. Prior to the application of the first layer of grout, the concrete surface was cleaned and wet with water to ensure a proper bond between the grout and the substrate. Subsequently, a first layer of grout with a thickness of 3 mm was applied and levelled to ensure a consistent thickness throughout the length of the composite. Immediately after applying the first layer of grout, the steel fabric was positioned on top of the mortar and gently pressed in, and a second layer of grout was applied. This process was repeated for two and three layers as required. The free end of the steel fabric/fabrics (clamping side) was embedded in a two-part epoxy and sandwiched between aluminium plates. The strengthened specimens were then covered with a wet hessian to enhance the hydration process and were stored in laboratory condition until the day of testing.

A horizontal single-lap shear bond test setup was adopted in this study. To apply the pull-out force, a 50-kN hydraulic actuator with an integrated load cell was used. The data reported during the test included applied load, slip of SRG composite, and strain in cords. The load was acquired from the integrated load cell connected to a data acquisition system while the slip of the loaded edge of the fabric relative to the composite and the substrate was measured by means of four LVDTs reacting against a plate attached to the steel fabric. The slip of the composite was then taken as the average difference between the LVDTs on the substrate and those on the composite. To measure the strains in the cords, a Digital Image Correlation (DIC) system was utilised using targets on steel cords. However, the outputs of this latter system will not be presented in this study.

Results and Discussion

The results of the shear bond tests including average failure load (P_{av}), average stress (f_{av}), average slip (s_{av}), and mode of failure are given in Table 1. The average stress was calculated as the failure load divided by the cross-sectional area of the steel cords. The resulting average stress-slip curves are shown in Figure 2.

Table 1. *Shear bond test results*

Series	Density of cords (cords/in)	Number of layers	Number of cords	Average load P_{av} (kN) [CV]	Average stress f_{av} (MPa) [CV]	Average slip s_{av} (mm) [CV]	Mode of failure
SB-L41	4	1	15	20.0 [19%]	2473 [19%]	2.13 [42%]	a
SB-L42		2	30	20.3 [14%]	1257 [14%]	1.59 [36%]	b
SB-L43		3	45	22.5 [12%]	927 [12%]	1.18 [26%]	b
SB-L81	8	1	30	16.7 [6%]	1030 [6%]	1.30 [16%]	c
SB-L82		2	60	27.7 [6%]	857 [6%]	1.15 [42%]	b and c
SB-L83		3	90	30.6 [12%]	631 [12%]	0.92 [20%]	b

CV= coefficient of variation
a= tensile failure of the fabric (rupture)
b= shear failure within the concrete cover (detachement of the whole composite)
c= shear failure within the composite (detachment of the upper layer of the composite)

In terms of average stress, there was a reduction of approximately 49% and 62% for two and three layers of low-density steel fabric, respectively, compared to one layer of the same fabric. On the other hand, for medium-density steel fabric the reduction was approximately 17% and 39% for two and three layers, respectively, compared to one layer of the same density.

A similar trend can be also observed for slip, as increasing the number of layers led to a decrease in the average slip in the range of 25% and 45% for two and three layers of 4 cords/in fabric, respectively, and 11.5% and 29% for two and three layers of 8 cord/in fabric, respectively, when compared to one layer of the same fabric.

In terms of failure load, all the specimens strengthened with low-density fabric (Series SB-L4) had almost a similar failure load ranging between 20 kN to 22.5 kN. However, their counterparts (Series SB-L8) had a higher deviation in failure load ranging from 16.7 kN to 30.6 kN.

The specimens strengthened with one layer of low-density steel fabric (Series SB-L41) developed the highest stress compared to the rest of the series and eventually failed by cords rupture [Figure 3a]. However, the specimens strengthened with medium-density steel fabric (Series SB-L81) experienced an inter-laminar shear failure [Figure 3b]. The rest of the series (Series SB-L42, Series SB-L43, Series SB-L82, and Series SB-L83) failed by a cohesive debonding at substrate-composite interface [Figure 3c-3f].

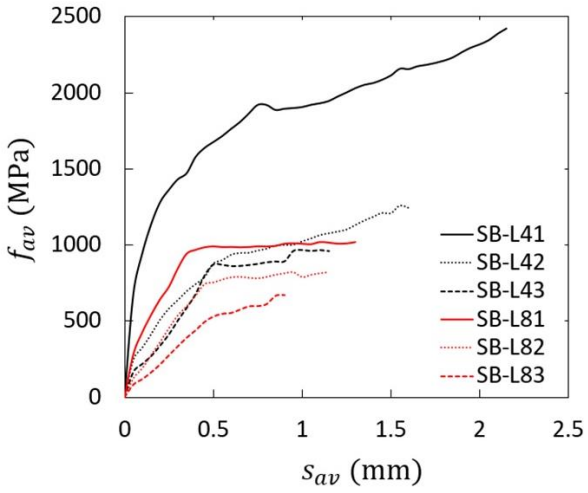

***Figure 2**. Shear bond test results*

Tensile rupture in the steel cords for series SB-L41 occurred at a load of 20 kN. The rupture of the cords in all specimens of this series provides evidence that sufficient shear bond strength developed at the interface between the composite and the substrate and also at the interface between the top and bottom layers of grout. All specimens in series SB-L81 failed for interlaminar shear at the level of the steel fabric at a load of 16.7 kN. The relatively dense structure of the steel fabric can result in poor penetration of the grout throughout the fabric and lead to higher localised stress promoting splitting.

All the specimens comprising two and three layers (except some specimens in series SB-L82) failed by cohesive debonding at the interface between the substrate and the composite. The large number of the steel cords resulted in more uniform distribution of stress within the composite and mobilised the full bond strength of the interface. Specimens with low-density steel fabric (series SB-L42 and SB-L43) failed at a load ranging from 17 kN to 24kN. However, the debonding load for their medium-density counterparts (series SB-L82 and SB-L83) was higher and ranging from 26kN to 34kN. The total number of steel cords for series SB-L82 and SB-L83 was 60 and 90 cords, respectively compared to 30 and 45 cords for Series SB-L42 and SB-L43, respectively. The large number of steel cords might help in a better distribution of the stress inside the composite and hence at the interface between the composite and the substrate which might, as a result, play a role in increasing the bond strength of that interface.

Conclusions

The aim of this paper was to investigate the shear bond behaviour in multi-layer SRG composites when applied to concrete substrates of low concrete strength. A total of six different configurations were tested, comprising one, two and three layers of low (4 cord/in) and medium (8 cord/in) density steel fabrics. The main results of this study are summarised below:

- Increasing the number of steel fabric layers leads to a decrease in the stress in the steel cords, as well as the slip of the composite, at failure.
- Three failure modes were identified, including rupture of the cords, interlaminar shear at the level of the fabric and substrate-composite interface debonding.
- Cords rupture was achieved in specimens with one layer of low-density fabric, while interlaminar shear was observed for those with one layer of medium-density fabric.
- All specimens with more than one layer failed in bond at the substrate-composite interface.

- Although when using one layer of fabric the higher cord density can lead to high localised stresses and cause failure due to delamination, the use of multiple layers can lead to a more uniform distribution of stresses within the composite and promote debonding at the substrate-composite interface.

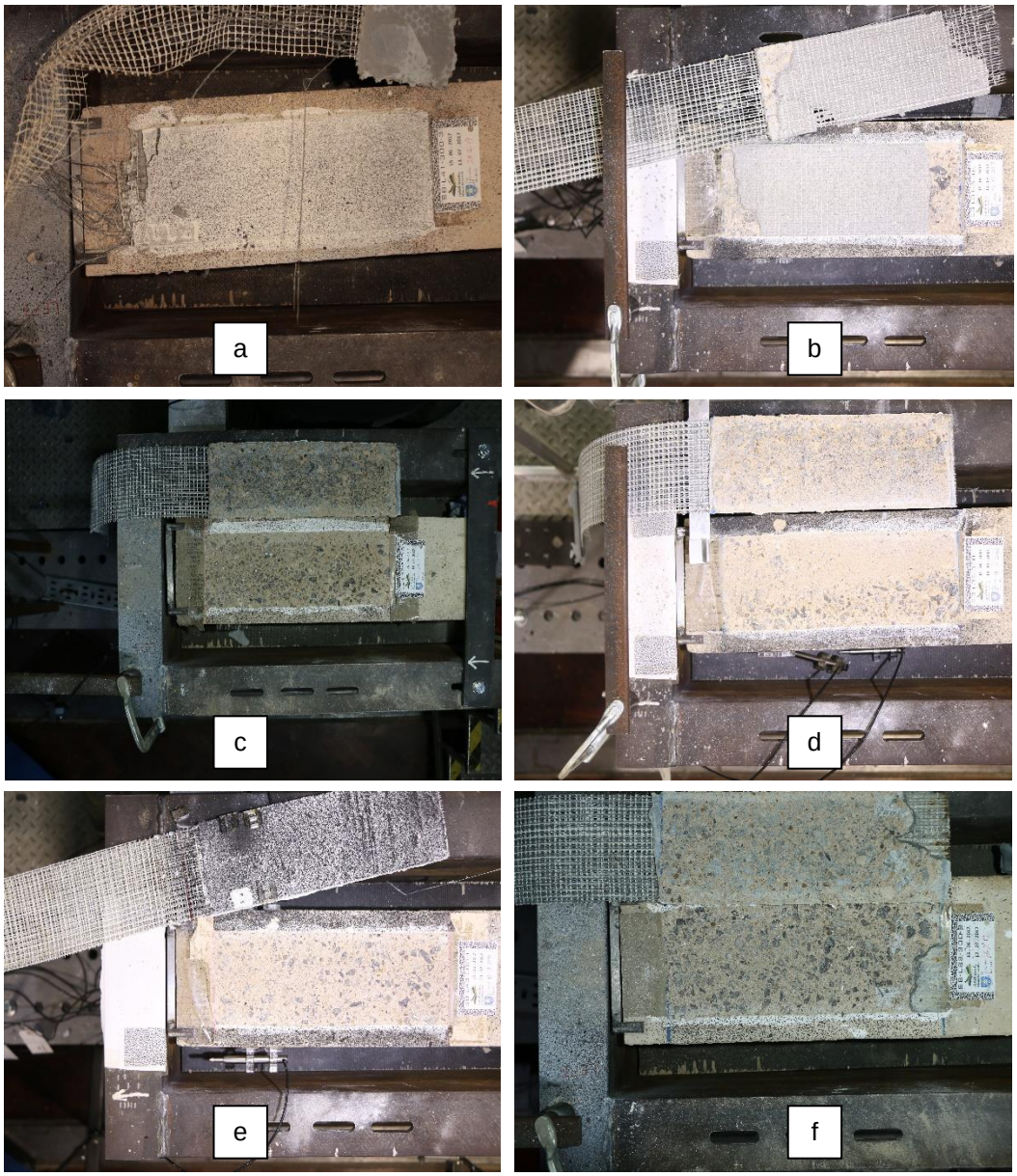

***Figure 3**. Mode of failure for (a) Series SB-L41, (b) Series SB-L81, (c) Series SB-L42, (d) Series SB-L82, (e) Series SB-L43, and (f) Series SB-L8*

Acknowledgement

The geo-polymer cement and the steel fabric were provided by Kerakoll S.p.A. The first author would like to thank the Saudi Arabian Cultural Bureau (UK) and Shaqra University (Saudi Arabia) for sponsoring his PhD research.

References

Wobbe, E., Silva, P., Barton B., Dharani, L., Birman, V., Nanni, A., Alkhrdaji, T., Thomas, J., Tnis, G., Flexural Capacity of RC beams externally bonded with SRP and SRG. *In: Proceedings of Society for the advancement of material and process engineering Symp.*, Long Beach, CA, USA, 2004.

Thermou, G. and Hajirasouliha, I. Compressive Behaviour of Concrete Columns Confined with Steel-Reinforced Grout Jackets. *Composites Part B: Engineering*, 138, 222-231 (2018).

Thermou, G.E., and Hajirasouliha, I. (2018) "Design-oriented models for concrete columns confined by steel-reinforced grout jackets" Construction and Building Materials, 178, 313-326.

De Santis, S., Ceroni, F., de Felice, G., Fagone, M., Ghiassi, B., Kwiecień, A., Lignola, G., Morganti, M., Santandrea, M., Valluzzi, M. and Viskovic, A., Round Robin Test on tensile and bond behaviour of Steel Reinforced Grout systems. *Composites Part B: Engineering*, 127, 100-120 (2017).

Sneed, L., Verre, S., Carloni, C. and Ombres, L., Flexural behavior of RC beams strengthened with steel-FRCM composite. *Engineering Structures*, 127, 686-699 (2016).

Bencardino, F., Condello, A. and Ashour, A., Single-lap shear bond tests on Steel Reinforced Geopolymeric Matrix-concrete joints. *Composites Part B: Engineering*, 110, 62-71 (2016).

Appendix D Shear Bond Behaviour of Multi-ply SRG composites for the Strengthening of Concrete Structures

SHEAR BOND BEHAVIOUR OF MULTI-PLY STEEL REINFORCED GROUT COMPOSITES FOR THE STRENGTHENING OF CONCRETE STRUCTURES

Georgia THERMOU[1], Stefano DE SANTIS[2], Gianmarco DE FELICE[3], Sultan ALOTAIBI[4,5], Francesca ROSCINI[6], Iman HAJIRASOULIHA[7], Maurizio GUADAGNINI[7]

Abstract: *Steel Reinforced Grout (SRG) composites, comprising Ultra High Tensile Strength Steel (UHTSS) textiles embedded in inorganic matrices, have experimentally proved effective for a number of structural retrofitting applications. Nevertheless, existing knowledge is mainly based on the behaviour of SRG systems with a single textile layer, whereas the use of more plies may be required when strengthening large structural members. This paper presents the preliminary results of an experimental study on SRG composites comprising multiple layers of galvanised UHTSS textiles within a geopolymer mortar. Single-lap bond tests were carried out to investigate the effect of number of plies (one, two or three) and fabric density (4 or 8 cords/in) on the SRG-to-concrete bond performance, which is crucial for the effectiveness of the retrofitting work.*

[1] Assistant Professor, University of Nottingham, Nottingham, UK, Georgia.Thermou@nottingham.ac.uk
[2] Researcher, Roma Tre University, Rome, Italy
[3] Professor, Roma Tre University, Rome, Italy
[4] Lecturer, Shaqra University, Dawadmi, Saudi Arabia
[5] PhD student, University of Sheffield, Sheffield, UK
[6] Research Assistant, Roma Tre University, Rome, Italy
[7] Senior lecturer, University of Sheffield, Sheffield, UK

INTRODUCTION

Fibre Reinforced Polymers (FRPs) are used extensively in retrofitting applications worldwide. However, several disadvantages, mainly related to the use of resins, such as the poor behaviour to fire conditions, the relatively high cost of epoxy resins and the lack of vapour permeability with adverse effects on reinforced concrete structures, render them less appealing with high environmental cost (Thermou et al. 2015). The last few years, a new generation of mortar-based systems, named Fabric Reinforced Cementitious Matrix (FRCM) composites, has been developed. Recent studies have demonstrated the efficiency of these systems in providing excellent application on wet surfaces, good performance at high temperatures, and excellent durability. The Steel-Reinforced Grout system is a relatively new system that consists of Ultra High Tensile Strength Steel (UHTSS) unidirectional textiles embedded in cement, lime or geo-polymer matrices. The cords are spaced at different distances (i.e., different density textiles are available) and fixed to a non-structural glass fibre mesh.

The response of the FRCM systems relies on the bond quality at the textile-to-matrix and substrate-to-matrix interfaces. Understanding the shear transfer mechanisms in mortar-based composite system is fundamental for their further development and use in structural applications. In general, mortar-based systems may exhibit different failure modes, differently from FRPs, which generally fail within the substrate (de Felice et al. 2018).

De Santis et al (2017) carried out a large round-robin test campaign to investigate the bond behaviour in SRG system on masonry substrates. They tested four SRG systems made of a combination of three different textiles and four mortar matrices. SRG systems were comprised of only one layer of reinforcement and were applied for a length of 260 mm upon the substrates. They found that the bond performance is dependent on a set of parameters including the mechanical characteristics of the steel textile and the matrix, the bond between the cords and the matrix, surface preparation, curing conditions, and test setup. Six modes of failure were identified including debonding of SRG composite with and without fragments of the substrate, detachment of the steel textile and the top layer of the matrix, slippage of steel textile with and without cracking of the loaded end of the composite, and rupture of cords.

The bond behaviour of SRG system on concrete substrate was studied by Sneed et al (2016) and Bencardino et al (2017). Sneed et al (2016) used a single-layer SRG composite with a 4 cords/in textile embedded in a thixotropic mineral mortar. The external layer of the matrix was omitted for half of the specimens in order to assess its role in the stress transfer mechanism. All the tested specimens, including the ones without external layers, failed due to debonding at textile-matrix interface. Load-slip behaviour for specimens with and without external layer of matrix was almost similar and was represented by a linear stage followed by a slight reduction in stiffness. Bencardino et al (2017) also investigated the bond characteristics of SRG composites on concrete substrates. SRG composite was made of stainless steel textile embedded in an inorganic fireproof matrix. Four bond lengths were examined including 100 mm, 150 mm, 200 mm, 250 mm, 300 mm, and 400 mm. It was found that the load-global slip of the tested specimens is comparable to that of FRP system. It was also reported that failure occurred at the textile-to-matrix interface, which implies that the bond behaviour of SRG system is not dependent on the mechanical properties of the substrate. By examining different bond lengths, it was concluded that the effective transfer length for this system is roughly 200 mm.

The SRG composite system has been used effectively as externally bonded reinforcement for the flexural strengthening of RC beams and the use of multiple layers of fabric was investigated in some recent works on reinforced concrete members reinforced in flexure (Napoli and Realfonzo 2015). Nevertheless, the shear transfer mechanism developed along the multiple layers of the steel fabric and the overall mechanical behaviour of multi-

ply SRG composites has not been studied in detail yet. A first attempt to develop a deeper understanding on the mechanical performance of multi-ply SRG composites has been made by lap-tensile tests in (Thermou et al. 2018). The objective of this study is to investigate the bond behaviour of multi-ply SRG composites applied to concrete substrates. For this purpose, a total of 18 single-lap shear bond tests were carried out on SRG composites made of one, two, and three layers of galvanised UHTSS textiles within a geopolymer mortar applied to concrete prisms.

EXPERIMENTAL PROGRAMME

A total of 18 direct single-lap shear bond tests were carried out on plain concrete specimens. Specimens were labelled following the notation SB-MXY where SB stands for shear bond tests, M denotes medium compressive strength substrate, X indicates the density of the steel textile (X=4 for textiles of 4 cords/in and X=8 for textiles of 8 cords/in), and finally Y is for the number of steel textile piles (Y=1, 2, 3 for one, two and three layers, respectively). A total of six series of specimens were tested including SB-M41, SB-M42, SB-M43, SB-M81, SB-M82, SB-M83. Each series had three nominally identical specimens.

Materials

Two types of steel textiles were used for this investigation with the same mechanical characteristics but different density textiles (4 cords/in and 8 cords/in). The textile is made by unidirectional Ultra High Tensile Strength Steel (UHTSS) cords fixed to a non-structural glass fibre mesh. Each cord is made by twisting 2 galvanised steel filaments on three rectilinear ones at a high torque angle. The equivalent thicknesses of the two textiles are 0.084 mm and 0.168 mm. The cords have a breaking load of 1.6 kN at a strain of 2%. The tensile strength and the modulus of elasticity of the textile are 23200 MPa and 186 GPa respectively (De Santis et al. 2017). The grout used to make SRG composite was made by mixing geopolymer mortar with water at a mixing ratio of 0.20. The 28-day compressive strength of concrete specimens was 27 MPa.

SPECIMENS PREPARATION

The bonded area of the SRG reinforcement had a length of 300 mm, a width of 100 mm, and a thickness of 6 mm, 9 mm, and 12 mm for 1, 2 and 3 layers of steel textiles, respectively. To enhance the bond between the substrate and the composite, substrate was grinded using an electrical grinder. Prior to the application of SRG composite, the substrate was cleaned from dust and moisten with water. A first layer of grout was applied, and the thickness was controlled by means of a specially designed acrylic mould. Immediately after applying the first layer of grout, steel textile was placed and gently impregnated, and another layer of grout is applied. This process was repeated for the specimens provided with 2 and 3 layers of textile. Following the recommendation developed by RILEM TC 250-CSM (de Felice et al. 2018), the SRG strip was applied 50 mm off the edge of the concrete specimen to avoid edge effect. The dry part of the steel textile (outside the composite) was 400 mm long. To grip the steel textile, its end was impregnated in a two-part epoxy and placed between two aluminium plates.

TEST SETUP

A 50-kN hydraulic actuator was used to apply a horizontal force. The specimen was placed inside a reaction frame with its back edge being secured to the frame to avoid back uplifting. Slip was measured using 4 LVDTs reacting against a plate fixed to the steel textile such that two LVDTs were attached to the composite and the other two were attached to the substrate [Figure 1]. Load was acquired from the integrated load cell connected to data acquisition system.

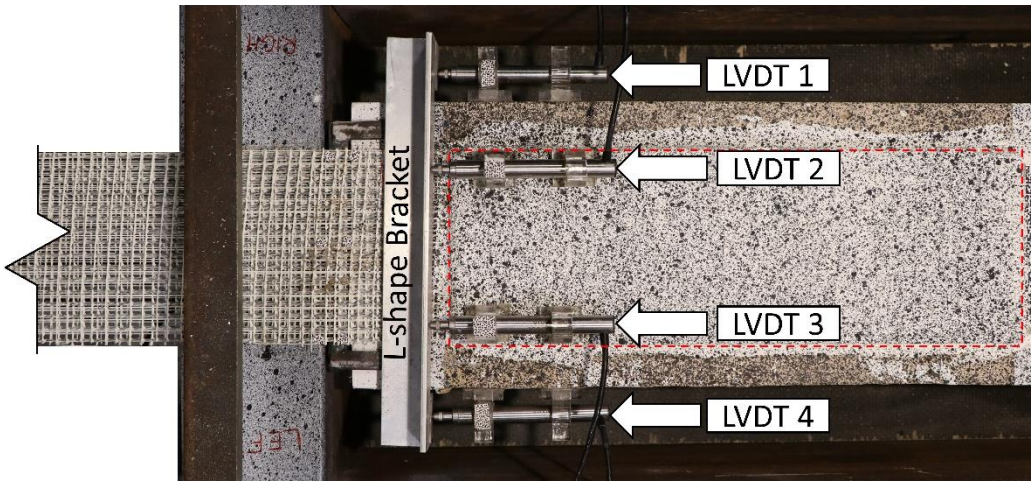

Figure 1. *Instrumentation of the shear bond test*

RESULTS AND DISCUSSION

Shear bond tests results are provided in Table 1 including average load at failure, corresponding average axial stress in the textile, slip at failure, and finally mode of failure for each series. Average stress was calculated by dividing the failure load by the total cross-sectional area of steel cords for each series. Slip refers to the relative slip between the upper layer of SRG composite and the substrate.

Table 1. *Shear bond test results*

Series	**Steel textile density** (cords/in)	**Number of layers**	**Number of cords**	**Average load at failure** (kN)	**Average axial stress** (N/mm^2)	**Slip at failure** (mm)	**Mode of failure**
SB-M41	4	1	15	21 [27%][1]	2399	2.05 [5%]	a[2]
SB-M42		2	30	21.7 [15%]	1341	1.40 [11%]	b[3]
SB-M43		3	45	22.4 [9%]	925	0.89 [53%]	b
SB-M81	8	1	30	15.8 [6%]	977	1.22 [14%]	c[4]
SB-M82		2	60	26 [8%]	804	1.05 [34%]	b, c
SB-M83		3	90	26.2 [8%]	541	0.99 [44%]	b

1. Coefficient of variation
2. a= mixed mode of failure comprising cords rupture and bond failure at substrate-composite interface
3. b= cohesive bond failure at substrate-composite interface
4. c= interlaminar shearing at textile-grout interface

The difference in the average failure load between all specimens comprising low-density steel textiles (i.e., series SB-M4) was almost negligible. On the other hand, for their counterparts (i.e., series SB-M8), there was an increase of approximately 65 % in the average failure load for specimens strengthened with two layers of steel textile (SB-M82) compared to that of the specimens strengthened with only one layer of textile (SB-M81). However, the average load at failure for series SB-M83 was almost the same as series SB-M82.

In terms of average axial stress, there is a reduction of approximately 44% and 61% for series SB-M42 and SB-M43, respectively, compared to series SB-M41, whereas the reduction for their counterparts was 18% and 45% for series SB-82 and SB-M83, respectively, compared to series SB-M81. Although series SB-M42 and SB-M81 had the same number of cords (i.e., 30 cords), the stress for SB-M42 was 27% higher than that of SB-M81 as this latter failed earlier at the textile-to-matrix interface.

In terms of slip, series SB-M41 developed the largest slip among all tested series. In general, there is a decreasing trend for slip as the number of steel textile layers is increased with this trend being more notable for the series utilising low-density textile. However, apart from series SB-M41, slip was comparable and ranged from 1.4 mm to 0.89 mm.

In Figure 2, stress-slip envelopes are presented for each series. All series showed a first stage characterized by a linear branch associated with the elastic behaviour of the system. The stiffness of the linear stage is higher for the series comprising only one layer of steel textile. As the number of textile layer was increased the slope of the linear segment decreased. This linear stage is followed by a nonlinear stage as a result of local damage at both substrate-to-matrix and textile-to-matrix interfaces. Some series showed a third stage where the slip was increasing at almost constant load (e.g., series SB-M81 in Figure 2b).

Figure 3 provides a comparison in terms of stress-slip response for series comprising low-density and medium-density steel textiles separately.

Figures 4(a)-(f) present the specimens at the end of the tests for each series. Three different modes of failure were observed including failure by tensile rupture in steel cords followed by a cohesive failure at substrate-composite interface (mode a), pure cohesive failure in bond between the SRG composite and the substrate with a higher involvement of the latter (mode b), and interlaminar shearing between the steel textile and the grout (mode c). The first mode of failure was observed for series SB-M41 where some cords reached their maximum stress suggesting a non-uniform stress distribution, which may be due to possible misalignment or manufacturing imperfections. This local tensile rupture was immediately followed by a cohesive debonding at the substrate-to-matrix interface.

Almost all specimens strengthened with two and three layers of steel textiles characterised a pure cohesive debonding at the substrate-to-matrix interface with fragments of the substrate and the SRG composite was almost intact after detachment. Series SB-M81 and two specimens of series SB-M82 developed an interlaminar shear failure at textile-to-matrix interface such that the upper layer of grout and steel textile detached from the bottom layer of grout. The relatively denser structure of steel textiles of 8 cords/in proved responsible for triggering bond failure at the interface between the steel textile and the grout. Indeed, none of the series that have low-density textile failed at textile-to-matrix interface as both layers of grout developed a better bond compared to that of the composites with medium-density textiles.

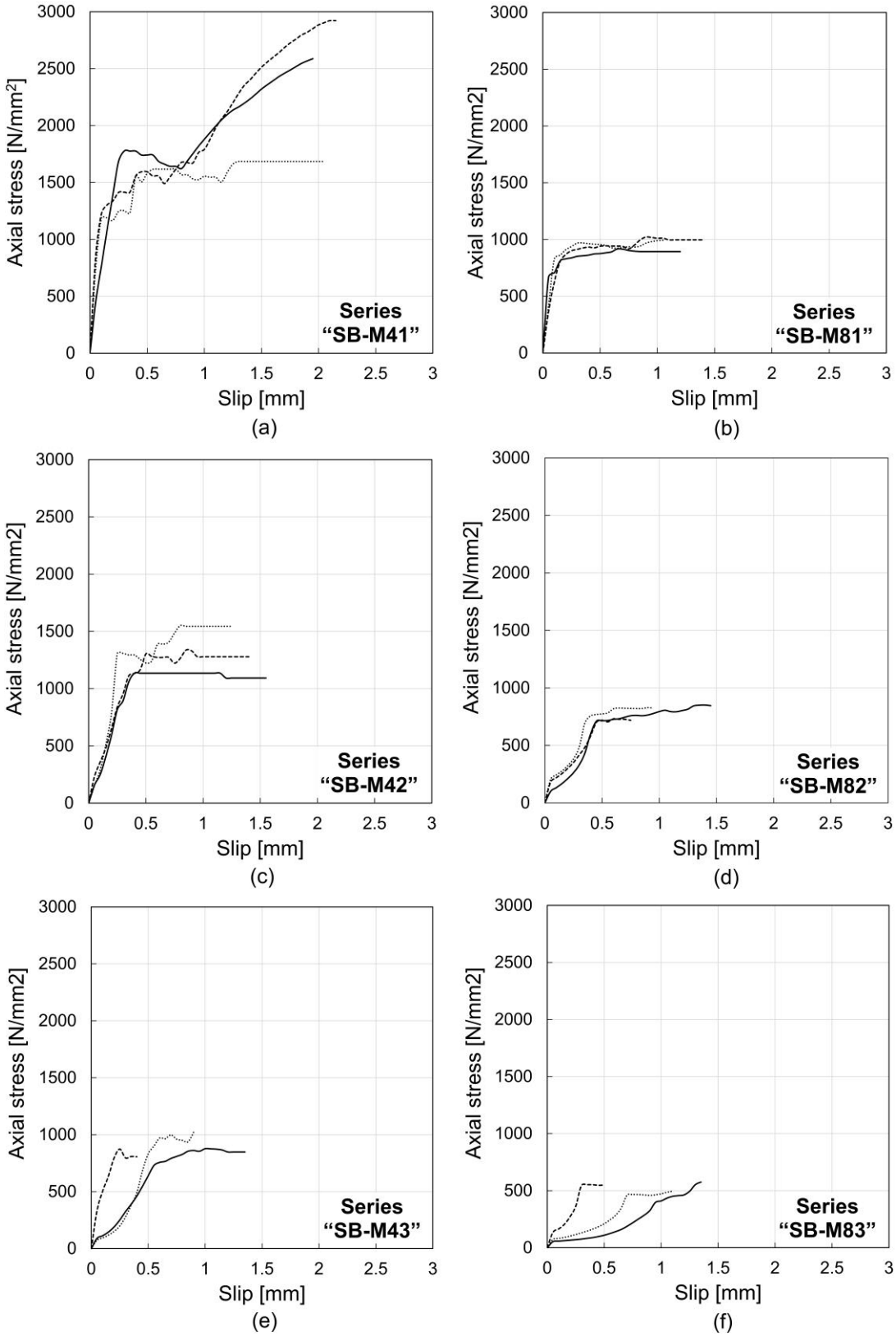

Figure 2. *Stress-slip envelope curves for (a) Series SB-M41, (b) Series SB-M81, (c) Series SB-M42, (d) Series SB-M82, (e) Series SB-M43, and (f) Series SB-M83*

All specimens strengthened with two and three layers of both steel textiles almost experienced a cohesive debonding failure at substrate-to-matrix interface. The debonding load was on average 22 kN and 26 kN for series comprising low-density and medium-density steel textiles, respectively. This can be attributed to the improved stress transfer mechanism in composites utilising medium-density textiles as the stress is better dissipated over a larger area of the matrix thanks to the larger number of cords (60 and 90 cords for series SB-M82 and SB-M83, respectively, and 30 and 45 cords for series SB-M42 and SB-M43, respectively).

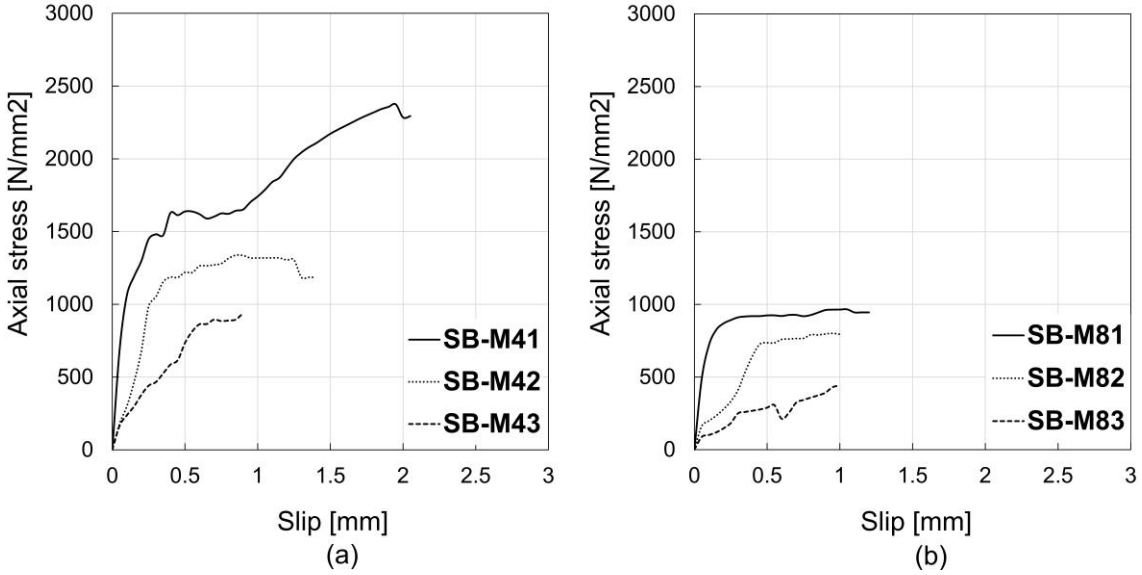

Figure 3. *Stress-slip curves for one, two, and three layers of (a) Low-density steel textile (4 cords/in) and (b) Medium-density steel textile (8 cords/in)*

CONCLUSIONS

The bond behaviour of SRG systems comprising steel textiles of two different densities applied to a medium compressive strength substrate was investigated in this paper. To this end, a total of 18 single-lap shear bond tests were carried out on concrete prisms strengthened with SRG system of one, two, and three layers of textile. It was concluded that the increase of the number of textile layers resulted in a reduction of average axial stress in the textile and average slip. Stress-slip response showed a stage of linear branch followed by nonlinear behaviour and for some series a third stage where the slip increased with a constant load. Three different modes of failure were observed including rupture of cords followed by a cohesive debonding at substrate-to-matrix interface, pure cohesive debonding at substrate-to-matrix interface involving the substrate, and an interlaminar shear failure at textile-to-matrix interface. It was, also, found that composites made of multi-ply textile of medium density steel textiles tend to have a better dissipation of stresses within the composite and hence increasing the interfacial debonding load.

ACKNOWLEDGEMENTS

The fourth author would like to thank the Saudi Arabian Cultural Bureau (UK) and Shaqra University (Saudi Arabia) for sponsoring his PhD research. Special thanks are attributed to Kerakoll S.p.A. for providing the materials.

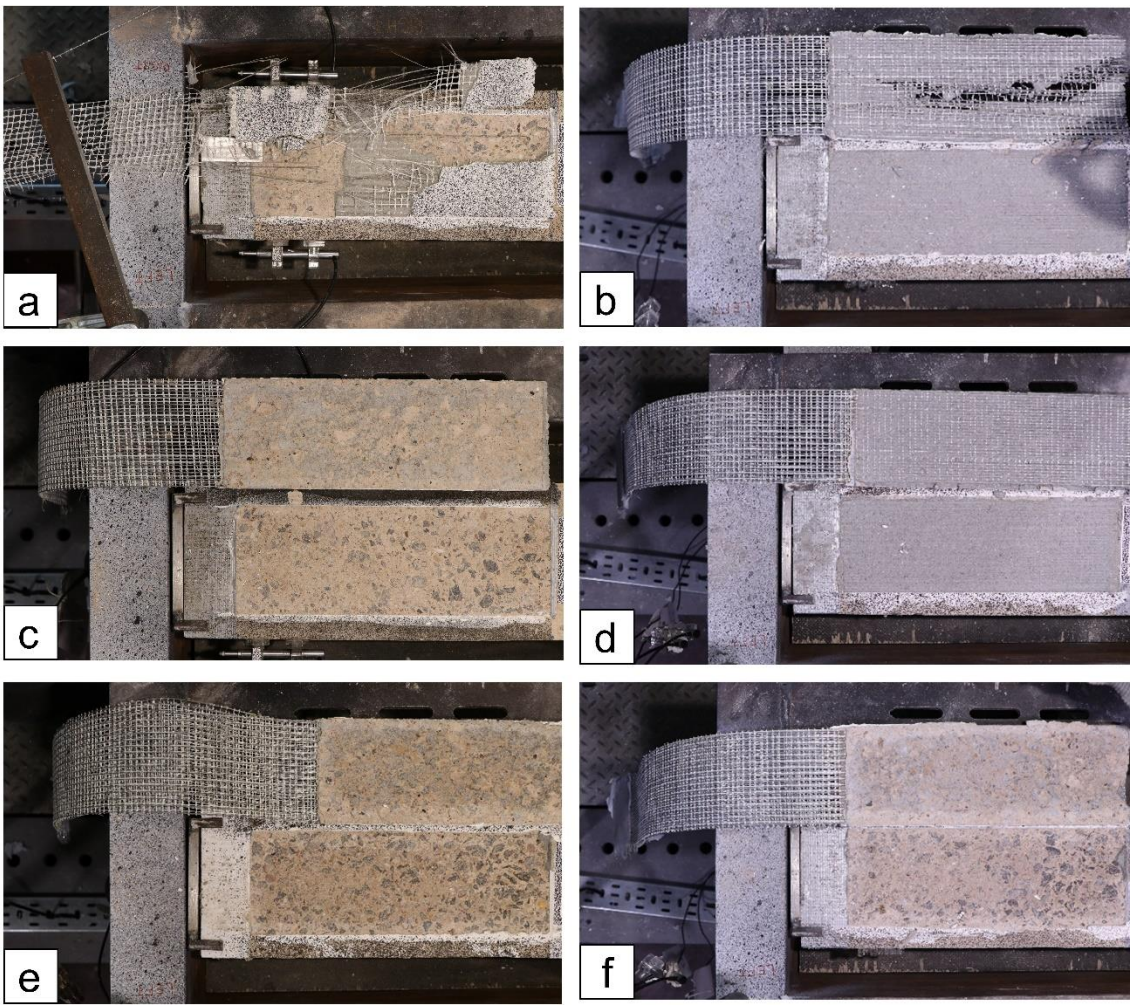

Figure 4. *Mode of failure of different specimens from (a) Series SB-M41, (b) Series SB-M81, (c) Series SB-M42, (d) Series SB-M82, (e) Series SB-M43, and (f) Series SB-M83*

REFERENCES

Ascione F, Lamberti M, Napoli A, Razaqpur G and Realfonzo R (2017), An experimental investigation on the bond behavior of steel reinforced polymers on concrete substrate. *Composite Structures*, 181: 58-72

Bencardino F, Condello A and Ashour A (2016), Single-lap shear bond tests on Steel Reinforced Geopolymeric Matrix-concrete joints. *Composites Part B: Engineering*, 110: 62-71

De Santis S, Ceroni F, de Felice G, Fagone M, Ghiassi B, Kwiecień A, Lignola G, Morganti M, Santandrea M, Valluzzi M and Viskovic A (2017), Round Robin Test on tensile and bond behaviour of Steel Reinforced Grout systems, *Composites Part B: Engineering*, 127: 100-120

Napoli A, Realfonzo R (2015) "Reinforced concrete beams strengthened with SRP/SRG systems: Experimental investigation" Construction and Building Materials, 93, 654-677.

Sneed L, Verre S, Carloni C and Ombres L (2016), Flexural behavior of RC beams strengthened with steel-FRCM composite. *Engineering Structures*, 127: 686-699

Thermou, G.E., Katakalos, K. and Manos, G. (2015). “Concrete Confinement with Steel-Reinforced Grout Jackets.” Materials and Structures, 48(5), 1355-1376.

de Felice G, Aiello MA, Caggegi C, Ceroni F, De Santis S, Garbin E, Gattesco N, Hojdys Ł, Krajewski P, Kwiecień A, Leone M, Lignola GP, Mazzotti C, Oliveira D, Papanicolaou C, Poggi C, Triantafillou T, Valluzzi MR, Viskovic A. Recommendation of RILEM TC 250-CSM: Test method for Textile Reinforced Mortar to substrate bond characterization. Materials and Structures 2018;51(4):95.

Thermou GE, de Felice G, De Santis S, Alotaibi S, Roscini F, Hajirasouliha I, Guadagnini M. Mechanical characterization of multi-ply steel reinforced grout composites for the strengthening of concrete structures. Proc. Int. Conf. CICE 2018, 9th International Conference on Fibre-Reinforced Polymer (FRP) Composites in Civil Engineering. Paris, France, 17-19 July 2018.

Appendix E Flexural Strengthening of RC Beams with SRG

Special session on
Advances in textile reinforced mortars for strengthening applications

Flexural Strengthening of RC Beams with SRG

S.S. Alotaibi[1,2], G.E. Thermou[3], I. Hajirasouliha[2], M. Guadagnini[2]

[1] Department of Civil Engineering, Shaqra University, Saudi Arabia
[2] Department of Civil and Structural Engineering, The University of Sheffield, UK
[3] Department of Civil Engineering, The University of Nottingham, UK

ABSTRACT

This paper presents the results of an experimental programme designed to assess the performance of SRG as flexural strengthening system for RC beams. A total of six beams with a clear span of 2300mm and a rectangular cross section of 150mm x 250mm were tested under a four-point bending configuration. The parameters investigated in this study are: 1) the number of SRG layers (one and two); and 2) the density of the SRG fabric (4 and 8 cords/in). The SRG system was fully anchored at one end of the beam to induce any possible debonding failure on the opposite shear span, which was fully instrumented with LVDTs and a DIC system to monitor slip at the free end of the SRG (located 150mm away from the support) and strain development along the bottom face of the beam. The use of one or two layers of the light density steel fabric (4 cords/in), or one layer of the medium density fabric (8 cords/in), enabled the full mobilization of the SRG mechanical properties and promoted flexural failures governed by yielding of the internal steel reinforcement followed by rupture of the externally bonded steel fabric. The use of a strengthening system with relatively higher stiffness (i.e., two layers of 8 cords/in) resulted in the premature debonding of the SRG, which initiated as end-anchorage debonding and subsequently propagated towards the opposite support in a brittle manner.

Appendix F Bond Behaviour of Multi-ply SRG Composites

Bond Behaviour of Multi-Ply Steel Reinforced Grout Composites

G.E. Thermou[8*], S. De Santis[9], G. de Felice[10], S. Alotaibi[11,12],
F. Roscini[13], I. Hajirasouliha[14], M. Guadagnini[7]

ABSTRACT

This paper presents an experimental investigation on Steel Reinforced Grout (SRG) systems comprising multiple layers of galvanized UHTSS textiles, with either 4 or 8 cords/in density, embedded within a geopolymer mortar. Lap-splice tests and single-lap bond tests were performed to develop an improved understanding of the textile-to-textile load transfer capacity and of the SRG-to-concrete substrate bond behaviour. The effects of number of textile plies, cord density and compressive strength of concrete on the bond behaviour are analysed.

KEYWORDS: bond and interfacial stresses; digital image correlation (DIC); fabric reinforced cementitious matrix (FRCM); textile reinforced mortar (TRM); lap-splice test; shear bond test; strengthening.

[8]Assistant Professor, University of Nottingham, Nottingham, UK
[9] Assistant Professor, Roma Tre University, Rome, Italy
[10] Professor, Roma Tre University, Rome, Italy
[11] Lecturer, Shaqra University, Dawadmi, Saudi Arabia
[12] PhD student, The University of Sheffield, Sheffield, UK
[13] Marie Curie IF, The University of Sheffield, Sheffield, UK
[14] Senior Lecturer, The University of Sheffield, Sheffield, UK
* Corresponding author; georgia.thermou@nottingham.ac.uk

1.0 INTRODUCTION

Aging of the structures due to the continuous deterioration caused by environmental conditions and extreme events (e.g., earthquakes) can significantly affect their structural performance and resilience over time [1]. Changes in use or, as for infrastructures, increasing traffic volumes, may also result in increasing load demands. Additionally, updating building codes generally corresponds to rising required safety, such that existing structures may become noncompliant with the most recent standards. When demolition is not an option due to either the prohibitive cost or the cultural and historical significance of the structure, retrofitting is the only solution. Depending on the performance targets and level of retrofitting, global or local intervention methods could be selected [2]. In the past three decades, the use of Fibre Reinforced Polymers (FRPs) has emerged as one of the most effective local strengthening methods. Nevertheless, FRPs have shown some drawbacks, such as high cost, poor fire resistance, lack of vapour permeability, toxic nature of epoxy, and lack of reversibility [3-4]. In order to overcome many of these drawbacks, closely related to the use of an organic matrix as the bonding material, a new generation of composites, named as Fabric Reinforced Cementitious Matrix (FRCM), has been developed, in which inorganic matrices are used instead of resins [4-5].

The experimental studies performed in the last 15 years on the bond behaviour of FRCM systems have identified the complexity of the FRCM-to-substrate shear transfer mechanisms and the occurrence of multiple failure modes [5-7]. In the case of Steel Reinforced Grout (SRG) systems, which comprise unidirectional textiles of ultra-high tensile strength steel (UHTSS) cords, studies on bond behaviour have been conducted on both concrete [3, 8-10] and masonry [1, 5-6, 11-14] substrates. Different parameters have been investigated, such as the bond length [3, 13], the fabric density [1, 14], the surface preparation [3, 5], the matrix strength [6], the substrate strength [12] and the substrate curvature [13]. In general, in the previous studies the failure of FRCM systems can occur due to: (i) debonding either at the fabric-to-matrix interface [3] or at the substrate-to-matrix interface, sometimes involving a thin layer of substrate (cohesive failure in substrate) [12], (ii) slippage of the fabric [15] or (iii) fabric tensile rupture [14]. De Santis and de Felice [12] attributed the debonding at the substrate-to-matrix interface to the high strength of the matrix applied to a relatively weak substrate. They observed that the substrate to matrix detachment was mainly associated with short bonded lengths. They also concluded that slippage of the fabric was attributed to its poor interlocking with the grout, as was also observed in textiles comprising stainless steel ropes, whose surface is smoother than that of cords [1]. Some of the above-mentioned studies suggested an effective transfer length for SRG systems ranging from 150 mm to 300 mm [1, 3, 9]. Accordingly, and based also on the results of tests not only on SRG but also on other FRCM systems [16], a bond length of 300 mm is recommended by most testing guidelines [1, 17].

Despite the knowledge developed in the field of FRCM so far, all the previous studies have considered SRG systems comprising only one layer of steel textile. Nevertheless, multiple textile layers may be required in some applications, such as the flexural strengthening of large span reinforced concrete beams [18]. To date, existing knowledge on the shear transfer mechanism developed along the multiple layers of the steel fabric and on the overall behaviour of multi-ply SRG composites is still very limited, despite the crucial role it plays on the effectiveness of externally bonded reinforcements. This study aims to bridge this knowledge gap and to gain an improved understanding of the bond behaviour of multi-ply SRG reinforcements applied to concrete substrates. An experimental investigation was performed on SRG composites comprising unidirectional textiles made of galvanized UHTSS cords, with either 4 or 8 cords/in density, embedded in a geopolymer mortar, particularly suitable for strengthening of concrete elements. The effect of number of textile layers, steel cords density and compressive strength of the substrate was analysed through a series of complementary tests. Lap-splice tests were carried out to study the textile-to-textile load transfer capacity for different overlap lengths (from 100 mm to 300

mm). Additionally, single-lap shear bond tests were performed on multi-ply SRG composites (comprising 1, 2 or 3 plies) bonded to two types of concrete substrates (with a compressive strength of 14 N/mm^2 or 28 N/mm^2).

2 MATERIALS AND EXPERIMENTAL SETUPS

2.1 MATERIALS

The textiles investigated in this work comprise unidirectional ultra-high tensile strength steel (UHTSS) micro-cords, thermo-welded to a fibreglass micromesh. Each cord has a cross sectional area of 0.538 mm^2 and is obtained by joining 5 wires, 3 straight and 2 wrapped with a high torque angle to enhance the interlocking with the mortar. Wires have a cross sectional area of 0.11 mm^2 and are galvanized (coated with zinc) to improve their durability. Two different fabrics were tested, which differ only in cord density, using 4 cords/in (corresponding to 1.57 cords/cm, labelled as S4) and 8 cords/in (3.15 cords/cm; S8). In the former (S4), cords are evenly arranged such that the clear spacing between two cords is 5.45 mm, whereas, in the latter (S8), cords are paired such that the clear spacing between two pairs is 2.28 mm. S4 has a surface mass density of □=670 g/m^2 and a design thickness of t_f=0.084 mm, whereas S8 has □=1300 g/m^2 and t_f=0.169 mm. The textiles have an average tensile strength of about 3200N/mm^2, an ultimate strain of 2.2% and tensile modulus of elasticity of 186kN/mm^2 [1]. The matrix used to manufacture SRG composites is a pre-mixed geopolymer mortar with a crystalline reaction geo-binder base. According to manufacturer's datasheet [19], it has a compressive strength of 55 N/mm^2, tensile strength of 10 N/mm^2 and Young's modulus of 22 kN/mm^2. For manufacturing the composites, a water-to-mortar powder mix ratio of 1:5 was used.

2.2 DIRECT TENSILE TESTS

Direct tensile tests were carried out on prismatic specimens (coupons) with a total length of 600 mm, width of 50 mm and thickness of 10 mm. In the case of S4, the strip embedded in the coupon comprised 8 cords, whereas, in the case of S8, the strip had 16 cords. In total, 16 specimens were tested, 8 with S4 and 8 with S8. Coupons were manufactured in Perspex moulds, demoulded after 2 days, cured for 28 days in water and, finally, stored for 7 days under standard laboratory conditions before testing. Displacement controlled tests were carried out at a machine stroke displacement rate of 0.01 mm/s, using a hydraulic universal testing machine with 500 kN capacity. The specimens were gripped by the wedges of the machine, which applied a lateral pressure to avoid slippage [20]. The ends of the coupons were wrapped with glass fibre reinforced polymer (GFRP) [15] to ensure a uniform stress distribution within the loading areas and prevent mortar crushing.

The load was recorded by an integrated load cell and divided by the cross sectional area of the steel textile (4.30 mm^2 for S4 and 8.61 mm^2 for S8) to calculate the stress (f). The strain (□$_t$) was derived as the mean of the displacements recorded by two transducers divided by their gauge length (200 mm). Digital image correlation (DIC) was also applied. A digital camera was placed on a stiff frame at 1.1 m distance from the specimen, to check that the sensor and the surface of the coupon were parallel. Pictures were taken every 5 seconds during test execution and post-processed to derive the displacement field. Subsequently, two points were selected on the surface of the coupon, one in the upper portion and one in the lower one, based on the crack pattern (each point was taken in the middle between two cracks). The strain was then calculated as the relative displacement between these two points divided by their initial distance and used to validate the strain obtained from the transducers [21].

Specimens were labelled using the notation "DT-X-N", in which "DT" denotes direct tensile test, "X" denotes the density of steel fabric ("4" for S4 and "8" for S8), and "N" identifies the specimen number (from 1 to 8) within a set of nominally identical specimens.

2.3 LAP-SPLICE TESTS

Lap-splice tests were carried out to investigate the textile-to-textile load transfer capacity and were performed on prismatic specimens similar to those subjected to direct tensile tests. They had 600 mm total length, 50 mm width and 12 mm thickness, were cast in the same moulds and underwent the same curing process. The overlap length in the central portion of the coupon, (L') was 100 mm, 200 mm or 300 mm for different specimens (see Figure 1). The thickness of the mortar matrix between the plies along the overlap was 3 mm [9]. The symmetry along the thickness direction prevented the occurrence of parasitic bending moments caused by eccentricities. During manufacturing of the specimens, particular care was paid to align the textile strips, to keep a constant spacing between them, and to let an adequate amount of mortar pass through the voids between the cords. The ends of the specimens were wrapped with GFRP and the tests were performed following the same protocol as for the as was used for the direct tensile tests. Five nominally identical specimens were manufactured and tested for each value of L' (15 specimens for S4 and 15 specimens for S8).

Specimens were labelled using the notation "LS-X-Y-N", in which "LS" denotes lap-splice test, "X" denotes the density of steel fabric ("4" for S4 and "8" for S8), "Y" is the overlap length in mm (100, 200 and 300), and, finally, "N" identifies the specimen number (from 1 to 5) within a set of nominally identical specimens.

2.4 SHEAR BOND TESTS

Single-lap shear bond tests were performed on concrete substrates. A total of 42 plain concrete prisms with a length of 500 mm and a cross section of 150 mm × 150 mm (Figure 2(a)) were cast in two different batches. Half of the concrete prisms were characterised by low compressive strength (L - 14 N/mm^2) and the remaining half by a medium compressive strength (M - 28 N/mm^2).

SRG strips were bonded over a 300 mm long and 100 mm wide area. As shown in Figure 3(a), the bonded area was on the vertical face to one of the sides of the prism (perpendicular to the casting face) and, which exhibited a better distribution of fine and coarse aggregates. The bonded area started 50 mm away from the edge of the concrete block to avoid edge effects and exhibit a better distribution of fine and coarse aggregates [6]. Before installation, the concrete surface was grinded with an angle grinder to remove the thin smooth paste and expose the aggregate. The grinded surface was then cleaned from debris and dust (Figure 3(a)). The grinded surface was kept wet for one day prior to SRG application to ensure that the water-to-cement ratio in the matrix was not compromised by any hydration processes in the substrate. After the application of the first layer of grout (Figure 3(b)), the steel fabric was placed on top of the layer and gently pressed by hand until it was fully impregnated in the mortar (Figure 3(c)). An additional layer of grout was then laid on top. This process was repeated more times for multi-ply SRG composites and, in these cases, special attention was paid to ensure that the strips were aligned with each other and that the time of application was within the working time of the mortar. Each grout layer had a thickness of 3 mm, which was controlled by specially designed moulds. Finally, the specimens were covered with a hessian fabric, which was kept wet for three days to enhance the hydration process. The specimens were left in laboratory conditions for at least 28 days before testing.

In this case, specimens were labelled using the notation "SB-X-Y-Z-N", in which "SB" denotes shear bond test, "X" denotes the concrete compressive strength ("L" for low and "M" for medium), "Y" denotes the density of steel fabric ("4" for S4 and "8" for S8), "Z" is the number of plies (1, 2 or 3), and finally, "N" identifies the specimen number (from 1 to 3 or 4) within a set of nominally identical specimens.

To apply the load, the free end of the steel fabric was sandwiched between aluminium plates measuring 120 mm × 100 mm using a two-part epoxy adhesive. In the case of multiple layers of steel fabrics, an additional 3 mm thick aluminium plate was placed between successive layers to keep their spacing similar to that within the bonded

area. The aluminium plates were provided with holes to guarantee a uniform distribution of epoxy adhesive through the whole end-plate assembly area to prevent possible textile-to-plate sliding in the gripping area.

For the shear bond tests, a direct single pull-out shear setup was used. Specimens were placed in a reaction steel frame provided with an adjustable bed resting on four bolts (Figure 2(b)). The height and the level of the bed were controlled to ensure the alignment between the SRG strip and the gripping sandwich and prevent the development of undesirable stresses inside the composite. Moreover, the plate against which the concrete block was reacting, was fitted with a hemispherical joint to limit the possible misalignment resulting from imperfections in the moulds and errors during SRG installation. Finally, a T-cross section bracket attached to the reaction frame by means of two bolts (Figure 2(b)) was used to restrain the back of the block from uplifting. Subsequently, a pre-loading load of 2 kN was applied to eliminate any slack in the unbonded textile.

The tests were carried out in displacement control at the rate of 0.01 mm/s [6] using a 50 kN load cell. To measure the slip between composite and substrate, two linear variable displacement transducers (LVDTs) were attached to the edges of the loaded end of the bonded area, while another two LVDTs were attached to the concrete block (see Figures 2(b) and 4). The LVDTs were reacting against a U-shaped bracket attached to the bare fabric at an offset of 10 mm from the loaded end. To estimate the slip rate, the relative composite-to-substrate displacement at the loaded end of the bonded area was then calculated as the difference between the average displacement of the LVDTs on the concrete block and that of those on the SRG. Digital image correlation (DIC) was also used to measure the slip and the strain in the unbonded textile by tracking the movement of small targets (3 mm diameter) attached at different locations near the loaded end of the bonded area. Figure 4 provides a schematic representation of the loaded end of the SRG composite with all DIC targets.

3 RESULTS OF DIRECT TENSILE TESTS AND LAP-SPLICE TESTS

3.1 DIRECT TENSILE TESTS

Tables 1 and 2 collect the results of the direct tensile and lap-splice tests for specimens with S4 and S8 textile, respectively. In these tables, the peak stress (f_t), the peak strain (ε_t), and the tensile modulus of elasticity in the uncracked stage (E_I) and in the cracked stage (E_{II}) are listed. The stress-strain response curves in Figure 5 display an initial linear stage, in which the mortar matrix was uncracked, followed by a second stage where multiple transversal cracks developed. Once the crack pattern was stabilized (no new cracks appeared), the increase of external load was associated with an enlargement of existing cracks, until failure. Such a three-stage behaviour has already been observed on similar SRG composites comprising high-strength cement or geopolymer mortars [1]. SRG composites with S4 textile failed by nearly simultaneous rupture of all cords. In the case of S8, however rupture of the cords occurred in a more progressive manner due to the more pronounced uneven load distribution across the larger number of cords.

3.2 LAP-SPLICE TESTS

Lap-splice tests were characterized by an initial phase, in which the specimen was uncracked. Then the first (main) transversal crack developed at the end of the overlap on the side of the single textile layer. After this point, the width of the main crack increased with the increase of the applied load while other cracks progressively appeared on the portion of the coupon comprising one ply of textile (Figure 6(a)). On the contrary, the surface of the other portion remained uncracked. A longitudinal crack also appeared, and progressively extended, through the thickness of the coupon along the overlap (Figure 6(b)). All specimens failed by relative sliding between the textile layers, with the exception of only one specimen with S4 textile and 300 mm overlap length, in which rupture of the cords occurred.

Figure 7 illustrates the stress-slip response curves of the lap-splice tests. For better comparison, the peak stress values attained in the direct tensile tests and lap-splice tests on SRG specimens and their corresponding slip are plotted in Figure 8. The stress (f) in these figures is referred to one ply of textile, while the slip (s) is the relative displacement between the two portions of coupon separated by the main crack. As explained before, the main crack developed at the end of the overlap length, on the side of the coupon comprising one textile layer. To calculate such slip, two points on either side of the main crack were selected at the end of the test, and their relative displacement was derived from the DIC displacement field measurements. The values of peak stress (f_t) attained in lap-splice tests and direct tensile tests are also listed in Table 1 together with the ultimate slip (s_u), which is defined as the slip corresponding to f_t.

In the specimens comprising S4 textile, a brittle failure was observed with the shortest overlap length (L'=100 mm), whereas for L'=200 mm and L'=300 mm a nearly constant stress was detected after the peak, under increasing slip. In this phase of the test, the portion of the overlap involved in the load transfer process progressively shifted away from the main crack. The maximum stress reached by using L'=200 mm and L'=300 mm was similar to the SRG tensile strength, suggesting that the effective transfer length is between 100 mm and 200 mm. It should be considered that the peak stress in lap-splice tests might be expected to be slightly lower than that of direct tensile tests (in this study, by 9% on average) due to unavoidable misalignments and also the different clamping conditions of the textile on one side (at the overlap), which could cause an uneven stress distribution amongst the cords.

The response of SRG specimens with S8 textile was different from that of S4. The peak stress was lower (on average 37-39% of the tensile strength) due to the higher cord density, which let a smaller amount of mortar matrix pass through the cords and, therefore, led to a lower textile-to-textile load transfer capacity. As for S4, the effective transfer length for S8 was estimated to be between 100 mm and 200 mm.

4 RESULTS OF SHEAR BOND TESTS

4.1 FAILURE MODES

The classification adopted by TC RILEM 250 CSM [22] was used to characterise the modes of failure of the bond test specimens (Fig. 9). Based on the experimental results, the following three distinct modes of failure were observed:

- Textile rupture (denoted as "E1"in Fig. 9) was characterised by the tensile failure of the steel cords immediately outside the bonded area (Figs. 10(a, b)), generally starting from an edge cord and propagating to the rest of the cords. This mode of failure was observed in the specimens with one layer of 4 cords/in textiles (SB-L-4-1, SB-M-4-1, Tables 3 and 4);
- Debonding at the matrix-to-substrate interface (denoted as "B" in Fig. 9) was observed mainly in the specimens with 2 and 3 layers of 4 cords/in textiles (SB-L-4-2, SB-L-4-3, SB-M-4-2, SB-M-4-3, Tables 3 and 4) and also in specimens with 3 layers of 8 cords/in textiles (SB-L-8-3, SB-M-8-3, Tables 3 and 4). The SRG strip was fully detached, while remaining almost intact with chunks of concrete substrate (Figs. 10(c, d));
- Debonding at the interface between the bottom layer of grout and the steel fabric (Figs. 10(e, f)) (denoted as "C" in Fig. 9) was observed in specimens with 1 and 2 layers of 8 cords/in textiles (SB-L-8-1, SB-L-8-2, SB-M-8-1, SB-M-8-2, Tables 3 and 4).

4.2 STRESS-SLIP RESPONSE

Tables 3 and 4 present the key results obtained from the shear bond tests, namely:

- The maximum load (P_{max}) and the associated maximum axial stress (f_{max}) in the textile. f_{max} is defined as:

$$f_{max} = \frac{P_{max}}{n * A_{cord}} \quad (1)$$

where n is the number of steel cords and A_{cord} is the cross sectional area of one cord.

- The slip at the loaded end of the SRG strip ($s_{com\,(LVDT)}$) obtained from the average value of relative displacement measured by the LVDTs (see Fig. 4) as follows:

$$s_{com(LVDT)} = \frac{(LVDT_{sub,l} - LVDT_{com,l}) + (LVDT_{sub,r} - LVDT_{com,r})}{2} \quad (2)$$

- The slip at the loaded end of the SRG strip derived through DIC ($s_{com\,(DIC)}$), calculated as follows:

$$s_{com(DIC)} = \frac{(d_{com,l} - d_{sub,l}) + (d_{com,r} - d_{sub,r})}{2} \quad (3)$$

where the distances $d_{sub,l}$, $d_{sub,r}$, $d_{com,l}$ and $d_{com,r}$ are defined in Fig. 4.

- The slip between the cords and the grout, s_{cor}, measured as the relative displacement between a DIC target attached to one cord and a target attached to the loaded end of the SRG bonded area, minus the elongation of the cord between these two targets (Eq. 4).

$$s_{cor} = \frac{(d_{cor,l1} - d_{com,l}) - (\varepsilon_{cor,l} \times L_{l2}) + (d_{cor,r1} - d_{com,r}) - (\varepsilon_{cor,r} \times L_{r2})}{2} \quad (4)$$

where

$$\varepsilon_{cor,l} = \frac{(d_{cor,l1} - d_{cor,l2})}{L_{l1}} \; and \; \varepsilon_{cor,r} = \frac{(d_{cor,r1} - d_{cor,r2})}{L_{r1}} \quad (5)$$

The definition of the various distances measured are depicted in Fig. 4. The slip values presented in Tables 3 and 4 correspond to the maximum load, P_{max}.

Figures 11-12 show the stress-slip response curves obtained from the LVDTs, whilst Figure 13 shows the average maximum load and the average maximum axial stress for the specimens with different number of layers, as well as the observed failure mode. The average slip at maximum load for specimens with different layers of SRG is presented in Figure 14.

The average stress-slip response curves obtained from DIC and LVDTs are compared in Figure 15(a). A good agreement between the two measurement methods was observed for the tests on SRG reinforcements comprising 1 and 2 textile plies, whereas in the case of 3 layers, the curves obtained from DIC showed a stiffer behaviour than those obtained from LVDTs. This stiffer behaviour was associated with slippage between the cords and the bracket where the LVDTs were reacting against, which resulted in exaggerated readings of the LVDTs compared to DIC system.

Data from DIC shows a small slip of steel cords inside the SRG (less than 0.23 mm) for all tested series, with the highest slip being associated with composites comprising one layer of the low-density steel textile (series SB-L-4-1 and SB-M-4-1) as shown in Figure 15 (b).

4.3 INFLUENCE OF NUMBER OF LAYERS

The variation in the modes of failure observed in the SRG systems between 1 and 2, 3 layers of S4 textile (i.e. mode "E1" for one layer and mode "B" for 2 and 3 layers, see section 4.1) was not associated with clear changes in the average maximum load, which for the six specimen sets ranged between 17.5 kN and 20.5 kN (Tables 3 and

4). As a result of the addition of more plies, the peak axial stress reduced from 2170~2470N/mm^2 for 1 ply to 750~1150N/mm^2 for 2 and 3 plies (55~70% decrease). It should be noted that the test results were more scattered for multi-ply SRGs than for one ply. Based on the results obtained in this study, applying more than one layer of steel fabric with 4 cords/in does not increase the effective load capacity of the system.

In the case of SRG systems comprising S8 textile, the peak load (P_{max}) increased from 15 kN for 1 layer to 25~26 kN for 2 layers (62~73% increase) (Tables 3 and 4, series SB-L-8-1, SB-L-8-2, SB-M-8-1 and SB-M-8-2), while the same mode of failure was observed (mode "C" see section 4.1). The addition of a third layer changed the mode of failure to detachment at matrix-to-substrate interface (mode "B" see section 4.1) with the bond capacity reaching values of 26 and 29.5 kN for series SB-L-8-3 (Table 3) and SB-M-8-3 (Table 4), respectively. The change in the mode of failure from "C" to "B" is mainly attributed to the lower stress per cord and the lower bond stress between the cord and the mortar. However, the bond stress at the mortar – concrete interface reached higher stresses and failed. As for the peak axial stress in the textile, passing from 1 to 2 plies was associated to a reduction from 940~960N/mm^2 to 780~813N/mm^2 (13~19% reduction), respectively, whereas the addition of the third layer entailed a further decrease by 25~31% (the peak axial stress was 540~610N/mm^2 and the reduction with respect to 1 ply was 35~44%).

Finally, increasing the number of textile layers reduced the ultimate slip in the specimens strengthened with the low-density steel fabric. More specifically, in series SB-M-4, $s_{com\ (LVDT)}$ reduced, on average, from 1.9 mm (1 ply) to 1.0 mm (2 plies) and to 0.6 mm (3 plies) (Table 4), whereas for SB-L-4, $s_{com\ (LVDT)}$ reduced, on average from 1.9 mm (1 ply) to 0.8 mm (2 plies) and to 0.9 mm (3 plies) (Table 3). On the contrary, the effects on the ultimate slip detected for SRG systems with S8 textile were less significant due to the changes in the mode of failure ($s_{com\ (LVDT)}$ being 0.82~1 mm for SB-M-8 (Table 4) and 0.65~0.74 mm for SB-L-8 (Table 3)).

4.4 INFLUENCE OF TEXTILE DENSITY

The influence of textile density on the SRG-to-substrate load transfer mechanism has already been investigated in several studies that dealt with one-ply systems [e.g. 12]. In general, the larger spaces between the cords of the lower density textiles (S4) allow a larger amount of mortar to pass through the textile, which results in a better interlaminar shear capacity with respect to denser fabrics [1]. Analogous considerations can be made for any FRCM, independently from the utilised textile material [16]. The results achieved in the present investigation are consistent with existing literature.

SRG composites with one ply of S4 textile exhibited an average maximum load of approximately 19 kN (series SB-L-4-1 and SB-M-4-1, Tables 3 and 4), which was slightly higher than that of the systems with one ply of S8 (15 kN, series SB-L-8-1 and SB-M-8-1, Tables 3 and 4). The larger cross sectional area of S8 textile with respect to S4 highlights the influence of textile density on SRG effectiveness, since the peak axial stress of SRGs with S4 was, on average, 2.5 times higher than that with S8 (Table 4). In terms of failure mode, all specimens with one ply of S4 textile exhibited cord rupture (mode "E1") except from specimen SB-M-4-1-2, which failed by composite-to-substrate debonding (mode "B") at a lower failure load (12kN). The specimens with S8 textile (SB-L-8-1 and SB-M-8-1 series), instead, failed by debonding at the interface between fabric and matrix (mode "C").

Textile density affected the trends associated with the increase of plies (see Figures 13 and 14 and see also comments in Section 4.3). SRG systems with S4 textile exhibited similar peak loads independently from the number of plies, which was associated with a nearly linear reduction of peak axial stress with the increase in the number of textile plies. Furthermore, the failure mode changed from tensile rupture (mode "E1" Fig. 9) for 1-ply systems to debonding at the interface with the substrate (mode "B" Fig. 9) for multi-ply systems. On the contrary, composites with S8 exhibited an increase of peak load and a less pronounced decrease of stress, with a quasi-stabilization for

multi-ply systems, as the increase of P_{max} was proportional to the increase of cross-sectional area when passing from 2 to 3 plies. It is worth noting that the peak axial stress attained by SRGs with S4 was always higher than that with S8. Finally, for these specimens failure occurred at the interface between fabric and matrix (mode "C") for 1 and 2 plies, and between matrix and substrate (mode "B") for 3-ply SRGs.

The density of the steel textile affected the ultimate slip of the specimens strengthened with only one layer of textile. There was a reduction of approximately 60% and 50% in the ultimate slip when increasing the density of steel textile from 4 to 8 cords/in for series SB-L and SB-M, respectively. On the other hand, specimens strengthened with 2 and 3 layers exhibited a slight change in terms of ultimate slip when the textile density was increased from 4 to 8 cords/in.

4.5 INFLUENCE OF CONCRETE COMPRESSIVE STRENGTH

As seen in Tables 3 and 4, half of the tested specimens failed due to detachment at the substrate-to-matrix interface ("B"), suggesting that the mechanical properties of the concrete substrate may play a role in the bond behaviour of the composite system. However, from the tests results obtained in this study, no solid conclusions can be drawn on the influence of concrete compressive strength due to the complex nature of shear bond test, particularly when multiple layers of steel textile reinforcement are applied. Possible imperfections in fabrication might have introduced misalignments between the different textiles layers, thus resulting in a non-uniform distribution of stresses, and thus to variation of the modes of failures between detachment at matrix-to-substrate (mode "B") and textile-to-matrix interface (mode "C" Fig. 9).

5. CONCLUSIONS

An experimental study was performed on the bond behaviour of SRG systems comprising multiple layers of galvanized UHTSS textiles and a geopolymer mortar. Two different textiles were used with 4 cords/in and 8 cords/in density. First lap-splice tests were conducted to provide information on the textile-to-textile load transfer capacity. The effective transfer length was found to be between 100 mm and 200 mm for both fabrics. Further increase of the overlap length did not improve the load transfer capacity but led to a larger ultimate relative slip associated with a progressive shifting of the overlap area effectively involved in the load transfer process. Textile density highly affected the textile-to-textile bond capacity, which was higher for the SRG composites with 4 cords/in than for those with 8 cords/in, demonstrating that the textile-to-textile bond capacity relies on the amount of mortar passing through the voids between the cords.

Subsequently, single-lap shear bond tests provided information on the bond performance on concrete substrates. SRG systems comprising 4 cords/in textiles exhibited similar peak load values independently from the number of plies, and accordingly, the stress at detachment decreased linearly with the increase of the number of layers. The use of multi-ply SRG with low density textile, therefore, does not appear to be very effective for flexural strengthening applications. As for the failure mode, cord rupture (1 ply) was changed to debonding at the SRG-to-substrate interface (2 and 3 plies). The use of multiple layers of steel textile with 8 cords/in led to an increase of the maximum load that can be transferred from the SRG system to the substrate. Specimens with 1 and 2 plies failed by textile-to-matrix detachment, whereas in those with 3 plies failure took place at the interface between concrete substrate and SRG strip. The gain in strength with the increase of the number of layers was less than linear, which was associated with a decrease of the peak axial stress, indicating a lower efficiency of multi-ply SRGs with respect to those with one fabric layer. The concrete substrate was involved in the mode of failure (matrix-to-substrate interface) for 50% of the tested specimens. However, it was not clear what is the influence of the concrete compressive strength on the bond behaviour due to the complex nature of shear bond tests with multiple layers.

Further investigation is still needed on the bond behaviour of multi-ply SRG reinforcements in order to estimate their effectiveness, assess the ultimate strength of retrofitted structural members, and develop design formula that are oriented to the optimized use of reinforcement materials. Strengthening details (such as the use of mechanical connectors) should also be developed in order to ensure a fruitful knowledge transfer from the research to the structural rehabilitation practice.

ACKNOWLEDGMENTS

The materials for this investigation (steel textiles and mortar) were provided by Kerakoll S.p.A. (Sassuolo, MO, Italy). S.A. would like to thank Shaqra University in Saudi Arabia and Saudi Arabian Cultural Bureau in the UK for funding this part of his PhD research. S.D.S., G.d.F. and F.R. acknowledge funding from Regione Lazio for the Research Project "SICURA Sustainable technologies for the seismic protection of the cultural heritage" (2018-2020) and from the Italian Ministry of Education, University and Research (MIUR), for the grant attributed to the Department of Engineering of Roma Tre University, in the frame of the Departments of Excellence Initiative (2018-2022).

REFERENCES

1. S. De Santis, F. Ceroni, G. de Felice, M. Fagone, B. Ghiassi, A. Kwiecień, G. Lignola, M. Morganti, M. Santandrea, M. Valluzzi, A. Viskovic. Round Robin Test on tensile and bond behaviour of Steel Reinforced Grout systems. Compos B Eng 2017b: 127: 100-120.
2. G.E. Thermou, S.J. Pantazopoulou, A.S. Elnashai. Global interventions for seismic upgrading of substandard RC buildings. J Struct Eng 2012; 138(3): 387-401.
3. M. Matana, A. Nanni, L.R. Dharani, P. Silva, G. Tunis. Bond Performance of steel reinforced polymer and steel reinforced grout. In: Proceedings of BBFS Conference. Hong Kong, December, 2005.
4. X. Huang, V. Birman, A. Nanni, G. Tunis. Properties and potential for application of steel reinforced polymer and steel reinforced grout composites. Compos B Eng 2005; 36 (1): 73-82.
5. G. de Felice, S. De Santis, L. Garmendia, B. Ghiassi, P. Larrinaga, P.B. Lourenço, D.V. Oliveira, F. Paolacci, C.G., Papanicolaou. Mortar-based systems for externally bonded strengthening of masonry. Mater Struct 2014; 47(12): 2021-2037.
6. L. Ascione, G. de Felice, S. De Santis. A qualification method for externally bonded Fibre Reinforced Cementitious Matrix (FRCM) strengthening systems. Compos B Eng 2015; 78: 497-506
7. J. Donnini, V. Corinaldesi, A. Nanni. Mechanical properties of FRCM using carbon fabrics with different coating treatments. Compos B Eng 2016; 88: 220-228
8. E. Stievanin, F. Da Porto, M. Panizza, E. Garbin, C. Modena. Bond characterization between historical concrete substrate and SRG/SRP strengthening systems. In: Proceedings of SEMC Conference. Cape Town, September, 2013.
9. F. Bencardino, A. Condello, A. F. Ashour. Single-lap shear bond tests on Steel Reinforced Geopolymeric Matrix-concrete joints. Compos B Eng 2017; 110: 62-71
10. F. Ascione, M. Lamberti, A. Napoli, R. Realfonzo. Experimental bond behavior of Steel Reinforced Grout systems for strengthening concrete elements. Constr Build Mater 2020; 232: 117105
11. A. Razavizadeh, B. Ghiassi, D. V. Oliveira. Bond behaviour of SRG-strengthened masonry units: Testing and numerical modelling. Constr Build Mater 2014; 64: 387-397.

12. S. De Santis, G. de Felice. Steel reinforced grout systems for the strengthening of masonry structures. Compos Struct 2015; 134: 533-548.
13. S. De Santis. Bond behaviour of Steel Reinforced Grout for the extrados strengthening of masonry vaults. Constr Build Mater 2017; 150: 367-382
14. A. Bilotta, F. Ceroni, E. Nigro, M. Pecce. Experimental tests on FRCM strengthening systems for tuff masonry elements. Constr Build Mater 2017; 138: 114-133.
15. S. De Santis, F. Carozzi, G. de Felice, C. Poggi. Test methods for Textile Reinforced Mortar systems. Compos B Eng 2017a; 127: 121-132.
16. G. de Felice, G., D'Antino, A., De Santis, S., Meriggi, P., Roscini, F. Lessons learned on the tensile and bond behaviour of Fabric Reinforced Cementitious Matrix (FRCM) composites. Frontiers in Built Environment 2020; 6: 5.
17. G. de Felice G, Aiello MA, Caggegi C, Ceroni F, De Santis S, Garbin E, Gattesco N, Hojdys Ł, Krajewski P, Kwiecień A, Leone M, Lignola GP, Mazzotti C, Oliveira D, Papanicolaou C, Poggi C, Triantafillou T, Valluzzi MR, Viskovic A. Recommendation of RILEM TC 250-CSM: Test method for Textile Reinforced Mortar to substrate bond characterization. Mater Struct 2018; 51 (4): 95.
18. A. Napoli, R. Realfonzo. Reinforced concrete beams strengthened with SRP/SRG systems: Experimental investigation. Constr Build Mater 2015; 93: 654-677.
19. Products.kerakoll.com. 2020. Technical Data Sheet For Geo-Lite Mortar. [online] Available at: https://products.kerakoll.com/yep-repository/kerakoll/media/Geolite__rating_2019_EN.pdf
[Accessed 24 April 2020].
20. S. De Santis S, Hadad HA, De Caso y Basalo FJ, de Felice G, Nanni A. Acceptance Criteria for Tensile Characterization of Fabric Reinforced Cementitious Matrix (FRCM) Systems for Concrete and Masonry Repair. J Compos Const 2018; 22(6): 04018048. DOI: 10.1061/(ASCE)CC.1943-5614.0000886.
21. M. Tekieli, S. De Santis, G. de Felice, A. Kwiecień, F. Roscini. Application of Digital Image Correlation to composite reinforcements testing. Compos Struct 2017; 160: 670-688.
22. G. de Felice, M.A. Aiello, C. Caggegi, et al. Recommendation of RILEM Technical Committee 250-CSM: Test method for Textile Reinforced Mortar to substrate bond characterization. Mater Struct 2018; 51: 95

FIGURES

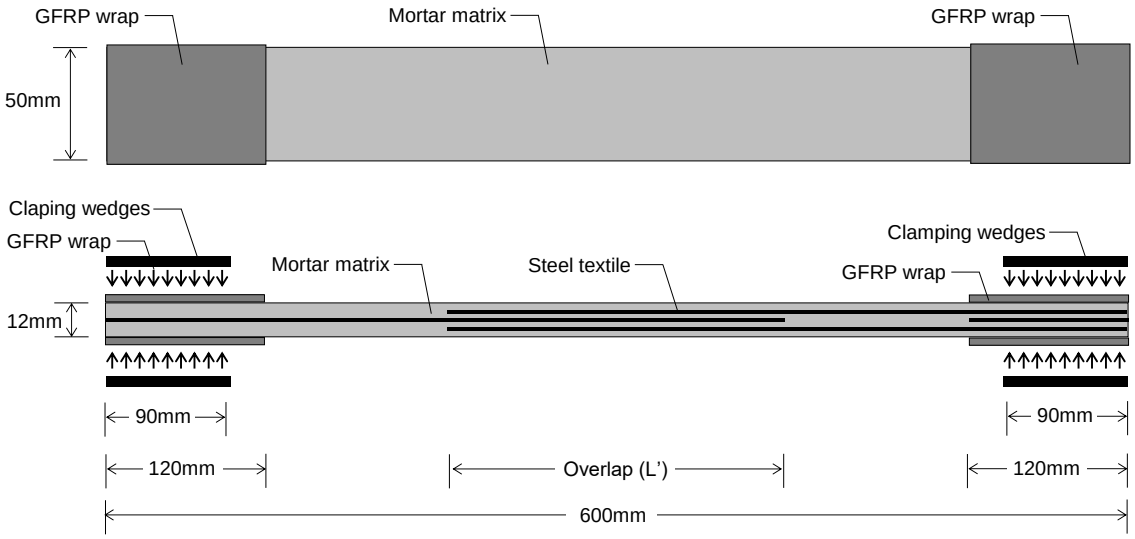

Figure 1. *Top and side view of SRG specimens for lap-splice tests.*

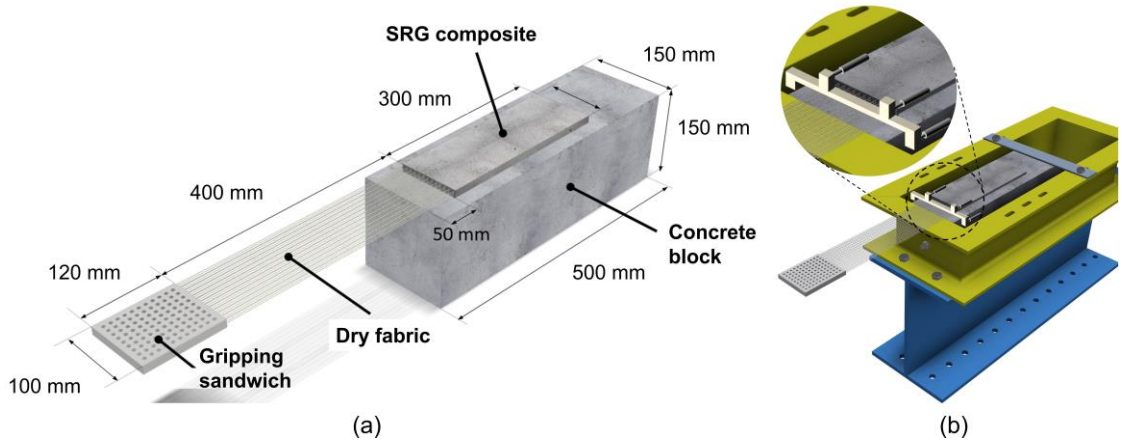

Figure 2. *(a) Geometry of specimens and (b) setup of single-lap shear bond test with a zoomed view on the loaded area.*

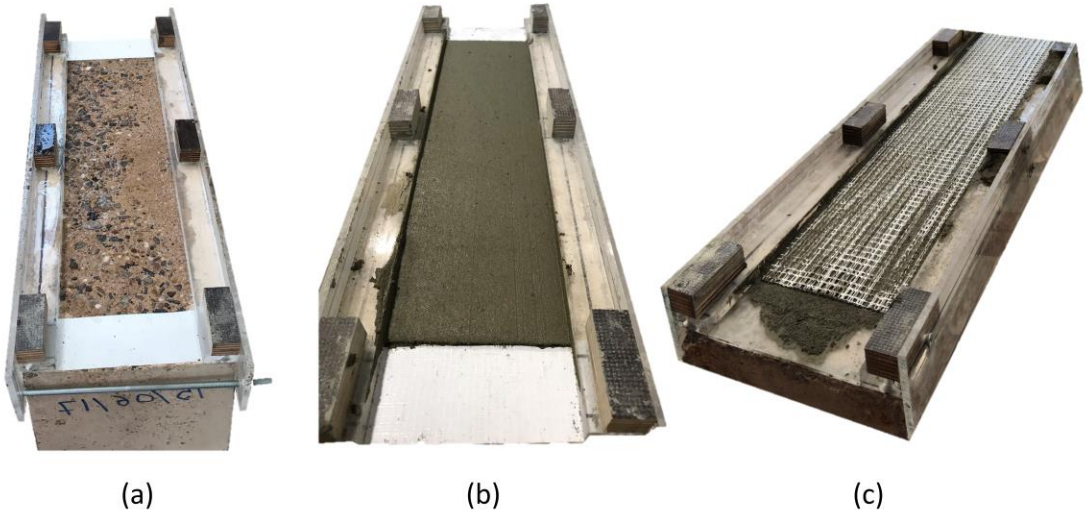

Figure 3. *Steps of the manufacturing process of specimens for shear bond tests: (a) grinded surface prior to the application of the first layer of grout, (b) application of the first layer of grout, and (c) first layer of steel textile placed on top of the grout layer.*

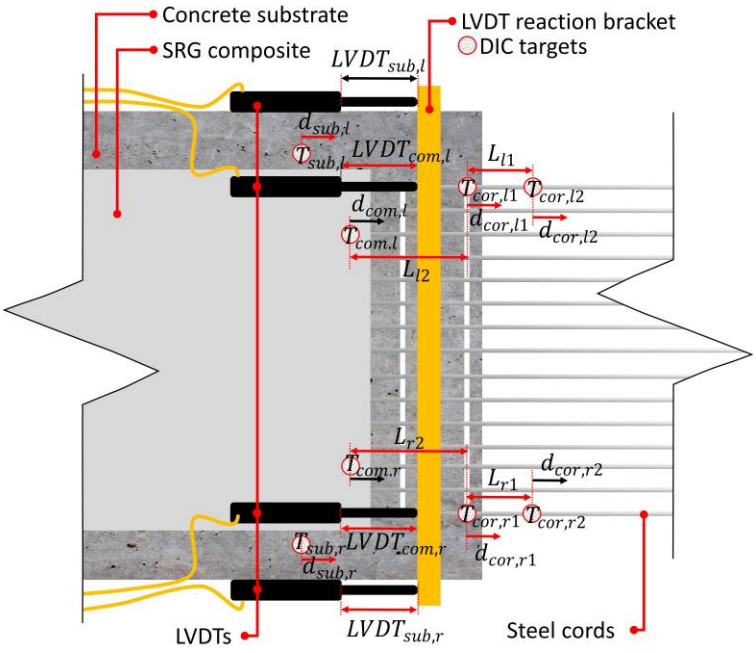

Figure 4. *Schematic presentation of the properties (slip of composite, slip of cords, and strain in cords) measured by using DIC system.*

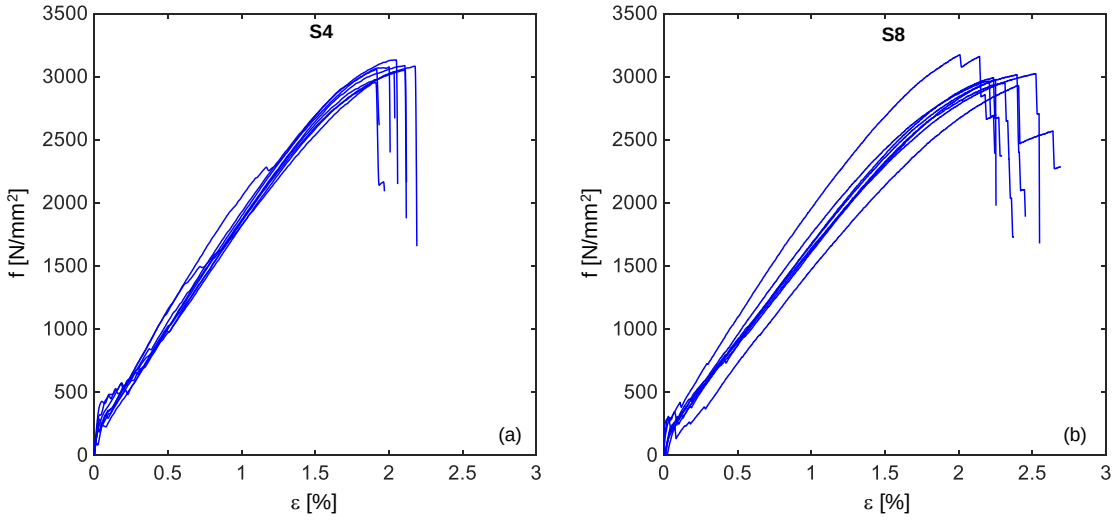

Figure 5. *Stress-strain response curves of direct tensile tests on SRG coupons comprising (a) S4 and (b) S8 textiles.*

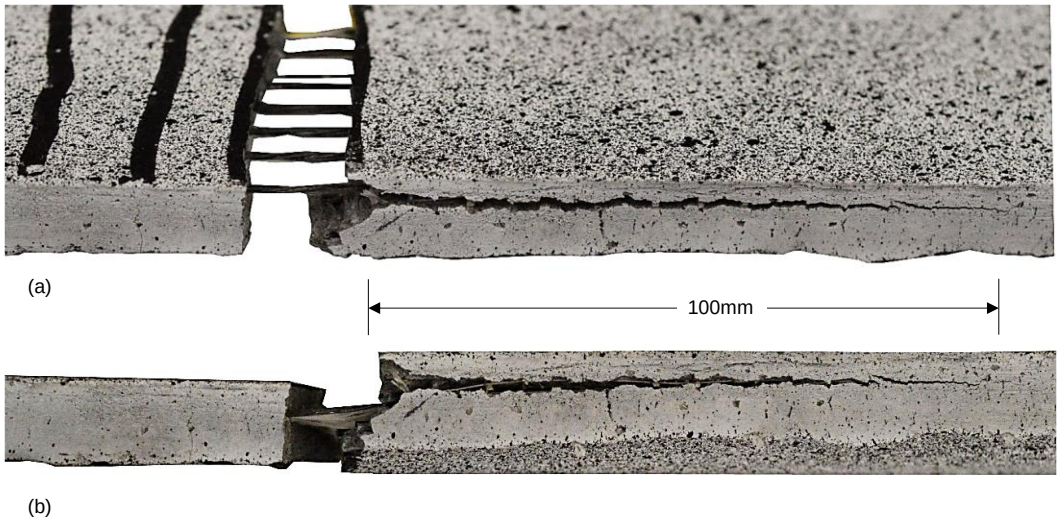

Figure 6. *(a) Isometric and (b) side views of the crack pattern observed in lap-splice tests (LS-4-100-2 specimen).*

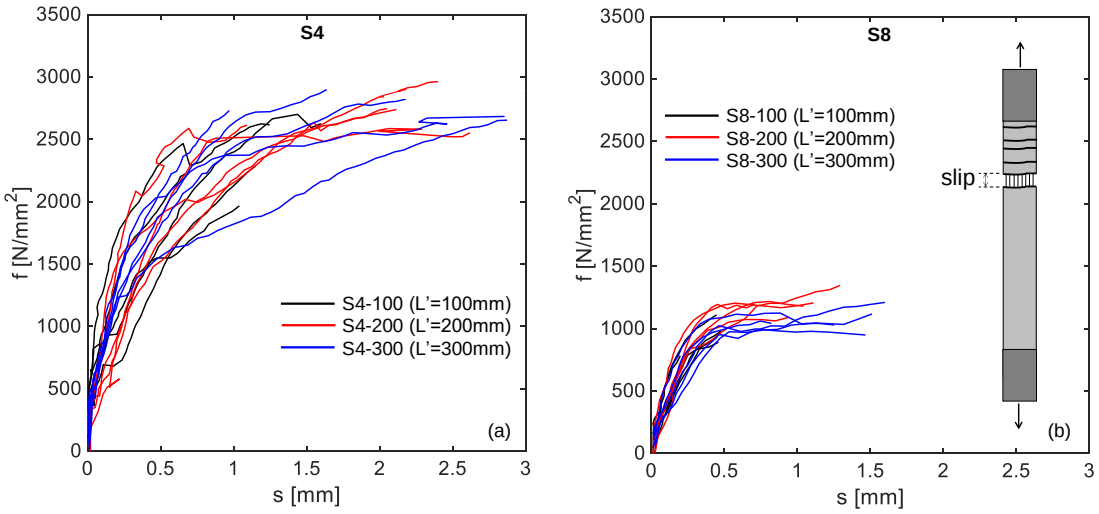

Figure 7. *Stress-slip response curves of lap-splice tests on SRG specimens comprising (a) S4 and (b) S8 textiles.*

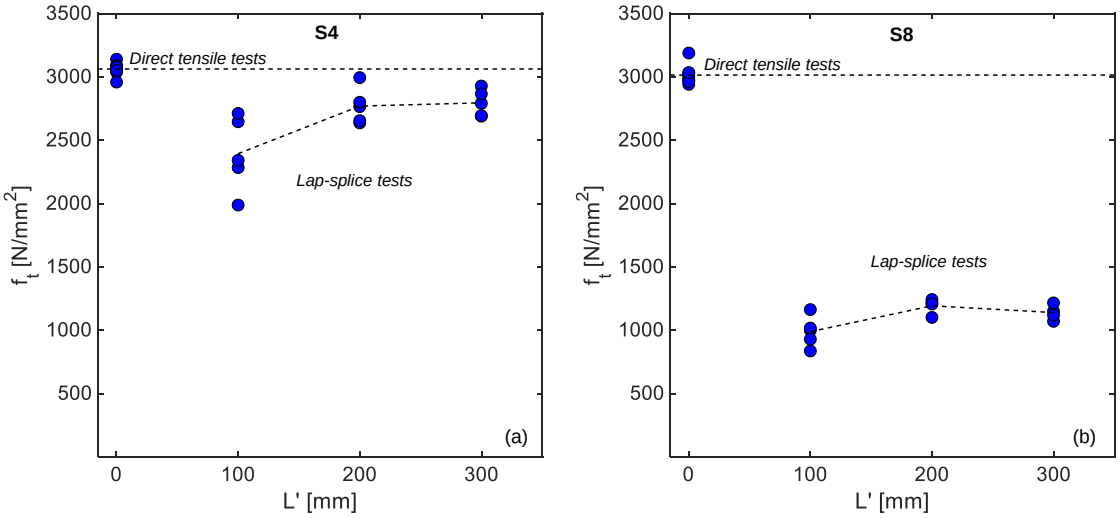

Figure 8. *Peak stress attained in direct tensile tests and in lap-splice tests on SRG specimens comprising (a) S4 and (b) S8 textiles.*

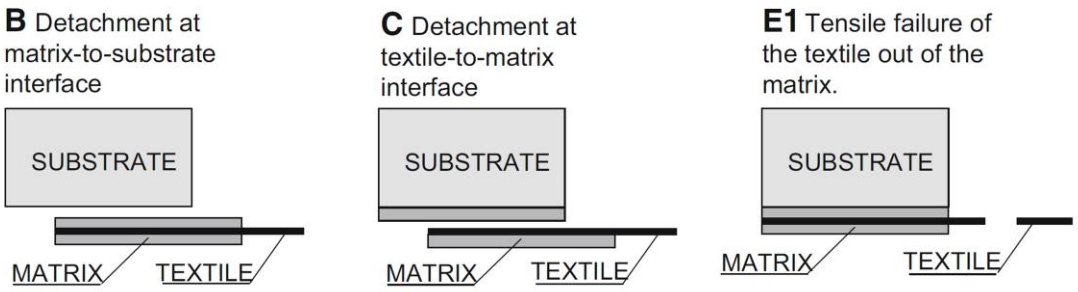

Figure 9. *Modes of failure observed in the bond tests according to TC RILEM 250 CSM [22].*

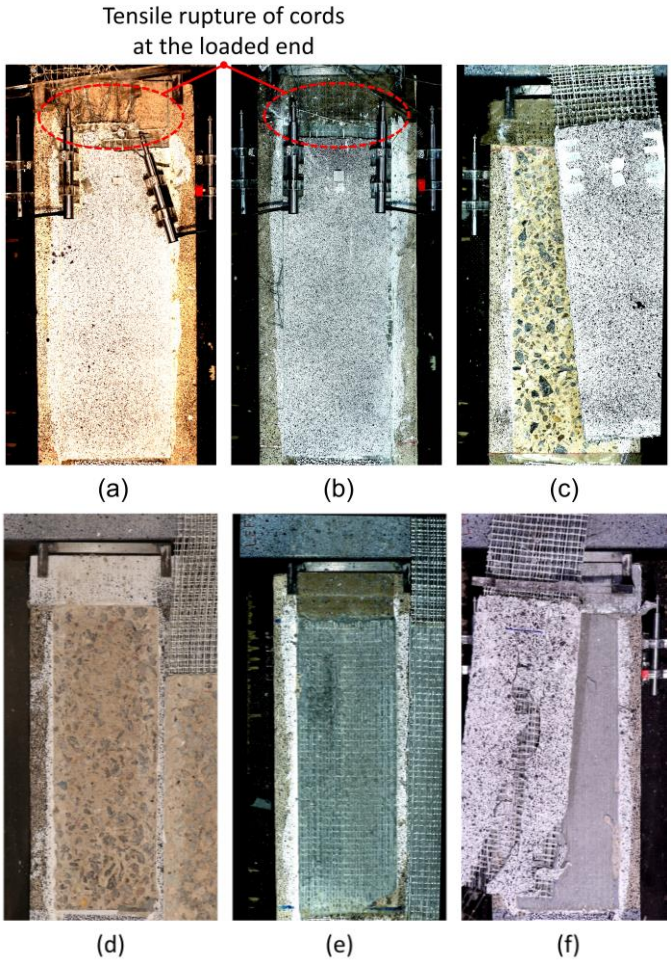

Figure 10. *Failure modes detected in shear bond tests: fabric rupture [Mode E1] in (a) SB-L substrates and (b) SB-M substrates, debonding at the substrate-to-matrix interface [Mode B] in (c) SB-L substrates and (d) SB-M substrates, detachment and the textile-to-matrix interface [Mode C] in (e) SB-L substrates and (f) SB-M substrates.*

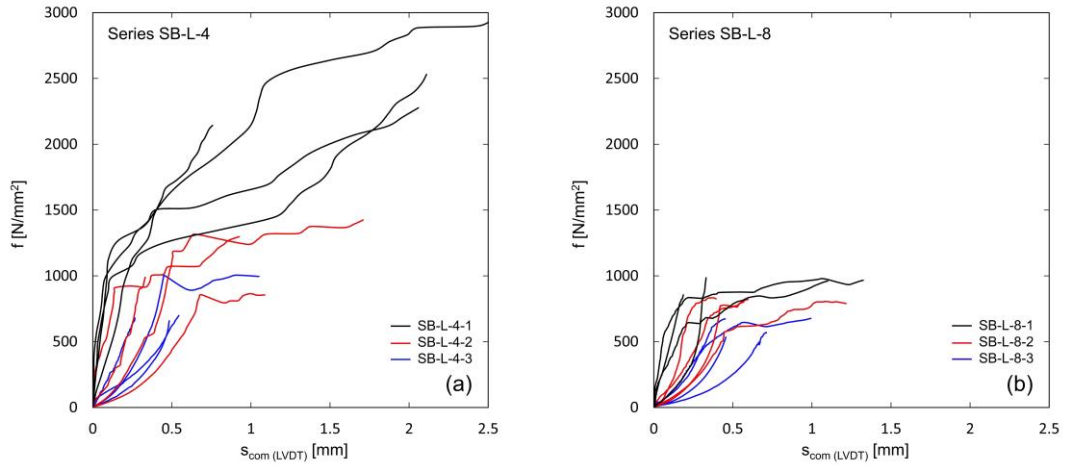

Figure 11. *Stress-slip response curves of shear bond tests on low compressive strength substrate: (a) SB-L-4 and (b) SB-L-8 series.*

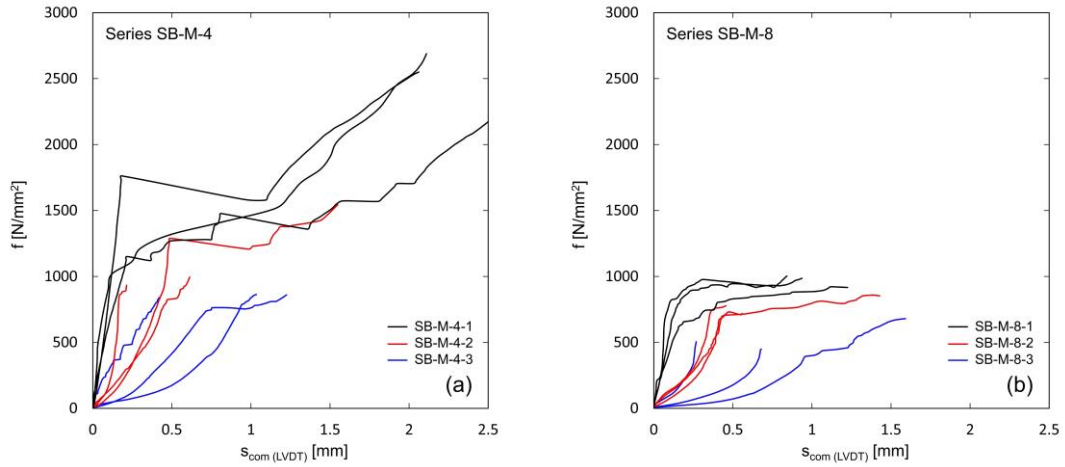

Figure 12. *Stress-slip response curves of shear bond tests on medium compressive strength substrate: (a) SB-M-4 and (b) SB-M-8 series.*

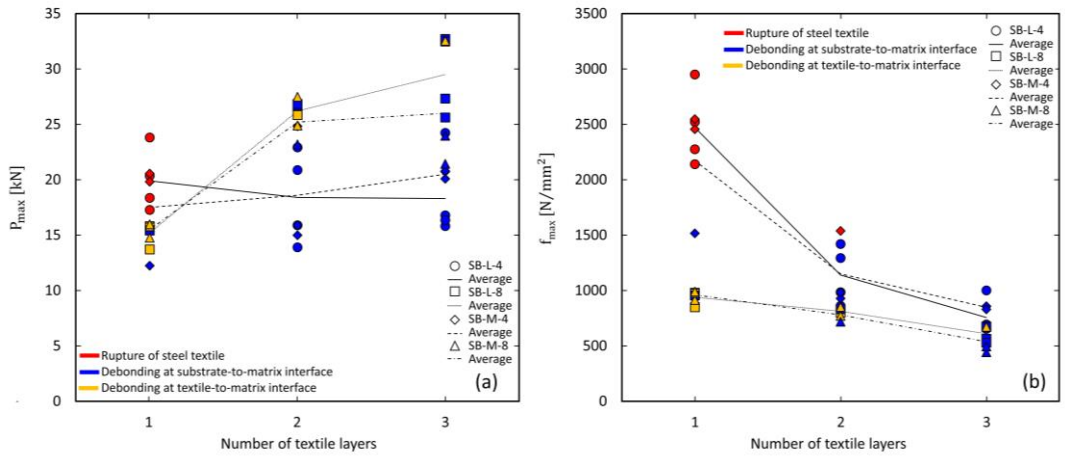

Figure 13. *(a) Peak load and (b) peak axial stress attained in shear bond tests vs. number of textile layers.*

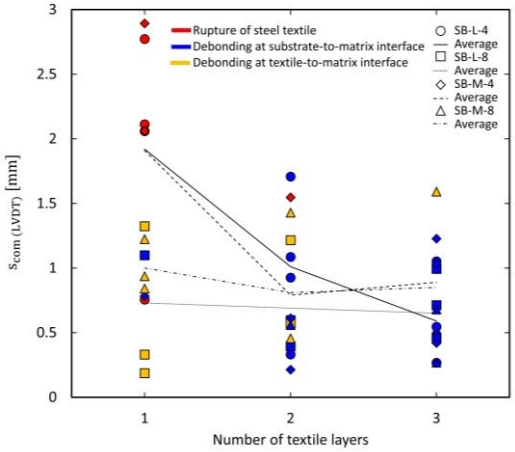

Figure 14. *Corresponding slip attained in shear bond tests vs. number of textile layers.*

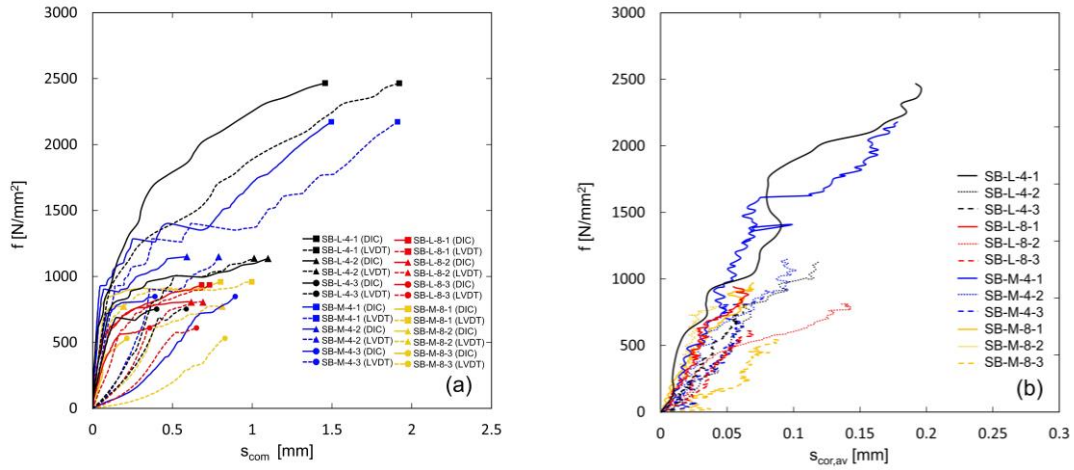

Figure 15. *The average stress-slip of composite response curves obtained from DIC system and LVDTs and (b) the average stress-slip of cords response curves.*

TABLES

Table 1. *Results of direct tensile tests and lap-splice tests for specimens with S4 textile*

Group	Specimen	f_t N/mm^2	ε_t %	E_I kN/mm^2	E_{II} kN/mm^2	s_u mm
DT-4	1	3134.6	2.05	1815	178.5	
	2	3089.4	2.12	1885	170.6	
	3	3084.2	2.19	1658	164.8	
	4	3041.5	2.06	1701	172.0	
	5	3054.5	2.13	1688	172.8	
	6	2958.6	1.93	1640	188.7	
	7	3080.3	2.04	1601	181.1	
	8	3063.8	1.95	1718	194.5	
	Average	3063.3	2.06	1713.3	177.9	
	St. dev.	50.7	0.09	93.9	9.9	
	CV (%)	2	4	5	5	
LS-4-100	1	2224.3				0.67
	2	2624.3				1.19
	3	1966.9				1.04
	4	2286.3				1.15
	5	2700.3				1.44
	Average	2360.4				1.10
	St. dev.	301.7				0.28
	CV (%)	13				25
LS-4-200	1	2739.3				2.11
	2	2588.1				0.69
	3	2745.7				2.05
	4	2962.7				2.40
	5	2613.6				1.09
	Average	2729.9				1.67
	St. dev.	148.4				0.74
	CV (%)	5				44
LS-4-300	1	2730.7				0.97
	2	2898.5				1.64
	3	2653.7				2.87
	4	2804.2				2.11
	5	2683.7				2.86
	Average	2754.2				2.09
	St. dev.	98.7				0.82
	CV (%)	4				39

Table 2. *Results of direct tensile tests and lap-splice tests for specimens with S8 textile*

Group	Specimen	f_t N/mm^2	ε_t %	E_I kN/mm^2	E_{II} kN/mm^2	s_u mm
DT-8	1	2973.5	2.21	1651	181.4	
	2	3188.1	2.01	1655	190.6	
	3	3002.4	2.24	1901	172.7	
	4	2959.3	2.25	1855	169.7	
	5	3028.1	2.39	1499	174.0	
	6	2942.7	2.40	1888	169.6	
	7	2961.8	2.31	1653	169.5	
	8	3034.4	2.49	1403	156.1	
	Average	3011.3	2.29	1688.1	172.9	
	St. dev.	78.8	0.15	182.8	10.0	
	CV (%)	2	6	11	6	
LS-8-100	1	2224.3				0.47
	2	2624.3				0.45
	3	1966.9				0.48
	4	2286.3				0.46
	5	2700.3				0.20
	Average	2360.4				0.41
	St. dev.	301.7				0.12
	CV (%)	13				29
LS-8-200	1	1206.0				1.11
	2	1217.2				0.81
	3	1091.9				0.94
	4	1346.2				1.29
	5	1197.1				0.71
	Average	1211.7				0.97
	St. dev.	90.4				0.23
	CV (%)	7				24
LS-8-300	1	1060.6				0.75
	2	1124.8				0.88
	3	1210.2				1.60
	4	1117.4				1.51
	5	1023.7				0.46
	Average	1107.4				1.04
	St. dev.	71.0				0.49
	CV (%)	6				48

Table 3. *Results of shear bond tests on low compressive strength concrete substrates (series SB-L)*

Group	Specimen	P_{max} kN	f_{max} N/mm^2	$s_{com(LVDT)}$ mm	$s_{com\ (DIC)}$ mm	$s_{cor\ (DIC)}$ mm	MoF
SB-L-4-1	1	17.27	2140	0.76	0.69	0.24	E1
	2	20.35	2522	2.11	1.22	0.12	E1
	3	18.36	2275	2.06	0.94	0.31	E1
	4	23.81	2951	2.77	2.98	0.21	E1
	Average	19.95	2472	1.93	1.46	0.22	E1
	St. dev.	2.87	356	0.84	1.04	0.08	
	CV (%)	15	15	44	72	37	
SB-L-4-2	1	13.90	861	1.09	0.91	0.16	B
	2	22.92	1420	1.71	1.77	0.14	B
	3	15.89	984	0.33	0.29	0.12	B
	4	20.88	1294	0.93	1.43	0.08	B
	Average	18.40	1140	1.02	1.1	0.13	B
	St. dev.	4.21	261	0.57	0.65	0.03	
	CV (%)	23	23	56	60	24	
SB-L-4-3	1	24.24	1001	1.05	1.15	0.06	B
	2	15.82	653	0.48	0.14	0.15	B
	3	16.79	694	0.55	0.17	0.04	B
	4	16.35	675	0.27	0.15	0.04	B
	Average	18.3	756	0.59	0.4	0.07	B
	St. dev.	3.98	164	0.33	0.5	0.05	
	CV (%)	22	22	56	125	72	
SB-L-8-1	1	13.71	849	0.19	0.11	0.03	C
	2	15.81	979	0.33	0.2	0.05	C
	3	15.69	972	1.32	1.33	0.12	C
	4	15.42	955	1.1	1.12	0.11	B-C
	Average	15.16	939	0.74	0.69	0.08	C
	St. dev.	0.98	61	0.56	0.62	0.04	
	CV (%)	7	7	76	90	50	
SB-L-8-2	1	26.34	816	0.6	0.51	0.12	B
	2	25.87	801	1.22	0.93	0.3	C
	3	25.84	801	0.57	0.24	0.09	C
	4	26.84	832	0.39	0.8	0.09	B-C
	Average	26.22	813	0.7	0.62	0.15	C
	St. dev.	0.47	15	0.36	0.31	0.1	
	CV (%)	2	2	52	50	67	
SB-L-8-3	1	27.32	564	0.71	0.18	0.09	B
	2	25.62	529	0.46	0.2	0.03	B
	3	32.71	676	0.99	0.64	0.1	B
	4	32.48	671	0.45	0.42	0.08	B
	Average	29.53	610	0.65	0.36	0.08	B
	St. dev.	3.6	75	0.26	0.22	0.03	
	CV (%)	13	13	40	62	38	

Table 4. *Results of shear bond tests on medium compressive strength concrete substrates (series SB-M)*

Group	Specimen	P_{max} kN	f_{max} N/mm^2	$s_{com\ (LVDT)}$ mm	$s_{com\ (DIC)}$ mm	$s_{cor\ (DIC)}$ mm	MoF
SB-M-4-1	1	20.56	2548	2.06	1.66	0.19	E1
	2	12.24	1516	0.78	0.26	0.2	B
	3	19.82	2456	2.89	2.57	0.16	E1
	Average	17.54	2173	1.91	1.5	0.18	E1
	St. dev.	4.6	571	1.06	1.16	0.02	
	CV (%)	27	27	56	78	12	
SB-M-4-2	1	14.99	929	0.21	0.12	0.1	B
	2	24.83	1538	1.55	1.51	0.17	E1
	3	15.87	983	0.61	0.14	0.06	B
	Average	18.56	1150	0.79	0.59	0.11	B
	St. dev.	5.44	337	0.69	0.8	0.06	
	CV (%)	30	30	88	136	55	
SB-M-4-3	1	20.72	856	1.23	0.43	0.1	B
	2	20.78	858	1.04	0.07	0.06	B
	3	20.08	829	0.42	0.68	0.14	B
	Average	20.53	848	0.9	0.39	0.1	B
	St. dev.	0.39	16	0.42	0.31	0.04	
	CV (%)	2	2	47	80	40	
SB-M-8-1	1	14.76	915	1.22	N/A	N/A	C
	2	15.79	978	0.94	0.86	0.04	C
	3	15.98	990	0.84	0.75	0.13	C
	Average	15.51	961	1	0.81	0.09	C
	St. dev.	0.66	40	0.2	0.08	0.06	
	CV (%)	5	5	20	10	67	
SB-M-8-2	1	27.48	851	1.43	N/A	N/A	C
	2	24.90	771	0.46	0.2	0.05	C
	3	23.19	719	0.56	N/A	N/A	B
	Average	25.19	780	0.82	0.2	0.05	C
	St. dev.	2.16	66	0.53			
	CV (%)	9	9	65			
SB-M-8-3	1	32.54	672	1.59	0.54	0.16	C
	2	21.43	443	0.68	0.07	0.04	B
	3	23.97	495	0.27	0.08	0.11	B
	Average	25.98	537	0.85	0.23	0.1	B
	St. dev.	5.82	120	0.68	0.27	0.06	
	CV (%)	23	23	80	118	60	

Appendix G Database of bond models

Cited in	Predicted Property	Model
Hiroyuki and Wu Model	Shear stress	$\tau_u = 0.27\,.\,L^{-0.669}$
[1]	Debonding load	$P_u = \tau_u\,.\,L\,.\,b_p$
Tanaka Model	Shear stress	$\tau_u = 6.13 - In(L)$
[1]	Debonding load	$P_u = \tau_u\,.\,L\,.\,b_p$
Maeda Model	Shear stress	$\tau_u = (110.2\,x10^{-6})\,.\,E_p\,.\,\ t$
[1]	Debonding load	$P_u = \tau_u\,.\,L_e\,.\,b_p$
	Effective length	$L_e = e^{2.1235-0.580\,.\ In(E_p\,.\,t_p)}$
Khalifa et al. Model	Shear stress	$\tau_u = (110.2\,x\,10^{-6})\,.\,(f_c'/42).E_p\,.\,\ t_p$
[1]	Debonding load	$P_u = \tau_u\,.\,L_e\,.\,b_p$
	Effective length	$L_e = e^{2.1235-0.580\,.\ In(E_p\,.\,t_p)}$
Sato Model	Shear stress	$\tau_u = 2.68\,x10^{-5}\,.\ (f_c')^{0.2}\,.E_p\,.\,\ t_p$
[1]	Debonding load	$P_u = \tau_u\,.\,L_e\,.\,(b_p + 7.4)$
	Effective length	$L_e = 1.89\,.\,(E_p\,.\,\ t_p)^{0.4}\ \ if\ L > L_e : \ L_e = L$
Iso's Model	Shear stress	$\tau_u = 0.93\,.\ (f_c')^{0.44}$
[1]	Debonding load	$P_u = \tau_u\,.\,L_e\,.\,\ b_p$
	Effective length	$L_e = 0.125\,.\,(E_p\,.\,\ t_p)^{0.57}\ \ if\ L > L_e : \ L_e = L$
Yang Model	Shear stress	$\tau_u = 0.50\,.\,\ f_t$

[1] Debonding load

$$P_u = \left(0.5 + 0.08\sqrt{0.01\,.E_p\,.\,t_p\,/f_t}\right).\tau_u\,.L_e\,.\,b_p$$

where,

$$L_e = 100\,mm$$

Izumo Model Debonding load

$$P_u = [3.8\,.\,(f_c')^{0.67} + 15.2]\,.\,L\,.\,E_p\,.t_p\,.\,b_p$$

[1] Debonding load

$$P_u = [3.4\,.\,(f_c')^{0.67} + 69]\,.\,L\,.\,E_p\,.t_p\,.\,b_p$$

Chen and Teng Model Debonding load

$$P_u = 0.427\,.\,\beta_p\,.\beta_L\,.\sqrt{f_c'}\,.\,L_e$$

[1]

$$\sigma_{up} = \alpha\,.\,\beta_p\,.\beta_L\,.\sqrt{E_p\,.\sqrt{f_c'}/t_p}$$

where,

$$\beta_p = \left[\frac{2 - (\,b_p/\,b_c)}{1 + (\,b_p/\,b_c)}\right]^{0.5} \quad \beta_L = \begin{cases} 1 & L \geq L_e \\ sin\left(\dfrac{\pi\,.L}{2\,.\,L_e}\right) & L < L_e \end{cases}$$

$recommended\ values\ for\ \alpha\ ranges\ between\ 0.38\ and\ 0.43$

Effective length

$$L_e = \sqrt{(E_p\,.\,t_p)/\sqrt{f_c'}} \quad \text{or} \quad L_e = \sqrt{(n\,.E_f\,.\,t_f)\,/\sqrt{f_c'}}$$

Chen et al. Debonding load

[1][2]

$$P_u = \begin{cases} \dfrac{b_p\,.\sqrt{2\,.G_f\,.\,E_p\,.\,t_p}}{\sqrt{1-\,\beta^2}} & L \geq \dfrac{1}{\lambda}\arccos\beta \\ \dfrac{b_p\,.\sqrt{2\,.G_f\,.\,E_p\,.\,t_p}\,\sin\,(\lambda\,.L)}{1-\,\beta\,.\cos(\lambda\,.L)} & L < \dfrac{1}{\lambda}\arccos\beta \end{cases}$$

where,

$$\lambda = \sqrt{\frac{\tau_f^2}{2\,.G_f\,.E_p\,.\,t_p}\,.(1 + \frac{b_p\,.E_p\,.\,t_p}{b_c\,.E_c\,.\,t_c})}$$

ACI 440.2R-08

ACI 440.2R-02

[1] [2] [3] [4] [5] [6] [7]

Effective strain

$$\varepsilon_{fd} = 0.41 \cdot \sqrt{\frac{f_c'}{n \cdot E_f \cdot t_f}} \qquad \leq 0.9 \cdot \varepsilon_{fu}$$

Effective strain

$$\varepsilon_{fd} = \begin{cases} \varepsilon_{cu} \cdot \left(\frac{h-c}{c}\right) - \varepsilon_{bi} & if \ \leq k_m \cdot \varepsilon_{fu} \\ k_m \cdot \varepsilon_{fu} & otherwise \end{cases}$$

Where

$$k_m = \frac{1}{60 \cdot \varepsilon_{fu}} \cdot \left(1 - \frac{n \cdot E_f \cdot t_f}{360{,}000}\right) \leq 0.90 \quad for \ n \cdot E_f \cdot t_f < 180 \ MPa$$

Otherwise

$$k_m = \frac{1}{60 \cdot \varepsilon_{fu}} \cdot \left(\frac{90{,}000}{n \cdot E_f \cdot t_f}\right) \leq 0.90$$

Holzenkämpfer Model

[1]

Debonding load

$$P_u = \begin{cases} 0.78 \cdot b_p \cdot \sqrt{2 \cdot G_f \cdot E_p \cdot t_p} & L \geq L_e \\ 0.78 \cdot b_p \cdot \sqrt{2 \cdot G_f \cdot E_p \cdot t_p} \cdot \alpha & L < L_e \end{cases}$$

Where,

$$\alpha = \left(\frac{L}{L_e}\right)\left(2 - \frac{L}{L_e}\right)$$

$$G_f = c_f \cdot f_t \cdot k_p^2$$

$$k_p = \sqrt{1.125 \cdot \left(\frac{2 - b_p/b_c}{1 + b_p/400}\right)}$$

Effective length

$$L_e = \sqrt{E_p \cdot t_p / 4 \cdot f_t}$$

Täljsten Model [1]	Debonding load	$P_u = b_b \,.\, \sqrt{\dfrac{2\,.\,G_f\,.\,E_p\,.\,t_p}{1+(E_p\,.\,t_p\,/E_c\,.\,t_c)}}$
Yuan and Wu Model [1]	Debonding load	$P_u = b_b \,.\, \sqrt{\dfrac{2\,.\,G_f\,.\,E_p\,.\,t_p}{1+(E_p\,.\,t_p\,.\,b_b\,/E_c\,.\,t_c\,.\,b_c)}}$
Neubauer and Rostásy Mode [1]	Debonding load	$P_u = \begin{cases} 0.64\,.\,k_p\,.\,b_p\,.\sqrt{E_p\,.\,t_p\,.f_t} & L \geq L_e \\ 0.64\,.\,k_p\,.\,b_p\,.\sqrt{E_p\,.\,t_p\,.f_t}\,.\alpha & L < L_e \end{cases}$ where, $\alpha = \left(\dfrac{L}{L_e}\right)\left(2-\dfrac{L}{L_e}\right)$ $k_p = ?$
Van Gemert Model [1]	Debonding load	$P_u = 0.5\,.\,b_b\,.\,L\,.\,f_t$
Challal et al. Model [1]	Shear stress	$\tau_u = 0.5\,.\,\tau_{max}^{debonding} = 2.7/(1+\,k_1\,.\tan 33^{\circ})$ where, $k_1 = \,t_p\,.(E_a\,.\,b_a\,/\,4\,.\,E_p\,.\,I_p\,.\,t_a)^{0.25}$
Yuan et al. Model [1]		$P_u = (\tau_f\,.\,b_b\,.\,\delta_f)/\Big(\,\lambda_2\big(\delta_f - \,\delta_1\big)\Big)\sin\,(\,\lambda_2\,.\,a)$ $a\ is\ determined\ by\ solvings:$ $\lambda_1 \tanh[\,\lambda_1(L-a)] = \;\lambda_2 \tan(\,\lambda_2\,.\,a)$ $\lambda_1^2 = (\tau_f/\delta_1\,.\,E_p\,.\,t_p)\,.\,(1+(\,E_p\,.\,t_p\,.\,b_b\,/E_c\,.\,t_c\,.\,b_c))$ $\lambda_2^2 = (\tau_f/(\delta_f - \,\delta_1)\,.\,E_p\,.\,t_p)\,.\,(1+(\,E_p\,.\,t_p\,.\,b_b\,/E_c\,.\,t_c\,.\,b_c))$

Nguyen et al. [1]	Effective length	$l_{dev} = c_c + \frac{d_p}{2} + \frac{4.61}{\lambda}$ where, $\lambda^2 = \frac{1}{E_p \,.\, t_p} \,.\, \frac{G_a \,.\, G_c}{G_c \,.\, t_a + G_a \,.\, c_c}$
CNR-DT 200 R1/2013 [3] [8] [7] [4] [5] [9] [10]	Debonding load	$P_u = b_f \,.\, \sqrt{2 \,.\, E_f \,.\, t_f \,.\, k_p \,.\, k_G \,.\, \sqrt{f_{cs} \,.\, f_{ts}}}$
	Effective length	$l_{ed} = \min\left\{\frac{1}{\gamma_{Rd} \,.\, f_{bd}} \,.\, \sqrt{\frac{\pi^2 \,.\, E_f \,.\, t_f \,.\, \Gamma_{Fd}}{2}}\,, 200\ mm\right\}$, Where: $f_{bd} = \frac{1 \,.\, \Gamma_{Fd}}{s_u}, with\ s_u = 0.25\ mm\ for\ FRP\ systems$ $\gamma_{Rd} = 1.25$ $\Gamma_{Fd} = \frac{k_p \,.\, k_G}{FC} \,.\, \sqrt{f_{cs} \,.\, f_{ts}}$ $k_p = \sqrt{\frac{2 - b_f/b}{1 + b_f/b}} \geq 1$ $k_G = 0.023\ mm\ or\ 0.037\ mm$
	Shear stress	$\tau_{max} = \frac{2 \,.\, G_f}{0.25}$
	Fracture energy	$G_f = 0.077 \,.\, k_p \,.\, \sqrt{f_{cs} \,.\, f_{ts}}$
	Effective strain	$\varepsilon_{fd} = min\left\{\frac{\eta_a \,.\, \varepsilon_{fk}}{\gamma_f}\ ;\ \varepsilon_{fdd}\right\}$, Where:

$$\varepsilon_{fdd} = \frac{k_q}{\gamma_{f,d}} \cdot \sqrt{\frac{1}{t_f \cdot E_f} \cdot \frac{2 \cdot k_b \cdot k_{G,2}}{FC} \cdot \sqrt{f_{cm} \cdot f_{ctm}}}$$

$$\varepsilon_{fdd} = \frac{k_{cr}}{\gamma_{fd} \cdot \sqrt{\gamma_c}} \cdot \sqrt{\frac{2 \cdot \Gamma_{Fk}}{t_f \cdot E_f}}$$

$$k_p = \sqrt{\frac{2 - b_f/b}{1 + b_f/b}} \geq 1 \; for \; b_f/b_c \geq 0.25$$

$$f_{ctm} = 0.30 \cdot (f_{ck})^{2/3} = 0.30 \cdot (f_{cm} - 8)^{2/3}$$

Italian Building Code consider a factor of 1.2 to account for the tensile strength of concrete in bending such that:

$$f_{ctm} = 1.2 \cdot 0.30 \cdot (f_{ck})^{2/3} = 1.2 \cdot 0.30 \cdot (f_{cm} - 8)^{2/3}$$ [see 18]

[11] Debonding load

$$P_{max} = \frac{2}{3} \cdot \beta \cdot \left(0.8 \cdot \sqrt{f_{cu}}\right) \cdot \left(\sqrt{\frac{E_f \cdot t_f}{2.8 \cdot f_{cm}}}\right) \cdot b_f ,$$

Where:

$$\beta = \begin{cases} 0.55 - minimal\ preparation \ldots\ldots \\ 0.85 - recommended\ preparation \\ 1.00 - superior\ preparation \ldots\ldots \end{cases}$$

Effective length

$$l_e = \sqrt{\frac{E_f \cdot t_f}{2.8 \cdot f_{ctm}}}$$

Fib 14

[11] Debonding load

$$P_{max} = 0.9 \cdot 0.64 \cdot 1 \cdot 1.06 \cdot \sqrt{\frac{2 - b_f/b_c}{1 + b_f/400}} \cdot b_f \cdot \sqrt{E_f \cdot t_f \cdot f_{ctm}}$$

Effective length

$$l_e = \sqrt{\frac{E_f \cdot t_f}{2 \cdot f_{ctm}}}$$

TR 55 [11]	Debonding load	$P_{max} = 0.5 \,.\, 1.06 \,.\, \sqrt{\frac{2 - b_f / b_c}{1 + b_f / 400}} \,.\, b_f \,.\, \sqrt{E_f \,.\, t_f \,.\, f_{ctk}}$
CNR -DT 200 [11]	Debonding load	$P_{max} = b_f \,.\, \sqrt{0.03 \,.\, \sqrt{\frac{2 - b_f / b_c}{1 + b_f / 400}}} \,.\, \sqrt{2} \,.\, E_f \,.\, t_f \,.\, \sqrt{f_{ck} \,.\, f_{ctm}}$
	Effective length	$l_e = \sqrt{\frac{E_f \,.\, t_f}{2 \,.\, f_{ctm}}}$
SIA 166 [11]	Debonding load	$P_{max} = 0.5 \,.\, b_f \,.\, \sqrt{E_f \,.\, t_f \,.\, f_{ctH}}$
CIDAR [11]	Debonding load	$P_{max} = 0.427 \,.\, \sqrt{\frac{2 - b_f / b_c}{1 + b_f / 400}} \,.\, b_f \,.\, \sqrt{E_f \,.\, t_f \,.\, \sqrt{f_c}}$
[12]	Debonding load	$P_u = 0.5 \,.\, \tau_f \,.\, b_f \,.\, \chi \,.\, L_e$, Where: $\chi = \begin{cases} 1, & L_b \geq L_e \\ \frac{L_b}{L_e} \,.\, \left(2 - \frac{L_b}{L_e}\right), & otherwise \end{cases}$
[13]	Debonding load	$P = n \,.\, b \,.\, \sqrt{4 \,.\, G \,.\, E \,.\, t}$
Faella et al 2002 [14]	Effective length	$l_e = \frac{\pi}{2} \,.\, \sqrt{\frac{E_f \,.\, t_f}{\tau_{max} / s_u}}$, Where: $s_u = \frac{0.41 \,.\, \beta}{f_{ct}^{0.5}}$

[15] Shear stress

$$\tau = \begin{cases} \tau_m \cdot \left(\frac{s}{s_o}\right), & if\ 0 \le s \le s_o \\ \tau_m \cdot \left(\tau_m - \tau_r\left(\frac{s - s_o}{s_1 - s_o}\right)\right), & if\ s_o < s \le s_1 \\ \tau_r, & if\ s_1 < s \le s_u \\ 0,000000, & if\ s > s_u \ldots 0. \end{cases}$$

Savoia et al [16] Shear stress

$$\tau = \tau_{max} \cdot \frac{u}{u_o} \cdot \left[\frac{2.86}{1.86 + \left(\frac{u}{u_o}\right)^{2.86}}\right],$$

Where:

$$\tau_{max} = 3.5 \cdot f_c^{0.19} \text{ and } u_o = 0.051\ mm$$

Teng et al [16] Shear stress

$$\tau = \begin{cases} \tau_{max} \cdot \frac{u}{u_o}, & if\ u \le u_o \\ \tau_{max} \cdot \frac{u_{f\,max} - u}{u_{f\,max} - u_o}, & if\ u \ge u_o \end{cases},$$

Where:

$$\tau_{max} = 1.5 \cdot \beta_w \cdot f_t$$

Teng et al [5] Debonding strain

$$\varepsilon_{deb} = 0.48 \cdot \beta_w \cdot \sqrt{\frac{\sqrt{f_c'}}{E_f \cdot t_f}},$$

Where:

$$\beta_w = \sqrt{\frac{2 - b_f/b}{1 + b_f/b}} \ge 1$$

Teng et al [5] Debonding strain

$$\varepsilon_{deb} = 0.171 \cdot \beta_p \cdot (4.32 - \alpha) \cdot f_{ctm} \cdot \sqrt{\frac{1}{E_f \cdot t_f}}$$

Where

		$\beta_p = \sqrt{\frac{2.25 - b_f/b_c}{1.25 + b_f/b_c}}$
		$\alpha = \left(10.53 \,.\, f_{ctm}^{-3/2} - 2/3\right)^{-1}$
Said and Wu [5] [7]	Debonding strain	$\varepsilon_{deb} = \frac{k \,.\, \left(0.23 \,.\, f_c'^{0.2}\right)}{(E_f \,.\, t_f)^{0.35}}$
[17]	Shear stress	$\tau\,(x) = t_p \,.\, \frac{df_p(x)}{dx}$
Carloni et al 2015 [18]	Shear stress	$\sigma_{deb} = \frac{P_{deb}}{n \,.\, b^* \,.\, t^*} = \sqrt{\frac{4 \,.E \,.\, G_{II\,f}}{t^*}}$, Where: $G_{II\,f} = \frac{k_p \,.k_G}{FC} \,.\sqrt{f_{cs} \,.\, f_{ts}}$ $k_p = \sqrt{\frac{2 - b_f/b}{1 + b_f/b}} \geq 1$
Obaidat et al. [10]	Shear stress	$\tau_{max} = 1.46 \,.\, G_a^{0.165} \,.\, f_{ct}^{1.033}$
	Fracture energy	$G_f = 0.52 \,.\, G_a^{-0.23} \,.\, f_{ct}^{0.26}$
Monti et al. [10]	Shear stress	$\tau_{max} = 1.8 \,.\, \beta_w \,.\, f_{ct}$
	Fracture energy	$G_f = 0.297 \,.\, f_{ct} \,.\, \beta_w^2$, Where: $\beta_w = \sqrt{\frac{1.5 \,.\, (2 - b_f/b_c)}{1 + b_f/100}}$
Lu et al. [10] [19] [7]	Shear stress	$\tau_{max} = 1.5 \,.\, \beta_w \,.\, f_{ct}$
	Fracture energy	$G_f = 0.308 \,.\, \beta_w^2 \,.\sqrt{f_{ct}}$,

Where:

$$\beta_w = \sqrt{\frac{2.25 - b_f/b_c}{1.25 + b_f/b_c}}$$

Debonding strain

$$\varepsilon_f^{IC} = 0.114 \,.\, (4.41 - \alpha) . \frac{\tau_{max}}{\sqrt{E_f \,.\, t_f}}$$

Where

$$\tau_{max} = 1.5 \,.\, \beta_w \,.\, f_t$$

$$\beta_p = \sqrt{\frac{2.25 - b_f/b_c}{1.25 + b_f/b_c}}$$

$$\alpha = 3.41 \,.\, \frac{0.228 \,.\, \sqrt{E_f \,.\, t_f}}{L_d}$$

[19] Debonding load

$$P_{2d} = P_{1d} \,.\, \left(\frac{K_2}{K_1}\right)^{0.5} . \sqrt{\left(2 \,.\, G_{FII} \,.\, l_f \,.\, b_f + 2 \,.\, W_s^p + 1\right)} \,,$$

Where:

$$G_{FII} = 0.297 \,.\, f_{ct} \,.\, \beta_w^2$$

$$\beta_w = \sqrt{\frac{1.5 \,.\, (2 - b_f/b_c)}{1 + b_f/100}}$$

$$W_s^p = f_{ym} \,.\, \varepsilon_c \,.\, \left(1 - \frac{c'}{c}\right) . A_s \,.\, a$$

[20] Shear stress

$$\tau = E_f \,.\, t_f \,.\, \frac{df(s)}{ds} \,.\, f(s)$$

Fracture energy

$$G_f = 0.5 \,.\, A^2 \,.\, E_f \,.\, t_f$$

Debonding load

$$F_{max,AN} = A \,.\, E_f \,.\, b_f \,.\, t_f$$

[21]

initiation stress $\tau_{lim} = 1.80 \,.\, k_b \,.\, f_{ct}$,

Where:

$$k_b = \sqrt{\frac{k \,.\, (2 - \frac{b}{B})}{1 + \frac{b}{B_{10}}}}$$

Fracture energy $G_f = k_p^2 \,.\, C_f \,.\, f_{ct}$,

Where:

$C_f = 0.202\ mm \sim 0.300\ mm$

[22]

Effective length

$$L = \begin{cases} \frac{2}{\lambda} & elastic \ \ldots\ldots\ldots\ldots \\ \frac{\arcsin\left(-\frac{\tau_o}{\tau_{max}}\right) + \frac{\pi}{2}}{\omega} & elastic - softening \\ \frac{2}{\lambda} + \frac{\arcsin\left(-\frac{\tau_o}{\tau_{max}}\right) + \frac{\pi}{2}}{\omega} & optimal \ldots\ldots\ldots\ldots \end{cases}$$

Fracture energy $G_f = \frac{1}{4 \,.\, E_f \,.\, t^*} \,.\, (\frac{P_{deb}}{n \,.\, t^*})^2$

Debonding load $P_{deb} = \frac{p \,.\, \tau_{max}}{\sqrt{p \ .\, k_2 / \ E_f \,.\, A}} \,.\, \sqrt{1 + \frac{k_2}{k_1}}$

Shear stress

$$\tau = \begin{cases} k_1 \,.\, u & if\ u < u_{max} \ldots\ldots. \\ -k_2 \,.\, u + \ \tau_{max} \,.\, \left(\frac{k_1 + \ k_2}{k_1 \,.\, k_2}\right) & if\ u_{max} \le u \le u_o \\ -k_2 \,.\, u_B + \ \tau_{max} \,.\, \left(\frac{k_1 + \ k_2}{k_1}\right) & if\ u > u_0 \ldots\ldots\ldots\ldots \end{cases}$$

Dai et al

$\tau\,(s) = A \,.\, (e^{-\alpha \,.\, s} - \ e^{-2 \,.\, \alpha \,.\, s})$

[23]

Focacci and Carloni

[23]

$$\tau(s) = \begin{cases} \tau_0 + \dfrac{\tau_m + \tau_0}{s_m} . s & if\ 0 \le s \le s_m \\ \tau_{01} + \dfrac{\tau_{01}}{s_{01}} . s & if\ s_m \le s \le s_c \\ \tau_{02} + \dfrac{\tau_{02}}{s_f} . s & if\ s_c \le s \le s_f \end{cases}$$

Fib Model Code 2010

[24]

Debonding stress (beams)

$$f_{fbm} = k_c . k_m . k_b . \beta_l . \sqrt{\frac{2 . E_f}{t_f} . f_{cm}^{2/3}},$$

Where:

$$k_p = \sqrt{\frac{2 - b_f/b}{1 + b_f/b}} \ge 1$$

[25]

Debonding stress

$$\tau = \frac{1}{2} . \sqrt{f_{cm} . f_{ctm}} . \left[1 + \left(\frac{f_{cm}}{f_{ctm}} - 1\right) . \frac{\sigma}{f_{cm}}\right]$$

[26]

Debonding strain for shear bond tests

$$\varepsilon_{db} = \begin{cases} \sqrt{\dfrac{2 . G_F}{n_f . t_{1f} . E_f}} & for\ debonding\ within\ substrate \\ 2 . \sqrt{\dfrac{G_F}{t_{1f} . E_f}} & for\ debonding\ within\ composite \end{cases}$$

Debonding strain for beams

$$\varepsilon_{db} = K . \sqrt{\frac{2 . b_f . G_F}{E_f . A_f}}$$

Where

K is a coefficient that must be calibrated against the experimental results and its evaluation requires that results of flexural tests on RC beams and results of single-lap shear tests performed with the same composite material

Debonding strain in fibres

$$\varepsilon_{deb}^{\Delta M} = \frac{\Delta M}{0.9 . h . E_f . A_f}$$

$$\varepsilon_{deb}^{\Delta M} = 1.88 \sqrt{\frac{1}{t_f \,.\, E_f}}$$

$$\varepsilon_{deb}^{FS} = 1.79 \sqrt{\frac{1}{t_f \,.\, E_f}}$$

$$\varepsilon_{db} = 2.24 \,.\, (t_f \,.\, E_f)^{-0.52}$$

$$\varepsilon_{db} = 2.57 \,.\, (t_f \,.\, E_f)^{-0.53}$$

$$\varepsilon_{db} = K \,.\sqrt{2 \,.\, G_F} \,.\, \sqrt{\frac{1}{t_f \,.\, E_f}}$$

Where

$$\Delta M = \frac{\Delta F}{2} \,.\, L_1$$

[27] Debonding strain $\varepsilon_{max,th} = \alpha \,.\, (E_f \,.\, A_f)^{\beta} \,.\, (f_{c,s})^{\gamma}$

References

[1] E. Sayed-Ahmed, R. Bakay and N. Shrive, "Bond strength of FRP laminates to concrete: State-of-the-art review", Electronic Journal of Structural Engineering, vol. 9, pp. 45-61, 2009.

[2] ACI 440.2R-08, “Guide for the Design and Construction of Externally Bonded FRP Systems for Strengthening Concrete Structures,” American Concrete Institute, 2008.

[3] F. Bencardino and A. Condello, "Structural behaviour of RC beams externally strengthened in flexure with SRG and SRP systems", International Journal of Structural Engineering, vol. 5, no. 4, p. 346, 2014.

[4] S. De Santis, G. de Felice, A. Napoli and R. Realfonzo, "Strengthening of structures with Steel Reinforced Polymers: A state-of-the-art review", Composites Part B: Engineering, vol. 104, pp. 87-110, 2016.

[5] F. Bencardino and A. Condello, "Reliability and adaptability of the analytical models proposed for the FRP systems to the Steel Reinforced Polymer and Steel Reinforced Grout strengthening systems", Composites Part B: Engineering, vol. 76, pp. 249-259, 2015.

[6] A. Prota, G. Manfredi, A. Nanni, E. Cosenza and M. Pecce, "Flexural strengthening of RC beams using emerging materials: Ultimate behavior", in Proceedings of 2nd International Conference on FRP Composites in Civil Engineering (CICE 2004), Adelaide, Australia, 2004, pp. 163–170.

[7] L. Ombres, "Flexural analysis of reinforced concrete beams strengthened with a cement based high strength composite material", Composite Structures, vol. 94, no. 1, pp. 143-155, 2011.

[8] A. Balsamo, F. Nardone, I. Iovinella, F. Ceroni and M. Pecce, "Flexural strengthening of concrete beams with EB-FRP, SRP and SRCM: Experimental investigation", Composites Part B: Engineering, vol. 46, pp. 91-101, 2013.

[9] CNR-DT 200 R1/2013, “Guide for the Design and Construction of Externally Bonded FRP Systems for Strengthening Existing Structures”, Consiglio Nazionale delle Ricerche, 2013.

[10] F. Bencardino and A. Condello, "SRG/SRP–concrete bond–slip laws for externally strengthened RC beams", Composite Structures, vol. 132, pp. 804-815, 2015.

[11] A. Serbescu, M. Guadagnini and K. Pilakoutas, "Standardised double-shear test for determining bond of FRP to concrete and corresponding model development", Composites Part B: Engineering, vol. 55, pp. 277-297, 2013.

[12] E. Grande, M. Imbimbo and E. Sacco, "Modeling and numerical analysis of the bond behavior of masonry elements strengthened with SRP/SRG", Composites Part B: Engineering, vol. 55, pp. 128-138, 2013.

[13] V. Alecci, M. De Stefano, R. Luciano, L. Rovero and G. Stipo, "Experimental Investigation on Bond Behavior of Cement-Matrix–Based Composites for Strengthening of Masonry Structures", Journal of Composites for Construction, vol. 20, no. 1, p. 04015041, 2016.

[14] C. Mazzotti et al., "Design Procedures for the Use of Composites in Strengthening of Reinforced Concrete Structures: State-of-the-Art Report of the RILEM Technical Committee", Springer, 2016.

[15] A. Razavizadeh, B. Ghiassi and D. Oliveira, "Bond behavior of SRG-strengthened masonry units: Testing and numerical modeling", Construction and Building Materials, vol. 64, pp. 387-397, 2014.

[16] L. Ombres, "Debonding analysis of reinforced concrete beams strengthened with fibre reinforced cementitious mortar", Engineering Fracture Mechanics, vol. 81, pp. 94-109, 2012.

[17] L. Bizindavyi and K. Neale, "Transfer Lengths and Bond Strengths for Composites Bonded to Concrete", Journal of Composites for Construction, vol. 3, no. 4, pp. 153-160, 1999.

[18] C. Carloni, T. D'Antino, L. Sneed and C. Pellegrino, "Three-Dimensional Numerical Modeling of Single-Lap Direct Shear Tests of FRCM-Concrete Joints Using a Cohesive Damaged Contact Approach", Journal of Composites for Construction, vol. 22, no. 1, p. 04017048, 2018.

[19] F. Bencardino and A. Condello, "Eco-friendly external strengthening system for existing reinforced concrete beams", Composites Part B: Engineering, vol. 93, pp. 163-173, 2016.

[20] F. Bencardino, A. Condello and A. Ashour, "Single-lap shear bond tests on Steel Reinforced Geopolymeric Matrix-concrete joints", Composites Part B: Engineering, vol. 110, pp. 62-71, 2017.

[21] F. Bencardino and A. Condello, "Experimental study and numerical investigation of behavior of RC beams strengthened with steel reinforced grout", Computers and Concrete, vol. 14, no. 6, pp. 711-725, 2014.

[22] J. Salsavilca, J. Yacila, N. Tarque and G. Camata, "Experimental and analytical bond behaviour of masonry strengthened with steel reinforced grout (SRG)", Construction and Building Materials, vol. 238, 2020.

[23] M. Santandrea, F. Focacci, C. Mazzotti, F. Ubertini and C. Carloni, "Determination of the interfacial cohesive material law for SRG composites bonded to a masonry substrate", Engineering Failure Analysis, vol. 111, p. 104322, 2020.

[24] S. Raoof, L. Koutas and D. Bournas, "Textile-reinforced mortar (TRM) versus fibre-reinforced polymers (FRP) in flexural strengthening of RC beams", Construction and Building Materials, vol. 151, pp. 279-291, 2017.

[25] W. Figeys, L. Schueremans, K. Brosens and D. Van Gemert, "Strengthening of Concrete Structures using Steel Wire Reinforced Polymer", ACI Symposium Publication, vol. 230, 2005.

[26] F. Bencardino, C. Carloni, A. Condello, F. Focacci, A. Napoli and R. Realfonzo, "Flexural behaviour of RC members strengthened with FRCM: State-of-the-art and predictive formulas", Composites Part B: Engineering, vol. 148, pp. 132-148, 2018.

[27] F. Ceroni and P. Salzano, "Design provisions for FRCM systems bonded to concrete and masonry elements", Composites Part B: Engineering, vol. 143, pp. 230-242, 2018.

Appendix H Manufacturers' Datasheets

BUILDING RANGE / Mineral geo-mortars for monolithic repair and for structural strengthening of concrete

GeoLite®

Certified, eco-friendly mineral geo-mortar with a crystalline reaction geo-binder base, for passivation, restoration, finishing and monolithic protection of deteriorated concrete structures, ideal for use in GreenBuilding. Very low petrochemical polymer content, free from organic fibres. Thixotropic, normal setting.

GeoLite® is a thixotropic geo-mortar used to passivate, restore, finish and protect reinforced concrete structures such as beams, pillars, slabs, front sections, ramps, facades, decorative elements, cornices and civil engineering structures such as bridges, viaducts, tunnels and water channels. Suitable as an inorganic mineral matrix in composite reinforcement systems in the GeoSteel line.

CE EN 1504-2(C) · CE EN 1504-3 · CE EN 1504-7 · R4 CC · R4 PCC · MC METHOD 2.3 · CR METHOD 3.1 - 3.3 · SS METHOD 4.4 · PR METHOD 5.1 · RP METHOD 7.1 - 7.2 · IR METHOD 8.3 · CA METHOD 11.2 · PASSES CARBONATION RESISTANCE

GREENBUILDING RATING®

GeoLite®
- Category: Inorganic Mineral Products
- Class: Mineral geo-mortars for monolithic repair and for structural strengthening of concrete
- Rating: Eco 3

eco3	Natural Mineral ≥ 50%	Recycled Mineral ≥ 50%	CO_2 ≤ 250 g/kg	Low Emission IAQ Indoor Air Quality	Recyclable
			CO_2/kg emission 239 g	Very low VOC emissions	Can be recycled as inert material

RATING SYSTEM ACCREDITED BY CERTIFICATION BODY SGS

PRODUCT STRENGTHS

- **GEO-BINDER**. Exclusive use of the innovative Kerakoll geo-binder with geo-polymer crystallisation revolutionises mortars used to repair concrete, guaranteeing levels of safety never before achieved and unique eco-friendly performance.
- **MONOLITHIC**. The first geo-mortar that forms a monolithic conglomerate that will surround, protect and strengthen reinforced concrete works without the need to apply several layers. The only mortar that is certified to passivate, restore, finish, correct and protect in a single layer.
- **CRYSTALLISING**. The naturally stable, monolithic repairs carried out with GeoLite® crystallise with the concrete to guarantee the durability of a mineral rock.
- **QUICK**. The first geo-mor²ar that requires just one day's work to achieve complete restoration, as compared with the six days required by traditional restoration mortar cycles involving several layers.
- **TAILORED**. The first range of geo-mortars with different setting times (> 80 – 40 – 10 min.) that can be mixed together to customise setting times according to conditions on the building site.

ECO NOTES

- Based on geo-binder
- Eco-friendly concrete restoration
- Very low petrochemical polymer content
- Free from organic fibres
- With low CO_2 emissions
- With very low volatile organic compound emissions
- Can be recycled as mineral inert material, avoiding waste disposal costs and environmental impact

AREAS OF USE

Use
Passivation, localised and generalised restoration; finishing and monolithic protection of reinforced concrete structures, such as beams, pillars, slabs, front sections, ramps, exposed walls, decorative elements, cornices and civil engineering structures such as bridges, viaducts, tunnels, water channels.
Specific for medium or large size operations, machine application, finishing of large surface areas.
Suitable as an inorganic mineral matrix in composite reinforcement systems from the GeoSteel range, for the static and seismic adaptation or improvement of reinforced concrete or masonry structural elements.
Ideal for GreenBuilding and Restoration of Modern Architecture.

INSTRUCTIONS FOR USE

Preparation of substrates
Before applying GeoLite® roughen the surface of the concrete substrate (to a depth of at least 5 mm) by mechanical scarification or hydro-demolition, thoroughly removing all weakened concrete; after this all rust must be removed from the reinforcing rods, which must be cleaned by brushing (manual or mechanical) or sandblasting. After this, clean the substrate, removing any remaining dust, grease, oil or other contaminants using compressed air or a high pressure washer, wet the surface until it is fully saturated leaving no excess water what so ever. Alternatively, Geolite® Base guarantees proper absorption when applied to highly absorbent, cement-based substrates, and encourages natural crystallisation of the geo-mortar. Before applying GeoLite®, check that the resistance class of the supporting concrete is suitable.

* ÉMISSION DANS L'AIR INTÉRIEUR Information sur le niveau d'émission de substances volatiles dans l'air intérieur, présentant un risque de toxicité par inhalation, sur une échelle de classe allant de A+ (très faibles émissions) à C (fortes émissions).

KERAKOLL The GreenBuilding Company

00094GeoLite® Code: E784 2014/07 EN

INSTRUCTIONS FOR USE

High-thickness patching on large surface areas: a suitable metallic reinforcement needs to be anchored to the substrate using anchoring pins.

Preparation
Prepare GeoLite® by mixing 25 kg of powder with the amount of water indicated on the packaging (we advise using the whole bag). A cement mixer can be used – mix until the mortar is smooth with no lumps; a suitable mortar machine can also be used to mix and then spray the product. When mixing small quantities, use a bucket and drill-type mixing device with a low-rev agitator.
Store the product away from any sources of humidity and out of direct sunlight.

Application
In localised/generalised restoration work in which GeoLite® is applied in thicknesses from 2 mm to 40 mm (maximum per layer), apply the mortar by hand using a trowel or mortar spray machine.
To create structural reinforcements, systems in which GeoLite® acts as an inorganic mineral matrix, apply an initial layer of geo-mortar, to guarantee a sufficient amount of material on the suitably prepared support (minimum thickness 5 – 8 mm) to regulate it and allow laying and incorporation of the strengthening textile. After applying the steel textile, apply a second layer so as to incorporate the reinforcement completely and close up any underlying gaps.
GeoLite® can be applied manually (with a steel spreader) or by machine in a minimum thickness of 2 mm, to make a protective finishing. Allow the surfaces to cure for at least 24 hrs.

Cleaning
Residual traces of GeoLite® can be removed from tools and machines using water before the product hardens.

ABSTRACT

Passivation, localised and generalised centimetre-thick monolithic restoration of deteriorated concrete structural elements and civil engineering structures, millimetre-thick monolithic protective finishing with manual or machine application of certified, thixotropic, eco-friendly, normal setting geo-mortar with a crystalline reaction zirconia and geo-binder base, extremely low petrochemical polymer content and free from organic fibres, specific for the passivation, restoration, finishing and guaranteed, long-lasting, monolithic protection of concrete structures, such as GeoLite® by Kerakoll® Spa, GreenBuilding Rating® Eco 3, that is CE-marked and compliant with the performance requirements of Standard EN 1504-7 (passivation of reinforcing bars), EN 1504-3, Class R4 (volumetric reconstruction and finishing) and EN 1504-2 (protection of surfaces), according to Principles 2, 3, 4, 5, 7, 8 and 11 as defined by EN 1504-9.

TECHNICAL DATA COMPLIANT WITH KERAKOLL QUALITY STANDARD

Appearance	Powder	
Apparent volumetric mass	1340 kg/m³	UEAtc
Aggregate mineral content	Silica - carbonate	
Grading	0 – 0,5 mm	EN 12192-1
Shelf life	≈ 12 months in the original packaging in dry environment	
Pack	25 kg bags	
Mixing water	≈ 5.1 l / 1 x 25 kg bag	
Flow of the mixture	140 – 160 mm	EN 13395-1
Density of the mixture	≈ 2050 kg/m³	
pH of the mixture	≥ 12,5	
Start/End of setting	> 70 – 80 min. (≈ 200 – 220 min. at +5 °C) – (> 50 – 60 min. at +30 °C)	
Temperature range for application	from +5 °C to +40 °C	
Minimum thickness	2 mm	
Maximum thickness per layer	40 mm	
Coverage	≈ 17 kg/m² per cm of thickness	

Values taken at +21 °C, 60% R.H. and no ventilation. Data may vary depending on specific conditions at the building site.

00694GeoLite® Code: E784 2014/07 EN

KERAKOLL
The GreenBuilding Company

INSTRUCTIONS FOR USE

High-thickness patching on large surface areas: a suitable metallic reinforcement needs to be anchored to the substrate using anchoring pins.

Preparation
Prepare GeoLite® by mixing 25 kg of powder with the amount of water indicated on the packaging (we advise using the whole bag). A cement mixer can be used – mix until the mortar is smooth with no lumps; a suitable mortar machine can also be used to mix and then spray the product. When mixing small quantities, use a bucket and drill-type mixing device with a low-rev agitator.
Store the product away from any sources of humidity and out of direct sunlight.

Application
In localised/generalised restoration work in which GeoLite® is applied in thicknesses from 2 mm to 40 mm (maximum per layer), apply the mortar by hand using a trowel or mortar spray machine.
To create structural reinforcements, systems in which GeoLite® acts as an inorganic mineral matrix, apply an initial layer of geo-mortar, to guarantee a sufficient amount of material on the suitably prepared support (minimum thickness 5 – 8 mm) to regulate it and allow laying and incorporation of the strengthening textile. After applying the steel textile, apply a second layer so as to incorporate the reinforcement completely and close up any underlying gaps.
GeoLite® can be applied manually (with a steel spreader) or by machine in a minimum thickness of 2 mm, to make a protective finishing. Allow the surfaces to cure for at least 24 hrs.

Cleaning
Residual traces of GeoLite® can be removed from tools and machines using water before the product hardens.

ABSTRACT

Passivation, localised and generalised centimetre-thick monolithic restoration of deteriorated concrete structural elements and civil engineering structures, millimetre-thick monolithic protective finishing with manual or machine application of certified, thixotropic, eco-friendly, normal setting geo-mortar with a crystalline reaction zirconia and geo-binder base, extremely low petrochemical polymer content and free from organic fibres, specific for the passivation, restoration, finishing and guaranteed, long-lasting, monolithic protection of concrete structures, such as GeoLite® by Kerakoll® Spa, GreenBuilding Rating® Eco 3, that is CE-marked and compliant with the performance requirements of Standard EN 1504-7 (passivation of reinforcing bars), EN 1504-3, Class R4 (volumetric reconstruction and finishing) and EN 1504-2 (protection of surfaces), according to Principles 2, 3, 4, 5, 7, 8 and 11 as defined by EN 1504-9.

TECHNICAL DATA COMPLIANT WITH KERAKOLL QUALITY STANDARD

Appearance	Powder	
Apparent volumetric mass	1340 kg/m³	UEAtc
Aggregate mineral content	Silica - carbonate	
Grading	0 – 0,5 mm	EN 12192-1
Shelf life	≈ 12 months in the original packaging in dry environment	
Pack	25 kg bags	
Mixing water	≈ 5.1 l / 1 x 25 kg bag	
Flow of the mixture	140 – 160 mm	EN 13395-1
Density of the mixture	≈ 2050 kg/m³	
pH of the mixture	≥ 12,5	
Start/End of setting	> 70 – 80 min. (≈ 200 – 220 min. at +5 °C) – (> 50 – 60 min. at +30 °C)	
Temperature range for application	from +5 °C to +40 °C	
Minimum thickness	2 mm	
Maximum thickness per layer	40 mm	
Coverage	≈ 17 kg/m² per cm of thickness	

Values taken at +21 °C, 60% R.H. and no ventilation. Data may vary depending on specific conditions at the building site.

00694GeoLite® Code: E784 2014/07 EN

KERAKOLL
The GreenBuilding Company

PERFORMANCE

HIGH-TECH

Performance characteristic	Test Method	Requirements of standard EN 1504-7	GeoLite® Performance
Corrosion protection	EN 15183	no corrosion	value exceeded
Shear adhesion	EN 15184	≥ 80% of the value of the uncovered bar	value exceeded
Performance characteristic	**Test Method**	**Requirements of standard EN 1504-3, class R4**	**GeoLite® Performance in CC and PCC conditions**
Compressive strength	EN 12190	≥ 45 MPa (28 days)	> 15 MPa (24 hrs)
			> 40 MPa (7 days)
			> 55 MPa (28 days)
Flexural tensile strength	EN 196/1	None	> 5 MPa (24 hrs)
			> 8 MPa (7 days)
			> 10 MPa (28 days)
Adhesive bond	EN 1542	≥ 2 MPa (28 days)	> 2 MPa (28 days)
Resistance to carbonation	EN 13295	depth of carbonation ≤ reference concrete [MC (0,45)]	value exceeded
Modulus of elasticity under compression	EN 13412	≥ 20 GPa (28 days)	25 GPa (28 days)
Thermal compatibility with freeze/thaw cycles with de-icing salts	EN 13687-1	bond strength after 50 cycles ≥ 2 MPa	> 2 MPa
Thermal compatibility with freeze/thaw cycles with de-icing salts	EN 13687-1	bond strength after 50 cycles ≥ 2 MPa	> 2 MPa
Capillary absorption	EN 13057	≤ 0,5 $kg \cdot m^{-2} \cdot h^{-0,5}$	< 0,5 $kg \cdot m^{-2} \cdot h^{-0,5}$
Chloride ion content (Determined on the product in powder form)	EN 1015-17	≤ 0,05%	< 0,05%
Reaction to fire	EN 13501-1	Euroclass	A1
Performance characteristic	**Test Method**	**Requirements of standard EN 1504-2 (C)**	**GeoLite® Performance**
Permeability to water vapour	EN ISO 7783-2	Reference class	class **I**: s_D < 5 m
Capillary absorption and water permeability	EN 1062-3	w < 0,1 $kg \cdot m^{-2} \cdot h^{-0,5}$	w < 0,1 $kg \cdot m^{-2} \cdot h^{-0,5}$
Bond strength by pull off	EN 1542	≥ 0,8 MPa	> 2 MPa
Linear shrinkage	EN 12617-1	≤ 0,3%	< 0,3%
Thermal expansion coefficient	EN 1770	$\alpha_T \leq 30 \cdot 10^{-6} \cdot k^{-1}$	$\alpha_T < 30 \cdot 10^{-6} \cdot k^{-1}$
Resistance to abrasion	EN ISO 5470-1	loss of weight < 3000 mg	value exceeded
Adhesion following thermal shock	EN 13687-2	≥ 2 N/mm²	> 2 N/mm²
Resistance to impact	EN ISO 6272-1	Reference class	Class III : ≥ 20 Nm
Hazardous substances		compliant with point 5.4	

QUALITÀ DELL'ARIA INTERNA (IAQ) VOC - EMISSIONI SOSTANZE ORGANICHE VOLATILI

Conformity	EC 1-R plus GEV-Emicode	GEV certified 3539/11.01.02

00094GeoLite® Code: E784 2014/07 EN

KERAKOLL
The GreenBuilding Company

WARNING

- **Product for professional use**
- abide by any standards and national regulations
- use at temperatures between +5 °C and +40 °C
- do not add binders or additives to the mixture
- do not apply to dirty, loose and flaking surfaces
- do not apply on gypsum, metal or wood
- following application, protect from direct sunlight and wind
- allow the product to cure during the first 24 hours
- if necessary, ask for the safety data sheet
- for any other issues, contact the Kerakoll Worldwide Global Service +39 0536 811 516 - globalservice@kerakoll.com

00694GeoLite® Code: E784 2014/07 EN

Kerakoll Quality System ISO 9001 CERTIFIED IT10/0327 | Kerakoll Quality System ISO 14001 CERTIFIED IT242729/UK | Kerakoll Quality System BS 18001 CERTIFIED IT255412/UK

KERAKOLL The GreenBuilding Company

KERAKOLL S.p.a.
Via dell'Artigianato, 9 - 41049 Sassuolo (MO) Italy
Tel +39 0536 816 511 - Fax +39 0536 816 581
info@kerakoll.com - www.kerakoll.com

BUILDING RANGE / Steel bars and sheets for structural strengthening of reinforced concrete and masonry structures

GeoSteel G600

GeoSteel G600 Hardwire™ is a unidirectional sheet made of ultra-high strength galvanized steel micro-cords, fixed to a fibreglass micromesh to facilitate installation, which can be installed using a GeoCalce® Fino or GeoLite® or GeoLite® Gel matrix according to project and building site requirements.

The structural strengthening GeoSteel sheet is thus extremely easy to handle and shape, and combines excellent mechanical and installation properties with high durability thanks to galvanization of the individual wires. Galvanized steel fiber sheets guarantee unique structural and mechanical properties, much higher than traditional carbon-glass-aramide fibre sheets, making them particularly effective in the various structural strengthening and seismic upgrade or compliance retrofit solutions, as well as the creation of suitable connection systems, when combined with GeoSteel Injector&Connector.

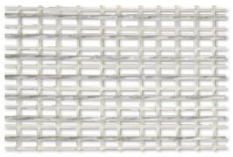

PRODUCT STRENGTHS

- High durability thanks to the special steel wire galvanization process, tested using strict durability tests in a chloride, freeze-thaw and high humidity environment
- Specifically intended for structural strengthening using:
  - GeoCalce® Fino, with pure natural hydraulic NHL 3.5 lime and mineral geo-binder base, ideal for retrofitting structural elements made of brick, natural stone, and tuff masonry and substrates that require advanced breathability along with high mechanical adhesion
  - GeoLite®, with mineral geo-binder base, ideal for retrofitting structural elements in reinforced concrete, prestressed reinforced concrete or good consistency masonry
  - GeoLite® Gel, epoxy-based mineral adhesive, ideal for structural retrofitting sections made of reinforced concrete, prestressed reinforced concrete, wood and steel
- Can be tensioned to create structural reinforcements and active devices using particular mechanical anchoring systems, thanks to the unique characteristics of the textile which do not require advance impregnation of the sheet, and at the same time allow it to be anchored and fastened with metal plates without having to take particular precautions, as is necessary for all the other types of fibre and textile on the market
- Can be shaped using GeoSteel Bender which allows the sheet to be modelled easily without altering its mechanical properties to create surround brackets for beams and pillars and other bent elements required during structural consolidation works

AREAS OF USE

Use

- Static and seismic upgrade or compliance retrofit of structural elements in brick, natural stone, tuff, reinforced concrete, prestressed reinforced concrete, wood, and steel walls
- Consolidation of brick masonry, natural stone and tuff arches, vaults and domes
- Confinement and wrapping of masonry and reinforced concrete structural elements
- Flexural, shear, and confinement strengthening of brick, natural stone, tuff, and masonry panels and reinforced concrete sections
- Flexural, shear, and confinement strengthening for timber elements
- Flexural strengthening for steel girders
- Execution of top ring beams or in breach in reinforced masonry
- Execution of special single- or double-fibre thread connectors for anchoring sheets and grids and executing reinforced injections

INSTRUCTIONS FOR USE

Preparation

The ultra-high strength galvanized steel fibre sheet, GeoSteel G600 Hardwire™, is ready-to-use.
The sheet can be cut at right angles to the cords with manual or electric shears, or parallel with the cords using a normal box cutter. The sheet, cut into strips even just a few cm wide and a number of metres long, ensures perfect stability without in any way compromising the workability of the material and its application.

Preparation of substrates

The substrate must be properly prepared and cleaned, always in accordance with the instructions dictated by the construction supervisor.
When the substrates are not damaged, simply clean and remove any dust or oils that could compromise the adhesion of the system, using compressed air or pressure water.
When the substrate is clearly degraded, uneven, or damaged by significant events, proceed as follows, always in accordance with the construction supervisor:

1. For masonry, tuff, and natural stone substrates:
   - Completely remove residues from previous processes that could compromise adhesion, and any quantity of inconsistent rendering mortars from between the stones;

0075GeoSteel G600 Code: E865 2014/07

KERAKOLL
The GreenBuilding Company

INSTRUCTIONS FOR USE

- Saturation, spray, or brush application, if required, of certified natural stabilizing cortical consolidant with base of pure stabilised potassium silicate in aqueous solution such as Biocalce® Silicato Consolidante or water-based eco-friendly solvent-free stabilizing agent, such as Rasobuild® Eco Consolidante;
- Reconstruction, if necessary, of material continuity according to design instructions and the construction supervisor.
- Levelling previously consolidated surfaces with geo-mortar with a base of pure natural hydraulic lime NHL 3.5 and mineral geo-binder such as GeoCalce® or GeoCalce® Fino, depending on the thickness required;

2. For substrates in reinforced concrete or prestressed reinforced concrete:
   - Thorough removal of weakened concrete if necessary, through mechanical scarification or hydro-demolition, making sure to roughen the substrate to a depth of at least 5 mm;
   - Removal of rust, if any, from reinforcing bars, which must be cleaned by brushing (manual or mechanical) or sandblasting;
   - Monolithic reconstruction or smoothing of the section, if needed, using geo-mortar based on a mineral geo-binder such as GeoLite®.
   - When applying the reinforcing system with an inorganic matrix, make sure that the substrate is appropriately dampened (follow the directions on the GeoLite® or GeoCalce® data sheets).
   - When applying the reinforcing system with an organic matrix, the substrate must be dry and free of humidity (follow the instructions on the GeoLite® Gel data sheet).

Application

Execution of steel fibre structural reinforcement in Steel Reinforced Mortar (combination of steel fibre and GeoCalce® Fino or GeoLite®), or Steel Reinforced Polymer (combination of steel fibre and GeoLite® Gel epoxy mineral adhesive) will be followed by application of a first layer of geo-mortar, making sure there is sufficient material for the substrate (average thickness ≈ 3 - 5 mm) to even it out and to lay and incorporate the reinforcing sheet. When using an epoxy mineral adhesive matrix, the substrate can be levelled using GeoLite® or GeoCalce®, taking care to allow the geo-mortar to cure for long enough to ensure that the humidity of the substrate is appropriate for application of GeoLite® Gel. The first layer of adhesive must be an average thickness of ≈ 2 - 3 mm. Afterward, working over the matrix while it is still wet, apply the ultra-high strength galvanized steel fibre sheet GeoSteel G600 Hardwire™, making sure that the sheet is perfectly incorporated into the matrix by pressing with a spreader or steel roller, and also checking that it comes out between the cords to ensure optimum adhesion between the first and second layers of matrix. At longitudinal overlapping points, overlay two layers of steel fibre sheet by least 15 cm for epoxy matrix and 30 cm for inorganic matrices. For organic and inorganic matrix, working wet on wet, perform the final protective smoothing (≈ 1 - 2 mm thick for organic matrix, ≈ 2 - 3 mm thick for inorganic), in order to fully incorporate the reinforcement and fill in any underlying voids. If there are additional layers after the first, proceed with laying of the second layer of steel fibre over the matrix while it is still wet, repeating the steps described above. In the event that the system installed with epoxy matrix must be plastered or concealed by smoothing, we recommend that, while the resin is still wet, you apply a spray of mineral quartz to provide better adhesion for subsequent layers.
If the reinforcing system is installed in especially aggressive environments, or you otherwise wish to ensure additional protection beyond that already provided by the matrix, we recommend applying:
- GeoLite® Microsilicato on reinforcement systems with GeoLite® or GeoCalce® Fino matrix;
- Kerakover Eco Acrilex Flex on reinforcement systems with GeoLite® Gel matrix.

If the works are in permanent or occasional contact with water, the cycles described above must be replaced with a polyurethane epoxy cycle or an osmotic cement depending on the needs of the worksite and the design specifications.
For technical specifications, application, and preparation of the matrix, as well as protective systems adequate for the matrix type, consult the relevant data sheets.

Creating a GeoSteel Connector

A steel-fibre thread connector system is created by including a band of fabric of appropriate width from the GeoSteel Hardwire™ line to provide the minimum number of cords in the connector according to the design, in order to achieve the required tensile strength; make sure to unravel the end of the fabric band by cutting the supportive mesh, making the cut parallel to the cords themselves to the length of the edge you want to create on the masonry. In the event of a connector with threads on both sides, this operation must be performed on both ends of the duly arranged fibre strip. Once the sheet is cut, roll the band onto itself, taking care to create a cylinder of an appropriate diameter compared to the hole.
Install the connector that has been created into the hole, and then insert the Geosteel glass fibre-reinforced polypropylene GeoSteel Injector&Connector, so that the end of the fibre bends 90°. Finally, using the special hole located on the head of the piece, inject the pourable mortar, such as GeoCalce® Fluido, to grout the fibre-thread connector system. When this phase is complete, the GeoSteel Injector&Connector must be duly sealed with the cap provided.
Depending on the type of substrate (concrete or masonry) for grouting the connector, as an alternative to the use of pourable natural hydraulic lime, the designer may choose to use pourable cement-based mortar Kerabuild® Eco Binder, thixotropic epoxy resin GeoLite® Gel or superfluid Kerabuild® Epofill.

Provided below is a table listing the tensile strength of a connector as a function of the type of GeoSteel Hardwire™ sheet and the corresponding widths of the band adopted:

Sheet	Width of the band (cm)	Number of Cords*	Tensile breaking load
GeoSteel G600	10	16	> 24 kN
GeoSteel G600	15	23	> 35 kN

*n° cords/cm = 1,57;
tensile breaking load of a cord > 1500 N.

In the event that a connector with another strength or a different number of cords from those listed is required, simply calculate the appropriate width of the band by dividing the required strength by the strength of one cord and then by the number of cords present per unit of width in the type of sheet selected.
Test reports are available upon request to determine the calculation parameters.

0075GeoSteel G600 Code: E865 2014/07

KERAKOLL
The GreenBuilding Company

ABSTRACT

SRM-GeoCalce® GeoSteel G600

Execution of structural reinforcement or repair, seismic upgrade of masonry, tuff, or natural stone elements and structures using a composite system based on ultra-high strength galvanized steel fibre sheet GeoSteel G600 Hardwire™ from Kerakoll Spa, with net fibre weight of ≈ 600 g/m², with the following mechanical characteristics: sheet tensile strength > 2800 MPa; sheet elastic modulus > 190 GPa; sheet break deformation > 1.50%; nominal area of a cord 3x2 (5 wires) = 0.538 mm²; no. cords per cm = 1.57; sheet equivalent thickness = 0.084 mm, impregnated with certified inorganic matrix of natural, structural, breathable, eco-friendly geo-mortar based on pure natural hydraulic lime NHL 3.5 and mineral geo-binder, such as GeoCalce® Fino by Kerakoll Spa, to be applied directly on the structure requiring reinforcement.

The procedure is conducted as follows:

1. *Any restoration of degraded, weakened, non-cohesive, or non-planar surfaces with GeoCalce® by Kerakoll Spa, in the case of masonry substrates, or GeoLite® by Kerakoll Spa, in the case of reinforced concrete substrates, and in all cases as dictated and approved by the construction supervisor;*
2. *Lay a first layer, an average of ≈ 3 - 5 mm thick of geo-mortar with pure natural NHL 3.5 and mineral geo-binder base, such as GeoCalce® Fino by Kerakoll Spa;*
3. *While the mortar is still wet, lay the ultra-high strength galvanized steel fibre sheet GeoSteel G600 Hardwire™ by Kerakoll Spa, and by pressing firmly with a smooth spreader or metal roller, make sure that the sheet is completely impregnated and avoid allowing any gaps or air bubbles to form, because these can compromise the adhesion of the sheet to the matrix or to the substrate;*
4. *Working wet on wet, apply the second layer of geo-mortar based on pure natural lime NHL 3.5 and mineral geo-binder, such as GeoCalce® Fino by Kerakoll Spa, ≈ 2 – 3 mm thick to fully incorporate the reinforcing sheet and fill in any remaining underlying gaps;*
5. *Repeat steps (3 and (4 if necessary for all subsequent reinforcing layers called for by the design.*

Delivery and installation of all the materials described above as well as everything else required to finish the job is included. The following are excluded: restoration of degraded areas and repair of the substrate; anchoring devices using connectors or metal plates; material acceptance tests; pre- and post-procedure testing, all aids required to perform the work.

The price is by unit of reinforcing surfaces actually laid, including overlaps and anchoring sections.

SRM-GeoLite® GeoSteel G600

Execution of structural reinforcement or repair, or seismic upgrade or compliance retrofit of reinforced cement, masonry, tuff, or natural stone elements and structures using a composite system based on ultra-high strength galvanized steel fibre sheet GeoSteel G600 Hardwire™ from Kerakoll Spa, with net fibre weight of ≈ 600 g/m², with the following mechanical characteristics: sheet tensile strength > 2800 MPa; sheet elastic modulus > 190 GPa; sheet break deformation > 1.50%; nominal area of a cord 3x2 (5 wires) = 0.538 mm²; no. cords per cm = 1.57; sheet equivalent thickness = 0.084 mm, impregnated with inorganic matrix of eco-friendly, thixotropic, normal-setting certified mineral geo-mortar, based on crystalline reaction geo-binder and zirconium, with very low petrochemical polymer content and free of organic fibres, specifically for passivation, restoration, smoothing, and guaranteed, long-lasting monolithic protection of structures in concrete, such as GeoLite® by Kerakoll Spa, to be applied directly on the structure requiring reinforcement.

The procedure is conducted as follows:

1. *Any restoration of degraded, weakened, non-cohesive, or non-planar surfaces shall be performed with GeoCalce® by Kerakoll Spa, in the case of masonry substrates, or GeoLite® by Kerakoll Spa, in the case of reinforced concrete substrates, and in all cases as dictated and approved by the construction supervisor;*
2. *Spread a first layer of approximate average thickness of ≈ 3 - 5 mm of geo-mortar with mineral geo-binder base, such as GeoLite® by Kerakoll Spa;*
3. *While the mortar is still wet, lay the ultra-high strength galvanized steel fibre sheet GeoSteel G600 Hardwire™ by Kerakoll Spa, and by pressing firmly with a smooth spreader or metal roller, make sure that the sheet is completely impregnated and avoid allowing any gaps or air bubbles to form, because these can compromise the adhesion of the sheet to the matrix or to the substrate;*
4. *Working wet on wet, apply the second layer of geo-mortar, such as GeoLite® by Kerakoll Spa, approximately ≈ 2 -3 mm thick, until the reinforcing sheet is fully incorporated and any underlying voids are filled;*
5. *Repeat steps (3 and (4 if necessary for all subsequent reinforcing layers called for by the design.*

Delivery and installation of all the materials described above as well as everything else required to finish the job is included. The following are excluded: restoration of degraded areas and repair of the substrate; anchoring devices using connectors or metal plates; material acceptance tests; pre- and post-procedure testing, all aids required to perform the work.

The price is by unit of reinforcing surfaces actually laid, including overlaps and anchoring sections.

SRP GeoSteel G600

Execution of structural reinforcement or repair, or seismic upgrade or compliance retrofit of reinforced cement, masonry, wood and steel using a composite system based on ultra-high strength galvanized steel fibre sheet GeoSteel G600 Hardwire™ from Kerakoll Spa, with net fibre weight of ≈ 600 g/m², with the following mechanical characteristics: sheet tensile strength > 2800 MPa; sheet elastic modulus > 190 GPa; sheet break deformation >1.50%; nominal area of a cord 3x2 (5 wires) = 0.538 mm²; no. cords per cm = 1.57; sheet equivalent thickness = 0.084 mm, impregnated with epoxy mineral matrix such as GeoLite® Gel by Kerakoll Spa to be applied directly on the structure requiring reinforcement without any need for primer.

The procedure is conducted as follows:

1. *Any restoration of degraded, weakened, non-cohesive, or non-planar surfaces shall be performed with GeoCalce® by Kerakoll Spa, in the case of masonry substrates, or GeoLite® by Kerakoll Spa, in the case of reinforced concrete substrates, and in all cases as dictated and approved by the construction supervisor;*
2. *Application of a first layer approximately average thickness of ≈ 2 - 3 mm of epoxy mineral adhesive such as GeoLite® Gel by Kerakoll Spa;*
3. *While the epoxy mineral adhesive is still wet, lay the ultra-high strength galvanized steel fibre sheet GeoSteel G600 Hardwire™ by Kerakoll Spa, and by pressing firmly with a smooth spreader or metal roller, make sure that the sheet is completely impregnated and avoid allowing any gaps or air bubbles to form, because these can compromise the adhesion of the reinforcing system to the substrate;*
4. *Working wet on wet, lay the second layer of matrix, such as GeoLite® Gel by Kerakoll Spa, at an average thickness of ≈ 1 – 2 mm, until the reinforcing sheet is completely covered;*
5. *Repeat steps (3 and (4 if necessary for all subsequent reinforcing layers called for by the design.*

Delivery and installation of all the materials described above as well as everything else required to finish the job is included. The following are excluded: restoration of degraded areas and repair of the substrate; anchoring devices using connectors or metal plates; material acceptance tests; pre- and post-procedure testing, all aids required to perform the work.

The price is by unit of reinforcing surfaces actually laid, including overlaps and anchoring sections.

0075GeoSteel G600 Code: E865 2014/07

KERAKOLL
The GreenBuilding Company

TECHNICAL DATA COMPLIANT WITH KERAKOLL QUALITY STANDARD

Wire			
	- characteristic tensile stress	σ_{wire}	> 2900 MPa
	- elastic modulus	E_{wire}	> 205 GPa
	- area	A_{wire}	0,1076 mm²
Dry sheet/Cord			
Cord 3x2 obtained by joining 5 filaments, of which 3 straight and 2 wrapped with a high torque angle			
	- actual area of a cord 3x2 (5 wires)	A_{cord}	0,538 mm²
	- n° cords/cm		1,57 cords/cm
	- mass (inclusive of thermal welding)		≈ 670 g/m²
	- equivalent thickness of sheet	t_{sheet}	≈ 0,084 mm
	- tensile breaking load of a cord		> 1500 N
	- tensile strength of the sheet	σ_{sheet}	> 2800 MPa
	- tensile strength by unit of width	σ_{sheet}	> 2,35 kN/cm
	- normal elastic modulus of sheet	E_{sheet}	> 190 GPa
	- break warp of the sheet	ε_{sheet}	> 1,50%
Pack	50 m rolls (h 30 cm)		
Weight of 1 roll	≈ 24 kg including packaging		

WARNING

- **Product for professional use**
- abide by any standards and national regulations
- when handling the sheet wear protective clothing and goggles, and follow the instructions regarding methods for applying the material
- contact with the skin: no special measures required
- storage on the work site: store under cover in a dry place, well away from substances that might damage it or its ability to adhere to the chosen matrix
- if necessary, ask for the safety data sheet
- for any other issues, contact the Kerakoll Worldwide Global Service +39 0536 811 516 - globalservice@kerakoll.com

0075GeoSteel G600 Code: E865 2014/07

KERAKOLL S.p.a.
Via dell'Artigianato, 9 - 41049 Sassuolo (MO) Italy
Tel +39 0536 816 511 - Fax +39 0536 816 581
info@kerakoll.com - www.kerakoll.com

BUILDING RANGE / Repair and reinforcement of reinforced concrete and masonry

GeoSteel G1200

GeoSteel G1200 sheet, in Hardwire™ extra-high strength galvanised steel fibre, is a unidirectional sheet made of extra-high strength galvanized steel micro-cords, fixed to a fibreglass micromesh to facilitate installation, which can be installed using a GeoCalce® F Antisismico, GeoLite® or GeoLite® Gel matrix according to project and building site requirements.

The structural strengthening GeoSteel sheet is thus extremely easy to handle and shape, and combines excellent mechanical and installation properties with high durability thanks to galvanization of the individual wires. Galvanized steel fiber sheets guarantee unique structural and mechanical properties, much higher than traditional carbon-glass-aramide fibre sheets, making them particularly effective in the various structural strengthening and seismic upgrade or compliance retrofit solutions, as well as the creation of suitable connection systems, when combined with GeoSteel Injector&Connector.

PRODUCT STRENGTHS

- High durability thanks to the special steel wire galvanization process, tested using strict durability tests in a chloride, freeze-thaw and high humidity environment
- Specifically intended for structural strengthening using:
  - GeoCalce® F Antisismico, fine-grain, structural, breathable geo-mortar with pure natural NHL 3.5 and geo-binder, ideal for retrofitting structural elements in brick, natural stone, and tuff masonry and substrates that require advanced breathability along with high mechanical adhesion
  - GeoLite®, with mineral geo-binder base, ideal for retrofitting structural elements in reinforced concrete, prestressed reinforced concrete or good consistency masonry
  - GeoLite® Gel, epoxy-based mineral adhesive, ideal for structural fixing of sections of reinforced concrete, prestressed reinforced concrete, wood, good consistency masonry and steel
- Can be tensioned to create structural reinforcements and active devices using particular mechanical anchoring systems, thanks to the unique characteristics of the textile which do not require advance impregnation of the sheet, and at the same time allow it to be anchored and fastened with metal plates without having to take particular precautions, as is necessary for all the other types of fibre and textile on the market
- Can be shaped using GeoSteel benders which allow the sheet to be modelled easily without altering its mechanical properties to create surround brackets for beams and pillars and other bent elements required during structural consolidation works

AREAS OF USE

Use

- Static and seismic upgrade or compliance retrofit of structural elements in brick, natural stone, tuff, reinforced concrete, prestressed reinforced concrete, wood, and steel walls
- Consolidation of brick masonry, natural stone and tuff arches, vaults and domes
- Confinement and wrapping of masonry or reinforced concrete structural elements
- Flexural, shear, and confinement strengthening of brick, natural stone, tuff, and masonry panels and reinforced concrete sections
- Flexural, shear, and confinement strengthening for timber elements
- Flexural strengthening for steel girders
- Execution of top ring beams or in breach in reinforced masonry
- Execution of special single- or double-fibre thread connectors for anchoring sheets and grids and executing reinforced injections
- Consolidation and reinforcement of exposed stone walls using widespread areas of mesh

INSTRUCTIONS FOR USE

Preparation

The GeoSteel G1200 sheet, in Hardwire™ extra-high strength galvanized steel fibre is ready-to-use.
The sheet can be cut at right angles to the cords with manual or electric shears, or parallel with the cords using a normal box cutter. The sheet, cut into strips even just a few cm wide and a number of metres long, ensures perfect stability without in any way compromising the workability of the material and its application.

Preparation of substrates

The substrate must be properly prepared and cleaned, always in accordance with the instructions dictated by the construction supervisor.
In the case of substrates that are not degraded, prepare the surfaces as indicated in the technical data sheet for GeoCalce® F Antisismico, GeoLite® or GeoLite® Gel.
When the substrate is clearly degraded, uneven, or damaged by significant events, proceed as follows, always in accordance with the construction supervisor:

1. For masonry, tuff and natural stone substrates:
   - Completely remove residues from previous processes that could compromise adhesion, and any quantity of inconsistent rendering mortars from between the stones;

GeoSteel G1200 Code: E1010 2017/05-EN

KERAKOLL The GreenBuilding Company

INSTRUCTIONS FOR USE

- Saturation, spray, or brush application, if required, of certified natural stabilizing cortical consolidant with base of pure stabilised potassium silicate in aqueous solution such as Biocalce® Silicato Consolidante or water-based eco-friendly solvent-free stabilizing agent, such as Rasobuild® Eco Consolidante;
- Reconstruction, if necessary, of material continuity according to design instructions and the construction supervisor
- Evening out previously consolidated surfaces with structural geo-mortar with a base of pure natural hydraulic lime NHL 3.5 and geo-binder such as GeoCalce® G Antisismico or GeoCalce® F Antisismico, depending on the thickness required;
- When applying the reinforcing system with an inorganic matrix, make sure that the substrate is adequately dampened and with a roughness of at least 5 mm (follow the instructions on the GeoCalce® F Antisismico or GeoLite® data sheet).
- When applying the reinforcing system with an organic matrix, the substrate must be dry and free of humidity and with a roughness of at least 0.5 mm (follow the instructions on the GeoLite® Gel data sheet).

2. For substrates in reinforced concrete or prestressed reinforced concrete:
   - Thorough removal of weakened concrete if necessary, through mechanical scarification or hydro-demolition, making sure to roughen the substrate to a depth of at least 5 mm;
   - Removal of rust, if any, from reinforcing bars, which must be cleaned by brushing (manual or mechanical) or sandblasting;
   - Monolithic reconstruction or smoothing of the section, if needed, using geo-mortar based on a mineral geo-binder such as GeoLite®.
   - When applying the reinforcing system with an inorganic matrix, make sure that the substrate is adequately dampened and with a roughness of at least 5 mm (follow the instructions on the GeoLite® data sheet).
   - When applying the reinforcing system with an organic matrix, the substrate must be dry and free of humidity and with a roughness of at least 0.5 mm (follow the instructions on the GeoLite® Gel data sheet).

Application

Execution of steel fibre structural reinforcement in Steel Reinforced Mortar (combination of steel fibre and GeoCalce® F Antisismico or GeoLite®), or GeoSteel S-FRP (combination of steel fibre and GeoLite® Gel epoxy mineral adhesive) will be followed by application of a first coat of geo-mortar, making sure there is sufficient material for the substrate (average thickness ≈ 3-5 mm) to even it out and to lay and incorporate the reinforcing textile. Before applying the first layer of geo-mortar, the substrate must be cleaned, suitably dampened and roughened, by means of sanding or mechanical scarification, so as to achieve a sufficient roughness (follow the indications on the technical sheet for GeoCalce® F Antisismico or GeoLite®). When using an epoxy mineral adhesive matrix, the substrate can be evened out using GeoLite®, for reinforced concrete substrates, GeoCalce® G Antisismico or GeoCalce® or GeoCalce® F Antisismico for masonry substrates, taking care to allow the geo-mortar to cure for long enough to ensure that the humidity of the substrate is appropriate for application of GeoLite® Gel. Indeed, before application of the first layer of GeoLite® Gel, the substrate must be clean, dry, free from damp and roughened, by sanding or mechanical scarification, to a depth of at least 0.5 mm. The first layer of adhesive must be an average thickness of ≈ 1-2 mm. Afterward, working over the matrix while it is still wet, apply the GeoSteel G1200 sheet in Hardwire™ extra-high strength galvanized steel fibre, making sure that the sheet is perfectly incorporated into the matrix by pressing with a spreader or steel roller, and also checking that it comes out between the cords to ensure optimum adhesion between the first and second layers of matrix. At longitudinal overlapping points, overlay two layers of steel fibre sheet by least 15 cm for epoxy matrix and 30 cm for inorganic matrices. For organic and inorganic matrix, working fresh on fresh, perform the final protective smoothing (overall thickness of the reinforcement for organic matrix ≈ 2-3 mm, overall thickness of the reinforcement for mineral matrix ≈ 5-8 mm), in order to fully incorporate the reinforcement and fill in any underlying voids. If there are additional layers after the first, proceed with laying of the second layer of steel fibre over the matrix while it is still wet. In the event that the system installed with epoxy matrix must be plastered or concealed by smoothing, we recommend that, while the resin is still wet, you apply a spray of mineral quartz to provide better adhesion for subsequent layers.

If the reinforcing system is installed in especially aggressive environments, or you otherwise wish to ensure additional protection beyond that already provided by the matrix, we recommend applying:

- GeoLite® MicroSilicato on reinforcement systems with GeoLite® or GeoCalce® F Antisismico matrix;
- Kerakover Eco Acrilex Flex on reinforcement systems with GeoLite® Gel matrix.

If the works are in permanent or occasional contact with water, the cycles described above must be replaced with a polyurethane epoxy cycle or an osmotic cement depending on the needs of the worksite and the design specifications.

For technical specifications, application, and preparation of the matrix, as well as protective systems adequate for the matrix type, consult the relevant data sheets.

Creating a GeoSteel Connector

A steel-fibre thread connector system is created by including a band of fabric of appropriate width from the GeoSteel Hardwire™ line to provide the minimum number of cords in the connector according to the design, in order to achieve the required tensile strength; make sure to unravel the end of the fabric band by cutting the supportive mesh, making the cut parallel to the cords themselves to the length of the edge you want to create on the masonry. In the event of a connector with threads on both sides, this operation must be performed on both ends of the duly arranged fibre strip. Once the sheet is cut, roll the band onto itself, taking care to create a cylinder of an appropriate diameter compared to the hole.

Install the connector that has been created into the hole, and then insert the Geosteel glass fibre-reinforced polypropylene GeoSteel Injector&Connector, so that the end of the fibre bends 90°. Finally, using the special hole located on the head of the piece, inject the pourable mortar, such as GeoCalce® FL Antisismico, to grout the fibre-thread connector system. When this phase is complete, the GeoSteel Injector&Connector must be duly sealed with the cap provided.

Depending on the type of substrate (concrete or masonry) for grouting the connector, as an alternative to the use of pourable natural hydraulic lime, the designer may choose to use pourable GeoLite® Magma geo-mortar, GeoLite® Gel thixotropic epoxy resin, or superfluid Kerabuild Epofill.

Provided below is a table listing the tensile strength of a connector as a function of the type of GeoSteel Hardwire™ sheet and the corresponding widths of the band adopted:

Sheet	Width of the band (cm)	Number of Cords*	Tensile breaking load
GeoSteel G1200	10	32	> 47 kN
GeoSteel G1200	15	47	> 70 kN

n° cords/cm = 3.19;
tensile breaking load of a cord > 1500 N.

GeoSteel G1200 Code: E1010 2017/05-EN

KERAKOLL
The GreenBuilding Company

INSTRUCTIONS FOR USE

In the event that a connector with another strength or a different number of cords from those listed is required, simply calculate the appropriate width of the band by dividing the required strength by the strength of one cord and then by the number of cords present per unit of width in the type of sheet selected.
Test reports are available upon request to determine the calculation parameters.

ABSTRACT

SRM-GeoCalce® F Antisismico&GeoSteel G1200

Execution of structural reinforcement or repair, seismic upgrade of masonry, tuff, or natural stone elements and structures using a composite system based on GeoSteel G1200 sheet in Hardwire™ extra-high strength galvanized steel fibre from Kerakoll Spa, with net fibre weight of ≈ 1,200 g/m2, with the following mechanical performance characteristics: tensile strength of the sheet > 2800 MPa; normal elastic modulus of sheet > 190 GPa; break warp of the sheet > 2 %; actual area of a cord 3x2 (5 wires) = 0.538 mm²; no. cords per cm = 3.14; equivalent thickness of the sheet = 0.169 mm, impregnated with inorganic matrix of fine-grain, structural, breathable geo-mortar with pure natural hydraulic lime NHL 3.5 and geo-binder, such as GeoCalce® F Antisismico by Kerakoll Spa, to be applied directly on the structure requiring reinforcement.
The procedure is conducted as follows:

1. *Any restoration of degraded, weakened, non-cohesive, or non-planar surfaces, using GeoCalce® G Antisismico or GeoCalce® F Antisismico by Kerakoll Spa and in any case as prescribed and approved by the construction supervisor;*
2. *Lay a first layer, an average of ≈ 3-5 mm thick of fine-grain, structural, geo-mortar with pure natural NHL 3.5 and geo-binder base, such as GeoCalce® F Antisismico by Kerakoll Spa;*
3. *While the mortar is still wet, lay the GeoSteel G1200 sheet in Hardwire™ extra-high strength galvanized steel fibre by Kerakoll Spa, and by pressing firmly with a smooth spreader or metal roller, make sure that the textile is completely impregnated and avoid allowing any gaps or air bubbles to form, because these can compromise the adhesion of the sheet to the matrix or to the substrate;*
4. *Working fresh on fresh, lay the second layer of fine-grain, structural, geo-mortar based on pure natural lime NHL 3.5 and geo-binder, such as GeoCalce® F Antisismico by Kerakoll Spa, ≈ 2-5 mm thick to fully incorporate the reinforcing sheet and fill in any remaining underlying gaps;*
5. *Repeat steps (3 and (4 if necessary for all subsequent reinforcing layers called for by the design.*

delivery and installation of all the materials described above as well as everything else required to finish the job is included. The following are excluded: restoration of degraded areas and repair of the substrate; anchoring devices using connectors or metal plates; material acceptance tests; pre- and post-procedure testing, all aids required to perform the work. The price is by unit of reinforcing surfaces actually laid, including overlaps and anchoring sections.

SRM-GeoLite®&GeoSteel G1200

Execution of structural reinforcement or repair, or seismic upgrade or compliance retrofit of reinforced cement, masonry, tuff, or natural stone elements and structures using a composite system based on GeoSteel G1200 sheet in Hardwire™ extra-high strength galvanized steel fibre from Kerakoll Spa, with net fibre weight of ≈ 1,200 g/m², with the following mechanical performance characteristics: tensile strength of the sheet > 3000 MPa; normal elastic modulus of sheet > 190 GPa; break warp of the sheet > 2%; actual area of a cord 3x2 (5 wires) = 0.538 mm²; no. cords per cm = 3.14; equivalent thickness of sheet = 0.169 mm, impregnated with inorganic matrix of eco-friendly, thixotropic, normal-setting certified mineral geo-mortar, based on crystalline reaction geo-binder and zirconium, with very low petrochemical polymer content and free of organic fibres, specifically for passivation, restoration, smoothing, and guaranteed, long-lasting monolithic protection of structures in concrete, such as GeoLite® by Kerakoll Spa, to be applied directly on the structure requiring reinforcement.
The procedure is conducted as follows:

1. *Any restoration of degraded, weakened, non-cohesive, or non-planar surfaces with GeoCalce® G Antisismico or GeoCalce® F Antisismico by Kerakoll Spa, in the case of masonry substrates, or GeoLite® by Kerakoll Spa, in the case of reinforced concrete substrates, and in all cases as dictated and approved by the construction supervisor;*
2. *Preparation of the substrate for application of the first layer of geo-mortar, the substrate must be adequately roughened by sanding or mechanical scarification (taking care to guarantee a roughness of at least 5 mm), clean and suitably dampened;*
3. *Spread a first layer of approximate average thickness of 3-5 mm of geo-mortar with mineral geo-binder base, such as GeoLite® by Kerakoll Spa;*
4. *While the mortar is still wet, lay the GeoSteel G1200 sheet in Hardwire™ extra-high strength galvanized steel fibre by Kerakoll Spa, and by pressing firmly with a smooth spreader or metal roller, make sure that the textile is completely impregnated and avoid allowing any gaps or air bubbles to form, because these can compromise the adhesion of the sheet to the matrix or to the substrate;*
5. *Working fresh on fresh, apply the second layer of geo-mortar, such as GeoLite® by Kerakoll Spa, approximately ≈ 2-3 mm thick, until the reinforcing textile is fully incorporated and any underlying voids are filled, giving an overall reinforcement thickness of ≈ 5-8 mm;*
6. *Repeat steps (3 and (4 if necessary for all subsequent reinforcing layers called for by the design.*
6. *Repeat steps (3 and (4 if necessary for all subsequent reinforcing layers called for by the design.*

Delivery and installation of all the materials described above as well as everything else required to finish the job is included. The following are excluded: restoration of degraded areas and repair of the substrate; anchoring devices using connectors or metal plates; material acceptance tests; pre- and post-procedure testing, all aids required to perform the work.
The price is by unit of reinforcing surfaces actually laid, including overlaps and anchoring sections.

GeoSteel S-FRP G1200

Execution of structural reinforcement or repair, or seismic upgrade or compliance retrofit of reinforced cement, masonry, wood and steel using a composite system based on GeoSteel G1200 sheet in Hardwire™ extra-high strength galvanized steel fibre from Kerakoll Spa, with net fibre weight of ≈ 1,200 g/m2, with the following mechanical performance characteristics: tensile strength of the sheet > 3000 MPa; normal elastic modulus of the sheet > 190 GPa; break warp of the sheet >2%; actual area of a cord 3x2 (5 wires) = 0.538 mm²; no. cords per cm = 3.14; equivalent thickness of the sheet = 0.169 mm, impregnated with epoxy mineral matrix such as GeoLite® Gel by Kerakoll Spa to be applied directly on the structure requiring reinforcement without any need for primer.
The procedure is conducted as follows:

1. *Any restoration of degraded, weakened, non-cohesive, or non-planar surfaces with GeoCalce® G Antisismico or GeoCalce® F Antisismico by Kerakoll Spa, in the case of masonry substrates, or GeoLite® by Kerakoll Spa, in the case of reinforced concrete substrates, and in all cases as dictated and approved by the construction supervisor;*

GeoSteel G1200 Code: E1010 2017/05-EN

KERAKOLL
The GreenBuilding Company

ABSTRACT

2. *Preparation of the substrate for application of the first layer of GeoLite® Gel, the substrate must be adequately roughened by sanding or mechanical scarification (taking care to guarantee a roughness of at least 0.5 mm), clean and free from damp;*
3. *Application of a first layer approximately average thickness of ≈ 2-3 mm of epoxy mineral adhesive such as GeoLite® Gel by Kerakoll Spa;*
4. *While the epoxy mineral adhesive is still fresh, lay the GeoSteel G1200 sheet in Hardwire™ extra-high strength galvanized steel fibre by Kerakoll Spa, and by pressing firmly with a smooth spreader or metal roller, make sure that the sheet is completely impregnated and avoid allowing any gaps or air bubbles to form, because these can compromise the adhesion of the reinforcing system to the substrate;*
5. *Working fresh on fresh, apply the second matrix layer such as GeoLite® Gel by Kerakoll Spa, until the reinforcement textile is completely covered to give an overall reinforcement thickness of ≈ 2-3 mm;*
6. *Repeat steps (3 and (4 if necessary for all subsequent reinforcing layers called for by the design.*

delivery and installation of all the materials described above as well as everything else required to finish the job is included. The following are excluded: restoration of degraded areas and repair of the substrate; anchoring devices using connectors or metal plates; material acceptance tests; pre- and post-procedure testing, all aids required to perform the work. The price is by unit of reinforcing surfaces actually laid, including overlaps and anchoring sections.

TECHNICAL DATA COMPLIANT WITH KERAKOLL QUALITY STANDARD

Wire		
- characteristic tensile stress	σwire	> 2900 MPa
- Elastic modulus	Ewire	> 205 GPa
- area	Awire	0,1076 mm²
Cord 3x2 obtained by joining 5 filaments, of which 3 straight and 2 wrapped with a high torque angle		
- actual area of a cord 3x2 (5 wires)	Acord	0,538 mm²
- n° cords/cm		3.19 cords/cm
- tensile breaking load of a cord		> 1500 N
Values are for non-impregnated sheet		
Tensile strength of the tape, typical value	σsheet	> 3000 MPa
tensile strength by unit of width	σsheet	> 4,72 kN/cm
normal elastic modulus of sheet	Esheet	> 190 GPa
Break warp of the tape, typical value	εsheet	> 2%
Fibre density	ρ_{fib}	≈ 7,955 g/cm³
Equivalent thickness	t_f	≈ 0,169 mm
mass (inclusive of thermal welding)		≈ 1200 g/m²
Mass of the textile by unit of area		≈ 1200 g/m²
Pack		40 m rolls (h 30 cm)
Weight of 1 roll		≈ 18 kg including packaging

WARNING

- **Product for professional use**
- abide by any standards and national regulations
- when handling the sheet wear protective clothing and goggles, and follow the instructions regarding methods for applying the material
- contact with the skin: no special measures required
- storage on the work site: store under cover in a dry place, well away from substances that might damage it or its ability to adhere to the chosen matrix
- if necessary, ask for the safety data sheet
- for any other issues, contact the Kerakoll Worldwide Global Service +39 0536 811 516 - globalservice@kerakoll.com

GeoSteel G1200 Code: E1010 2017/05-EN

Kerakoll Quality System ISO 9001 CERTIFIED IT10/0327
Kerakoll Quality System ISO 14001 CERTIFIED IT242729/UK
Kerakoll Quality System BS 18001 CERTIFIED IT255412/UK

KERAKOLL The GreenBuilding Company

KERAKOLL S.p.a.
Via dell'Artigianato, 9 - 41049 Sassuolo (MO) Italy
Tel +39 0536 816 511 - Fax +39 0536 816 581
info@kerakoll.com - www.kerakoll.com